Inaugural dissertation for obtaining the doctoral degree of the Combined Faculty of Mathematics, Engineering and Natural Sciences of the Ruprecht - Karls - University Heidelberg

Presented by
M.Sc. Marie Bordas
Born in Villecresnes, France
Date of Oral Examination: 08.12.2022

Deciphering the role and the mechanism of B-cell Non-Hodgkin Lymphoma-derived small Extracellular Vesicles in modulating the phenotype of myeloid cells.

Referees:

Prof. Dr. Viktor Umansky

Prof. Dr. Peter Lichter

Declaration

I hereby declare that I have written the submitted dissertation “Deciphering the role and the mechanism of B-cell Non-Hodgkin Lymphoma-derived small Extracellular Vesicles in modulating the phenotype of myeloid cells.” myself and in this process have not used any other sources than those expressly indicated.
I hereby declare that I have not applied to be examined at any other institution, nor have I used the dissertation in this or any other form at any other institution as an examination paper, nor submitted it to any other faculty as a dissertation.

Marie Bordas.

1. Summary

Non-Hodgkin Lymphomas (NHL) represent one of the most common cancers worldwide. Among the most common forms of NHL are found Chronic Lymphocytic Leukemia (CLL), Diffuse Large B-cell Leukemia (DLBCL), and Follicular Lymphoma (FL). NHL is characterized by an expansion of myeloid cells with pro-tumoral properties, such as Tumor-associated macrophages (TAMs) or Myeloid-derived Suppressor Cells (MDSCs). However, little is known about the tumoral mechanisms leading to the expansion of those cell populations.

It was recently suggested that small extracellular vesicles (sEVs) secreted by tumor cells may contribute to the polarization of myeloid cells. Indeed, the treatment of myeloid cells with CLL-derived sEVs leads to an upregulation of PD-L1 at the surface of myeloid cells and an increased secretion of pro-inflammatory cytokines. Interestingly, CLL-derived sEVs were enriched in yRNA4, a small non-coding RNA. Treatment of myeloid cells with yRNA4 induces a similar response of myeloid cells to treatment with CLL-derived sEVs. This effect depends on the Toll-Like Receptor (TLR) 7, a member of the TLR family, and may be relevant for all small RNAs contained in sEVs. In this dissertation, I first investigated the involvement of other TLR in response to treatment with CLL-derived sEVs. I searched for candidate sEV-proteins that could drive the polarization of myeloid cells into a pro-tumoral phenotype. In parallel, I investigated the role played by yRNA4 in the polarization of myeloid cells.

As a first step, this dissertation presents a new approach for isolating and characterizing sEVs from human or murine lymphoid tissues. This approach combines differential centrifugation with size-exclusion chromatography, and turned out to be superior to previously used ultracentrifugation on a sucrose density cushion in terms of purity and yield of sEVs.

A second step shows that the proteomic signature induced in myeloid cells following treatment with CLL-derived sEVs was broader than the signature induced in myeloid cells by yRNA4. The capacity of sEVs to induce a pro-inflammatory phenotype was tested using murine myeloid cells deficient for either TLR4, TLR7, or Myd88. Loss of TLR4 but not TLR7 nor Myd88 in myeloid cells leads to an impaired polarization of myeloid cells by tumor-derived sEVs. The activation of TLR2 and TLR4 following treatment with tumor-derived sEVs was also proven by using reporter cell assays.

Next, I searched for potential TLR ligands present in NHL-derived sEVs. A proteomic comparison was performed with sEVs derived from the lymph nodes (LNs) of patients diagnosed with two subtypes of NHL, DLBCL and FL, as well as sEVs from patients with reactive lymph nodes as a non-tumoral control. Tumor LNs from DLBCL or FL patients were enriched in sEVs compared to reactive LNs. However, we observed a differential signature between the proteome of DLBCL-derived and FL-derived sEVs. Proteins unique to DLBCL-derived sEVs were primarily related to RNA processing, while proteins unique to FL-derived sEVs were more related to metabolism, among other pathways. Interestingly, sEVs from all

sources were found to be particularly enriched with Heat Shock Proteins (HSP), a family of proteins known to be endogenous ligands of TLRs.

Finally, a knock-out of yRNA4 was induced using the CRISPR/Cas9 approach in the cell line HG-3, modeling CLL. The knock-out was validated using classical and real-time quantitative polymerase chain reactions and a Northern-blot assay. yRNA4 knock-out did not impair the capacity of the cells to secrete sEVs, nor their morphology, as investigated using transmission electron microscopy. However, sEVs derived from the yRNA4-deficient cell line showed a decreased capacity to induce the inflammatory phenotype in myeloid cells. The results raise the new hypothesis, that the reduced capacity of yRNA4-KO sEVs is due not only to the sole absence of yRNA4 but that the deletion of yRNA4 may impact the protein cargo loaded into the sEVs.

Altogether, this dissertation allowed to decipher deeper the mechanisms by which tumor-derived sEVs influence the phenotype of myeloid cells. This mechanism was shown to be mediated by TLR2, TLR4 and TLR7; and the bioactive ligands include single-stranded RNAs such as yRNA4, as well as proteins, in particular the Heat-Shock Proteins. In the future, these findings may help finding new therapeutical targets to inhibit the modulation of the tumor microenvironment by tumor cells.

2. Zusammenfassung

Das Non-Hodgkin Lymphom (NHL) ist eine der häufigsten Krebsarten weltweit. Zu den weitverbreitesten Formen des NHL gehören die chronische lymphatische Leukämie (CLL), das diffus großzellige B-Zell-Lymphom (DLBCL) und das follikuläre Lymphom (FL). Eine Expansion myeloider Zellen mit tumorfördernden Eigenschaften wie tumor-assoziierten Makrophagen (TAMs) oder myeloiden Suppressorzellen (MDSC) ist charakteristisch für NHL. Allerdings ist wenig über die Mechanismen bekannt, welche zur Expansion dieser Zellpopulationen führen.

Kleine extrazelluläre Vesikel (sEVs), die von Tumorzellen sezerniert werden, wurden kürzlich als möglicher Beitrag zu dieser Polarisierung myeloider Zellen vorgeschlagen. Tatsächlich führt die Behandlung von Monozyten mit CLL-abgeleiteten sEVs zu einer Hochregulation von PD-L1 auf der Monozytenoberfläche und einer erhöhten Sekretion von proinflammatorischen Zytokinen. Interessanterweise war yRNA4, eine kleine nicht-kodierende RNA, in CLL-abgeleiteten sEVs angereichert. Behandlung von Monozyten mit yRNA4 induziert einen ähnlichen Effekt wie CLL-abgeleitete sEVs. Dieser Effekt ist abhängig von Toll-like-Rezeptor (TLR) 7, der zur Familie der TLRs gehört und womöglich für alle in sEVs enthaltenen kleinen RNAs relevant ist. In dieser Doktorarbeit untersuchte ich zunächst die Beteiligung anderer TLRs an der Reaktion auf Behandlung mit CLL-abgeleiteten sEVs. Ich suchte mögliche Kandidaten für sEV-Proteine, welche die Polarisierung der Monozyten in einen tumorfördernden Phänotyp antreiben. Parallel dazu ermittelte ich die Rolle von yRNA4 in der Polarisierung von Makrophagen.

In einem ersten Schritt stellt diese Doktorarbeit einen neuen Ansatz zur Isolierung und Charakterisierung von sEVs aus humanem oder murinem lymphatischen Gewebe vor. Dieser Ansatz kombiniert differenzielle Zentrifugation mit Größenausschluss-Chromatographie und erwies sich in Bezug auf Reinheit und Ausbeute von sEVs als Verbesserung gegenüber der zuvor verwendeten Ultrazentrifugation mit Saccharose-Dichtekissen.
Im zweiten Schritt wird gezeigt, dass die in Monozyten durch Behandlung mit CLL-abgeleiteten sEVs induzierte proteomische Signatur breiter gefächert als die durch yRNA4 induzierte Signatur ist. Das Vermögen von sEVs, einen tumorfördernden Phänotyp zu indizieren, wurde unter Verwendung von murinen Monozyten getestet, denen entweder TLR4, TLR7 oder Myd88 fehlte. Durch den Verlust von TLR4 kommt es zu einer beeinträchtigten Polarisierung der Monozyten durch Tumor-abgeleitete sEVs, was jedoch weder für TLR7, noch für Myd88 zu beobachten war. Zudem wurde die Aktivierung von TLR2 und TLR4 nach Behandlung mit Tumor-abgeleiteten sEVs durch Experimente mit Reporterzellen nachgewiesen.

Des Weiteren sollten potentielle TLR Liganden, die in NHL-abgeleiteten sEVs vorhanden sind, identifiziert werden. Es wurde ein Vergleich der Proteome von sEVs durchgeführt, welche aus Lymphknoten (LN) von Patienten stammten, bei denen NHL mit den beiden Sybtypen DLBCL und FL diagnostiziert wurde. Als tumorfreie Kontrolle dienten sEVs von Patienten mit reaktiven

Lymphknoten. In Tumor-Lymphknoten von DLBCL- oder FL-Patienten waren sEVs im Vergleich zu reaktiven Lymphknoten angereichtert. Jedoch beobachteten wir für DLBCL- und FL-abgeleitete sEVs eine unterschiedliche Proteomsignatur. Proteine, die ausschließlich in DLBCL-abgeleiteten sEVs vorkamen, standen in erster Linie im Zusammenhang mit RNA-Prozessierung, während Proteine spezifisch für FL-abgeleitete sEVs neben anderen Signalwegen eher mit dem Metabolismus in Verbindung stehen. Interessanterweise waren in sEVs von jedem Ursprung insbesondere Hitzeschockproteine (HSP) angereichert, einer Familie von Proteinen, welche als endogene TLR-Liganden bekannt sind.

Schließlich wurde ein Knockout der yRNA4 mit Hilfe eines CRISPR/Cas9 Ansatzes in der Zelllinie HG-3 induziert, welche als Modell für CLL dient. Dieser Knock-out wurde durch klassische und quantitative Echtzeit-Polymerasekettenreaktion (PCR) sowei einen Northern-Blot validiert. Der yRNA4-Knockout beeinträchtigte weder die Fähigkeit der Zellen, sEVs zu sezernieren, noch deren Morphologie, wie mittels Transmissionselektronenmikroskopie untersucht wurde. Jedoch zeigten sEVs, die von der yRNA4-defizienten Zelllinie stammten, eine verminderte Fähigkeit zur Induktion des inflammatorischen Phänotyps in Monozyten. Auf Grund dieser Ergebnisse kommt die neue Hypothese auf, dass die reduzierte Induktion durch yRNA4-KO sEVs nicht nur auf das alleinige Fehlen der yRNA4 zurückgeführt werden kann, sondern die Deletion von yRNA4 auch die in sEVs geladene Proteinfracht beeinflusst.

Zusammenfassend ermöglichte diese Doktorarbeit eine tiefergehende Analyse der Mechanismen, die dem Einfluss von sEVs auf den Phänotyp myeloider Zellen zu Grunde liegen. Es wurde gezeigt, dass dieser Mechanismus durch TLR2, TLR4 und TLR7 vermittelt wird. Bioaktive Liganden schließen sowohl einsträngige RNAs wie yRNA4 ein, als auch Proteine, insbesondere HSPs.

3. Related publications, Posters, and Talks

The following publications and posters are related to the projects presented in this dissertation.

Publications

1. **Bordas M**, Genard G, Ohl S, Nessling M, Richter K, Roider T, Dietrich S, Maaß KK, Seiffert M. Optimized Protocol for Isolation of Small Extracellular Vesicles from Human and Murine Lymphoid Tissues. *International Journal of Molecular Sciences*. 2020 Aug 4;21(15):5586. doi: 10.3390/ijms21155586. PMID: 32759826; PMCID: PMC7432511.
2. Roider T, Seufert J, Uvarovskii A, Frauhammer F, **Bordas M**, Abedpour N, Stolarczyk M, Mallm JP, Herbst SA, Bruch PM, Balke-Want H, Hundemer M, Rippe K, Goeppert B, Seiffert M, Brors B, Mechtersheimer G, Zenz T, Peifer M, Chapuy B, Schlesner M, Müller-Tidow C, Fröhling S, Huber W, Anders S, Dietrich S. Dissecting intratumour heterogeneity of nodal B-cell lymphomas at the transcriptional, genetic and drug-response levels. *Nature Cell Biology*. 2020 Jul;22(7):896-906. doi: 10.1038/s41556-020-0532-x. Epub 2020 Jun 15. PMID: 32541878.
3. Roessner PM, Llaó Cid L, Lupar E, Roider T, **Bordas M**, Schifflers C, Arseni L, Gaupel AC, Kilpert F, Krötschel M, Arnold SJ, Sellner L, Colomer D, Stilgenbauer S, Dietrich S, Lichter P, Izcue A, Seiffert M. EOMES and IL-10 regulate antitumor activity of T regulatory type 1 CD4+ T cells in chronic lymphocytic leukemia. *Leukemia*. 2021 Aug;35(8):2311-2324. doi: 10.1038/s41375-021-01136-1. Epub 2021 Feb 1. PMID: 33526861; PMCID: PMC8324479.
4. Llaó-Cid L, Roessner PM, Chapaprieta V, Öztürk S, Roider T, **Bordas M**, Izcue A, Colomer D, Dietrich S, Stilgenbauer S, Hanna B, Martín-Subero JI, Seiffert M. EOMES is essential for antitumor activity of CD8+ T cells in chronic lymphocytic leukemia. *Leukemia*. 2021 Nov;35(11):3152-3162. doi: 10.1038/s41375-021-01198-1. Epub 2021 Mar 17. PMID: 33731848; PMCID: PMC8550953.
5. Roider T, Brinkmann BJ, Kim V, Knoll M, Kolb C, Roessner PM, **Bordas M**, Dreger P, Müller-Tidow C, Huber W, Seiffert M, Dietrich S. Autologous culture model of nodal B-cell lymphoma identifies ex vivo determinants of response to bispecific antibodies. *Blood Advances*, 2021 Sep 29:bloodadvances.2021005400. doi: 10.1182/bloodadvances.2021005400. Epub ahead of print. PMID: 34587238.

Posters

- German Society of Extracellular Vesicles, Marbuch, Germany, October 2018. Tumor-derived exosomes modulate the microenvironment in Diffuse Large B-Cell Lymphoma. **Bordas M**, Schulz R, Haderk F, Lichter P, Seiffert M.
- FSP-B retreat, Germany, February 2020. Impact of lymphoma cell-derived extracellular vesicles and yRNA on myeloid cells and tumor growth. **Bordas M**, Ohl S, Zapatka M, Tuorto F, Nessling M, Haderk F, Lichter P, Seiffert M.
- DKFZ PhD Poster Presentation, Heidelberg, Germany, November 2020: Tumor-derived exosomes modulate myeloid cells andinduce a tumor-supportive microenvironment in Non-Hodgkin Lymphoma. **Bordas M**, Ohl S, Genard G, Maass K, Haderk F, Dietrich S, Seiffert M.
  Best Poster Prize
- ImmunoRad conference, Paris, France, September 2021: Carbon-ion therapy for immune activation in solid cancer: focus on small extracellular vesicles. Genard G, **Bordas M**, Moustafa M, Maass K, Seco J.
- German Society of Extracellular Vesicles, Freiburg, Germany, October 2021. Deciphering the cargo of Non-Hodgkin Lymphoma-derived small Extracellular Vesicles and their role in modulating the phenotype of myeloid cells. **Bordas M**, Genard G, Ohl S, Kasim M, Maass K, Müller T, Kriegsvelt J, Roider T, Dietrich S, Seiffert M.

Talks

- International TRAIN-EV conference, online, June 2021. Deciphering the cargo of Non-Hodgkin Lymphoma-derived small Extracellular Vesicles and their role in remodulating the phenotype of myeloid cells. **Bordas M**, Genard G, Maass K, Müller T, Kriegsvelt J, Roider T, Dietrich S, Seiffert M.
  Best Talk Prize

4. Table of contents

5. INTRODUCTION

5.1. CHAPTER I: B-cell Non-Hodgkin Lymphomas

5.1.1. Normal B-cell biology

5.1.1.1. Development and maturation of B-cells

Initially, B-cells arise from lymphoid progenitor cells (LPC) in the bone marrow (BM) of adults or in the fetal liver during the prenatal life. The LPC becomes a pro-B-cell by going through the rearrangement of the segments D_H and J_H coding for the heavy chain of the B-cell surface immunoglobulin. This rearrangement will be performed with the help of RAG1, and RAG2 proteins [1,2]. The RAG proteins can bind to recombination signal sequences (RSS) on the DNA, and are able to induce double-strand breaks [3,4]. At that pro-B-cell stage, the heavy chains are combined to surrogate light chains. Then, the newly DJ_H segment will be rearranged with the V_H-segment. At that stage, newly formed pre-B-cells are positively selected: only cells with a B-cell receptor (BCR) able to bind to an antigen receive pro-survival signals. In addition, V_L and J_L segments coding for the light chains will be rearranged [5,6]. The light chains do not have a D segment. Resulting immature B-cells will be negatively selected: if there is self-reactivity, the cell will be eliminated. In addition, immature B-cells will express not only surface IgM, but also IgD, and then become mature Naïve B-cells. Those cells are then ready to reach the secondary lymphoid organs (SLO), mainly the spleen [7–9]. Firstly, naïve B-cells (IgM+ IgD+) will cross the dark zone and go through somatic hypermutation (SMH) of receptor editing to increase their affinity to the antigen, thanks to the AID enzyme. Secondly, in the light zone, naïve B-cells go through class switch recombination, differentiate into memory B cells or plasmablasts, and circulate to other sentinel organs as lymph nodes. A schematic of B-cell differentiation and maturation is represented in Figure 1.

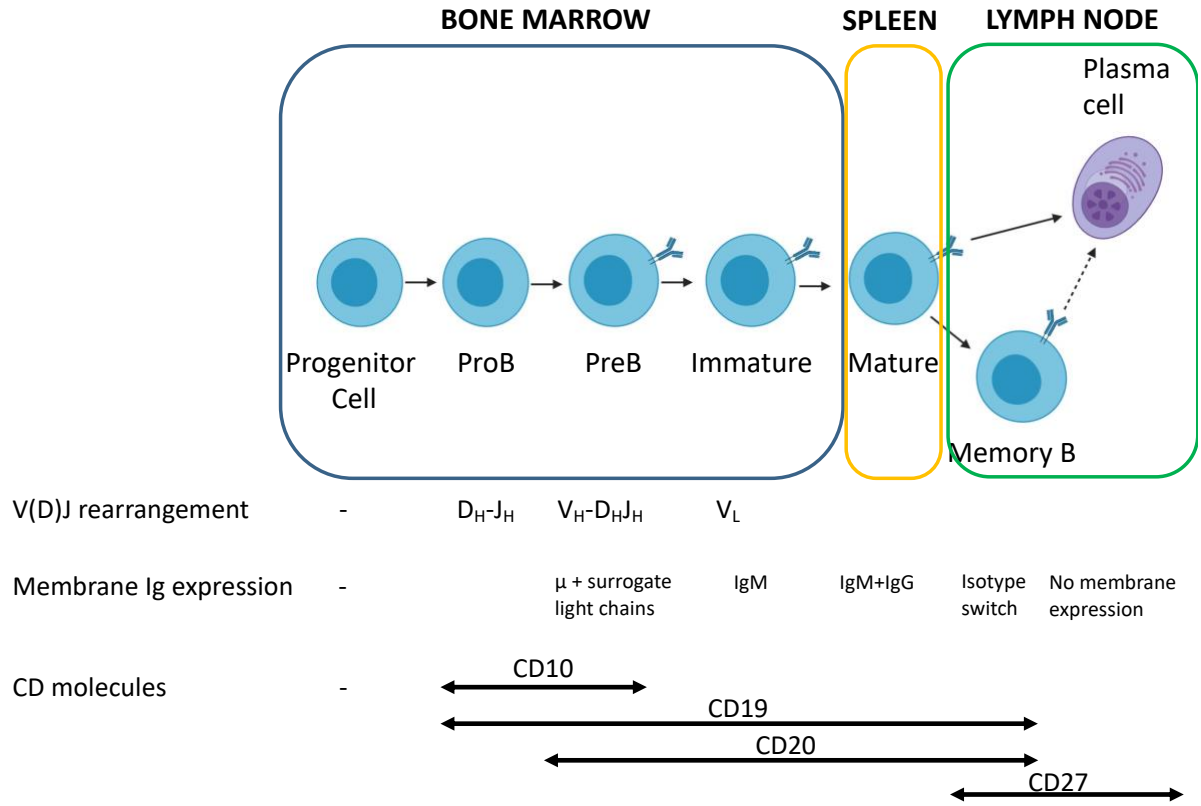

Figure 1: Schematic of the different B-cell development stages and associated changes of the BCR chain rearrangements, as well as immunoglobulin and CD surface markers. *Adapted from Immunology A Short Course, 7th Edition (Coico R. and Sunshine G. Wiley-Blackwell, 2015).*

5.1.1.2. B-cell role during adaptive immunity and the role of BCR

The BCR is a protein complex formed of an immunoglobulin expressed at the surface of the cell, as well as the two proteins CD79a and CD79b responsible for signal transduction [10,11].During a pathological condition, naïve mature B-cells can recognize circulating antigens or epitopes at the surface of pathogens through their BCR. Briefly, following binding to the BCR, the antigen is processed into peptides (proteolysis), and MHC-II proteins presents the peptides at the surface of B-cells [12,13]. CD4 helper T cells recognize the complex antigen-MHC-II and can activate B-cells in return. Following activation, B-cells proliferate, and resulting cells differentiate into plasma cells for antibody production following Ig class switch or into memory B cells. Mutations of molecules involved in the BCR signaling pathway are commonly found in lymphoid malignancies. Among the most commonly affected genes are *MYD88, CD79B, REL, PTEN, TRAF3, NFKBIE, AND TNFAIP3* [11].

5.1.2. B-cell Non-Hodgkin Lymphomas

5.1.2.1. Epidemiology of Non-Hodgkin Lymphomas

Contrary to B-cell Non-Hodgkin Lymphoma (NHL), Hodgkin Lymphoma (HL) is characterized by a few malignant cells, called Reed-Sternberg cells [14]. Because the ratio of malignant cells over microenvironmental cells is drastically different between HL and NHL, and because their gene signatures are so divergent, these two entities must be separately studied when looking at the microenvironment.

For this project, we decided to focus on B-cell NHL, in particular three entities that share similarities in terms of tumor genetics and behavior: Diffuse Large B-cell Lymphoma (DLBCL), Follicular Lymphoma (FL), and Chronic Lymphocytic Leukemia (CLL). Altogether, these 3 NHL subtypes represented 75% to 90% of all NHL cases in the USA between 2009 and 2011 [15–17]. Related statistics are presented in Table 1.

	DLBCL	CLL	FL
Proportion out of all NHL	30-40%	10-20%	5-15%
Median age at diagnosis	66	70	63
5-year relative survival at diagnosis	66,57%	90,92%	87,92%

Table 1: Comparison of statistics related to DLBCL, CLL and FL. Indicated statistics were recovered from SEER cancer statistics 2007-2013 [18,19].

5.1.2.2. Histology of B-cell NHL

Histologic analysis of hematoxylin and eosin-stained LN tissue sections remains a world-used approach for diagnosing of B-cell NHL. B-cell NHLs are characterized by the proliferation of B-cells in the lymph nodes and differ by the cancer cell morphology, genetic mutations, the maturation stage of the cancer cells, the clinical behavior, and the lymph node zone they arise from [20,21]. In DLBCL, the classical architecture of the LN is effaced due to the diffusion of tumor B-cells (Figure 2)[22]. On the contrary, in FL, the tumor cells form nodules similar to follicles. Furthermore, the tumor cells in FL are a mixture of small and large lymphoid cells. In CLL, the classical architecture of the LN is disappearing, and the LN shows a classical diffusion of small lymphocytes. The classification of subtypes depends on additional tests, including the search for specific markers by flow cytometry or immunohistochemistry, fluorescence in situ hybridization, or genetic screening.

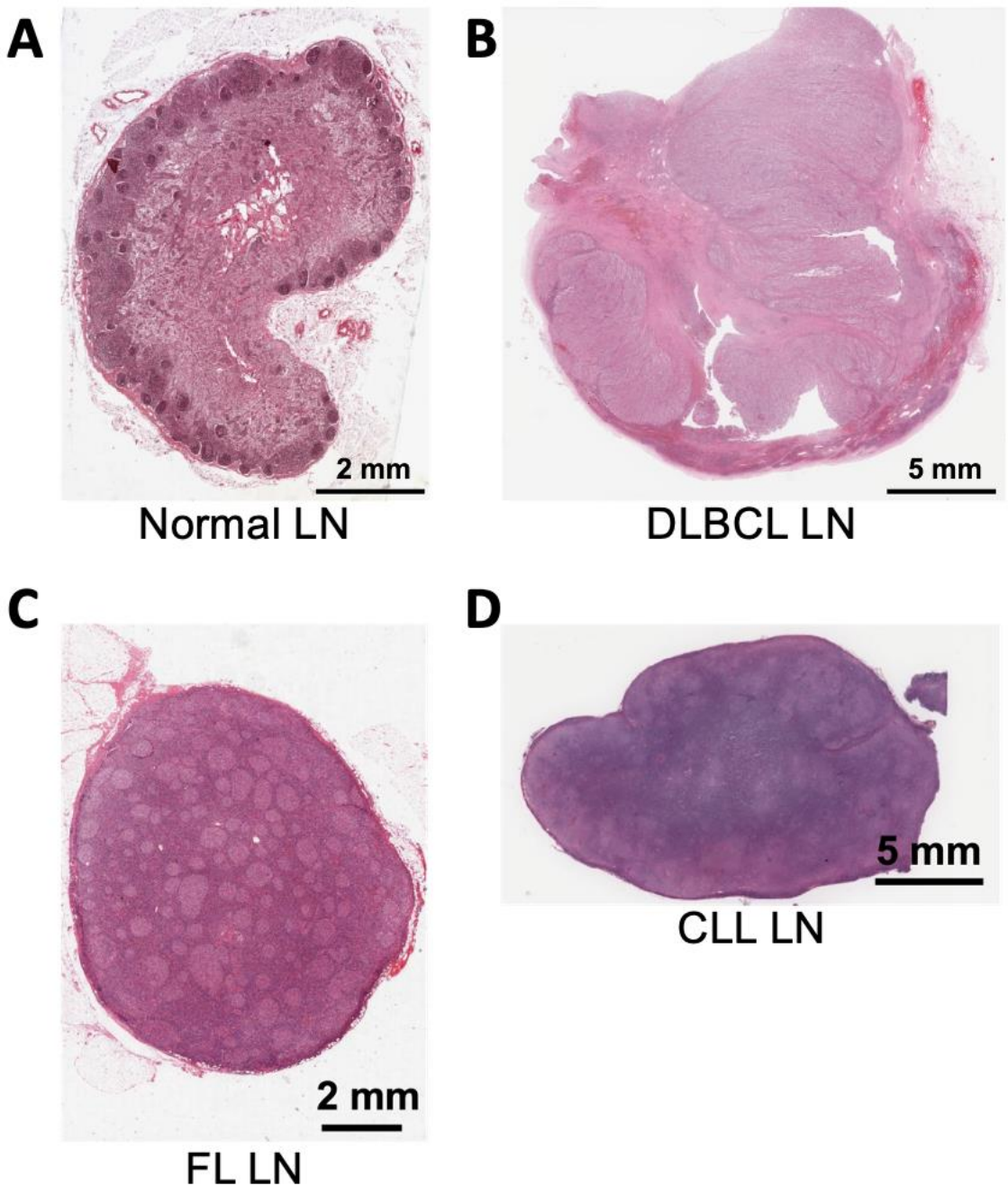

Figure 2: Hematoxylin and Eosin staining of lymph nodes with indicated pathological conditions. A) Normal LN. B) LN from 70 years old female showing a classical disappearance of the LN structure. The LN is enriched in very large cells (*not shown*). The patient was diagnosed for DLBCL. C) LN from 77 years old male with nodules-like structures. The patient was diagnosed for FL. D) LN from 75 years old female. Additional staining lead to diagnose the patient for CLL (*not shown*). Images were taken with permission from https://www.virtualpathology.leeds.ac.uk/.

5.1.2.3. Diffuse Large B-cell Lymphoma

DLBCL is a very heterogeneous group of diseases, with multiple classifications available. The tumor cells are generally large to medium-sized, with a high Ki-67 labeling index. The distinction between the most common germinal-center B-cell like (GCB) and activated B-cell-like (ABC) can be made due to the tumor cell of origin; however other subtypes have been described by the World Health Organization [23–28].

GCB-DLBCL

GCB-DLBCL derives from B-cells in the germinal center (GC) of secondary lymphoid organs. The most common genetic alteration in GCB-DLBCL is a translocation of chromosomes 14 and 18, leading to the translocation of anti-apoptotic gene *BCL-2* into the *IG* gene, leading to BCL-2 overexpression [29–31]. We also find translocation of the *IG* promoter and the *C-MYC* proto-oncogene in most patients [23,32], as well as other point mutations and amplification [33]. Translocations involving *BCL-6* are found in a majority of patients where the resulting upregulation of *BCL-6* represses cell cycle checkpoint-related genes [8,34]. Upregulation of mir-17-92 micro RNA cluster was also reported and drives suppression of the *PTEN* tumor suppressor and anti-apoptotic BIM protein [35]. Of note, *PTEN* deletions are a common mutation found in GCB-DLBCL patients [24]. Amplifications of the REL protein, a transcription factor necessary for B-cell proliferation were also reported as commonly found aberrations in GCB-DLBCL patients [24,36]. *REL* amplification in B-cells is responsible for the B-cell proliferation in the GC [37]. Gain-of-function mutations of *EZH2* are relatively common in GCB-DLBCL [25,27,28,38,39].

ABC-DLBCL

ABC-DLBCL derives from plasmablasts in the light zone of the GC. Some mutations are common to GCB- and ABC-DLBCL, such as *BCL6* translocations and *NOTCH* mutations [27]. Translocations are quite common in ABC-DLBCL patients, with 3q27 and 18q21 leading to the respective amplification of *BCL6* and *BCL2* [40,41]. The most recurrent mutations lead to constitutive activation of the NFkB pathway, including gain-of-function of the BCR coactivator *CD79*[42,43] or *MYD88* [28,44,45], and lost-of function of *TNFAIP3* [46,47]. *BLIMP1* deletion can also lead to a blockade of B-cell differentiation [48,49]. Tumor suppressor *TP53* mutations are also linked preferentially to ABC-DLBCL [23]. Genetic alterations of the proto-oncogene *MYC* can also be found in ABC-DLBCL with a lower prevalence than in GCB-DLBCL [33].

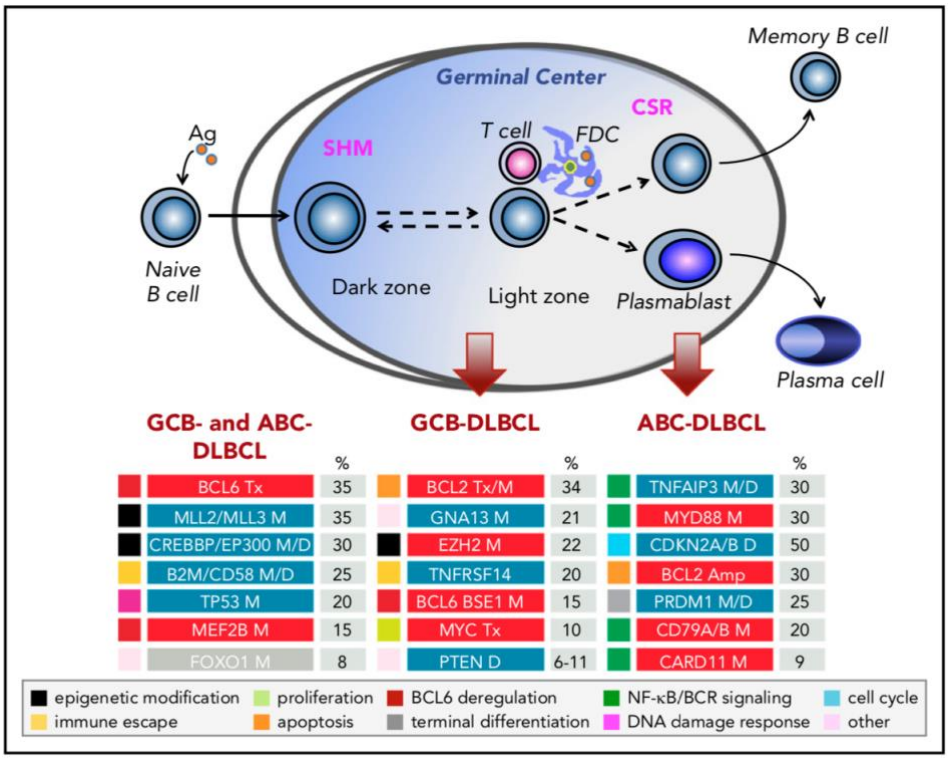

Figure 3: Schematic of the cellular origin and main genetic alterations associated with the most common DLBCL subtypes. The legend of the color code can be found at the bottom of the figure. Amp, amplification; Tx, chromosomal translocations; M, mutations; D, deletions. Reuse with permission from "Genetics of Diffuse-Large B-cell Lymphoma", by Pasqualucci L. and Dalla-Favera R., 2018, Blood Review Series.

The new classification of DLBCL

Two distinct analyses of the exome of respectively 574 and 304 DLBCL biopsy samples have led to the establishment of a new classification system for DLBCL, not based on the Cell-Of-Origin (the classical GCB/ABC/other distinction) but the genetic profile of the tumor.

In the first study, four subtypes of DLBCL were suggested: the MCD subtype with an overrepresentation of tumor harboring the *MYD88*^{L265P} and *CD79b* mutations, the BN2 subtype with an overrepresentation of *BCL6* fusions and *NOTCH2* mutations, the N1 subtype with an overrepresentation of mutations affecting the NOTCH pathway, and finally the EZB subtype with an overrepresentation of *EZH2* mutations and *BCL-2* translocations [27].

In the second study, five subtypes of DLBCL were suggested, called C1 to C5 [50]. C1 englobes patients with alterations of *BCL-6* and *NOTCH* similar to the BN2 subtype. C2 is enriched in *TP53*-inactivating mutational events. In C3, *BCL-2* and *EZH2* alterations are

overrepresented, similar to the EZB subtype. In C4, tumors with alterations in genes involved in the BCR pathways, among others, are enclosed. Finally, the C5 subtype seems to correspond to the MCD subtype with concomitant *MYD88^{L265P}* and *CD79b* mutations and *BCL-2* gain of function mutations [51].

Altogether the data indicate that the BN2/C1 and EZB/C3 subtypes are more responding to immunochemotherapy. The classification of DLBCL subtypes by genetic lesions may facilitate the medical care given to patients by providing better guidelines for the choice of targeted therapies [52].

Box 1: Extensive exome and transcriptome analysis of DLBCL LN biopsies have led to the development of a new classification of DLBCL subtypes, including recurrent genetic mutations and specific transcriptomic signatures.

5.1.2.4. Follicular Lymphoma

The genetic alterations in FL closely resemble those in DLBCL, including t(14;18)(q32;q21) *IGH/BCL-2* translocation, *BCL-2* mutations, *CREBBP, KMT2D*, or *EZH2* mutations [38,53]. BCR pathway-related genes are recurrently mutated in FL samples, with mutations in *CD79* genes, *CXCR4* and *BTK,* among others [54]. Additionally, histone-related genes are recurrently co-mutated in FL tumor cells. [54]. Histological transformation of FL into DLBCL can occur in 10-20% of patients and results from the clonal expansion of tumor cells carrying an accumulation of genetic anomalies with frequently found rearrangements of the *C-MYC* and *BCL-2* genes [55,56].

5.1.2.5. Chronic Lymphocytic Leukemia (CLL)

CLL frequently develops as an indolent disease characterized by the typical expansion of CD5-positive B cells in the peripheral blood and secondary lymphoid organs. The most important subgroups of CLL are based on the mutational status of the *IGVH* gene (Immunoglobulin heavy chain variable region). The cell-of-origin of mutated-*IGVH* CLL is a memory B-cell that has already passed the immunoglobulin rearrangement. In contrast, *IGVH*-unmutated CLL derives from the clonal expansion of a B-cell at a more immature stage and is associated with a worse prognosis [57,58].

Chromosomal alterations are a common cause of CLL, with four recurrent events found in patients: 13q14, 11q22-23, and 17p deletions, as well as trisomy 12[59]. The 13q14 region contains the microRNAs miR-15 and -16; their loss results in the clonal proliferation of CD5+ B-cells, likely through an increase of *BCL-2* levels [60–62]. The 11q22-23 region includes the tumor suppressor gene *ATM* required for the non-homologous end-joining repair during V and J segments rearrangement [63,64]. Animal knockout experiments of *ATM* located in the 11q locus promote the development of NHL-like disease [65,66]. *CUL5* is another suppressor gene in the 11q22-23 region, although its involvement in CLL biogenesis remains uninvestigated [67,68]. The

17p12 deletion affects the expression of *TP53* [69–71]. CLL biogenesis in trisomy 12 patients remains poorly investigated; however, trisomy 12 seems to be associated with a higher mutational rate in *NOTCH* and expression deregulation of the genes related to BCR co-activators [72,73]. Other point mutations have been suggested as CLL drivers, including the genes *TP53, NOTCH, SF3B1, MYD88, ATM,* and *BIRC3* [74–78].

5.1.3. Standard treatment approaches for B-cell NHL

Multiple classifications have been developed to guide physicians for the treatment of B-cell NHL patients. Those classifications take into consideration the age, mutational status, histology of the tumor, proliferation rate, and dissemination in lymph nodes, lymphocytosis in peripheral blood, tumor surface markers, etc., and require lymph node or blood biopsies.

5.1.3.1. DLBCL

The primary treatment for DLBCL remains the R-CHOP combination. R-CHOP includes Cyclophosphamide, Doxorubicin Hydrochloride, Vincristine, and Prednisone, in combination with Rituximab, an anti-CD20 antibody [79,80]. Using this combination therapy, 50% to 60% of patients are cured[81]. However, 20 to 30% of patients show relapses, and 15 to 25% do not respond to the R-CHOP standard care. This is particularly the case for double-hit lymphoma patients carrying rearrangement of both *MYC* and *BCL2*. In such cases, salvage treatments with other combinations of chemotherapeutic molecules associated with Rituximab can be proposed in combination with autologous hematopoietic stem cell (HSC) transplantation in some cases [81,82].

Furthermore, CD19-targeting CAR T-cell therapies have brought significant changes in the care of relapsed DLBCL patients and now represent a third-line therapy option. Three Phase 2 clinical trials have shown that CAR T cells lead to increased overall survival compared to patients receiving conventional therapy [83–86]. Although initially suggested for patients non-eligible for autologous HSC transplantation, recent studies indicate the superiority of CAR T cell therapy over autologous HSC transplantation [84,87].

5.1.3.2. FL

Asymptomatic patients usually do not receive treatment as preventive treatment did not show any survival advantage [88–90]. In the first stages, localized radiation treatment is an option for patients [91,92]. In the case of symptomatic and advanced or relapsed staged FL, patients are treated with anti-CD20 antibody therapy (Obinutuzumab, Rituximab, etc.). Anti-CD20 antibody-based therapy can be combined with chemotherapeutics such as alkylating agents or, in some cases, the CHOP-regimen [93]. Allogeneic, as well as autologous HSC transplantation, remain an option for relapsed FL [94]

5.1.3.3. CLL

The management of early-stage CLL patients usually relies on a wait-and-watch approach[95]. However, several therapeutic options exist following the progression of the disease. The FCR combination combined the purine analog Fludarabine, the alkylating agent Cyclophosphamide and the anti-CD20 antibody Rituximab and remains a standard of care. Later, inhibitors of the BCR-related kinases have shown remarkable outcomes in patients. Bruton's tyrosine kinase (BTK) inhibitors, including Ibrutinib are the most common drugs[96–98]. Ibrutinib is now regularly used as first-line therapy and shows a better control of the disease over time compared to other therapeutics [99,100]. The combination of Ibrutinib with the anti-CD20 antibody Rituximab did not show superiority to Ibrutinib only [101]. More recently, the combination of the anti-CD20 antibody Obinutuzumab with the BCL2 inhibitor Venetoclax was approved as a first-line therapy to treat CLL patients, with 49.5% of patients showing a complete response [95,102]. The choice of the therapy must take into consideration the genetic characteristic of the tumor, in particular the *IGHV* mutational status as well as deficiency of *TP53*. In the latter patient group, using BTK inhibitors remains the first-line treatment [103]. Lately, clinical studies have investigated the efficacy of the combined treatment Venetoclax + Ibrutinib, with high promises for TP53-deficient CLL patients.

5.2. B-cell NHL and communication with the microenvironment

5.2.1. The microenvironment as a main player of disease progression

Like most cancers, the development of B-cell NHL highly depends on the modulation of their microenvironment and the crosstalk between different cell types. This conclusion comes from the fact that primary cells cannot survive *in vitro* and go through spontaneous apoptosis. *In vivo*, studies have shown that the microenvironment promotes cell survival and chemoresistance. Therefore, for a few decades, scientific research aimed at investigating the changes in the microenvironment and attempted to find a way to eradicate tumor cells by targeting the microenvironment[104]. The localization of B-cell NHL can be numerous, mainly the lymph nodes and blood, but dissemination to the bone marrow, spleen, or other mucosa-associated lymphoid tissues (MALT) is frequently described. The cell types and their abundance in the tumor microenvironment depend on the tissue. Therefore, the path to fully understand the role of the microenvironment in cancer progression as well as the numerous mechanisms employed by tumor cells to modulate it remains long and requires extensive studies. Both *in vitro* and *in vivo* studies are necessary to answer such questions.

5.2.1.1. Stromal cells

This paragraph can be found in the Supplementary box 1.

5.2.1.2. Endothelial cells

This paragraph can be found in the Supplementary box 2.

5.2.2. Myeloid cells

5.2.2.1. Dendritic Cells

Dendritic cells are a heterogeneous population of Antigen-Presenting Cells (APCs) able to recognize pathogen-associated molecular patterns (PAMPs) through Pattern Recognition Receptors (PRRs) such as Toll-Like Receptors (TLRs). Following phagocytosis of pathogens, foreign proteins are processed into antigenic peptides and presented on surface MHC-II molecules. Upon their activation, DCs migrate to secondary lymphoid organs. The recognition of peptide/MHC-II complexes on their surface by helper T cells results in their polarization into either Th1, Th2 or regulatory T lymphocytes [105,106]. However, DCs can also cross-present tumor cell-derived antigens on MHC Class I molecules, leading to CD8 T cell activation [107–110]. Little is known about the role of DCs in the progression of B-cell NHL. It has been previously reported that the number of DCs is generally decreased in the LNs of NHL patients compared to reactive LNs [111,112], and that enrichment of intratumoral DCs was associated with better overall survival in DLBCL patients [113]. However, as NHL cells highly express the “don’t eat me” transmembrane protein CD47, it is likely that the phagocytic activity of DCs is inhibited in the tumor microenvironment through CD47 engagement with SIRPα, as similarly observed for other myeloid cell populations [114–116]. Another study suggested that the adhesion of FL cells to DCs may protect them from drug-induced apoptosis [117]. Additionally, DCs can upregulate PD-L1 expression on their surface, limiting the activation of T lymphocytes [118,119].

5.2.2.2. Circulating monocytes

Monocytes and monocyte-derived cells are a major player in the B-cell NHL tumor microenvironment and seem essential for tumor cell survival and proliferation. Firstly, monocytes have been shown to partially prevent the spontaneous apoptosis of B-cell NHL cells *in vitro* [120]. Secondly, depletion of monocytes or macrophages *in vivo* delays tumor growth in different B-cell NHL murine models [121–123]. An increased interest in the biology of monocytes in the context of B-cell NHL was raised as it was realized that patients present higher Absolute Monocyte Counts (AMC) in the blood and that the AMC of patients was inversely correlated with the disease outcome [124,125,126]. It has been proposed that B-cell NHL cells in the BM and SLOs directly attract monocytes through the secretion of multiple cytokines, typically CCL2, CCL3, CCL4, and CXCL5 [127]. Several studies analyzed monocyte subsets in the context of B-cell NHL. Our lab has previously revealed that CLL is linked to an accumulation of patrolling monocytes, defined as Ly6C^{low}CD43^{high} myeloid cells, in the spleen of Eμ-TCL1 adoptive transferred animals. Identical observations were made in the blood of an Eμ-Myc murine model [123]. The human counterpart of patrolling monocytes, the non-classical monocytes, were also

increased in the peripheral blood of CLL patients [125,128]. Such non-classical monocytes could give rise to Nurse-Like Cells in CLL (Box 2) or monocytic myeloid-derived suppressor cells (MoMDSCs). These myeloid cells harbor a pro-tumoral phenotype, characterized by increased secretion of pro-inflammatory cytokines and upregulation of immunosuppressive surface markers, including PD-L1, PD-L2, Arg1, IDO, and CD163 [123,129,130]. This phenotype is associated with T lymphocytes suppression and IL-10-dependant expansion of regulatory T lymphocytes [123,125]. MoMDSC-mediated suppression of T cells requires direct contact which leads to the downregulation of CD62L on the surface of both $CD4^+$ and $CD8^+$ T lymphocytes and limits their rolling and migratory capacities [131].

Nurse-Like cells (NLCs) in CLL

In the presence of CLL cells, myeloid cells can differentiate into NLCs, particularly in the lymphoid tissues [132,133]. NLCs are characterized by high expression of surface CD68 and CD163, with CD163 expression level associated with increased CLL cell proliferation and poor prognosis [134]. Gene expression profiling of NLCs revealed that NLCs resemble tumor-associated M2-like macrophages, although some expressed genes are generally typical for M1-like macrophages [135,136]. NLCs can send pro-survival signals to CLL cells and are active mediators of drug resistance [134,137,138]. NLCs secrete both APRIL and BAFF, promoting CLL cell survival [139]. Blockade of BAFF-Receptor in CLL cells improves ibrutinib-induced apoptosis of CLL cells [140]. Interestingly, *in vitro* reprogramming of NLCs into M1-type macrophages using IFN-γ seems to enhance their phagocytosis potential and synergize with anti-CD20 rituximab treatment for CLL cell elimination [141]. NLCs also express surface CD31, a ligand of CD38 which is present on CLL cells and whose activation leads to cell survival and proliferation through downstream upregulation of *BCL-2* and *BCL-XL* upregulation [142,143].

Box 2: Characteristics of Nurse-Like Cells and their influence on the tumor microenvironement in the context of CLL

5.2.2.3. Macrophages and Tumor-Associated Macrophages (TAMs)

Macrophages are terminally differentiated myeloid cells able to perform phagocytosis of pathogens, present antigens and neo-antigens to lymphocytes, and secrete cytokines to modulate the immune response. Although the classification of macrophages remains controversial, it is generally admitted that they can harbour different states of polarization, whose extremes are classically presented as M1 and M2 polarization states. Briefly, M1-macrophages produce pro-inflammatory cytokines and are considered an anti-tumoral immune cell subset, whereas M2-macrophages tend to have anti-inflammatory and anti-tumoral properties [144,145]. Tumor cells can recruit and induce a stronger M2-polarization of macrophages through the secretion of cytokines. It is thought that the polarization towards an M2 phenotype is caused by inhibition of the *NOTCH* signalling pathway [146–148]. In addition to CD68 expressed by all macrophages, Tumor-Associated Macrophages (TAMs) are M2-like

macrophages specifically expressing the CD163 surface marker. Many studies have shown a correlation between CD68+ or CD163+ macrophages with poor disease outcomes (Table 2). The same conclusions were drawn for CLL-associated TAMs, called NLCs. Depletion of macrophages in murine models can decrease tumor progression in B-cell NHL xenograft models [149].

Publication	Entity	Conclusion
[149]	DLBCL	High number of CD163+ macrophages is correlated with poor disease outcome.
[150]	FL (treated patients)	Number of CD68+ macrophages is correlated with poor disease outcome. *
[151]	FL (treated patients)	High number of CD68+ macrophages is correlated with poor disease outcome *
[152]	DLBCL	High number of CD163+ macrophages is correlated with poor disease outcome.
Blood (2015) 126 (23): 5023.	DLBCL (treated patients)	High number of CD163+ macrophages is correlated with poor disease outcome.
[153]	FL (treated patients)	High number of CD68+ macrophages is correlated with poor disease outcome

Table 2: Summary table of publications showing in DLBCL and in FL a correlation between the number of CD163+ tumor-associated macrophages (TAMs) and a poor disease outcome. *The opposite correlation is seen in Rituximab-treated patients. Indeed, it has been reported that the use of anti-CD20 antibodies like Rituximab induce opsonisation of tumor cells and a better phagocytosis by TAM [154].

TAMs use multiple mechanisms to promote tumor progression, including.

- ⇒ Inhibition of cytotoxic T cell function by upregulation of the surface ligand PD-L1[155,156]
- ⇒ Increased angiogenesis through secretion of VEGF and Legumain[149,157,158]
- ⇒ Modulation of the extracellular matrix by secretion of metalloproteinases[159]
- ⇒ Increase of anti-inflammatory cytokines: IL-10, CCL17, TGF-β[160–162]. These cytokines promote the recruitment of regulatory T cells and inhibit the function of effector T cells.
- ⇒ Inhibited phagocytic activity by expression of SIRPα [114,163]
- ⇒ Increased expression of IDO1 and IL4I1, leading to modulation of aromatic amino acid metabolism. The resulting metabolites can inhibit effector T cells, promote the recruitment/maintenance of regulatory T cells, as well as neovascularization [164–167]

Although it has not been shown explicitly for B-cell NHL-related TAMs, it is likely that, as in other cancer types, B-cell NHL TAMs can directly promote tumor cell survival by modulation of the *NF-kB, M-TOR,* or *STAT3/STAT5* signaling pathways in tumor cells [168–170]. This mechanism could rely on the transmembrane presentation of IL-15 or BAFF/APRIL secretion by TAMs, which induce healthy and tumor B-cell proliferation [171]. TAMs can also secrete high levels of Arginase1, leading to increased metabolism of L-arginine and secretion of metabolites

promoting tumor cell proliferation [172]. Additionally, high tumor infiltration by TAMs is associated with a faster transformation of FL cells [173]

5.2.2.4. Targeting myeloid cells in B-cell NHL

Due to the heterogeneity of myeloid cell subsets in the B-cell NHL microenvironment and the numerous mechanisms they use to modulate the immune system, they represent an attractive target for the treatment of B-cell NHL, as well as other cancers[130,174]. Targeting tumor-associated myeloid cells could enhance the efficacy of immunotherapies[175,176] and different approaches tested to induce such an effect are summarized in Table 3.

Mechanism of action	Reference of the study	Conclusions of the study
Inhibition of arginase	Pilanc et al., Frontiers in Oncology, 2021	Efficient inhibition of arginase in glioma-associated macrophages reduced secretion of immunosuppressive cytokines, ameliorated cytotoxic activity of NK function, increased T cell infiltration and ameliorated response to anti-PD1 therapy in a murine model of glioma.
	Sosnowska et al. Oncoimmunology, 2021	Inhibition of arginase induced T cell proliferation and improved survival of lung cancer murine models.
Inhibition of CSF-1 *(responsible for myeloid cell differentiation)*	Holmgaard et al., Oncoimmunology, 2016	Blockade of CSF-1 by a blocking antibody decreased the number of moMDSC in a murine model of breast cancer, and enhanced efficacy of anti-CTLA4 and anti-PD-1 treatment
	Zhu et al., Cancer Research, 2014	Anti-CSF1antibody or CSFR1 inhibitors reduced the amount of moMDSCs and enhanced anti-CTLA4 and anti-PD1 efficacy by increasing the number of effector T cells.
	Valero et al., Leukemia, 2021	Blockade of CSF-1R reversed M2-polarization of macrophages, and enhanced rituximab efficacy in a xenograft model of FL.
Inhibition of IDO	Holmgaard et al., JEM, 2013	Combined treatment of melanoma murine models with inhibitor of IDO and anti-CTLA4 overcame anti-CTLA4 resistance detected in animals treated with anti-CTLA4 antibody alone. The better control

		of tumor progression correlated with an increase of intratumoral effector T cells
	Yu et al., J. Immunol., 2013	Inhibition of IDO enhanced CART cells-mediated control of tumor progression in murine models of Mantle Cell Lymphoma and Burkitt's Lymphoma
Inhibition of HDAC (inducer of M2-polarization)	Li et al., Oncogene, 2021	Inhibition of HDAC reduced tumor infiltration by MDSCs in breast cancer and melanoma murine models and was associated with reprogramming of TAMs into M1-like macrophages,. Animals treated with combined HDAC inhibitor and anti-PDL1 showed survival advantage over anti-PDL1-treated animals. *HDAC inhibition can also have a direct pro-apoptotic effect on B-cell NHL cells (Chen et al. Front Cell Dev Biol, 2020).
Inhibition of CCR2	Flores-Toro et al., PNAS, 2020	Inhibition of CCR2 reduced tumor infiltration by MDSCs, reduced T-cell exhaustion and improved response to Anti-PD-1 therapy in murine models of glioma.
	Mitchem et al., Cancer Research, 2013.	Inhibition of CCR2 synergized with chemotherapy to reduce tumor in pancreatic murine model and was linked to depletion of infiltrating TAMs and moMDSCs.
Anti-SIRPa, anti-CD47	Chao et al., Cell, 2010	Combined Anti-CD47/Rituximab therapy improved the phagocytic activity of macrophages compared to both treatments alone, and eradicated lymphoma in xenotransplant murine models of B-cell NHL.
	Lin et al., PloSOne, 2017	Blockade of CD47 promoted the phagocytosis of lymphoma cells by macrophages *in vitro*.
	Liu et al., JCI Insight, 2020	Blockade of SIRPa combined to rituximab enhanced the phagocytosis of macrophages in co-culture as well as CD47/SIRPa double humanized melanoma mouse model.

Activation of TLRs	Farias et al., Sci. Rep., 2021	TLR4 agonist synergized with anti-PD-L1 to control tumor progression in a murine model of melanoma
	Reilley et al., Journal for ImmunoTherapy of Cancer, 2019	TLR9 agonist synergized with anti-PD-L1 or anti-CTL4 to control tumor progression in a murine model of melanoma

Table 3: Summarizing table of reported assays aiming to target myeloid cells in different models of cancer, and conclusions of the mentioned studies.

5.2.3. T cells

This paragraph can be found in the Supplementary box 3.

5.3. CHAPTER II: RECENTLY DESCRIBED EXTRACELLULAR VESICLES (EVs) AS MEDIATORS OF THE MICROENVIRONMENTAL COMMUNICATION

5.3.1. History of EVs

The history of EV research starts in 1983 with several manuscripts simultaneously published [177–179]. Those studies showed that reticulocyte precursors migrate to the blood, where they differentiate into mature reticulocytes. However, reticulocyte precursors, which are enriched in Transferrin receptors, lose most of them during this maturation step. Using electron microscopy, researchers found that Transferrin receptors are externalized via small vesicles (Figure 4). The first EVs were thus thought to be “garbage” bags.

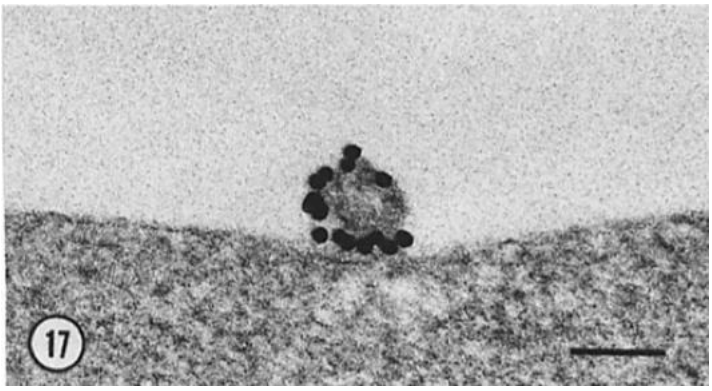

Figure 4: Transferrin Receptor was labeled with Gold-conjugated nanoparticles. Externalization of transferrin receptors out of reticulocytes was observed using electron microscopy. Scale bar = 100nm. *From Harding et al., Journal of Cell Biology, 1983*.

In the 1990s, the work from Raposo *et al*. showed the capacity of Antigen-Presenting Cells (APC) to secrete vesicles containing MHC-II-Antigen complexes [180,181]. Those vesicles were found to be co-released with inflammatory mediators. The following decade was enriched in publications deciphering the molecular mechanism for EV biogenesis and secretion, thus highlighting the existence of different EV subpopulations. In the 2000s, EV-related research reported the “universal” secretion of EVs by cells and their diverse functions, as well as optimization of isolation and validation technics [182].

Nowadays, the EV research community worldwide has been expanded and can be divided into three main branches:

- ⇒ Continuing to characterize EVs and their heterogeneity, the associated pathways related to their biogenesis, as well as the uptake mechanisms by recipient cells,
- ⇒ Functional studies of EV-mediated cell-to-cell communication in pathologies,
- ⇒ Therapeutic use of EVs as vaccines, tissue regeneration tools, or drug delivery systems.

5.3.2. Types of EVs

Virtually all cell types nanovesicles secrete EVs from prokaryotic to eukaryotic systems. They are composed of a lipidic bilayer similar to the cell membrane, and they can carry cargos of proteins, lipids, and nucleic acids [183]. Additionally, EVs can present surface proteins, which can be used as markers for specific EV populations [184,185]. EVs can be internalized by recipient cells, in which they deliver functional proteins and nucleic acids [186,187]. Little is known about their diffusion in complex organisms, but it is thought that EVs can be transported from one organ to another due to their small size and their secretion in body fluids. A recent study suggested the implication of an active mechanism for specific populations of EVs to escape the extracellular matrix [188].

Although the definition of EVs is continuously interrogated, we generally distinguish four subtypes of eukaryotic-derived EVs based on their size, composition, and origin. Table 4 provides a simplified overview of the main features for each of the four populations is provided.

Type of EV	Description
Microvesicles (MV)	Microvesicles are a heterogeneous population with vesicle size ranging from 50nm to 1µm. Contrary to small extracellular vesicles (sEVs), MVs are released through direct budding from the plasma membrane [189,190]. Due to their mode of secretion, we generally consider that the loading of MV is a passive mechanism. However, comparative profiles of the proteome and transcriptome of MV to cytoplasm content are lacking.
Apoptotic bodies (ApoBD)	ApoBD are released by apoptotic cells only for the rapid clearance of cell material and related antigens [191]. ApoBD are distinguished from other EV by their size (800-5000nm), and just like MV, they are formed through direct budding of the cell membrane, thus carrying similar markers. [56].
Small extracellular vesicles (sEVs)	sEVs are very small EVs (30-200nm) and originate from the endocytic pathway [192,193]. Due to their mechanism of release, described more in detail in the next paragraphs, sEVs' loading seems to be the result of both active and passive mechanisms [194,195]. sEVs carry specific markers that allow their distinction from other EV subtypes [196].
Exomeres	Exomeres were described for the first time in 2018 when EVs were isolated using a new separation technic, the asymmetric-flow field-flow fractionation (AF4)[197]. Exomeres size generally does not exceed 50nm [198]. Exomeres carry similar proteins, nucleic acids, and lipids than other EVs, but are enriched in metabolic-related elements [197]. Their secretion pathway is likely similar to the one of sEVs [198].

Table 4: Overview of EV subtypes and their characteristics in terms of size and biogenesis mechanism.

Of note, this dissertation is exclusively focusing on sEVs.

5.3.3. Small Extracellular Vesicles (exosomes)

5.3.3.1. Biogenesis

sEVs derive from the endocytic pathway. The endocytic pathway is a cellular mechanism by which external complexes are internalized by the invagination of the plasma membrane and form vesicles called endosomes [199,200]. Those endosomes present an inverted membrane orientation. They can fuse, become Late Endosomes, and take up material from the Golgi or Endoplasmic reticulum [201]. Late Endosome membrane can invaginate itself, forming vesicles called Intraluminal Vesicles or ILV inside the multivesicular bodies (MVB). MVB can fuse either with the lysosome for degradation or the plasma membrane, and secreted particles are the so-called sEVs, with the same membrane orientation as the cell [199–201]. A schematic of the mechanism is presented in Figure 5.

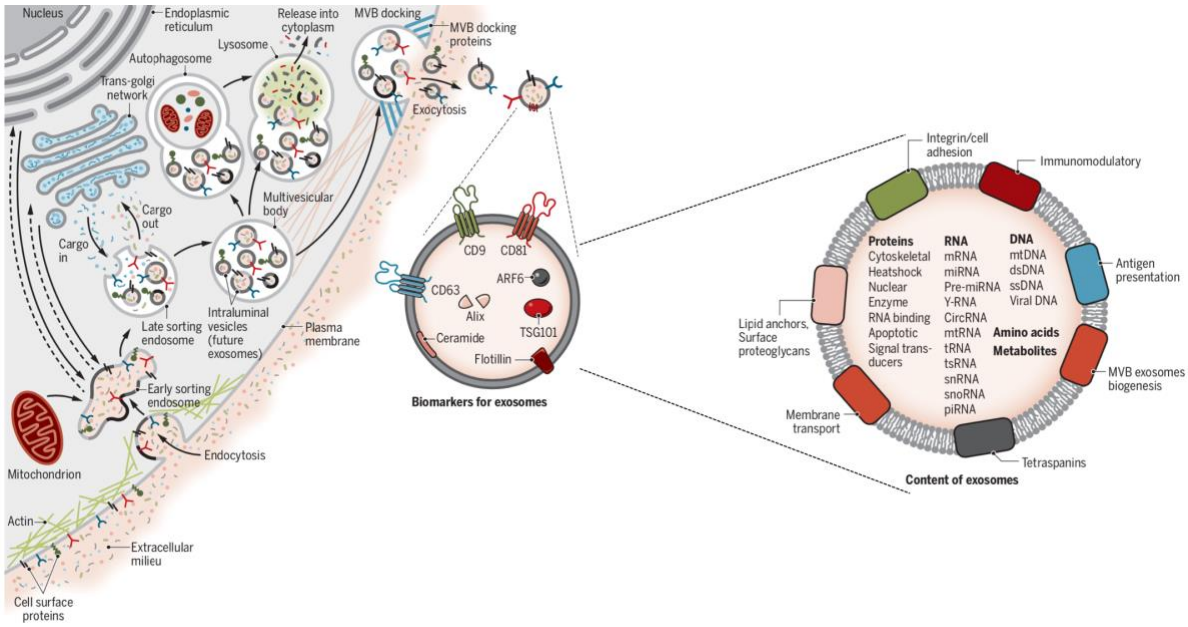

Figure 5: Mechanism of biogenesis and secretion of sEVs, including involved cellular organelles and content of secreted sEVs (sEVs = exosomes). From Kalluri and Lebleu, Science, 2020. *Reused with permission*.

<u>The ESCRT-dependant mechanism for sEVs biogenesis</u>

Several studies reported: 1) the presence of ESCRT components in sEVs, and 2) a decreased secretion of sEVs upon knock-out of ESCRT components, revealing its role in sEV secretion [202,203]. The ESCRT machinery is made of 4 subunits (ESCRT-0, ESCRT-I, ESCRT-II, ESCRT-III) and acts as follows [204,205]:

⇒ Step 1: Cell membrane lipids and ubiquitinated proteins cluster as a microdomain at the surface of the cells.

⇒ Step 2: ESCRT-0 and ESCRT-I contain ubiquitin-binding domains that recognize ubiquitinated proteins, and they can also recognize the membrane lipids. They assemble on the intracellular side of the membrane, where the microdomains mentioned in Step 1 are found

⇒ Step 3: ESCRT-0 and ESCRT-I recruit ESCRT-II and ESCRT-III.

⇒ Step 4: ESCRT-II and ESCRT-III induce the budding of the cell membrane and the scission, forming the endosome and then Multivesicular Bodies (MVB).

The ESCRT-independent pathway for sEVs biogenesis

Multiple ESCRT-independent mechanisms have also been proposed, although they remain poorly investigated:

⇒ The Syndecan-syntenin-ALIX pathway [206]: the Syntenin proteoglycans can interact with ALIX with the help of an intracellular adaptor Syntenin. This complex induces the budding of the membrane and the formation of endosomes.

⇒ Tetraspanin-dependant mechanism [207]: surface tetraspanins as CD81 can form microdomains necessary for specific sorting of cargos and formation of ILV

⇒ Rab31-dependant mechanism[208]: Rab proteins are membrane proteins involved in the movement of actin and tubulin and are known to be involved in the formation of vesicles. Upregulation of Rab proteins in cancer tends to be associated with pro-tumoral function by regulating hypoxia, activation of oncogenic pathways, and apoptosis[209]. Rab31 has been shown to inhibit the fusion of MVBs to the lysosome actively and thus redirects the fate of ILVs, contained inside the MVB towards secretion as sEVs.

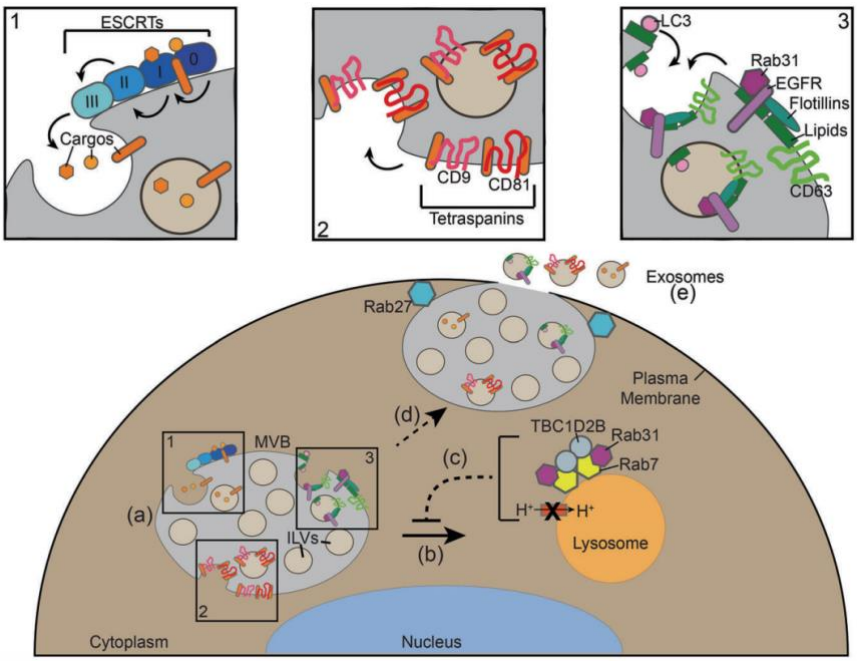

Figure 6: Schematic overview of the pathways involved in sEV biogenesis. (1) Proteins of the ESCRT machinery assemble at the surface of the multivesicular bodies (MVBs) recruit proteins

and promotes the formation of Intraluminal vesicles (ILVs). (2) Tetraspanin clusters promote the formations of ILVs. (3) Flotillins and autophagy-related proteins recruit Rab31 and promote the secretion of ILVs by blocking their migration to the lysosomes. From Kenefic, Zhang and Lyden, Cell Research, 2020. Reused with permission.

5.3.3.2. Bioactive molecules in small EV

DNA

The presence of DNA in sEVs remains controversial. If DNA can be isolated from sEV preparations, it remains unclear if it is located inside the sEV or stuck to the surface of the vesicles. In the early 2010s, several studies reported that DNA isolated from sEV preparation was mainly dsDNA[210,211]. In 2019, Yokoi, Villar-Prados and colleagues reported that sEVs isolated from the ovarian cancer cell line OVCAR-5 contain genomic DNA (gDNA). Using Whole Genome Sequencing, they have shown that the Copy Number Variations (CNVs) profile found in the sEV-derived DNA was strongly overlapping with the one from the parental cell line[212]. One hypothesis is that DNA isolated from sEV preparations may be influenced by the isolation method. By combining different isolation techniques based on density separation and magnetic selection of $CD63^+$ sEVs, another team could separate the sEV fraction from the so-called “non-vesicular” fraction of the sEV preparations. They could show that both DNA and histones are more enriched in the non-vesicular fraction and therefore claimed that DNA commonly isolated from sEV preparations is co-precipitated with sEVs[213]. However, using asymmetric flow-field fractionation, Zhang et al. could separate small sEVs (60-80nm) and large sEVs (90-120nm) and detected DNA fragments up to 10kbp. Of note, several studies have now shown that somatic mutations could be sequenced from the plasma-derived sEVs of patients, such as KRAS mutations for metastatic colorectal cancer[214].

Messenger RNAs (mRNAs)

Although mRNAs represent a minority of RNAs in the sEVs, it has been shown that mRNA can be transported from one cell to another through sEVs. Some of the mRNAs found in the sEVs are not detected in the cytoplasm of the parental cells, highlighting an active loading of those RNAs into the sEVs. Additionally, such mRNA can be efficiently translated into proteins by the recipient cell of sEVs[215]. Such findings are now translated into clinical development. For example, the Capricor company proposed to deliver the SARS-CoV-2 Spike protein (S) coding mRNA S^{w1} or the nucleocapsid protein (N)-coding mRNA LSNME using sEV[216].To promote the active loading of the mRNAs into the sEV, the mRNA sequences were fused to the coding sequence of Lamp1, a protein highly expressed in sEV. *In vivo* treatment of mice with these vaccine sEVs led to CD4+ and CD8+ T-cell activation and proliferation in response to respective treatment with N or S peptides.

MicroRNAs (mirRNA)

MiRNAs are highly enriched in sEVs and their loading in sEVs is the result of an active sorting mechanism, which remains poorly characterized[217,218]. Following antigen recognition, microRNAs transferred from T lymphocytes to antigen-presenting cells (APCs) by sEVs are actively inhibiting target mRNA translation[219]. MiRNAs found in the sEVs of cancer patients (isolated from serum or urine) are promising biomarkers of disease in non-invasive liquid biopsies. For example, sEV-derived miR-21 was suggested as an effective disease biomarker in several cancer subtypes, particularly prostate cancer [220,221]. Serum sEVs were significantly enriched in miR-155 in patients with DLBCL or Hodgkin Lymphoma[222,223]. Serum sEV-derived miR-155 was also suggested as a biomarker of resistance to classical R-CHOP therapy in DLBCL patients. The delivery of microRNAs by sEVs is also being developed as a therapeutic tool[224].

Other small RNAs

Small RNAs represent the majority of nucleic acids found in sEVs. When proceeding to total RNA extraction and profile analysis, RNAs of sEVs can be detected as a peak of around 200 base pairs (bp), independently of the sEVs origin[213]. Multiple sorts of small RNAs can be found in sEVs: microRNAs (miRNAs), mitochondrial RNAs (mtRNAs), transfer RNAs (tRNAs), small nuclear RNAs (snRNAs), small nucleolar RNAs (snoRNAs), piwi-interacting RNAs (piRNAs), tRNA-derived small RNAs (tsRNAs), Y RNAs and circular RNAs (circRNAs)[199], as well as long non-coding RNAs (lncRNAs; not considered as small RNAs). Pre-miRNAs are also found in the sEVs. However RNases involved in their cleavage, such as Dicer and Argonaute, have been rarely found in the proteome of sEVs[225]. However, it was shown that oncogene mutations, as in the KRAS gene, may regulate the loading of such RNases into the sEVs[226]. A description of the different small RNA families detected in the sEVs can be found in Supplementary box 4. Additionally, sEVs are highly enriched in Y RNAs, which will be described in the following paragraph [227]. Data comparing the small-RNA transcriptome of sEVs to the cell of origin have shown that some small RNAs are specifically enriched in sEVs, indicating the presence of an active loading mechanism of small RNAs into the sEVs[228]. As RNA-binding proteins (RBPs) represent up to 25% of the proteins found in sEVs, small RNAs and to RBPs are likely loaded as a complex into the sEVs [225,228].

yRNAs

yRNAs, also called Y RNAs or RNYs, are a family of highly conserved small non-coding RNAs (yRNA1, yRNA3, yRNA4, yRNA5) which exist either as full-length transcripts (~100bp) or fragments (~25bp) once cleaved by RNase L[227]. Human yRNAs are all located within a 45kb genome region located on chromosome 7[229] . Numerous pseudogenes for yRNAs have been described in the human genome[230]. They accumulate in the nucleus and the cytoplasm of eukaryotic cells. yRNAs are often described as part of ribonucleoprotein complexes and were

suggested to act as scaffolding RNAs[231]. Y RNAs are made of a specific stem-loop structure (Figure 7) with several domains allowing the binding of several proteins simultaneously[229,230].

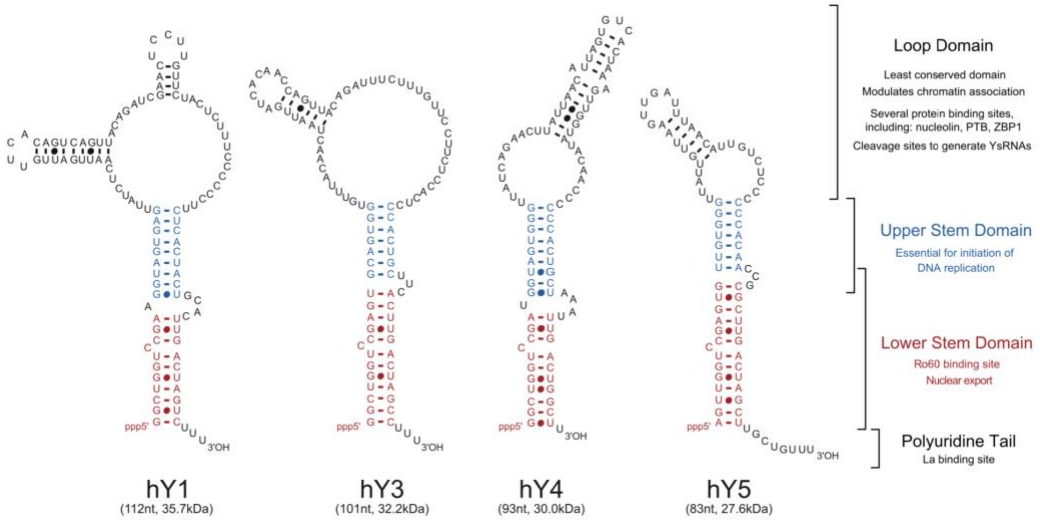

Figure 7: Sequence and structure of the four yRNA family members. *From Kowalski and Krude, The International Journal of Biochemistry & Cell Biology,* 2015.

Several yRNA-partner proteins have already been identified, with some proteins showing specific binding to a specific yRNA (Table 5). One of the most described interacting proteins with yRNA is Ro60. yRNAs were first discovered when scientists studied systemic lupus erythematosus (SLE), an auto-immune disease. In SLE, the ring-shaped Ro-60kDa (Ro60) protein is an auto-antigen. Ro60 is an RNA-binding protein that forms complexes with yRNAs by a binding sequence located on the stem of the yRNAs (Figure 7). yRNA-Ro60 complexes have been proposed to regulate the non-coding RNA population and eliminate misfolded non-coding RNAs in environmental stress[229,232]. Additionally, studies indicated a role for yRNAs in DNA replication[227,233–235]. This effect is believed to be redundant to all yRNAs. In line with this hypothesis, the deletion of yRNA5 in 293T cells did not confer a growth deficiency to the cells[236]. Of note, no studies are available at the moment that successfully differentiate the function of full-length yRNAs and yRNA fragments.

The existence of cell-free yRNAs remains controversial. yRNAs were initially suggested to be found both in encapsulated form as in extracellular vesicles and in a circulating form as cell-free-RNAs in the serum[230]. Recently, both circulating and sEV-encapsulated yRNAs were enriched in the plasma of cancer patients, with yRNA4 levels in sEVs from the plasma of pediatric patients with T-cell lymphoma positively correlating with disease stage and negatively correlating with treatment responsiveness[237]. Jeppesen et al. used state-of-the-art approaches to separate non-vesicular (NV) proteins from sEVs and, using small RNA-sequencing, proved that all four human yRNAs are detected in the cells, large EVs, sEVs and non-vesicular fractions. yRNAs were equally found in the non-vesicular and the sEV-derived fractions[213]. Full-length yRNAs and yRNA fragments were enriched in all fractions at a similar level. yRNA

are also circulating in the serum, particularly in the fetal bovine serum used for cell culture. RNA-sequencing of Fetal Bovine Serum (FBS)-derived sEVs and non-vesicular fractions revealed that bovine yRNAs reads can be mapped to the human genome[238]

References	Protein name	Protein function in cells	Method to identify Y-RNA binding proteins	Y1	Y3	Y4	Y5	Entry in vesicle pedia	Source of EV
Hendrick et al. (45); Köhn et al.(89)	Ro60	Binds misfolded RNA	Immunoprecipitation (anti-Ro60), RNA affinity purification	++	++	++	++	Yes	Blood/cell lines
Hendrick et al. (45); Köhn et al.(89)	La (SSB)	Binds 3′ poly-(U) tail of RNA pol III transcripts	Immunoprecipitation (anti-La), RNA affinity purification	++	++	++	++	Yes	Cell lines
Fouraux et al. (60)	Nucleolin	Associates with intranucleolar chromatin	Immunoprecipitation (anti-Ro60 and anti-La)	++	++	–	–	Yes	Blood/urine/cell lines
Fabini et al. (61)	hnRNP I (PTBP1)	Pre-mRNA splicing	RNA affinity purification	++	++	–	–	No	–
Fabini et al. (61); Köhn et al.(89)	hnRNP K	Pre-mRNA binding	RNA affinity purification	++	++	–	–	Yes	urine/cell lines
Thomson et al. (79)	Ago	RNAi mediated gene-silencing	Immunoprecipitation (anti-Ago)		n.d.			No	–
Cheng et al. (90)	Calreticulin	Calcium-binding chaperone	Electrophoretic mobility shift assay (EMSA)	++	++	++	++	Yes	Blood/pleural effusions/saliva/ urine/cell lines
Hogg and Collins (69)	L5 (RPL5)	Component of ribosome	RNA affinity purification	–	–	–	++	Yes	Saliva/urine/cell lines
Bouffard et al. (91); Hogg and Collins (69)	RoBPI (PUF60)	Pre-mRNA splicing, apoptosis and transcription regulation	Yeast three-hybrid assay, immunoprecipitation, RNA-immunoprecipitation (Ro60)	++	++	–	++	Yes	Cell lines
Hogg and Collins (69)	IFIT5	Interferon-induced RNA binding protein, senses viral 5′triphosphorylated RNA	RNA affinity purification	n.d	n.d.	n.d.	++	Yes	Urine/cell lines
Köhn et al. (58); Sim et al.(62); Kohn et al. (89)	ZBP1 (IFGB2P1, IMP1)	Recruits mRNAs to protein-RNA complexes, allowing mRNA transport and transient storage	Immunoprecipitation (anti-Ro60-FLAG), RNA affinity purification	+	++	n.d.	n.d	Yes	Cell lines
Sim et al. (58); Köhn et al. (89)	YBX1	Regulation of mRNA transcription, splicing, translation and stability	Immunoprecipitation (anti-Ro60-FLAG), RNA affinity purification	++	++	++	+	Yes	Cell lines
Sim et al. (58)	YBX3	Binds to GM-CSF promoter. Also binds full-length mRNA and short RNA	Immunoprecipitation (anti-Ro60-FLAG)		n.d			No	–
Sim et al. (58)	MOV10	Required for miRNA-mediated gene silencing. Involved in human hepatitis delta virus transcription	Immunoprecipitation (anti-Ro60-FLAG)		n.d.			Yes	Urine/cell lines
Yamazaki et al. (92); Köhn et al. (89)	Matrin-3	Nuclear matrix protein, nuclear retention of RNA, involved in antiviral response	RNA affinity purification	++	++	–	–	Yes	Urine/cell lines
Köhn et al. (89)	ELAVL1 (HuR)	Stabilizes mRNA and regulates translation	RNA affinity purification	–	++	–	–	Yes	Cell lines
Köhn et al. (89)	CPSF1	Involved in mRNA poly-adenylation	RNA affinity purification	++	++	–	–	Yes	Cell lines
Köhn et al. (89)	CPSF2	Involved in mRNA poly-adenylation	RNA-immunoprecipitation	++	++	–	–	Yes	Cell lines
Köhn et al. (89)	FIP1L1	Involved in mRNA poly-adenylation	RNA-immunoprecipitation	++	++	–	–	No	–
Köhn et al. (89)	SYMPK	Histone mRNA 3′-end processing	RNA-immunoprecipitation	++	++	+	+	Yes	Urine/cell lines
Bogerd et al. (93); Apolonia et al. (94)	APOBEC3G	Inhibitor of retrovirus replication, broad antiviral activity	RNA-immunoprecipitation		n.d.			Yes	Cell lines
Bogerd et al. (93); Apolonia et al. (94)	APOBEC3F	Inhibitor of retrovirus replication, broad antiviral activity	RNA-immunoprecipitation		n.d.			Yes	Cell lines
Tebaldi et al. (73)	HuD (ELAVL4)	Translational enhancer of mTORC1-responsive genes, regulation of mRNA abundance and alternative splicing	RNA-immunoprecipitation	–	++	–	n.d.	No	–

Indicated are known functions of the human variants of these proteins. Binding to the different Y-RNA subtypes is indicated with +, – and ++, or not-determined (n.d.). Furthermore, identification of these proteins in EV is indicated based on entry in the Vesiclepedia database of EV-associated proteins, as well as the source of EV in which these proteins were detected.

Table 5: List of proteins known to interact with yRNAs and their associated function. *From Driedonks T. and Nolte-'t Hoen E.N.M, Frontiers in Immunology, 2019.*

Proteins

In a recent study, Kugeratski et al. performed super-SILAC Mass Spectrometry on sEVs derived from 14 cell lines. Gene Ontology Molecular Function analysis revealed that proteins ubiquitously found in sEVs are mainly involved in RNA or nucleic acid binding activity[239]. RNA-binding proteins (RBPs), such as the Y-box protein 1 (YBX1), are commonly found in sEVs. YBX1 contributes to the loading of specific microRNA into the sEVs[240,241]. Argonaute2 (AGO2) is also detected in sEVs from different sources[228]. AGO2 sorting into EV is a regulated mechanism, and the increase or decrease of AGO2 sorting into EV influences the enrichment of specific miRNAs in the sEVs. It has been suggested that sEV-derived AGO2 protein contributes to the processing of precursor miRNA in sEVs[242]. The loading of RNA-binding proteins into sEVs may depend on the LC3 protein, initially described as a mediator of the autophagy pathway[243]. Suggested ubiquitously enriched proteins in sEVs also involved GTPases and proteins of the Ras family[239]. Among GTPases, Rab proteins are highly enriched in sEVs. If it is known that Rab proteins are essential for sEVs secretion, it remains nonetheless unclear if sEV-derived Rab proteins have a function once delivered to recipient cells. The proteins of the APOBEC3 family, which are known to bind to yRNAs, are also regularly reported to be enriched in sEVs (Box 3).

Apolipoprotein B mRNA editing enzyme catalytic polypeptide-like (APOBEC) are a family of 11 proteins, also called DNA cytidine deaminases, responsible for C>U edition in RNAs. They were initially described to be involved in the innate immune response for the modification and degradation of single-stranded viral DNA[244,245]. APOBEC exists as mono-, di- or oligomers[245]. APOBEC proteins form complexes with proteins such as Ro60 or yRNAs[245]. The expression of APOBEC3 is increased in myeloid cells following the activation of Toll-Like Receptors[244]. However, additional functions of APOBEC than control of viral infection have been reported. APOBEC3 has been shown to regulate the inhibitory function of miRNA. On one side, it has been shown that APOBEC3G can interact with AGO2 and inhibits the formation of the miRISC complexes and the miRNAs [246]. On the other side, APOBEC3G can compete with DEAD-END (DND1), which blocks the interaction between the miRNAs and their target mRNA, thus restoring their function[247]. More interestingly, it was recently shown that following activation, RNAs in myeloid cells go through an increased C>U editing, which is increased in M1-macrophages compared to M2-macrophages[248]. RNA editing in macrophages is decreased in APOBEC3A knock-down myeloid cells. APOBEC3A and APOBEC3B were also reported to induce DNA somatic point mutations or chromosomal rearrangements leading to cancer development or drug resistance[249–251]. APOBEC proteins are regularly found in sEVs.

Box 3: The APOBEC protein family and their link to sEVs

5.3.3.3. Others

sEVs are naturally enriched in lipids and metabolites. However, little is known about their function in sEVs, apart from forming the lipidic membrane. Cholesterol, Sphingomyelins, Phosphatidylcholines, and Phosphatidylserines are the most enriched molecules[252]. Metabolomic analysis of sEVs derived from platelets or urine revealed important differences in the metabolome depending on the origin of the fluid. However, common metabolites to both sources of sEVs are particularly enriched in organic acids, nucleotides, and sugars.

5.3.4. Tumor-derived sEV remodulate the phenotype of myeloid cells

5.3.4.1. General

Because the content of tumor-derived sEVs differs depending on the tumor tissue, drawing a precise portrait of their effect on myeloid cells is, if not impossible, very challenging. However, some characteristics of myeloid cells following treatment with tumor-derived sEVs were broadly observed independently of the origin of the tumor-derived sEVs. Tumor-derived sEVs generally promote a pro-tumoral phenotype of myeloid cells, or their differentiation into M2-polarized macrophages, Myeloid-Derived Suppressor Cells (MDSCs), or Tumor-associated macrophages (TAM)[253–256]. This phenotype is associated with the secretion of tumor-promoting cytokines such as IL6, CCL2, CCL4, CCL7, IL-10, CXCL12, TNF-α, and IL1-β[254,256–258]. The survival of myeloid cells is promoted by tumor-derived sEVs, most likely through the transfer of GTPases. Treatment of myeloid cells with tumor-derived sEVs is always associated with an upregulation of the inhibitory ligand PD-L1 at the surface of the cells[254,258]. PD-L1 upregulation induced by tumor-derived sEVs seems to be dependent on the activation of Toll-Like Receptors and subsequent phosphorylation of STAT3, leading to the activation of NF-κB [284,288,289]. Additionally, tumor-derived sEVs were reported to inhibit the differentiation of myeloid cells into DCs [260,261]. Myeloid cells treated with tumor-derived sEVs show a reorganization of the cytoskeleton, which is associated with the formation of lamellipodia and increased migration[254].

5.3.4.2. Modulation through Toll Like receptors (TLRs)

Toll-Like Receptor function

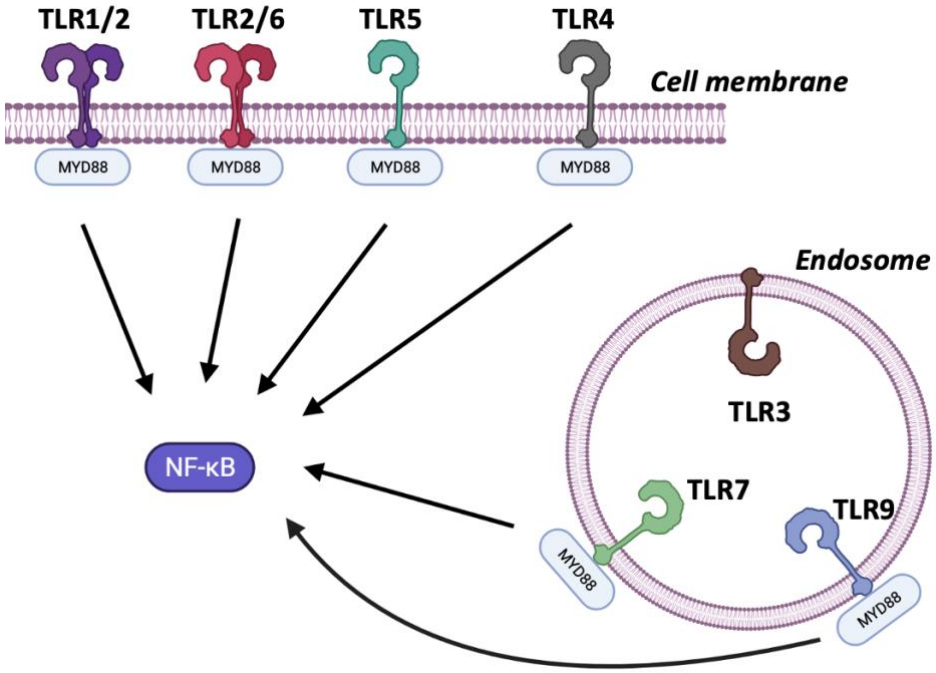

TLRs are crucial players of the innate immune system. Together with other receptors such as C-type lectins or RIG-I-like receptors, they form a class of receptors called Pattern-Recognition Receptors (PRRs) [262]. PRRs are mainly expressed by antigen-presenting cells. TLRs can act as homodimers or heterodimers to recognize pathogen-associated molecular patterns (PAMPs). TLR2 is found as heterodimer with TLR1 or TLR6 and recognizes lipoproteins, peptidoglycans, mannan etc[262]. TLR4 can recognize bacterial lipopolysaccharides, whereas TLR5 recognizes flagellin. On the endosomal membrane, TLR3 can recognize double-stranded RNAs[263]. TLR7 recognizes single-stranded RNAs. Although initially thought of as non-functional, human cells seem to carry endosomal TLR8, which shares functions with TLR7[263,264]. Finally, TLR9 recognizes single-stranded CpG DNA. TLR10 on the cell surface and TLR12 and TLR13 on the endosome membrane have been more recently described, but their affinity remains poorly characterized. The pathway following TLR activation is quite well described and available at: https://www.cellsignal.com/pathways/toll-like-receptor-signaling-pathway. In brief, all TLRs, except for TLR3, depend on the adaptor protein Myd88 for the transduction of the signal. Other members involved in the signalling cascade are IRAK and IRF proteins. Activation of TLR-related signaling pathways result in the translocation of the transcription factors NF-kB, AP-1, and IRF7 (among others) to the nucleus and leads to the secretion of pro-inflammatory cytokines and interferons [265]. Using Myd88-KO cells, a Myd88-independent pathway relying on the TRIF adaptor protein downstream of TLR3 and TLR4 activation was also described[266,267].

Exosomes activate TLRs

Tumor-derived sEVs depend highly on TLRs to modulate the phenotype of myeloid cells. First, small RNAs contained in the sEVs can activate TLR7 and TLR8. This is true for microRNA as well as Y RNAs[258,259]. Additionally, it cannot be excluded that sEV-derived small RNAs can activate other TLRs, as shown for the sEV-derived miR-203-induced activation of TLR4 on DCs [268]. Activation of TLR by sEVs has a dual effect on the phenotype of myeloid cells, with both pro-and anti-tumoral features. However, the balance tends towards a pro-tumoral phenotype. Indeed, sEVS derived from lung cancer can promote metastasis, an effect abolished in TLR2-KO mice [269]. Metastasis was also suggested to be promoted by melanoma, lung carcinoma, and breast cancer-derived sEVs through activation of TLR2 and TLR4[270]. In general, tumor-derived sEVs are often reported to be potent activators of TLR2 and TLR4 on recipient cells such as myeloid cells or mesenchymal stem cells[269,271,272]. sEV-derived TLR-ligands proposed to initiate this activation include HMGB1 and Heat-Shock-Proteins[270,273–275]. To activate TLRs, ligand proteins must be expressed at the surface of sEVs. HMGB1 and HSP are proteins existing both as transmembrane, intraexosomal, intracellular and soluble forms. However, the presence of HMGB1 at the surface or inside sEVs remains controversial, with HMGB1 being several times reported as a negative marker of sEVs[213,239]. Additionally, it remains unclear if the transmembrane forms of these proteins can activate TLR similarly to their soluble form. Of note, sEVs are not only able to activate TLRs, but they also contain soluble forms of TLRs, which are recurrently detected in the proteome of sEVs. Whether sEV-derived TLRs have a function in recipient cells remains unresolved.

5.3.5. State-of-the-art: sEVs in B-cell NHL

Several studies have reported that the amount of absolute sEVs and, particularly B-cell-derived sEVs, is increased in the serum of CLL patients [258,276,277], which is reduced upon treatment with ibrutinib [276]. sEVs from NHL patients present a specific small-RNA and proteomic signature [276,278,279]. In particular, the small RNA signature of CLL-derived sEVs is characterized by an enrichment of miR-29a, miR-29b, miR-155, miR-150, and let-7g [276,278,280]. Stromal can take up CLL-derived sEVs, leading to a Cancer-Associated Fibroblast phenotype, with an increased proliferation[278,280]. In response to treatment with CLL-derived sEVs, stromal cells release more pro-inflammatory cytokines and pro-tumoral factors such as BAFF and APRIL, a mechanism mediated by increased phosphorylation of kinases and NfkB activation[278]. FL-derived sEVs modulate the phenotype of macrophages by promoting upregulation of FasL and are associated with an increased risk of transformation of FL into DLBCL [281]. Using CLL as a model, Haderk et al. have shown that myeloid cells, following treatment with tumor-derived sEVs, showed an increased expression of the inhibitory ligand PD-L1 and secretion of pro-inflammatory cytokines. B-cell NHL sEVs not only impact the stromal and myeloid cells but also promote the expansion of Treg and apoptosis of CD8+ lymphocytes and NK cells [277]. Additionally, B-cell NHL sEVs have been described as promoters of chemoresistance and angiogenesis [277,282].

5.4. CHAPTER III: Unresolved question and limitations to consider when studying the biology of sEV

5.4.1. Culture conditions

Research on the role of EVs and sEVs is a recent field that encounters limitations due to a lack of standardization of the methods used to isolate and characterize EVs. Innumerable factors can potentially influence the rate of sEVs secretion by the cells, as well as the biogenesis route leading to modification, among others, of the heterogeneity of secreted sEVs and their content. The first parameters to control are the cell culture conditions.

5.4.1.1. Cell containers

Up to now, it remains poorly investigated if cells cultured in different types of plates, flasks, or bioreactors can influence the sEVs produced by the cells. However, one study performed metabolomics on sEVs derived from flasks or bioreactors and concluded that a differential metabolomic signature is found in sEVs depending on the cell culture container [283].

5.4.1.2. Growth medium

Several studies have already underlined how the growth media can affect the produced sEVs. It has been recently reported that the sEV secretion rate of HEK293T cells was modified when cells were cultured in Opti-MEM medium or DMEM medium supplemented with 10% of FBS [284]. Additionally, supplementation of the medium with albumin, globulin, or fibronectin also influenced the secretion rate, as it was already shown for glucose[285]. An excellent review by Lehrich et al. summarizing all effects due to the processing of sEV-depleted FBS is available in the JEV, 2021[286]. Briefly, the depletion of sEVs in FBS was reported by several groups to influence the cell viability, the switch from 3D- to monolayer growth, and the migration potential of the cells. Indeed, the ultracentrifugation of FBS results in the partial depletion of lipids or other growth factors from the medium [286]. An alternative is commonly used by several groups, switching to a serum-free medium for up to 48 hours during the time of supernatant collection. However, the authors of the study highlight that depletion of serum from the medium induces immediate stress on the cultured cells[286].

5.4.1.3. Other parameters

The cell confluency, the initial number of seeded cells, the passage frequency, oxygen rate or, contamination of the cells by mycoplasma are other parameters suggested to influence the yield and purity of sEVs[287].

5.4.1.4. Influence of isolation technique and co-isolation of bioactive molecules

sEV isolation methods

Increased interest in sEV-related research led to important developments regarding the standardization of sEV isolation techniques. Several studies have established that different isolation approaches lead to different subtypes of collected sEVs. Table 6 summarizes the current approaches the sEV community uses.

Method	Description
Ultracentrifugation	Cell culture supernatant is centrifuged at 100,000g for 2 hours. The step can be repeated by removing the supernatant and washing the pellet containing sEVs and remaining soluble proteins in PBS.
Density gradient	The supernatant is centrifuged at 100,000g for 2 hours. The pellet containing sEVs and soluble proteins is resuspended in a small volume and applied on a sucrose density gradient. During the second step of ultracentrifugation, the proteins and sEVs are separated due to their different density. An additional washing step in PBS is performed.
Filtration	The supernatant goes through a filter of specific pore size, allowing only sEVs and smaller particles to go through.
Size-exclusion chromatography	The supernatant is applied onto a column containing a gel with pores. Smaller particles such as proteins are retained within the pores of the columns, whereas sEVs are directly eluted.
Polymer-based precipitation	The supernatant is mixed with polymers of high molecular weight, and low-speed centrifugation or filtration allows to separate sEVs from their original fluid.
Magnetic bead capture	The supernatant is labeled with antibodies recognizing a specific sEV maker such as CD63. The antibodies are linked to magnetic beads. The antibody-exosomes complexes are retained by magnetism.

Table 6: Summary of the main techniques used for the isolations of sEVs and brief description of the approach.

Influence of the isolation method on sEV preparations yield, purity and content

The choice of the isolation technique is of crucial importance for a research project. For each available technique, pros and cons must be taken into consideration, depending on the use of the isolated sEVs. Although polymer-based precipitation using commercially available kits is the approach leading to the highest yield of recovered sEVs, it has been reported that the resulting sEV preparations were toxic when used for the treatment of cells, most likely due to an important contamination of the sEVs with polymer proteins and chemicals [288–290]. For the

same reason, polymer-based precipitation is not recommended for Mass-Spectrometry analysis. Magnetic capture is an approach leading to the collection of a little but very pure sEV preparation. Magnetic captures are mainly using anti-CD63 antibodies to separate sEVs from other components of the supernatant[288]. However, it should be reminded that CD63-negative sEV populations have also been described, which are lost in the case of magnetic capture. Size-Exclusion Chromatography (SEC) has been reported to result in a high yield of sEVs, although the resulting product shows the highest contamination rate by lipoproteins[290]. Contamination by lipoproteins is particularly significant when isolating sEVs from plasma. Ultracentrifugation and density-gradient ultracentrifugation are associated with recovering of little but highly pure sEVs[291]. However, the repetition of ultracentrifugation steps may damage the integrity of sEVs [291]. Proteomic analysis of sEVs isolated from the same parental cell lines but using different isolation methods revealed differences in the signature of the sEVs, despite an acceptable overlap[239,292]. The same conclusions were reported for the small RNA content[291]. These results highlight that different isolation techniques lead to the isolation of slightly different subpopulations of sEVs.

5.4.2. Influence of storage conditions

sEVs are spheroid structures composed of a lipidic membrane containing proteins and nucleic acids, among other biomolecules. Therefore, the storage conditions must be optimized to avoid the degradation of sEV-derived components. The international MISEV guidelines 2018 highlight how the storage conditions of the sEV-containing fluid (plasma, blood, supernatant, etc.) and the isolated sEVs can influence their integrity and function [293]. sEVs are mainly stored at 4°C, -20°C, or -70/-80°C. Contradictory studies reported either that the temperature of the storage, to a maximum of one week, did not influence the concentration of sEVs, or that only the storage at -80°C prevents the loss of sEVs as detected by nanoparticle Tracking analysis [294]. A difference in the results may depend on the fluid of origin of the isolated sEVs. One hypothesis is that storage at different temperatures may result in the loss of different sEVs populations[294,295]. Some studies reported that storage at -70°C, but not 4°C, leads to a loss of properties of anti-bacterial EVs [296]. For storage at -70/-80°C, the addition of DMSO may improve the preservation of the membrane and avoid ice crystals. However, even adding DMSO does not prevent the gradual loss of material that correlates with the time-length of the storage [297]. As a sub conclusion, the storage of sEV-containing fluids and sEV preparations should be optimized depending on the application. This is particularly important when testing the biological function of sEVs, which can be impacted by the temperature and the length of the storage. Because of the lack of standardization, the storage conditions should always be very well described when results are being reported.

5.4.3. Acquisition of physiologically relevant results

5.4.3.1. Doses of sEV

Due to an significant loss of sEV during the isolation method, estimating the number of sEVs secreted by cells during a specific period of time remains challenging. Additional tracking approaches are being developed to investigate this question further, one approach consisting in fusing a fluorescent or luminescence gene to an sEV-derived marker, such as CD63 or CD9[298–301]. One limitation when performing a functional assay to understand the function of sEVs is to choose a dose or concentration that are physiologically relevant. *In vitro* experiments can estimate the ratio of sEV per cell that is efficient to induce a biological effect or is toxic for the cells. *In vivo* experiments have proven that the dose of sEVs can influence their biodistribution. However, it remains unclear if the sEV-labelling approaches used in such studies did not modify the biodistribution themselves[297].

5.4.3.2. Isolation technique-mediated enrichment of sEVs specific subpopulations

As previously explained, sEVs are a heterogeneous population, with subpopulations being most likely enriched differentially depending on the isolation technique. Subpopulations of sEVs are now differentiated based on the surface tetraspanin profile (CD63, CD9, and CD81) on sEVs. Tetraspanins are known to cooperate with specific integrins, also found at the surface of sEVs, and integrins at the surface of sEVs can modify their organ biodistribution [302,303].

5.4.3.3. Limitation to *in vivo* studies

When performing *in vivo* experiments, not only the dose of sEVs and the biodistribution must be considered, but also the high rate of sEV-clearance or accumulation by the liver or other organs such as the spleen, which are particularly influenced by the route of administration, and the site of injection [304]. Experiments aiming at using sEVs for drug-delivery purposes should consider that sEVs are easily taken up by macrophages by phagocytosis [305]. However, Kamerkar et al. suggested that expression of CD47 at the surface of sEVs efficiently decreases their phagocytosis by myeloid cells [306]. A patent in the United-States now protects the use of CD47-overexpressing EVs.

5.4.4. sEVs are a promising therapeutic tool

The relevance of EVs as a promising diagnostic and therapeutic tool, particularly in the field of cancer, has gained much attention in the scientific community over the last couple of years. This promise led to the development of multiple spin-off companies developing EV-based

products to treat a multitude of diseases. These companies receive important funding from national agencies to develop their research and production activities. Several products developed by these companies are now reaching phase I of clinical trials[307]. So far, EV-based drugs are proposed to be used for two main functions: as vaccines, if they are loaded with a tumor antigen that can activate an anti-tumor response by the immune system, or as a drug or nucleic acid delivery system, their nanoscale size conferring them an increased potential to reach distant sites of injection, and potentially cross the blood-brain barrier, making them of particular interest for the treatment of brain tumors [308]. One of the advantages of EVs compared to cell therapy is their low immunogenicity and toxicity. As a proof-of-principle, the injection of human EVs into fully immunocompetent murine animals has been shown not to be associated with side effects despite the inter-species aspect of such treatment. Additionally, the manufacturing processes for EV production are and keep being optimized by several companies worldwide. EV production processes remain similar to the ones used producing antibodies for mono- or polyclonal therapies; however, they have the advantage of not necessarily requiring the use of animals as cell donors. In addition to their potential as diagnostic or treatment tools in the field of cancer or auto-immune diseases, EVs have been suggested as an optional tool to fight infectious diseases. It has been recently brought to the light of the COVID-19 pandemic, where EVs were shown to have the capacity to be used as decoy agents for the human protein ACE2 essential for SARS-CoV-2 virus cell infection [309], or as mRNA delivery system for vaccination[216]. Techniques are under optimization to improve the efficient loading of mRNA into sEVs, with nanoporation being a promising direction [310,311]. In parallel, one challenge that remains to be addressed is selecting an appropriate cell source for sEV production to ensure both product safety and efficient large-scale sEV production. So far, studies are focusing mainly on Mesenchymal Stromal Cells (MSCs) [312,313]. However, due to the absence of genomic or mitochondrial DNA, red blood cell sEVs have been suggested as sEV producers for therapeutic purposes[314,315].

6. AIMS OF THE THESIS

6.1. Improving cell culture, isolation techniques and storage of sEV preparations

The choice of the isolation approach for sEVs is of primary importance and must be carefully considered based on the further application. In a first step, I aimed to compare the efficiency of differential centrifugation combined to either 1-ultracentrifugation on sucrose density gradient or 2-size-exclusion chromatography on commercially available columns (Single qEV, Izon, France), in terms of yield, purity, and function of recovered sEVs. Additionally, I compared the effect cell culture medium contents, flasks and bioreactors, on the function, sEV secretion and type of secreted sEVs. Finally, I aimed at investigating if the storage of sEV preparations at -80°C may impact their biological function, compared to sEVs stored at 4°C.

6.2. Activation of Toll-Like Receptors in myeloid cells following treatment with B-cell NHL sEVs

To investigate if TLRs are highly involved in the acquisition of a pro-tumoral phenotype by myeloid cells following the uptake of CLL-derived sEVs, *in vitro* experiments were performed using knock-out murine models for different TLRs or TLR-pathway components, as well as reporter cell lines for TLRs.

6.3. Bioactive molecules responsible for myeloid cells activation in B-cell NHL

To explore the proteome of CLL-derived sEVs in primary samples as well as to investigate for potential proteins inducing the sEV-mediated protumoral phenotype in myeloid cells, a proteomic analysis of sEVs derived from the lymph nodes of DLBCL, FL or non-tumor patients was performed using Mass-Spectrometry.

6.4. Resolving the relevance of intra-sEV-derived yRNA4 for sEV-induced induction of a pro-tumoral phenotype in myeloid cells

A knock-out of the yRNA4 gene was performed using the CRISPR/Cas9 approach, in the CLL HG3 cell line (HG3 yRNA4-KO). The KO was validated by PCR using genomic DNA as well as by Northern-Blot. The potential of sEVs from the WT or the yRNA-KO cell line in inducing a pro-tumoral phenotype in myeloid cells was investigated using *in vitro* functional assays. The difference of expression of the other yRNA family members was investigated by RT-qPCR, and a potential difference of protein cargo loaded into the sEVs, in the presence or absence of yRNA4, was investigated by Mass-Spectrometry.

7. MATERIAL AND METHODS

7.1. Material

7.1.1. Cell culture (incl. monocyte isolation and functional assay)

RPMI 1640	Sigma-Aldrich, Steinheim	R8758
Fetal Bovine Serum (FBS)	Sigma-Aldrich, Steinheim	F7524
Dulbecco's Phosphate Buffered Saline (PBS)	Sigma-Aldrich, Steinheim	D8537
2-Mercaptoethanol (55 mM)	Thermo Fisher Scientific, Waltham	21985-023
Dimethylsulfoxid (DMSO)	Sigma-Aldrich, Steinheim	41639
CELLine Classic bioreactor flask CL 1000	Sigma-Aldrich, Steinheim	Z688029
Penicillin-Streptomycin (10,000 U/mL)	Invitrogen, Whaltham	15140122
HEPES (1M)	Life Technologies, Carlsbad	15630056
Sodium Pyruvate (100 mM)-100 mL	Life Technologies, Carlsbad	11360070
Effectene Transfection Reagent (1 ml)	Qiagen, Hilden	301425
Recombinant human M-CSF	Peprotech, Rocky Hill	300-25-10
EasySep™ Mouse Monocyte Isolation Kit	Stem cell	#19861
RBC Lysis Buffer (10X)	Biozol Diagnostica	BLD-420301
CD14 MicroBeads, human	Miltenyi Biotec GmbH	130-050-201
LS Columns	Miltenyi Biotec GmbH	130-042-401
Biocoll	Biochrom	L6115
Leucosep Röhrchen	Greiner	227290
70µM Zellsiebe	Neolab	352350
Vicell sample vials	Beckman Coulter	383721
GentleMACSTM C Tubes	Miltenyi Biotec, Bergisch Gladbach	130-093-237
Falcon 70µm Cell strainer	Corning, New York	352350
Conical Tubes 15mL	Corning, New York	91014
Conical Tubes 50mL	Corning, New York	91054
Mr. Frosty Freezing container	Nunc, Rosklide	5100-0001

Pipette tips	Steinbenner Laborsystem, Wisenbach	TP50010, TP50020, TP50100, TP50200, TP51250
hY4 full length (hY4 96nt), RNA	5'GGCUGGUCCGAUGG UAGUGGGUUAUCAGA ACUUAUUAACAUUAG UGUCACUAAAGUUGG UAUACAACCCCCCAC UGCUAAAUUUGACUG GC UUUUU-3'	IBA, Göttingen

7.1.2. Flow cytometry

Fixable Viability Dye eFluor®506	Thermo Fisher Scientific, Waltham	65-0866-14
APC/Cyanine7 anti-human CD14 Antibody	Biolegend, San Diego	325620
PE/Cyanine7 anti-human CD16 Antibody	Biolegend, San Diego	302016
APC anti-human CD274 (B7-H1, PD-L1) Antibody	Biolegend, San Diego	329708
PE/Cyanine7 anti-mouse/human CD11b Antibody	Biolegend, San Diego	101216
PE/Dazzle™ 594 anti-mouse CX3CR1 Antibody	Biolegend, San Diego	149014
APC anti-mouse F4/80 Antibody	Biolegend, San Diego	123116
Brilliant Violet 711™ anti-human HLA-DR Antibody	Biolegend, San Diego	307644
PE Mouse IgG2b, κ Isotype Ctrl Antibody	Biolegend, San Diego	400314
Alexa Fluor® 647 anti-mouse CD192 (CCR2) Antibody	Biolegend, San Diego	150604
FITC anti-mouse F4/80 Antibody	eBioscience, San Diego	123107
PE anti-mouse CD54 Antibody	Biolegend, San Diego	116108
CD274 (PD-L1, B7-H1) Antibody, PerCP-eFluor™ 710	eBioscience, San Diego	46-5982-82
Fc Receptor Binding Inhibitor Antibody	Life Technologies, Carlsbad	14-9161-73
APC anti-human CD19 Antibody	Biolegend, San Diego	302212

PE anti-human CD54 Antibody	Biolegend, San Diego	353105
Alexa Fluor® 647 anti-mouse CD192 (CCR2) Antibody	Biolegend, San Diego	150604
CD274 (PD-L1, B7-H1) Antibody	Life Technologies, Carlsbad	46598282
MHC Class II (I-A/I-E) Antibody, Alexa Fluor® 700	eBioscience, San Diego	56-5321-82
eBioscience™ IC Fixation Buffer	eBioscience, San Diego	00-8222-49
LEGENDplex™ Human MCP-1 Capture Bead A8, 13X	Biolegend, San Diego	740813
LEGENDplex™ Human IL-6 Capture Bead A10, 13X	Biolegend, San Diego	740124
LEGENDplex™ Human Inflammation Panel 1 Standard	Biolegend, San Diego	740811
LEGENDplex™ Human Inflammation Panel 1 Detection Antibodies	Biolegend, San Diego	740810
LEGENDplex™ Buffer Set A1	Biolegend, San Diego	740525
Annexin V Binding Buffer	Biolegend, San Diego	422201
Annexin V FITC	Biolegend, San Diego	640906
7-AAD Viability Staining Solution	Biolegend, San Diego	420403
APC anti-human CD62L Antibody	Biolegend, San Diego	304810

7.1.3. **Molecular biology** (incl. PCR, RT-qPCR, blotting reagents)

GeneRuler 1 kb Plus DNA Ladder	Thermo Fisher Scientific, Waltham	SM1331
RIPA Buffer	Sigma-Aldrich, Steinheim	R0278
Qubit Protein Assay Kit-100 assays	Life Technologies, Carlsbad	Q33211
RNA loading dye	Life Technologies, Carlsbad	R0641
Qubit tubes	Life Technologies, Carlsbad	Q32856
miScript SYBR Green PCR Kit	Qiagen, Hilden	218073
RNA 6000 Pico kit	Agilent, Santa Barbara	5067-1513
RNA 6000 Pico Ladder	Agilent, Santa Barbara	5067-1535
QIAamp DNA Mini Kit (50)	Qiagen, Hilden	51304

CARESTREAM(R) KODAK(R) BIOMAX(R) MR FILM	Sigma-Aldrich, Steinheim	Z350397-50EA
DEPC BioChemica 5	Applichem, Darmstadt	A0881,0020
COLUMN G-25 ILLUSTRA MICROSPIN	Thermo Fisher Scientific, Waltham	11743309
ULTRAhyb Ultrasensitive Hybridization Buffer-125 mL	Life Technologies, Carlsbad	AM8670
miScript RT II kit	Qiagen, Hilden	218160
Extra Thick Blot Filter Paper, Precut, 7.5 x 10 cm	Biorad, Hercules	1703965
T4 Polynucleotide Kinase (PNK)	New England Biolabs, Ipswich	M0201S
15% Mini-PROTEAN TBE-Urea Gel, 10 well, 30 µl	Biorad, Hercules	4566053
Hot Start Taq 2X Master Mix	New England Biolabs, Ipswich	M0496S
Monarch® DNA Gel Extraction Kit	New England Biolabs, Ipswich	T1020
10X RIPA Buffer15ML	Abcam, Cambridge	ab156034
Nuclease-free Water	Invitrogen, Whaltham	AM9937
0,2ml 8-strip PCR Tubes	Starlab, Brussels	A1402-3700-C
Proteinase K	Sigma-Aldrich, Steinheim	3115879001
Qiagen RNeasy® Micro Kit	Qiagen, Hilden	74004
Antioxidant	Life Technologies, Carlsbad	NP0005
Reducing agent	Life Technologies, Carlsbad	NP0004
NuPAGE Novex 4-12% Bis-Tris Protein Gels, 1.5 mm, 10 well	Life Technologies, Carlsbad	NP0335BOX
Ponceau	Sigma-Aldrich, Steinheim	P7170
Page Ruler 10kD-250kD	Life Technologies, Carlsbad	26619
Gel Green	Biotrend, Köln	B-41005

7.1.4. Isolation of sEVs

qEVsingle / 35nm	Izon, Lyon	SP6
Thinwall Polyallomer tubes, 38.5 mL, 25 x 89 mm	Beckman Coulter, Brea	326823

OpenTop Polyallomer tube 14x95mm	Beranek, Torrance	5031
OptiPrep™ Density Gradient Medium	Sigma-Aldrich, Steinheim	D1556
0,22um filter	Merck, Darmstadt	16467555
Filter system, 250mL, 0.22 uM	Sigma-Aldrich, Steinheim	SIAL1096-12EA

7.1.5. Western-Blots

Calnexin Antibody (H and Ms)	Hölzel Biotech, Köln	A01240-40
Cytochrome C antibody (H and Ms)	Hölzel Biotech, Köln	A01507-40
CD81 antibody (Ms)	Hölzel Biotech, Köln	ABC-AM8561b
APOBEC3D/APOBEC3F Polyclonal Antibody (H)	Biolegend, San Diego	PA5-39357
CD9 Monoclonal Antibody (H)	Biolegend, San Diego	10626D
CD81 antibody (H and Ms)	ProSci, Fort Collins	5195
Purified anti-Hsp70 Antibody (H)	Biolegend, San Diego	648001
Pierce ECL Plus Western Blotting Substrate-25 mL	Life Technologies, Carlsbad	31134
Purified anti-CD63 Antibody (Ms)	Biolegend, San Diego	143901
Purified anti-CD9 Antibody (Ms)	Biolegend, San Diego	124802
Purified CD81 Antibody (Ms)	Biolegend, San Diego	104901
Purified anti-Cytochrome C Antibody (H and Ms)	Biolegend, San Diego	612503
Anti-Calnexin antibody (H and Ms)	Abcam, Cambridge	ab213243
Anti-APOBEC3G antibody (H)	LSBio, Seattle	LS-C404537-60

7.1.6. Sequences of primers

CR2 FWD	GGTCCTCGGGATTTCTTGTGG
CR2 REV	GAACAACTGTACCTTATCACGGT
CCL22 FWD	ATCGCCTACAGACTGCACTC
CCL22 REV	GACGGTAACGGACGTAATCAC
IL5 FWD	TGGAGCTGCCTACGTGTATG
IL5 REV	TTCGATGAGTAGAAAGCAGTGC
NT5E FWD	TGATGAACGCAACAATGGCAC
NT5E REV	AAATGTGCCTCCAAAGGGCA

CXCL12 FWD	GCCCTTCAGATTGTAGCCCG
CXCL12 REV	GTGGGTCTAGCGGAAAGTCC
IL12A FWD	AACATGCTCCAGAAGGCCAG
IL12A REV	TAAACAGGCCTCCACTGTGC
CXCL12 FWD	GCCCTTCAGATTGTAGCCCG
CXCL12 REV	GTGGGTCTAGCGGAAAGTCC
SLAMF8 FWD	TGAGGCTATCTGGCGATCTCT
SLAMF8 REV	CTGGGCACTGCATCGTACA
CD86 FWD	GGAGCCTTAGGAGGTACGGG
CD86 REV	ACTCAGTCCCATAGTGCTGTCA
164 PCR yRNA4 FWD	GTGTTCGTGGGTGAGGAGTT
166 Sequencing yRNA4	CGTTTCTATTGCTGGGCATT
SeqI PCR yRNA4 REV	CTGCCCAGGAATCAGCTTT
ActB FWD	CACCATTGGCAATGAGCGGTTC
ActB REV	AGGTCTTTGCGGATGTCCACGT
GAPDH FWD	GTCTCCTCTGACTTCAACAGCG
GAPDH REV	ACCACCCTGTTGCTGTAGCCAA
Y1_loop-F	GATCGAACTCCTTGTTCTACTC
Y1_loop-F	AGATTTCTTTGTTCCTTCTCCACTC
Y1_loop-F	GTGTCACTAAAGTTGGTATACAAC
Y1_loop-F	GTTAAGTTGATTTAACATTGTCTC
hsa-miR-21-5p	TAGCTTATCAGACTGATGTTGA

7.1.7. Antibody for TEM

HLA-DR/DP Antibody (MEM-136)	Santa Cruz Biotechnologies, Dallas

7.1.8. Equipment

Vi-CELL XR	Beckman Coulter, Brea
BD LSRFortessaTM	BD Biosciences, Franklin Lanes
Centrifuge 5810 R	Eppendorf, Hamburg

Centrifuge cell culture	
SW40T rotor	Beckman Coulter, Brea
Ultracentrifuge	
Western Blot Transfer device	Bio-Rad Laboratories, Hercules
Qubit fluorometer	Thermo Fisher Scientific, Waltham
Nanosight LM10	Malvern Instruments, Worcestershire
MACS Magnet and stand	Miltenyi Biotec, Bergisch Gladbach

7.1.9. Database, resources and softwares

NCBI Ensembl Genome	https://www.ensembl.org/index.html
NCBI Blast	https://blast.ncbi.nlm.nih.gov/Blast.cgi
PubMed	https://pubmed.ncbi.nlm.nih.gov/
Exocarta	http://www.exocarta.org/
Metascape	https://metascape.org/gp/index.html
Panther	http://www.pantherdb.org/
Interactivenn	http://www.interactivenn.net/
R	https://www.rstudio.com/
FlowJo	https://www.flowjo.com/
Prism	https://www.graphpad.com/scientific-software/prism/
BD FACSDiva™ Software	BD Biosciences, Franklin Lanes
TIDE	https://tide.nki.nl/
ChopChop	https://chopchop.cbu.uib.no/

7.2. Methods

7.2.1. Cell lines and cell culture conditions

7.2.1.1. Cell lines characteristics

The following cell lines were used for the project:

MEC1	B-cell Chronic Lymphocytic Leukemia (CLL) cell line derived from a 58-year-old male patient. The MEC-1 cell line is Epstein-Barr-Virus positive. The MEC-1 cell line is a suspension cell line characterized by the surface expression of CD19, CD20 and HLA-DR among other markers. MEC1 cells are characterized by a mutation of the IGVH genes and an overexpression of Bcl2 and Bax overexpression[316]
HG3	B-cell Chronic Lymphocytic Leukemia cell line derived from a 70-year-old male patient. The HG-3 cell line is Epstein-Barr-Virus positive. The HG-3 cell line is a suspension cell line characterized by the surface expression of CD5, CD19, CD20, CD80 and HLA-DR among other markers. HG-3 cells are IGVH unmutated and carry a 13q14 deletion[317]
TCL1-355	The TCL1-355 cell line was immortalized from the splenocytes of a Eμ-TCL1 murine model of CLL by triple-knockdown of CDKN2A, CDKN2B and TP53. [318]

7.2.1.2. Preparation of sEV-free Fetal Calf Serum (FCS)

To produce sEV-free FCS, FCS (Sigma-Aldrich) was centrifuged at 100,000*g* for 18 hours at 4°C. The supernatant was collected, and the pellet containing sEVs discarded. The FCS supernatant was then filtered two times using a 0.22µm vacuum filtration unit. Efficient depletion of sEVs in FCS was regularly checked by NTA.

7.2.1.3. Cell culture in classical flasks

The cell lines were obtained from previously frozen vials stored in liquid nitrogen in the lab. Mycoplasma contamination was frequently checked using the Mycoplasma Testing Service offered by Eurofins Scientific. Cells were seeded in T150 flasks at a concentration of $0{,}5.10^6$ cells/mL in RPMI medium supplemented by 10% FSC *or* sEV-free FCS supplemented with Penicillin (10U/mL), Streptomycin (10µg/mL) (Gibco, 11548876) and L-Glutamin (2mM, Gibco, 11539876). All cells were incubated in a 10% CO_2 incubator at 37°C and passed every 2 to 3 days. Cell viability and concentration was assessed using a Vicell XR Cell Viability Analyzer (Beckman Coulter, Germany).

7.2.1.4. Cell culture in CellLINE 1000 bioreactor flask

The CellLINE 1000 bioreactors are compartmentalized in two: the upper part – the “medium compartment” - presents a volume capacity of 500mL and the lower part – the “cell compartment” – 15mL. The two compartments are separated by a 10 kD molecular weight cut-off membrane, corresponding to a particle radius of approximatively 1.59nm. Therefore, the membrane retains the bigger proteins as well as vesicles secreted by the cells in the cell compartment, whereas nutrients (glucose, glutamine etc.) can be transferred from the medium compartment to the cell compartment. As a result, vesicles are collected in a non-diluted volume, which is easier for further processing of the supernatant and isolation of sEVs. For the culture, a total of 20-40.10^6 MEC-1 or HG-3 cells were resuspended in 15mL of sEV-free medium and seeded into the cell compartment. The medium compartment was filled with RPMI medium supplemented with Penicillin (10U/mL), Streptomycin (10µg/mL) (Gibco, 11548876) and L-Glutamin (2mM, Gibco, 11539876). The flask was placed into a 10% CO_2-incubator at 37°C. The medium was changed, and the cells were passed every 5 to 7 days.

7.2.1.5. Collection of supernatants from murine spleens and human lymph nodes

Spleen from adopted transferred Eµ-TCL1 animals

Eµ-TCL1 mice on C57BL/6 background were kindly provided by Carlo Croce (Ohio State University). For the adoptive transfer of C57BL/6 recipient animals, B-cells enriched from the spleen of primary Eµ-TCL1 animals and cryopreserved in the biobank of the team were used. For the adoptive transfer of Eµ-TCL1 tumors, 1–2.10^7 of Eµ-TCL1 B-cells were transplanted intraperitoneally (*i.p.*) into C57BL/6 WT animals (Charles Rivers). Tumor load was monitored in the blood weekly: briefly, blood was collected from the submandibular vein, and erythrocytes lysed in ACK (Ammonium-Chloride-Potassium) buffer. Cells were washed in PBS and resuspended in PBS supplemented with 2% FCS (2% FCS-PBS). Cells were stained with a panel including a viability dye, anti-CD45, anti-CD5 and anti-CD19 antibodies for 30 minutes on ice, protected from light. Cells were washed in 2% FCS-PBS, resuspended in 100-200 µL of 2% FCS-PBS, and directly analysed on a BD LSRFortessa™ Cell Analyzer (BD Biosciences). The tumor load was assessed as the proportion of CD5+ cells among viable CD45+CD19+ cells as show in Figure 8. Animals with a tumor load superior to 85% were sacrificed for spleen isolation. The spleens were manually dissociated using a 40µm cell strainer and a plunger. All animal experiments were carried out according to institutional and governmental guidelines approved by the local authorities (Regierungspräsidium Karlsruhe, permit number G98/16, approved on 13 July 2016).

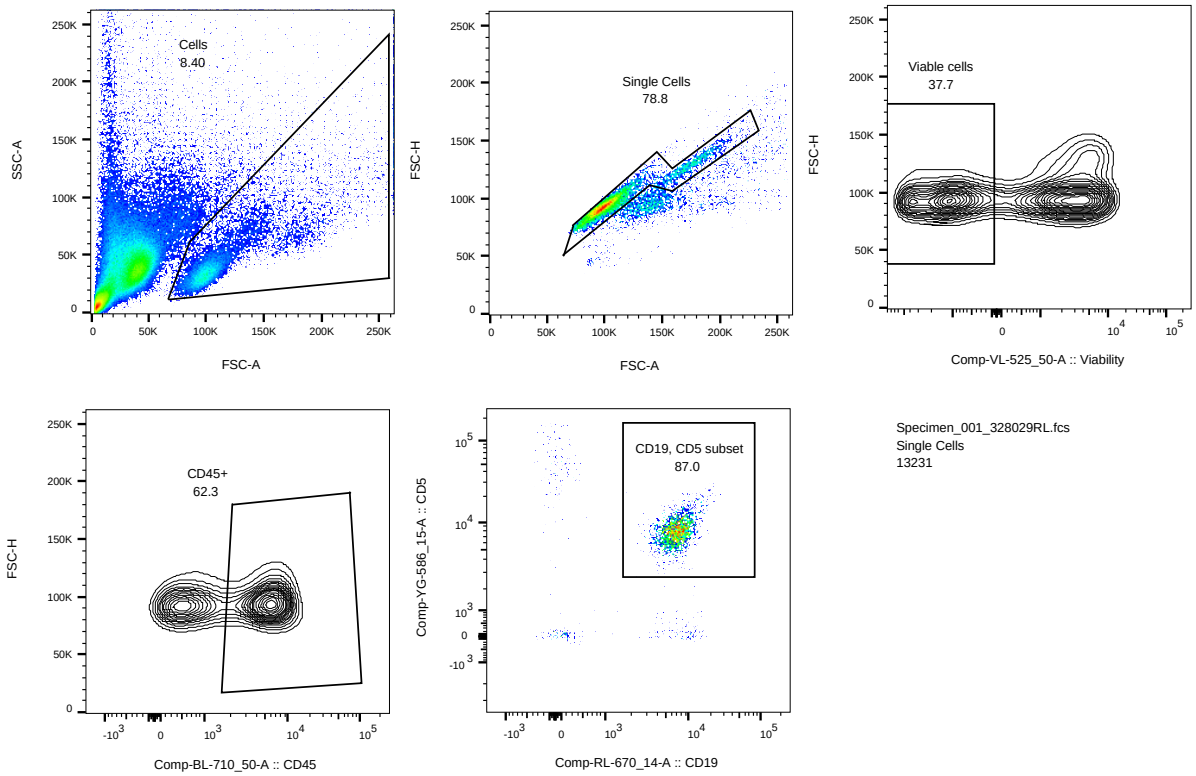

Figure 8: Gating strategy to assess the tumor load. Peripheral blood cells were stained for viability, CD45, CD19 and CD5. The tumor load was assessed as the percentage of $CD19^{+}CD5^{+}$ cells among all $CD45^{+}$ cells.

Lymph node supernatants

Following resection, lymph nodes pieces were collected and processed in the lab of our collaborator, Prof. Dr. med. Sascha Dietrich. Briefly, the lymph nodes were cut in small pieces using scissors in sEV-free medium and mechanically dissociated using a mortar and pestle until obtention of single cell suspensions. Following centrifugation at 300*g* for 10 minutes at 4°C, the supernatant was collected and handed to us. Transport of the supernatants was performed on ice.

7.2.2. Isolation of sEVs

7.2.2.1. Differential centrifugation

The protocol was adapted from a previously established protocol in the lab. To remove cell debris, supernatants from cell lines, murine spleens or human lymph nodes were centrifuged at 300*g* for 10 minutes at 4°C. Supernatants were collected and centrifuged at 2000x g for 20 min at 4 ◦C. The supernatants were collected and the pellets containing apoptotic bodies were discarded. To separate sEVs and proteins from microvesicles, the supernatants were centrifuged at 10,000× g for 40 min at 4 ◦C. The supernatants were collected and transferred into ultracentrifugation tubes and centrifuged at 100,000× g for 2h at 4 ◦C using a Swinging-Bucket Rotor. Resulting 100,000× g pellets were resuspended in 200µL of 0.22-µm-filtered

PBS. The preparations were applied on a sucrose cushion (see part B) or on a Size-Exclusion Chromatography (SEC) column.

7.2.2.2. sEV isolation on a sucrose density cushion

Following the differential centrifugation, preparations containing sEVs and soluble proteins were diluted with 0.22-µm-filtered PBS to reach a volume of 7mL. The diluted preparation was applied onto 4mL of a 40% sucrose cushion with a density of 1.12 g/mL, and centrifuge at 100,000x g for 2h at 4°C. Following the ultracentrifugation, two phases could be observed: the upper phase, containing the proteins (~6,5mL) was discarded, and the second phase containing sEV (~3,5mL) was transferred in a new ultracentrifuge tube. The pellet containing proteins complexes of high molecular weight was discarded. The sEVs were washed in 0.22-µm-filtered PBS by a final centrifugation at 100,000g for 2h at 4°C. The supernatant was discarded and sEVs resuspended in 0.22-µm-filtered PBS.

7.2.2.3. sEV isolation using single qEV columns from IZON, France.

Following the differential centrifugation, preparations containing sEVs and soluble proteins were applied onto commercially available SEC columns (IZON qEV single column). The samples were allowed to enter the column, and then the column was filled with 0.22µm-filtered PBS. Elution fractions were collected from the moment the preparations were applied onto the column as following: a first fraction of 1mL was collected corresponding to the void volume of the column, and then 7 fractions of 250µL were collected.

7.2.3. Validation of sEV preparations

7.2.3.1. Analysis of sEV preparations by Nanoparticle Tracking Analysis

sEV preparations were diluted 1:500 to 1:2000 in 0.22-µm-filtered PBS, to reach a final volume of 1mL and analysed on a Nanosight LM-10 (Malvern Panalytical). Camera level and detection threshold were set up at 13 and 5, respectively. The absence of background was verified using 0.2-µm-filtered PBS. For each sample, 1-3 videos of 30-60s each were recorded and analysed using the NTA 3.0 software version (Malvern Instruments).

7.2.3.2. Immunoblotting

The following part was extracted from Bordas et al. IJMS 2020 and was written in collaboration with Geraldine Genard.

[sEVs and respective parental cells were lysed in RIPA buffer (Abcam, Cambridge, UK), and whole protein lysates were quantified via BCA™ Protein Assay Kit (Thermo Fisher Scientific Inc., USA). Per lane, 2.8 µg (human samples) to 3.4 µg (mouse samples) of protein were

loaded onto 10% polyacrylamide gels. Following SDS-PAGE and protein transfer, membranes were blocked in 5% bovine serum albumin in Tris-buffered saline (TBS)-Tween 0.1%, and primary antibodies against FLOTILLIN-1 (1:1,000, Cell Signaling Technology, Danvers, MA, USA #18634), CD81 (1:400, ProSci Inc., San Diego, CA, USA #5195), CD9 (1:1,000, Cell Signalling Technology, Danvers, MA, USA #13174), TSG101 (1:1.000, BD Bioscience, San Jose, CA, USA #612697), ALIX (1:1,000, Cell Signalling Technology, Danvers, MA, USA #2171) CALNEXIN (1:500, GeneScript #A0124040), CYTOCHROME C (1:750, GeneScript, Piscataway, NJ, USA#A0150740), GM130 (1:1,000, Cell Signaling Technology, Danvers, MA, USA #12480), ATP5A (1:1,000, Abcam, Cambridge, UK #ab14748) were used in indicated dilutions in 5% bovine serum albumin in TBS-Tween 0.1%. Signals were visualized after secondary antibody hybridization by chemiluminescence detection reagent (Bio-Rad Lab, Hercules CA, USA #1705061) with GE Healthcare Amersham Imager 600 (GE Healthcare, Chicago, IL, USA).]

7.2.3.3. Analysis of sEV by Transmission Electron Microscopy.

The following part was extracted from Bordas et al. IJMS 2020 and was written in collaboration with Michelle Nessling and Karsten Richter from the DKFZ Electron Microscopy platform.
[sEV fractions were adsorbed onto glow discharged carbon coated grids, washed in aqua bidest and negatively stained with 2% aqueous uranyl acetate. For immuno-EM, carbon-coated formvar grids were used and the immune reaction was performed after buffer wash including incubation with blocking agent (Aurion, Wageningen, The Netherlands), dilution series of primary antibody HLA-DR (Santa Cruz, Dallas, TX, USA #sc-51618) and Protein A-Au reporter (CMC, UMC Utrecht, The Netherlands). Micrographs were taken with a Zeiss EM 910 or EM 912 at 100 kV (Carl Zeiss, Oberkochen, Germany) using a slow scan CCD camera (TRS, Moorenweis, Germany).]

7.2.3.4. Analysis of sEV protein content

Using Bisynchronic Assay (BCA)

In a 1.5mL centrifuge tube, a 9µL aliquot was collected from the sEVs preparation, diluted with 1µL of 10X 10X radioimmunoprecipitation assay buffer (RIPA; Abcam ab156034), briefly vortexed, and incubated on a rotating wheel at 4°C for 30 min. Following the incubation, the aliquots were centrifuged at 16,000x g at 4°C for 20 min. The supernatant was collected and used for BCA following manufacturer's instructions (Thermo Fisher, 23225).

Using Qubit Protein assay

In a 1.5mL centrifuge tube, a 9µL aliquot was collected from the sEVs preparations, diluted with 1µL of 2%-SDS, briefly vortexed, and incubated on ice for 20 min. Following the

incubation, the aliquots were centrifuged at 16,000x g at 4°C for 20 min. The supernatant was collected and used for Qubit protein quantification following manufacturer's instructions (Invitrogen Q33211).

7.2.4. Storage of sEV preparations

Initially, sEVs were stored at -80°C following isolation. These preparations are referred as "frozen" sEVs in the Results section. As it was observed during the project that the freezing step impact their functionality (See part X), the storage conditions were modified. For functional assays, sEVs preparations were isolated up to 7 days prior the day of the experiment and kept at 4°C. These preparations are referred as "fresh" sEVs. However, sEVs preparations aimed to be used for the isolation of proteins of small RNAs were kept at -80°C until processing.

7.2.5. Patients' informations

SampleID	Gender	Year of birth	Diagnosis	Classification	% Ki-67 positivity in malignant cells	Notes	Date of first diagnosis	Prior Therapy	Date of Surgery	Size of the collected piece of LN	Number of cells isolated
20LN0211	F	1974	rLN		NA				28/01/20	1 small piece	>1x10^8
20LN0250	M	1949	No malignancy found in this LN	SLL/CLL diagnosed after transbronchial needle	NA		05 2020		26/06/20	1 very small piece	2x10^7
20LN0252	M	1981	rLN		NA	Dermatopathic? Tattoo-associated?			09/07/20	1 small piece	>1x10^8
20LN0253	F	1977	rLN		NA				10/07/20	1 small piece	3x10^7
20LN0242	M	1957	DLBCL	GCB unknown; CD20-CD30+	80	Progression; St.p. CHOP 2019/20 -> PR	09 2019	Chemotherapy	02/06/20	1 big piece	5x10^7
20LN0251	M	1966	DLBCL	non-GCB	90	Relapse; St.p. R-CHOEP + Radiotherapy 2013 -> CR	01 2013	Chemoimmunotherapy and radiotherapy 2013	30/06/20	1 big piece	>5x10^8
20LN0230	M	1962	DLBCL	non-GCB	80	Relapse; St.p. R-CHOP, R-DHAP, ASCT 2019	01 2017	Multiple chemoimmunotherapies	22/04/20	1 small piece	2x10^6
20LN0265	M	1940	DLBCL	non-GCB	95		09 2020	None	26/08/20	1 medium piece	>1x10^8
20LN0229	M	1942	FL	Grade 1/2	20		04 2020	None	20/04/20	1 big piece	>5x10^8
20LN0254	M	1936	FL	Grade 1/2	30	Relapse; St.p. t-FL 2005 and 2011	04 2002	Multiple chemoimmunotherapies	13/07/20	1 medium piece	>1x10^8
20LN0261	F	1948	FL	Grade 1/2	30		08 2020	None	18/08/20	1 small piece	4x10^6
20LN0267	F	1962	FL	Grade 3a	70		10 2018	None	09/09/20	1 medium piece	1x10^8

Table 7: Characteristics of patients whose LN were used for sEV isolation and further proteome analysis, including the gender of the patients, year of birth, characterized disease in the collected biopsy sample as provided by the pathology department, prior treatment and year of diagnosis as well as information regarding the size of the collected piece of LN.

7.2.6. Isolation of proteins from sEVs for Mass-Spectrometry analysis

sEVs preparations were thawed on ice. 10X RIPA was added to the preparations to obtain a final concentration of 1X. The preparations were vortexed for 5 sec and incubated for 30 min at 4°C on a rotating wheel. The preparations were then centrifuged at 16,000x *g* for 20 min at 4°C. The supernatant containing proteins were collected in new 1.5mL tubes, and an aliquot collected for protein quantification using BCA protein quantification. The proteins were kept at -80°C until analysis.

7.2.7. Isolation of RNA and small RNA from cells and sEVs

The total RNA was isolated from cell pellet or sEV preparations using the RNeasy® Mini kit and following the manufacturer's instructions (Qiagen, Hilden). For sEV preparations, an equal volume of RLT buffer was mixed to the sEV preparations.

7.2.8. Northern-blot Analysis of yRNA4 enrichment

150ng of denatured RNA from parental cells was loaded per lane on 15% Tris/boric acid/EDTA (TBE)-urea gels and polyacrylamide gel electrophoresis (PAGE) was performed. Ethidium bromide staining was performed to visualize RNA on gels. Gels were washed in TBE buffer and samples were transferred to Hybond-N+ nylon membranes by semi-dry electro-blotting. A 32nt antisense oligonucleotide probe against the 5' end of hY4 (5'- AGTTCTGATAACCCACT ACCATCGGACCAGCC-3')[319] was labelled with 20 pmol [γ32-P]ATP (corresponding to 120 µCi) and used for detection of full- length hY4. T4 polynucleotide kinase allowed the labelling of 10 µM oligonucleotide probe. Samples were incubated for one hour at 37 □C, then inactivated for 10 min at 68 □C and purified on G25 microspin columns. Membranes were incubated in UltraHyb oligo hybridization buffer for 30 min at 37 □C, and the oligonucleotide probe applied for one hour at 37 □C. Membranes were washed twice in washing buffer 1 for 5 min at 37 □C, and in washing buffer 2 for 10 min at RT. The signals were obtained by development on radiography film.

7.2.9. Real-time quantitative Polymerase Chain Reaction (RT-qPCT)

RNA was extracted from the cell pellet of myeloid cells incubated for 8 hours with TEXs, yRNA4 or Effectene using the RNEasy kit (Qiagen, Hilden, Germany). Reverse transcription was performed with the SuperScript™ II Reverse Transcriptase from ThermoFisher (Waltham, MA, USA). Real-time quantitative Polymerase Chain Reaction was performed using the SYBR™ Green Master Mix (ThermoFisher, Waltham, MA, USA). The sequence of primers can be found below.

CR2 Fwd	GGTCCTCGGGATTTCTTGTGG
CR2 Rev	GAACAACTGTACCTTATCACGGT
CCL22 Fwd	ATCGCCTACAGACTGCACTC

CCL22 Rev	GACGGTAACGGACGTAATCAC
IL5 Fwd	TGGAGCTGCCTACGTGTATG
IL5 Rev	TTCGATGAGTAGAAAGCAGTGC
NT5E Fwd	GCCTGGGAGCTTACGATTTTG
NT5E Rev	TAGTGCCCTGGTACTGGTCG
CD86 Fwd	CTGCTCATCTATACACGGTTACC
CD86 Rev	GGAAACGTCGTACAGTTCTGTG
SLAMF8 Fwd	AGCCCTACTTCCCATTACAGT
SLAMF8 Rev	AGAGATCGCCAGATAGCCTCA
IL12A Fwd	CCTTGCACTTCTGAAGAGATTGA
IL12A Rev	ACAGGGCCATCATAAAAGAGGT
CCL3 Fwd	CGGTGTCATCTTCCTAACCA
CCL3 Rev	GACATATTTCTGGACCCACTC
CSF3 Fwd	GCTGCTTGAGCCAACTCCATA
CSF3 Rev	GAACGCGGTACGACACCTC
CSF3 Fwd	GCTGCTTGAGCCAACTCCATA
CSF3 Rev	GAACGCGGTACGACACCTC
TNR5 Fwd	CACACTGCCACCAGCACAA
TNRF Rev	GCCTTCTTCACAGGTGCAGAT
ActB Fwd	CACCATTGGCAATGAGCGGTTC
ActB Rev	AGGTCTTTGCGGATGTCCACGT
GAPDH Fwd	GTCTCCTCTGACTTCAACAGCG
ActB Rev	ACCACCCTGTTGCTGTAGCCAA

7.2.10. Real-time quantitative Polymerase Chain Reaction (RT-qPCT) for small RNA

Reverse transcription of RNA was performed with the miScript RT II kit (Qiagen, Hilden) using the HiFlex buffer and according to the manufacturer's instructions. 12µL of RNA was used per reaction. The obtained cDNA was quantified by Nanodrop (ThermoFisher, Waltham). For the RT-qPCR, the miScript SYBR Green PCR Kit was used (Qiagen, Hilden). For each reaction between 100 and 500ng of cDNA was used. The primers were described elswhere[320]. The following program was used:

Hold Stage	95°C 15min
PCR stage (50 cycles)	95°C 10sec 57°C 30sec 72°C 30sec
Melt Curve Stage	95°C 15sec 60°C 1min 95°C 15sec

The expression of the different yRNAs in sEVs were normalized to MiR-21 and compared between the HG3-derived and HG3 yRNA4-KO-derived sEVs using the ΔΔCt approach.

7.2.11. Functional assay on human myeloid cells

7.2.11.1. Isolation of myeloid cells

Peripheral blood buffy coat samples from healthy donors were obtained from the Institute for Clinical Transfusion Medicine and Cell Therapy (IKTZ, Heidelberg, Germany). Peripheral Blood Mononuclear cells (PBMCs) were isolated via Ficoll density separation. In brief, the blood was diluted 1:1 with PBS at room temperature (RT). 50mL Leucosep tubes were filled with 15mL of Ficoll (ref) and briefly centrifuge to allow the Ficoll solution to cross the porous membrane. 36mL of diluted blood were carefully added to the Leucosep tubes. The Leucosep tubes were then centrifuged at 1000x g for 20 minutes at RT without brake. The upper plasma phase was carefully removed and the PBMC layer collected in a new 50mL tube. The PBMCs were washed in PBS two times at 300x g for 10 minutes at 4°C. PBMCs pellets were then resuspended in ice-cold MACS Running buffer and automatically counted. PBMCs were labelled by CD14 MicroBeads (Milteny Biotech) instruction and CD14-positive myeloid cells enriched by positive magnetic selection following the manufacturer's instructions.

7.2.11.2. Experiment design

Myeloid cells were resuspended in RPMI medium supplemented with 10% of heat-inactivated FCS, 1% Penicillin/Streptomycin, 1% L-glutamin and 100ng/mL of hM-CSF. 200.10^3 myeloid cells were seeded per well in 48-well plates. Cells were treated with indicated amount of sEVs, full-length yRNA4 packaged in effectene, effectene or left untreated and incubated at 37°C. After an incubation of 8 hours, cells were harvested and the expression levels of PD-L1, CD54, HLA-DR and CCR2 were assessed by flow cytometry using a BD LSRFortessa™ Cell Analyzer (BD Biosciences) after gating on viable CD14+ cells.

7.2.11.3. Analysis of myeloid cells signature by antibody microarray (Sciomics).

Protein extraction, sample labelling and analysis on antibody microarrays was performed by Sciomics (Neckargemünd, Germany). Each protein was recognized by one or more antibodies, present in four replicates in the microarray. Raw data were analyzed using the LIMMA package of R-Bioconductor using the median signal intensities.

7.2.12. Functional assay on murine myeloid cells

7.2.12.1. Isolation of myeloid cells

Female WT, Myd88$^{-/-}$, or TLR7$^{-/-}$ C57BL/6 mice were sacrificed by CO_2 inhalation followed by cervical dislocation. Each experiment included at least 3 animals per condition. Femurs, tibias, and hips bones were isolated and kept in 2% FCS-PBS on ice until the next step. The bones were crushed in 2% FCS-PBS using a mortar and pestle and the supernatant filtered through a 40µm-strained. The cells were centrifuged at 300x g for 10 min at 4°C, the supernatant discarded. For the lyse of erythrocytes, the cell pellets were resuspended in ACK buffer and incubated at room temperature (RT) for 7 min. The cells were washed in 2% FCS-PBS and resuspended in autoMACS Running buffer. Myeloid cells were isolated by magnetic depletion using the EasySep™ Mouse Monocyte Isolation Kit and following the manufacturer's instructions.

7.2.12.2. Experiment design

Myeloid cells were resuspended in RPMI medium supplemented with 10% of heat-inactivated FCS, 1% Penicillin/Streptomycin, 1% L-glutamin and 100ng/mL of hM-CSF. 50-200.10^3 myeloid cells were seeded per well in 48-well plates. Cells were treated with indicated amount of sEVs, full-length yRNA4 packaged in effectene, effectene or left untreated and incubated at 37°C. After an incubation of 8 hours, cells were harvested and the expression levels of PD-L1, CD54, HLA-DR and CCR2 were assessed by flow cytometry using a BD LSRFortessa™ Cell Analyzer (BD Biosciences).

7.2.13. Flow-cytometry data acquisition and analysis

Myeloid cells were manually harvested by pipetting, washed by centrifugation, and resuspended in 50µL PBS supplemented by FC-block (BD, 564219) for human samples or PBS supplemented with 2% of Rat serum for murine samples. Samples were stained in a 96-cell plate, for 30 min on ice, protected from light. Following the incubation, the samples were washed with PBS, centrifuged, and resuspended in 50µL of MACS Running buffer (Milteny, 130-091-221). Appropriate FMO controls were prepared. Single-stain controls were prepared using UltraComp eBeads™ (ThermoFisher, 01-2222-41). Cells were directly analysed on a BD LSRFortessa™ Cell Analyzer (BD Biosciences).

7.2.14. Analysis of TLR4 and TLR2 activation using HEK reporter cells

TEXs were isolated by differential centrifugation combined to size exclusion chromatography as previously described and validated by Transmission Electron Microscopy, Nanoparticle

Tracking analysis and Qubit protein quantification (Thermofisher) as previously described[321]. 5x104 HEKBlue cells were seeded into a 96-well plate in 200 µL of HEKBlue Detection medium. Indicated doses of TEXs or positive control were added to the wells. For TLR2 reporter cell line, FSL-1 was used as a positive control at a concentration of 10 ng/mL; for TLR4 reporter cell line, LPS-B5-U was used as a positive control at a concentration of 10 ng/mL. The cells were incubated for 7 hours at 37°C, transferred to a SyngeryMX Reader where plate was read at 630nm every 2 minutes for up to 24 hours.

7.2.15. Mass Spectrometry analysis of LN-derived sEVs

For the timsTOF Pro PASEF acquisition, peptides were separated using the Easy nLC 1200 system fitted with an analytical column (Aurora Series Emitter Column with CSI fitting, C18, 1.6 µm, 75 µm x 25 cm) (Ion Optics). The outlet of the analytical column with a captive spray fitting was directly coupled to a timsTOF Pro (Bruker) mass spectrometer using a captive spray source. Solvent A was ddH2O (Biosolve Chimie), 0.1% (v/v) FA (Biosolve Chimie), 2% acetonitrile (ACN) (Pierce, Thermo Scientific), and solvent B was 100% ACN in dH2O, 0.1% (v/v) FA. The samples were loaded at a constant pressure. Peptides were eluted via the analytical column at a constant flow of 0.4 µL per minute at 55°C. During the elution, the percentage of solvent B was increased in a linear fashion from 4 to 17% in 30 minutes, then from 17 to 29% in 15 minutes, then from 29 to 37.5% in a further 5 minutes, and then to 100% in 10 minutes. Finally, the gradient was finished with 2.5 minutes at 4% solvent B to equilibrate the column. Peptides were introduced into the mass spectrometer via the standard Bruker captive spray source at default settings. The glass capillary was operated at 3500 V with 500 V end plate offset and 3 L/minute dry gas at 180°C. Full scan MS spectra with mass range m/z 100 to 1700 and a 1/k0 range from 0.85 to 1.3 V*s/cm2 with 100 ms ramp time were acquired with a rolling average switched on (10x). The duty cycle was locked at 100%, the ion polarity was set to positive, and the TIMS mode was enabled. The active exclusion window was set to 0.015 m/z, 1/k0 0.015 V*s/ cm2. The isolation width was set to mass 700-800 m/z, width 2 – 3 m/z and the collision energy to 1/k0 0.85-1.3 V*s/ cm2, energy 27- 45 eV.
The resulting raw spectral data were further analyzed with MaxQuant (version 1.6.17.0) using default settings.

For the analysis, the proteins were manually ranked per sample for the most enriched to the less enriched. Proteins present in 3 out of 4 samples per group were used to perform a Venn diagram. Pathway enrichment analysis was performed using the Metascape platform.

7.2.16. Knock-out of yRNA4 in HG3 cell lines

7.2.16.1. Design of the guide RNAs

The genome location and sequence of the human yRNA4 sequence was found on the Grch38.p13 version of the human genome available on the Ensembl website

(www.ensembl.org/). The yRNA4 gene is located on the forward strand of chromosome 7 and is located at the following position: chr7:148,963,315-148,963,410. The FASTA sequence of the yRNA4 flanked of its 1000 upstream and downstream bases was extracted for guide RNAs design. The guide RNA sequences were designed using the Chopchop website (http://chopchop.cbu.uib.no/). In total, we selected 6 guide RNAs to target the 5' region of yRNA4 and 6 guide RNAs to target the 3' region of yRNA4. The strategy of using to guide RNAs was preferred over a single guide RNA. Indeed, yRNA4 is a non-coding small RNA whose transcript is found in the mammalian cells either as full-length or fragment, with fragments having biological effects. Therefore, inducing a single double-strand break in the middle of the gene would not ensure a total inhibition of all the gene products. The sequence of the forward and reverse primers used for the cloning of the guide RNA is presented in Table X. The guide RNAs were selected based on their specificity for the region, to avoid off-targets; and their predicted efficiency. The targeted strand was not taken into consideration as the Cas9 induce double-stranded breaks.

Guide RNA	Primer name	Primer sequence	Target	Strand	GC content	MM0	MM1	MM2	MM3	Predicted efficiencv
1	RNY4-3-1-FWD	caccGCCGTTGTCCTCAAACAAGG	Targetting the 3' downstream sequence of yRNA4	+	55	1	0	0	3	68.97
	RNY4-3-1-REV	aaacCCTTGTTTGAGGACAACGGC								
2	RNY4-3-2-FWD	caccGAGGACAACGGCCCCGACTG		-	70	1	0	0	3	57.17
	RNY4-3-2-REV	aaacCAGTCGGGGCCGTTGTCCTC								
3	RNY4-3-3-FWD	caccGGGGCCGTTGTCCTCAAACA		+	60	1	0	0	4	56.50
	RNY4-3-3-REV	aaacTGTTTGAGGACAACGGCCCC								
4	RNY4-3-4-FWD	caccGTTCTGTGCAAACGCAAAGC			50	1	0	0	5	53.13
	RNY4-3-4-REV	aaacGCTTTGCGTTTGCACAGAAC								
5	RNY4-3-3-FWD	caccAAACGCAAAGCTGGCGGACA		-	55	1	0	0	5	52.20
	RNY4-3-3-REV	aaacTGTCCGCCAGCTTTGCGTTT								
6	RNY4-3-6-FWD	caccAACGGCCCCGACTGAGGCTC		-	70	1	0	0	5	25.37
	RNY4-3-6-REV	aaacGAGCCTCAGTCGGGGCCGTT								
7	RNY4-5-1-FWD	caccAATAGACGTAAATTACCAAA	Targetting the 5' upstream sequence of yRNA4	_	25	1	0	0	10	51.43
	RNY4-5-1-REV	aaacTTTGGTAATTTACGTCTATT								
8	RNY4-5-2-FWD	caccGTGGCTACTCTAAATAAGTT		_	35	1	0	1	10	43.73
	RNY4-5-2-REV	aaacAACTTATTTAGAGTAGCCAC								
9	RNY4-5-3-FWD	caccAAGGACAAGAGGCTTCCATT		+	45	1	0	0	13	55.52
	RNY4-5-3-REV	aaacAATGGAAGCCTCTTGTCCTT								
10	RNY4-5-4-FWD	caccATGTCTTCAGGTATTTGCAA		+	35	1	0	1	15	59.52
	RNY4-5-4-REV	aaacTTGCAAATACCTGAAGACAT								
11	RNY4-5-5-FWD	caccAAATAAATGTAGTTGCATGA		-	25	1	0	0	22	50.01
	RNY4-5-5-REV	aaacTCATGCAACTACATTTATTT								
12	RNY4-5-6-FWD	caccGAAGATAATCAGATAATGTA		+	25	1	0	0	25	49.63
	RNY4-5-6-REV	aaacTACATTATCTGATTATCTTC								

Table 8: List of guide RNA primers used for the deletion of yRNA4 by CRISPR/Cas9, including the targeted strand, GC content, mismatches required for a possible off-target effect and predicted efficiency as calculated by the ChopChop online tool.

7.2.16.2. Cloning of the gRNA into the plasmid

The protocol was adapted from the CRISPR Zhang Lab protocol.
In a first step, corresponding forward and reverse oligonucleotides were phosphorylated and annealed.

The reaction mix was prepared as followed:

1µL forward oligonucleotide (100µM)
1µL reverse oligonucleotide (100µM)

1µL 10X T4 Ligation Bugger
6.5µL ddH2O
0.5µL T4 Polynucleotide Kinase (New England Biolabs, M0201S)

10µL (Total volume)

The thermocycler program was set up as followed:

37°C 30 minutes
95°C 5 minutes
To 25°C by decreasing of 5°C per minutes.

The digestion of the plasmid and the integration of the annealed oligonucleotides into the pX458 plasmid vector by ligation were performed in a one-step reaction.

The reaction mix was prepared as followed:

100ng pX458 vector
2µL of annealed oligonucleotides diluted 1:250 in ddH2O
2µL of 10X FastDigest Buffer
1µL of DTT
1µL of ATP
1µL of FastDigest *BbsI* enzyme
0.5µL T7 DNA Ligase
XµL ddH2O

20µL (Total volume)

The thermocycler program was set up as followed:

37°C 5 minutes
23°C 5 minutes
Run the program for 6 cycles

4°C Hold

7.2.16.3. Transformation of competent bacteria and plasmid production

One Shot™ TOP10 Chemically Competent (Thermo Fisher) were used for the transformation by heat shock, following manufacturer's instructions. Ampicillin-Agar plates were streaked using 20µL of competent cells and incubated overnight at 37°C. Single colonies were picked up the following day and used for overnight cultures in 4mL of LB broth supplemented with Ampicillin at a concentration of 100µL/mL. The plasmids were isolated using the QIAgen Spin Miniprep Kit (27104) following manufacturer's instructions. The plasmids' quality and concentration were assessed using a Nanodrop 2000 (Thermo Fisher).

7.2.16.4. Transfection of HEK-293 cells to assess gRNA efficiency

HEK-293 cells were used to assess the gRNA efficiency. Transfection of HEK-293 cells was performed using Lipofectamine LTX & PLUS reagent (Invitrogen) following manufacturer's instructions for 6-well plates. 2.5µg of plasmid containing gRNA or the pMAX plasmid was used per well. After a 48-hour incubation, the cells were collected, and GFP-positive cells sorted on a BD Facs Aria (`??) sorter. DNA from sorted cells was extracted using the QIAamp DNA Mini Kit (Qiagen, 51304) following manufacturer's instructions. DNA were quantified on a Nanodrop 2000. The locus of interest was amplified by PCR as described below:

12.5µL Hot Start 2X Master Mix (New Englends Biolabs, M0496S)
2.5µL forward primer (10µM) GTGTTCGTGGGTGAGGAGTT
2.5µL reverse primer (10µM) CTGCCCAGGAATCAGCTTT
100ng of DNA
ddH_2O
Total Volume = 25µL

The program was set up as followed :

95°C	3 minutes
95°C	30 seconds
60°C	30 seconds
72°C	2 minutes
→ Repeat for 35 cycles	
72°C	5 minutes
4°C	Hold

The PCR products were run on a 2% Agarose-gel and the fragments were isolated using the Monarch® DNA Gel Extraction Kit (New England Biolabs, T1020S), according to manufacturer's instructions. PCR products were sequenced using the Sanger sequencing service from Eurofins Genomics. The efficiency of each gRNA in inducing insertions-deletions was assessed using the online TIDE program (https://tide.nki.nl/).

7.2.16.5. Electroporation of HG-3 cells

HG-3 cells were electroporated using a Neon Transfection System. HG-3 cells were passed one day prior the electroporation. On the day of the electroporation, HG-3 cells were collected and washed in PBS. 10^6 cells per condition were centrifuged at 300x g for 10 minutes at RT, and resuspended in 100µL of Resuspension Buffer T. Plasmids were added to 100µL of cells as described below:

Positive control	100µL of cells in T buffer + 2.5µg of pMAX vector
Sample	100µL of cells in T buffer + 2.5µg of pGuide n°2 + 2.5µg of pGuide n°10.

The parameters selected for the electroporation were: 3 pulses of 10ms, at a voltage of 1600V each. Following electroporation, the cells were directly in a 6-well plate containing 2mL of pre-warm, antibiotic-free medium.

7.2.16.6. Sorting of cells

48 hours following electroporation, HG-3 cells were collected, stained with the viability dye eFluor506, and GFP+ cells sorted on a BD FACSAria™ III (BD Biosciences). The gating strategy is represented below:

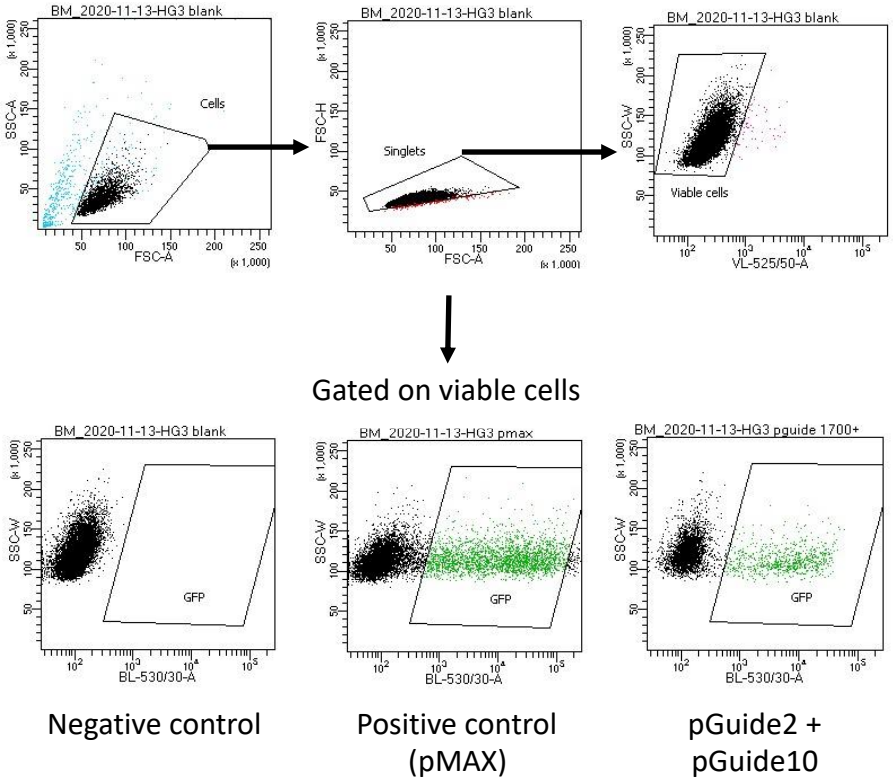

Following the sort, GFP+ cells electroporated with the 2 guide RNAs were resuspended in conditioned medium and placed in culture for 2 days.

7.2.16.7. Dilution for culture of single clones

48 hours following the sort, cells were collected and manually counted using a counting chamber. For the dilution, cells were resuspended in conditioned medium at a concentration of 2.5 cell per mL. 200µL were seeded per well in 96-well plates. These values were chosen to plate 0.5 cell per well and optimize the chances of seeding a single cell per well.

8. RESULTS

8.1. Testing the function of sEVs: the functional assay explained in detail

To answer most of the questions described in the aims of the thesis, an *in vitro* functional assay that is based on analysing the expression of surface markers by flow cytometry upon treatment of myeloid cells with sEVs was used as a read-out to assess the ability of the different sEV preparations to modify the phenotype of myeloid cells. Whether the phenotype acquired by myeloid cells following treatment with tumor-derived sEVs is balancing towards a pro- or an anti-tumoral response remains undetermined and would require extensive *in vivo* investigations. For this reason, myeloid cells treated with sEVs and showing an upregulation of PD-L1 are referred to “sEV-polarized”. Additional markers of myeloid cells sEV-induced polarization include ICAM-1 (CD54) and HLA-DR[322]. Both molecules are known to be upregulated in myeloid cells upon their activation. The technical aspect of the assay is described in detail in the Material and Methods part of this dissertation (7.2.11). A schematic

of the assay is represented in

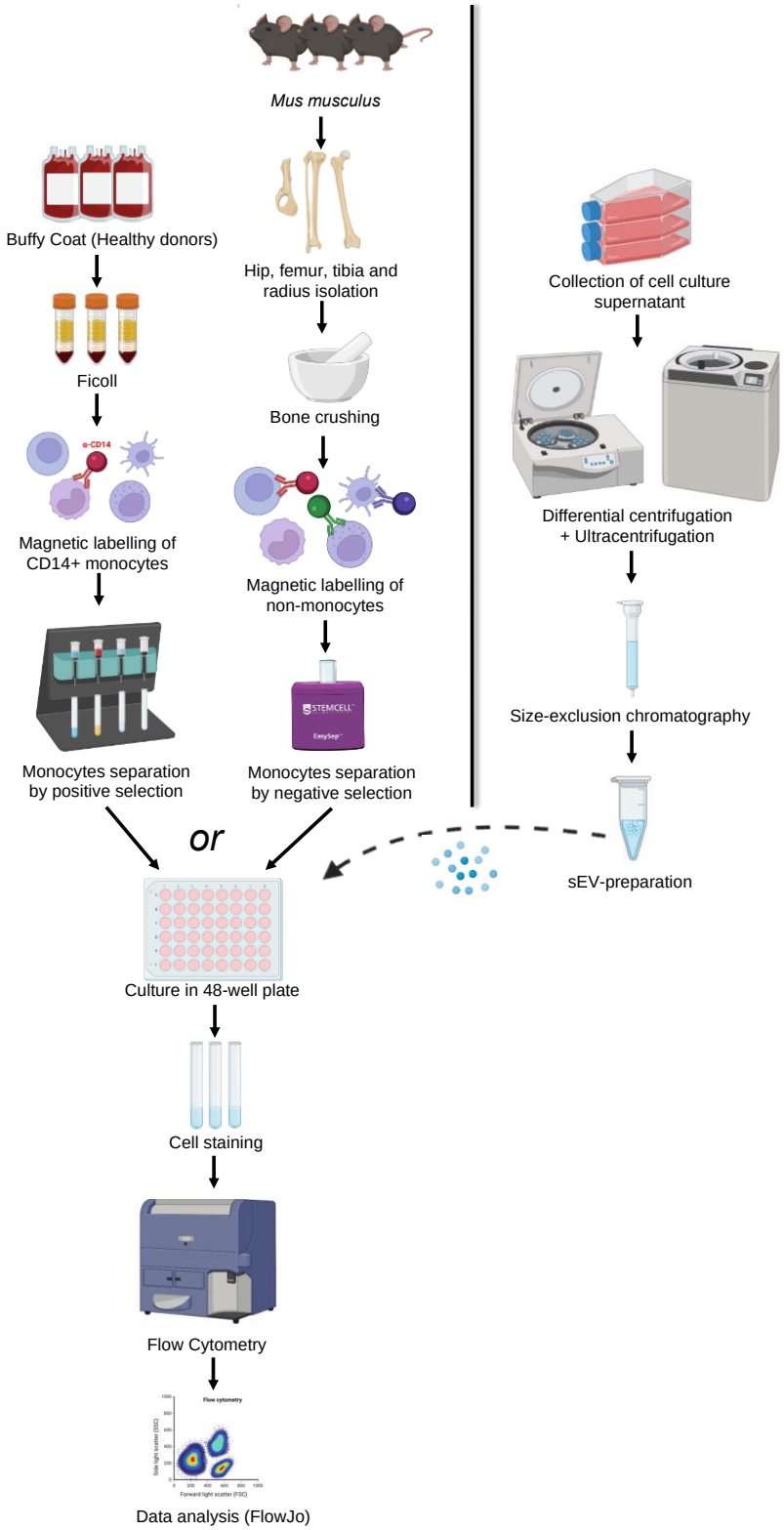

- Figure 9. Several markers of myeloid cells sEV-induced polarization were used as a read-out: PD-L1, CD54 and HLA-DR were used for both human or murine myeloid cells. In addition, CD62L and CD16 were sometimes included for human myeloid cells and CCR2 for murine myeloid cells. The assay was adapted from Haderk et al, *Science Immunology*, 2017 [258]. Explanations for the choice of the markers are presented in

.

Marker	Relevance
PD-L1	PD-L1 is an inhibitory ligand for PD-1. PD-L1/PD-1 interaction leads to the inhibition of T-lymphocytes' cytotoxicity and proliferation [323]
HLA-DR	HLA-DR is part of the MHC Class II receptors and contributes to antigen presentation to the T-cell receptors on CD4+ T cells.
CD54	Also called ICAM-1, CD54 is an adhesion molecule, promoting leukocytes endothelial transmigration. CD54 is upregulated on the surface of myeloid cells following activation [324]. CD54 also exists as a soluble form. The effect of membrane-bound or soluble CD54 on the immune function remains unclear; CD54 may stimulate the proliferation of CD8+ T lymphocytes but inhibit the proliferation of B lymphocytes [325,326]
CCR2	C-C Chemokine- receptor type 2 is the receptor for the proinflammatory chemokine CCL2. CCR2 expression is positively correlating to the number of circulating myeloid cells and expressed on inflammatory myeloid cells [327,328]. Genetic deletion or chemical blockade of CCR2 is associated with reduced recruitment and trafficking of myeloid cells [329,330]
CD62L	CD62L, also called L-selectin, is an adhesion protein. CD62L is associated with monocyte recruitment [331,332]. Downregulation of soluble CD62L secretion is associated with a decrease of T cell trafficking [131].
CD16	Fc gamma receptor involved in antibody-dependent cell-mediated cytotoxicity (ADCC) in myeloid cells [333].

Table 9: List of major surface markers used to assess myeloid cells activation following treatment with sEVs or controls, and their function in myeloid cells. PD-L1, CD54 and HLA-DR were used both for human or murine myeloid cells; CD62L and CD16 for human myeloid cells only, whereas CCR2 for murine myeloid cells.

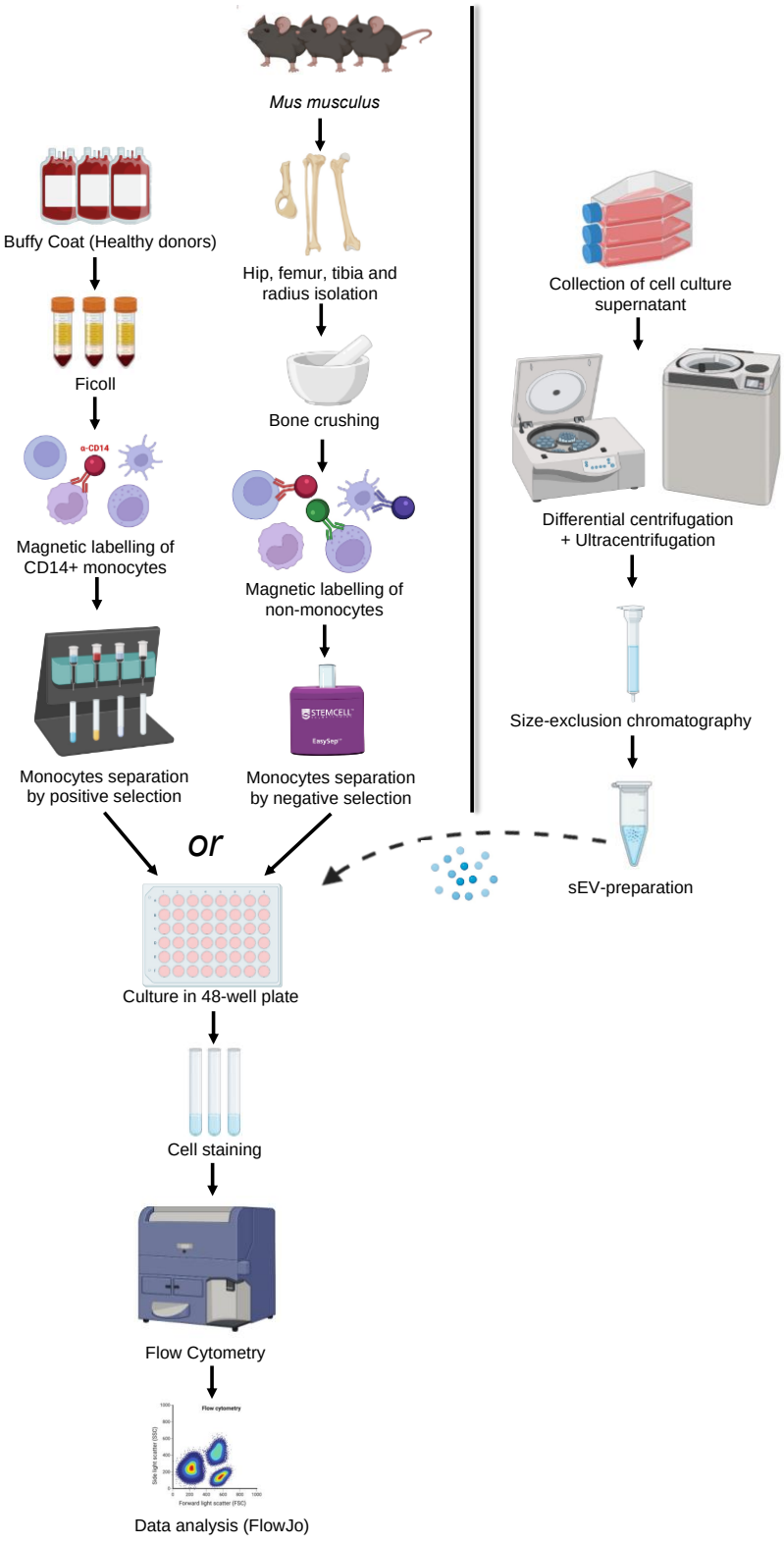
Mus musculus
Buffy Coat (Healthy donors)
Hip, femur, tibia and radius isolation
Collection of cell culture supernatant
Ficoll
Bone crushing
Differential centrifugation + Ultracentrifugation
α-CD14
Magnetic labelling of CD14+ monocytes
Magnetic labelling of non-monocytes
Size-exclusion chromatography
Monocytes separation by positive selection
Monocytes separation by negative selection
or
sEV-preparation
Culture in 48-well plate
Cell staining
Flow Cytometry
Flow cytometry
Data analysis (FlowJo)

Figure 9: Experimental outline to assess sEV-induced polarization of myeloid cells following treatment with sEVs or control condition. Myeloid cells are isolated from human peripheral blood or murine BM by magnetic selection. In parallel sEVs are isolated by differential centrifugation combined to size-exclusion chromatography (unless differently mentioned). Myeloid cells are treated with sEVs in culture followed by FC staining, acquisition, and analysis.

8.2. Optimization of the cell culture conditions, the isolation technique and the storage conditions of sEV-preparations

8.2.1. Optimization of the isolation method

The figures and legends presented in this chapter were extracted or adapted from the following publication: Bordas et al. IJMS, 2020. The initial draft of the manuscript was prepared by myself, but corrections have been added by co-authors as stipulated in the "Contributions" section of the publication.

Multiple approaches have been referenced for the isolation of sEVs, as described in the Introduction, 5.4.1.4. The approaches particularly differ in terms of yield and purity. Additionally, the choice of the approach must be selected based on the starting material used for sEV isolation (cell culture supernatant, plasma, solid tissue, etc). To enrich B-cell NHL-derived-sEVs, two sources of primary material were used: lymph nodes (LNs) freshly resected from patients suspected for B-cell NHL, and the spleen of adoptively-transferred Eμ-TCL1 mice, a CLL murine model showing accumulation of malignant B-cells in the spleen. However, optimal protocols for these two specific tissues were lacking at the starting time of the study. To select the optimal protocol, a comparison of two widespread-used techniques was performed: differential centrifugation combined to size-exclusion chromatography (SEC) and differential centrifugation combined to ultracentrifugation on sucrose density cushion. For the SEC, a commercially available IZON column was used. A schematic of the isolation steps is presented in Figure 10. A total of 3 LN-supernatants and 3 murine spleens were used and submitted to differential centrifugation (black squares, Figure 10). The 100K pellet containing sEVs and protein complexes was then split in two equal volumes. The first aliquot was used to proceed to the isolation of sEVs using the SEC (blue squares, Figure 10), whereas the second aliquot was used to proceed to the isolation of sEVs by ultracentrifugation on a sucrose density cushion (red squares, Figure 10), also called density gradient flotation, as previously described [334] . The first approach gives rise to a total of 8 eluate fractions, called F0 to F7, with F0 corresponding to the void volume of the column. The second approach gives rise to a single final product. The purity and the yield of the different products were compared using Nanoparticle tracking analysis (NTA) to assess the concentration and absolute number of particles recovered; protein quantification by bicinchoninic acid (BCA) assay; immunoblotting to assess the rate of co-isolated non-sEV-derived proteins; and transmission electron microscopy (TEM) to have a closer look at the shape and integrity of the isolated particles. The results are presented in the following sections.

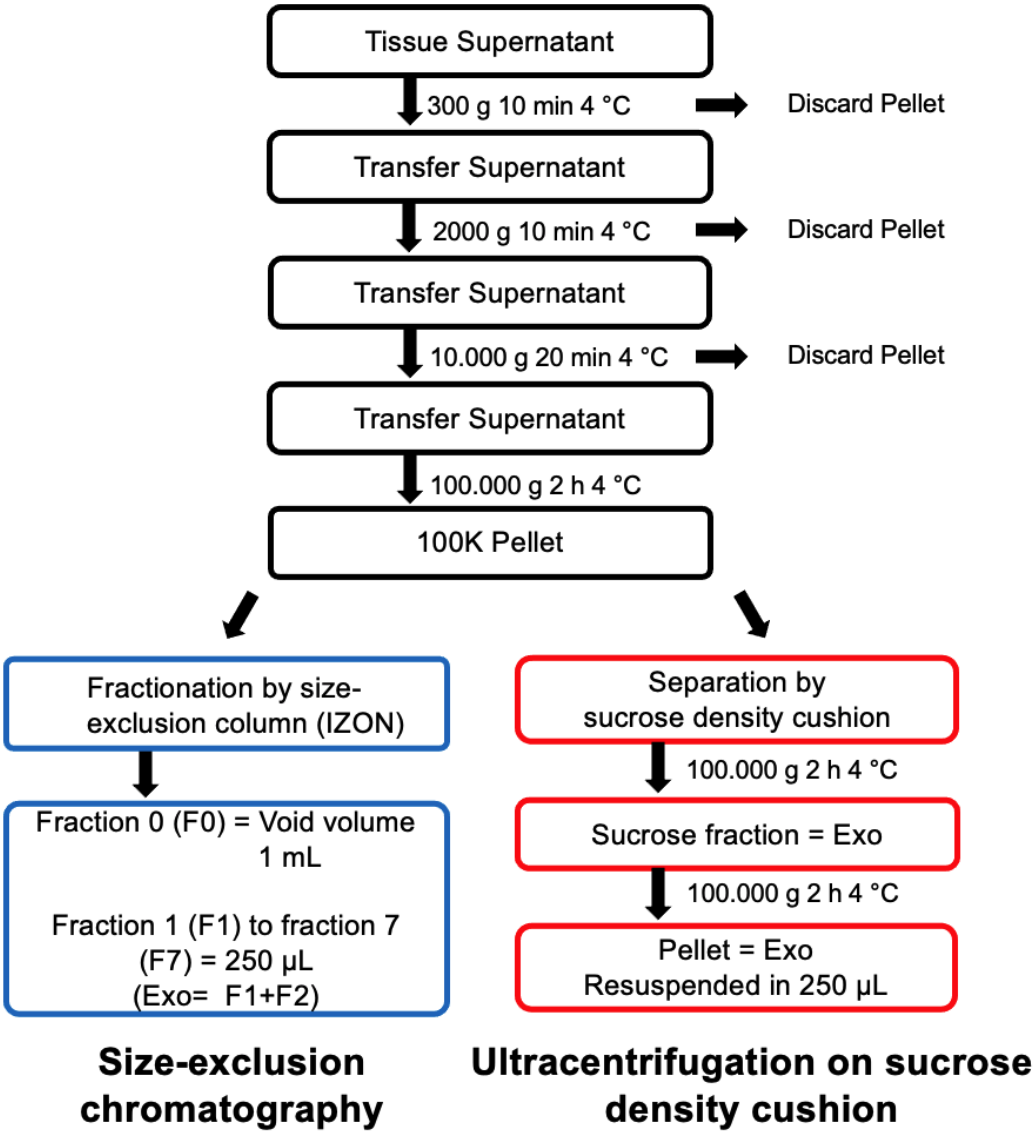

Figure 10: Experimental outline of the comparison of size-exclusion chromatography (SEC)-based versus sucrose density cushion-based sEV isolations. Supernatant of dissociated patients' LNs or murine spleens was separated by differential ultracentrifugation and the resulting 100K pellet was resuspended and split into two equal parts for direct method comparison. Equal volumes were loaded on either SEC columns or on a sucrose density cushion.

8.2.1.1. Results for LN supernatants

Three lymph nodes from undiagnosed lymphoma patients were used for the isolation of sEVs. The elution volume for each fraction collected from the IZON SEC column or for the sucrose density cushion (referred below as "CUSHION") were the same (250µL). The concentration and absolute number of particles was assessed by NTA (Figure 11, A). sEVs isolated using the IZON column were enriched in fractions 1,2 and 3. However, the fraction 2 was always the

most enriched fraction, and called peak fraction. The protein concentration in the peak fraction shows a 3.9 to 10.3-fold increase in the IZON peak fraction compared to the CUSHION product. In line with these results, the absolute number of recovered sEVs in the IZON fractions was higher in comparison to the CUSHION (Figure 11, A). Furthermore, the concentration of proteins was higher in the peak fraction (fraction 2) than the CUSHION (Figure 11, B). The same observation was true when looking at the absolute amount of recovered proteins. However, for the LNs from patients 221 and 228, the differences in terms of protein concentration in the IZON fractions and in the CUSHION were not as drastic as for the particle concentration. The results seem to indicate that the CUSHION approach results in an increase of co-isolated protein complexes in comparison to the IZON/SEC approach. No stringent differences could be observed between the mean size of sEVs found in the IZON fractions in comparison to the corresponding CUSHION samples (Figure 11, C).

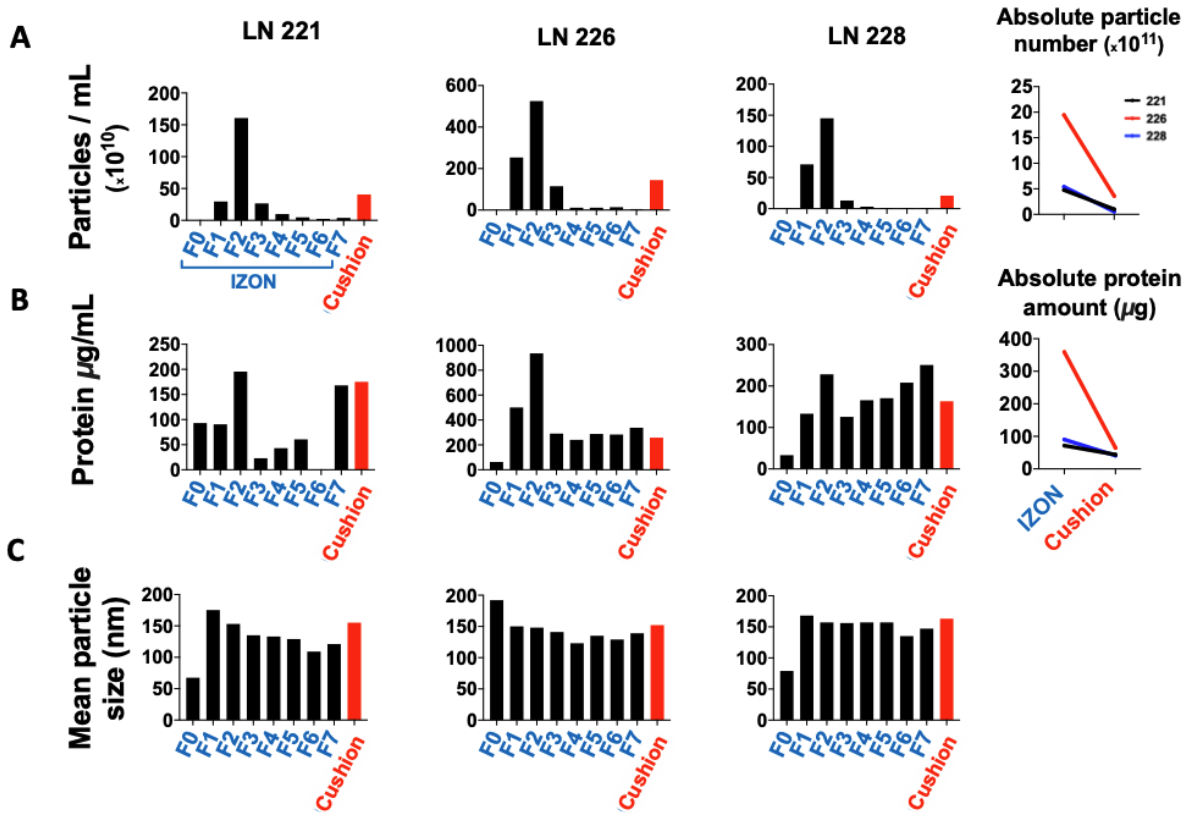

Figure 11: Quantitative comparison of sEVs isolated from human lymph nodes (LNs) using differential centrifugation combined to size-exclusion chromatography (“IZON”) or ultracentrifugation on a sucrose density cushion (“CUSHION”). Size-exclusion column (SEC) fractions (F0 = void volume, 1ml; F1, F2, F3, F4, F5, F6, F7 = serial fractions, 250 µl) and cushion fraction (pellet resuspended in 250 µl) were analyzed by Nanosight Tracking Analysis (NTA), bicinchoninic acid (BCA) protein quantification. (**A**) Left: Particle concentrations in IZON fractions F0-F7 and “cushion” fraction for three different human LN samples measured by NTA. Right: Absolute number of detected particles as sum of fraction 1 and fraction 2.. (**B**) Left: BCA protein quantification for IZON fraction F0-F7 and the “cushion” fraction. Right: Absolute

amount of protein in fraction 1 and fraction 2. (**C**) Mean particle size for IZON fraction F0-F7 and the “cushion” fraction analyzed by NTA.

In line with those results, the NTA analysis did not show any considerable difference between the profile of IZON fraction 2 or the CUSHION (Figure 12, A). The presence of positive and negative markers for sEVs was verified by immunoblot, as recommended by the MISEV guidelines 2018 [196] (Figure 12, B). The results show a strong enrichment of the sEV-derived markers Flotillin-1, CD81, CD9 and TSG101 in IZON fractions 1 and 2, as well as in fraction 3, although to a lower extent. Flotilin-1, CD81, CD9 but not TSG101 were also detected in the CUSHION. These results confirm the presence of sEVs in these specific samples. Additionally, for the same amount of loaded proteins, the enrichment of markers in the CUSHION was lower, in line with the hypothesis that the sucrose density cushion approach leads to an increased co-isolation of sEVs along with non-sEV-derived products than the IZON/SEC approach. Negative markers of sEVs were also tested. As expected, Cytochrome C (marker of mitochondria) and GM130 (marker of Golgi) were detected in the cell lysates, but in none of the sEVs products. Calnexin (marker or ER) was detected in the fractions 1 and 2 as well as the cushion product, although to a lower extent than in the cell lysate. The unexpected presence of Calnexin in the sEVs can result either from the co-isolation of non-sEV-derived proteins with the sEVs, or may also indicate a possible involvement of the ER during the sEV biogenesis. Similar results were previously observed and discussed elsewhere [335–337]. For each LN, IZON fraction 2 as well as the corresponding CUSHION were analyzed by TEM (Figure 12, C). The TEM pictures show an enrichment of particles in the IZON fraction 2 in comparison to the CUSHION. Additionally, the IZON samples show expected donut-shaped sEVs for all 3 samples, indicating that the integrity of the sEVs was preserved, whereas the corresponding CUSHION showed different products from one sample to another. In particular, the CUSHION sEVs from LN226 and LN228 seemed disrupted. A labelling of the preparations with a gold-labelled antibody directed against HLA-DR was also performed (Figure 12, D). Although HLA-DR is not specific to B-cells, it is highly enriched in Antigen-Presenting Cells (APCs) in general. Both approaches efficiently led to the isolation of sEVs derived from APCs. Unfortunately, antibodies recognizing specific B-cell markers such as CD20 were not suitable for TEM.

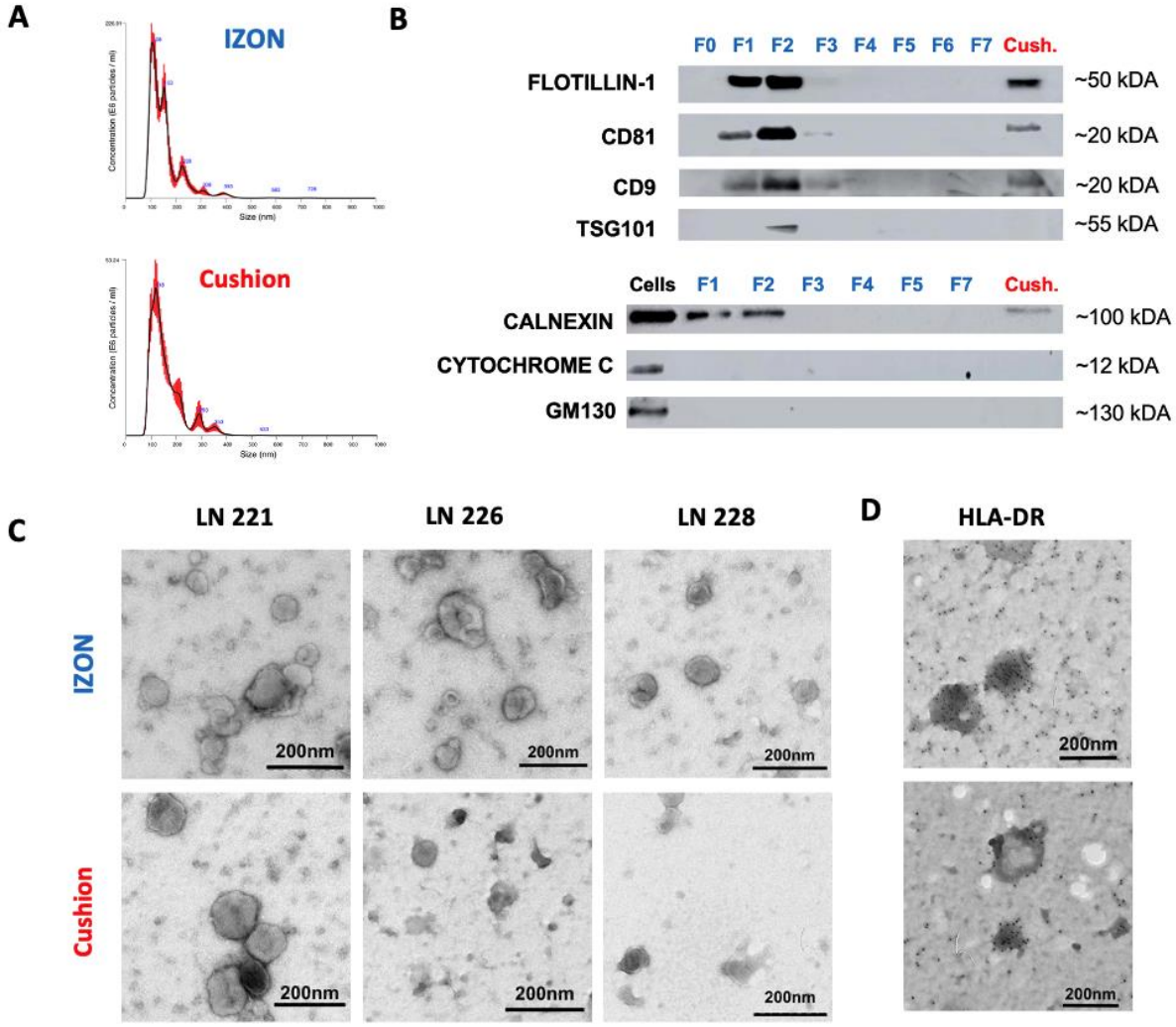

Figure 12: Characterization of sEV preparation by NTA-based size profile, immunoblotting and transmission electron microscop (TEM). (**A**) Representative particle distribution profile for LN221 IZON fraction 2 sample (top) and CUSHION sample analyzed by NTA (bottom). (**B**) Immunoblotting analysis of FLOTILLIN-1, CD81, CD9, TSG101, CALNEXIN, CYTOCHROME C and GM130 for indicated IZON fractions, the “cushion” fraction and parental cell lysates for one LN sample. (**C**) TEM images of IZON fraction 2 and the CUSHION for the 3 indicated samples. (**D**) Immunogold electron microscopy for HLA-DR of one human LN sample (Sample LN221). Scale bar 200 nm.

8.2.1.2. Results for Eμ-TCL1 spleen

Spleens from three adoptively transferred Eμ-TCL1 animals were processed as described in the Material and Methods (7.2.12). The spleens were collected exclusively for animals with a tumor load above 90%, as calculated by the percentage of CD5+CD19+ cells among all viable cells. sEVs were similarly isolated and analysed as for the lymph nodes. Isolation of sEVs on the IZON column resulted in an enrichment of particles in the IZON fractions 1 and 2, as for

the LNs (Figure 13, A). For the Spleen 42704, the particles were enriched in IZON fractions 2 and 3, a result that was attributed to the manual loading of the column. Comparison of the absolute amount of isolated particles confirmed that the IZON column leads to an increased yield of recovered particles in comparison to the CUSHION. However, the protein concentration of the IZON peak fractions were similar than in the corresponding CUSHION (Figure 13, B). This difference can possibly be due to an increased co-isolation of soluble proteins with sEVs when using the later approach. The superiority of the SEC approach in terms of yield was also seen at the protein level, when comparing the absolute amount of recovered proteins. The mean size of the particles as assessed by NTA, was similar between the IZON fractions and the CUSHION (Figure 13, C).

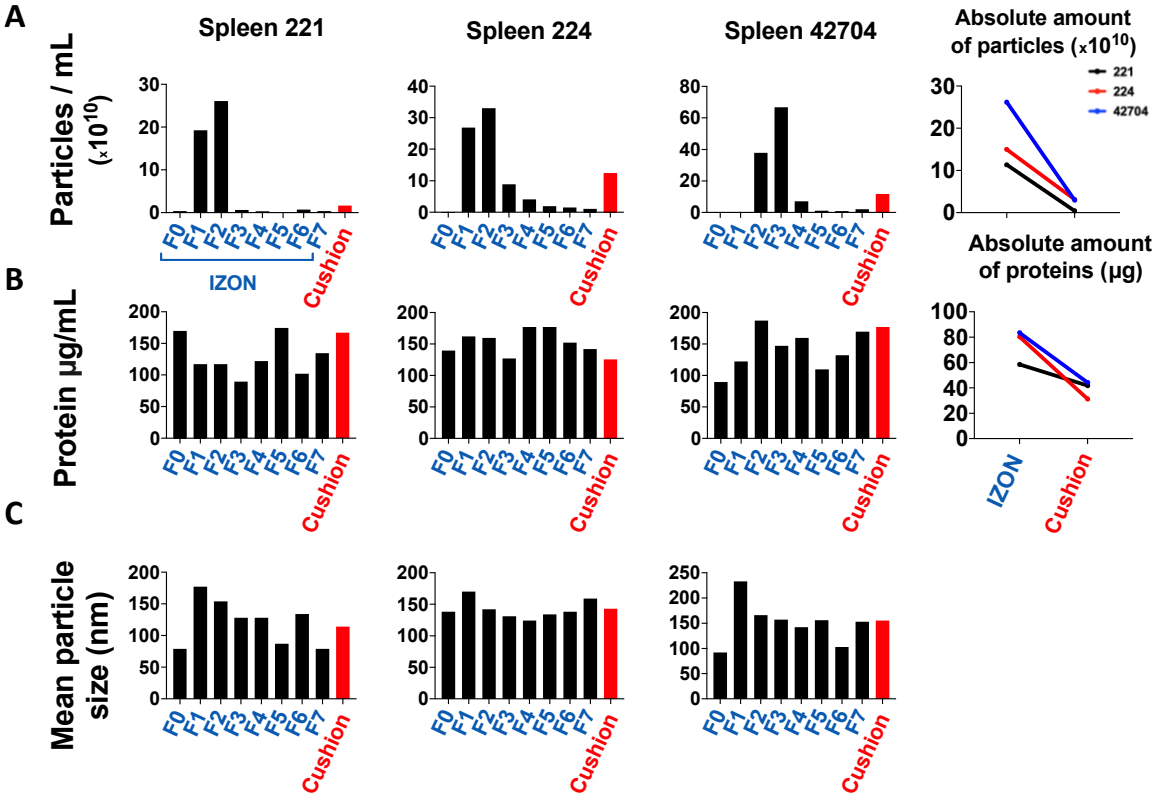

Figure 13: Isolation and characterization of murine spleen sEVs: (A) Left: sEV concentration in the different IZON Fractions and CUSHION preparations for three samples analyzed by NTA. Right: Absolute number of particles in indicated preparations. For each sample, the number of particles in the two peak fractions or in the cushion product was calculated. (B) Left: Protein quantification in the indicated preparations assessed by BCA assay. Right: Absolute amount of protein in indicated preparations. (C) Mean particle size of all fractions and the CUSHION preparations analyzed by NTA.

The NTA profiles showed differences in the distribution of the particle size depending on the isolation approach used (Figure 14, A). This difference can be due to the lower amount of particles recovered in the CUSHION, resulting in specific peaks on the particle size profile. Additionally, positive sEV-derived markers (FLOTILIN-1, ALIX and TSG101) as well as

negative sEV-derived markers (CALNEXIN, ATP5A) were validated by immunoblotting (Figure 14, B) While ALIX was particularly enriched in the IZON fractions 1 and 2 as well as in the CUSHION, the sEV-derived marker FLOTILIN-1 was enriched in the IZON fractions 1 and 2, but absent from the CUSHION. On the contrary, TSG101 was highly detected in the CUSHION, but only poorly detected in the IZON fractions 1 and 2. The difference in particle size distribution as well as sEV-derived markers could result from the isolation of different sEV subpopulations resulting from the use of different isolation methods. Analysis of the different samples (IZON Fraction 2 and CUSHION) was completed by TEM (Figure 14, C). IZON Fractions 2 from all three samples were similar, however the three different CUSHION preparations showed three different results. For CUSHION sEVs derived from the spleen 221, lipidic-like structures were observed. For the CUSHION sEVs derived from the spleens 224 and 42704, the identified vesicles did not present a typical sEV cup-shape structure. In two out of three CUSHION samples, small dark structures with a specific geometrical shape were present (Figure 14, D). The structures were typical of ferritin, in line with the brown-like color of the supernatant pellets following the first ultracentrifugation step (Figure 14, E). This co-isolation was not only highly reproducible but represents a very important component of the sEV preparations (Supplementary figure 1).

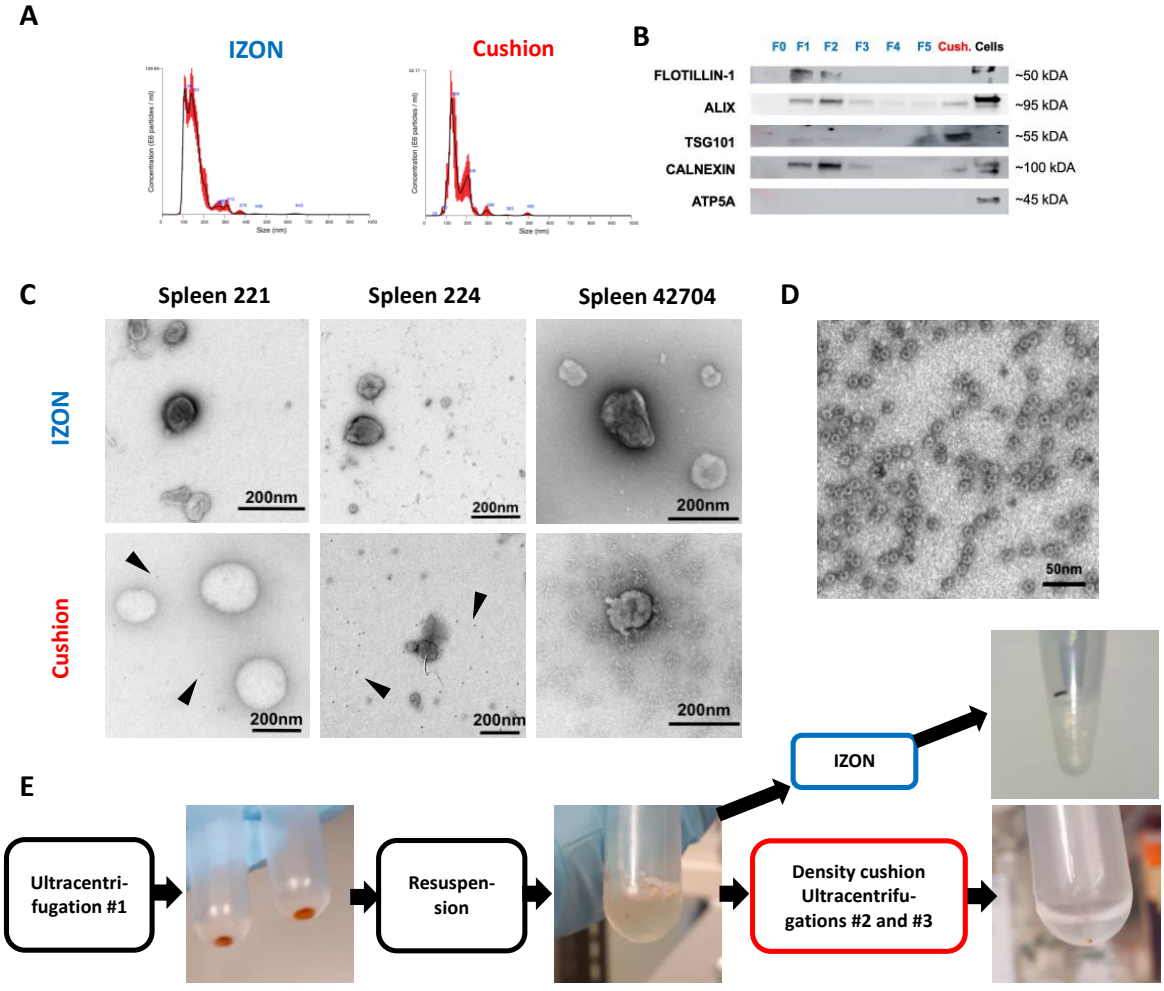

Figure 14: Characterization of sEV preparations by NTA-based size profile, immunoblotting and TEM. (**A**) One representative particle distribution profile for an IZON fraction 2 (left) and

a CUSHION preparation analyzed by NTA (Spleen 42704). (**B**) Immunoblotting analysis of FLOTILLIN-1, ALIX, TSG101, CALNEXIN and ATP5A for the different IZON fractions, the CUSHION preparation and parental cells for one spleen sample (Spleen 224). (**C**) TEM images of IZON peak fraction and CUSHION preparation for the three indicated samples. (**D**) TEM image of ferritin-like structures found in CUSHION preparations. (**E**) Pictures of the sEV pellet, resuspended sEVs prior to application on the sucrose density cushion, and final pellet in PBS before resuspension.

8.2.1.3. Differential response of myeloid cells treated with sEVs i solated either with SEC or with sucrose density cushion.

To compare if the sEVs isolated with the two methods show a differential potential to induce a polarization of myeloid cells, a functional assay was performed as previously described (8.1) and myeloid cells were incubated for 8 hours with IZON Fraction 2 sEVs, CUSHION sEVs, or left untreated. The phenotype of myeloid cells was characterized by FC. IZON and CUSHION sEVs could both induce an upregulation of PD-L1. However, the different sEV preparations isolated on a density cushion showed a more variable response (Figure 15, top row). Two out of three CUSHION sEVs failed to induce HLA-DR upregulation which was observed with all IZON sEVs. ICAM-1 was strongly upregulated by CUSHION sEVs, whereas only one IZON sample could induce an upregulation. Representative histograms are showed in Figure 15, B, bottom row.

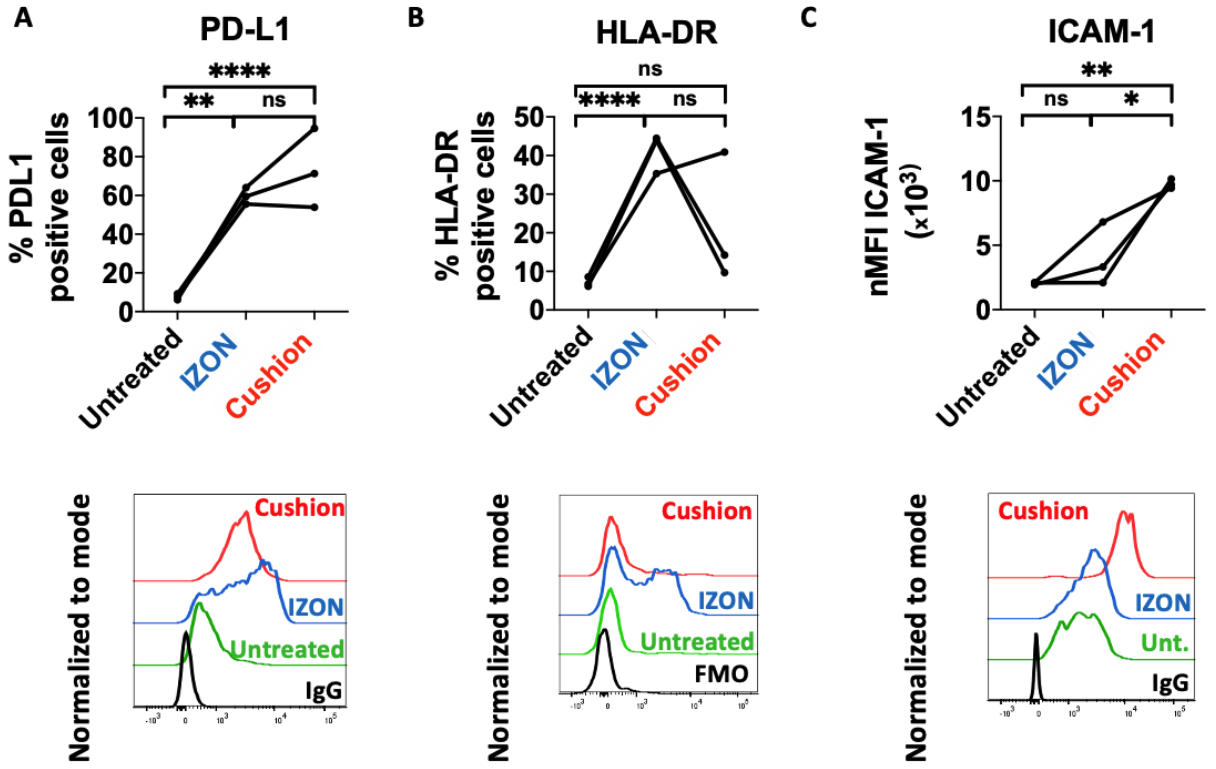

Figure 15: Response of murine myeloid cells upon sEV treatment. Bone marrow-derived myeloid cells were treated with 5 µg of the indicated sEV preparations for 8 hours and analyzed by flow cytometry gating on CD11b+F4/80+CX3CR1+Ly6C+ cells (n=3 mice per sEV

preparation). (A) Top: Percentage of PD-L1 positive cells among myeloid cells. Bottom: Representative histogram including isotype antibody staining as negative control (IgG). (B) Percentage of MHC-II/HLA-DR positive cells among myeloid cells. Bottom: Representative histogram including fluorescence-minus-one (FMO) staining as negative control. (C) Top: ICAM-1/CD54 expression presented as normalized mean fluorescence intensity (nMFI). Bottom: Representative histogram. P-values were determined by One-way ANOVA with Tukey's multiple comparisons test. *P < 0.05; **P < 0.0021; ***P < 0.0002; ****P < 0.0001.

8.2.2. Comparison of Eμ-TCL1 vs TCL1-355 sEVs

During the course of the project, an Eμ-TCL1 cell line was kindly provided by Dr. Dimitar Efremov, at the University of Trieste, called TCL1-355. The TCL1-355 cell line is described in the Material and Methods, 7.2.1.1. The use of a cell line to isolate murine CLL-derived sEVs represented an opportunity to isolate a pure population of CLL-derived sEVs, contrary to the sEVs coming from the spleen of adoptively transferred Eμ-TCL1 animals. Cell line-derived sEVs would also limit the use of animals for experiments. Both TCL1 cell line and spleen supernatants were used for the isolation of sEVs, whose potential to induce a polarization of myeloid cells was compared *in vitro*. sEVs isolated from the TCL1-355 cell line were analysed by TEM and showed a typical sEV-like structure (Figure 16, A). In order to check for a potential dose-response effect, three doses of sEVs were selected for this experiment: 1μg, 5μg and 10μg. The polarization of myeloid cells induced by sEVs was assessed by the surface expression of PD-L1, CD54, HLA-DR and CCR2 (Figure 16, B) following a treatment of 8 hours with the indicated sEVs or the Effectene control. The results revealed that sEVs isolated from the spleen (Eμ-TCL1) have an increased capacity to induce PD-L1 on myeloid cells compared to sEVs from the TCL1-355 cell line. In both cases, the increase of PD-L1 positively correlated to the dose of sEVs. Eμ-TCL1 sEVs also induced, almost systematically, a downregulation of CCR2, whereas such an effect was observed only occasionally with TCL1-355 sEVs. On the contrary, HLA-DR and CD54 seemed to be similarly upregulated by both sources of sEVs. The results indicate that sEVs isolated from the spleen of Eμ-TCL1 adoptively transferred animals share some common features with sEVs isolated from the TCL1-355 cell line. However, the Eμ-TCL1 sEV preparations may contain additional bioactive components activating additional pathways leading to a superior upregulation of PD-L1 and downregulation of CCR2. These could be either sEVs from a different cell origin than leukemic cells, or an increased co-isolation of protein complexes with sEVs due to the solid nature of the original tissue.

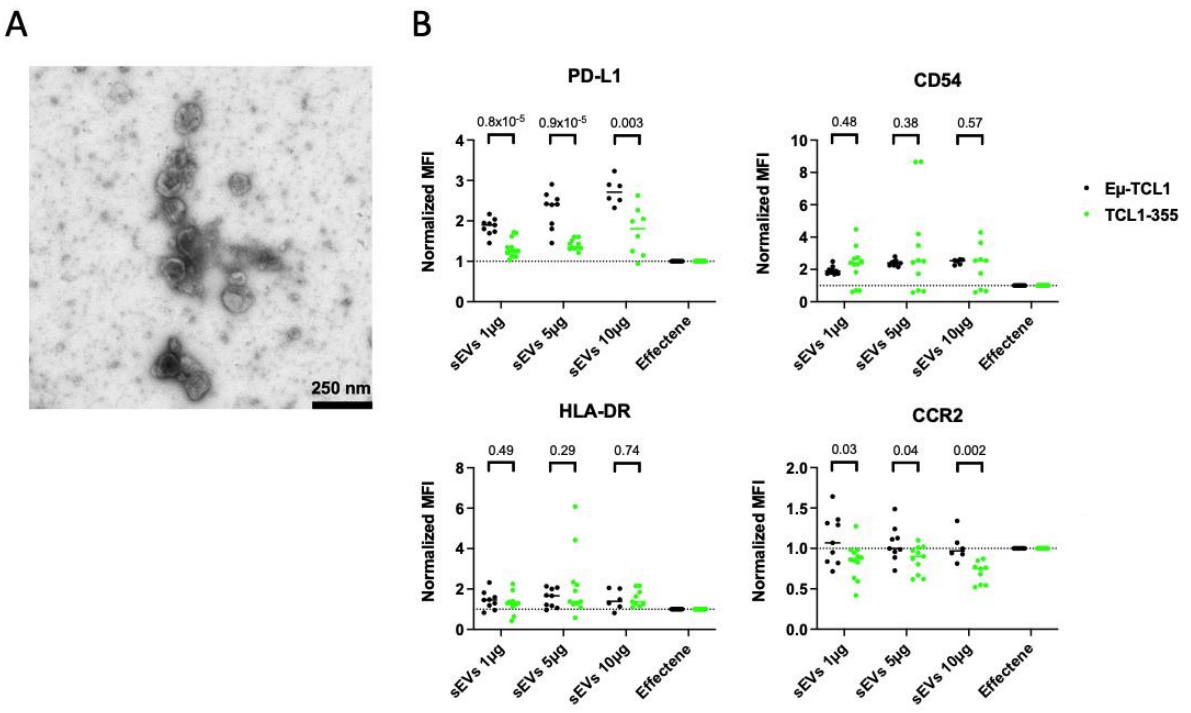

Figure 16: Comparison of sEVs isolated from the spleen of Eμ-TCL1 adoptively transferred animals with sEVs isolated from the TCL1-355 cell line. (**A**). Representative TEM picture of TCL1-355 derived sEVs. The sEVs show a classical donut-like shape and are smaller than 200nm. (**B**) Response of murine myeloid cells upon sEV treatment. Bone marrow-derived myeloid cells were treated with 1,5 or 10µg of Eμ-TCL1 or TCL1-355 sEVs, for 8 hours and analyzed by flow cytometry gating on CD11b+F4/80+CX3CR1+Ly6C+ cells. The expression of PD-L1, CD54/ICAM-1, HLA-DR and CCR2 are presented as normalized mean fluorescence intensity (nMFI). The normality of the values was verified by Shapiro test, and the indicated P-values were determined by unpaired t-tests.

8.2.3. Conclusion

Optimal isolation and storage conditions of sEVs remain an unresolved challenge. A multitude of approaches have been developed in the recent years to isolate sEVs, as described in paragraph 5.4.1.4. The different approaches present differences in terms of yield, purity and reproducibility. Therefore, the isolation method must be carefully selected, depending on the further use of the sEVs. Protocols aiming at improving isolation of sEVs from biofluids are numerous, but little is known about the isolation of sEVs from solid tissues. With the aim to further understand the role of B-cell NHL-sEVs by performing functional assays as well as proteomics, first, two methods for sEV isolation were compared prior any further step: differential centrifugation combined to size-exclusion chromatography (“SEC”) and differential centrifugation combined to ultracentrifugation on a sucrose density cushion (“CUSHION”). Altogether, the data indicate that SEC results not only in a higher yield of recovered sEVs, but also an increased purity, due to an improved separation of sEVs from soluble protein complexes. TEM images of the preparations showed that SEC seems to be more reproducible,

especially for sEVs coming from murine spleens. The results also suggests that the use of different methods may also lead to the isolation of different subpopulations of sEVs, as previously suggested [196,338]. Finally, it was shown that SEC but not the density cushion approach could efficiently separate the highly enriched ferritin-like molecules from the sEVs isolated from murine spleens. Nonetheless, it was shown later that sEVs isolated from the spleen of Eμ-TCL1 adoptively transferred animals show a slightly different potential to induce a polarization of myeloid cells than sEVs isolated from the TCL1-355 cell line, indicating that sEVs from the solid tissue may present a lower purity with co-isolated components affecting the read-out of the experiment. Therefore, it was decided to switch the sEV source over the course of the project.

8.3. Bioactive molecules responsible for myeloid cells activation in B-cell NHL

It was previously shown that CLL-derived sEVs can induce a so-called pro-tumoral phenotype in myeloid cells, characterized by an upregulation of PD-L1, a downregulation of CCR2, as well as an increased secretion of the CCL2 and CCL3 chemokines and the IL-6 cytokine [258]. Small-RNA sequencing of the sEVs revealed that one of the most enriched small RNA in the CLL-derived sEVs is the yRNA4. Treatment of myeloid cells with yRNA4 alone lead to a similar phenotype as for CLL-derived sEVs, when considering the markers mentioned above. To investigate similarities and differences in the signature induced by sEVs and by yRNA4, myeloid cells were treated with MEC1-sEVs, yRNA4 or the Effectene control as described in Figure 17A; the cell pellets from three technical replicates were used for protein extraction and the enrichment or depletion of specific proteins was analysed on a ScioCD antibody microarray (Sciomics, Neckargemünd, Germany).

The triggered response of myeloid cells following the different treatments was validated by assessing the cytokine concentration in the supernatant, using a Cytometric Bead Array (BD Biosciences). As expected, myeloid cells incubated with MEC1-sEVs or yRNA4 alone secreted increased amount of CCL2, CCL3 and IL6 in comparison to the control condition (Effectene) (Figure 17, B, top row). Although not statistically significant difference was obtained, the treatment of myeloid cells with MEC1-sEVs seemed superior to yRNA4 in inducing the secretion of CCL2, whereas the treatment with yRNA4 showed an increased capacity to induce secretion of CCL3 and IL-6 in comparison to MEC1-sEVs. Altogether the data validated the activation of myeloid cells in both conditions in comparison to the control condition. As a validation, the enrichment of the same cytokines as assessed by the microarray was analyzed (Figure 17, B, bottom row). CCL2, CCL3 and IL6 were found enriched in myeloid cells treated with MEC1-sEVs and yRNA4 alone in comparison to the Effectene control. Like the cytokine assay, the upregulation of CCL3 and IL6 was superior in yRNA4-treated myeloid cells than MEC1-sEVs-treated myeloid cells. However, the expression of CCL2 was not significantly different between the two different experimental conditions when using microarray-derived data. Next, differentially enriched proteins were plotted as a heatmap and confirmed that the technical replicates clustered together, and that all 3 treatments led to 3 distinct signatures in myeloid cells (Figure 17, C).

Differentially upregulated and downregulated proteins between each condition were plotted as a Venn diagram and Volcano plot (Figure 17, D and Supplementary figure 2). This revealed that more proteins were significantly different between MEC1-sEV-treated myeloid cells and the control condition than yRNA4-treated myeloid cells and control, highlighting that the treatment of myeloid cells with MEC1-sEVs leads to a broader response in myeloid cells than yRNA4-alone. A common signature was found in myeloid cells treated either by MEC1-sEVs or yRNA4. This signature includes 13 antibodies corresponding to 9 upregulated proteins (CCL2, CCL3, IL6, CCL4, IL1B, IL8, TNR5) and 2 downregulated proteins (CXCL16, EGLN), several antibodies being used on the array for the same protein. Furthermore, the list of

proteins upregulated following MEC1-sEVs treatment was analysed for enriched terms using the Metascape platform with cross-referenced gene lists from multiple ontology sources (Figure 17, E). Interestingly, two closely related pathways were enriched: the R-HAS-6783783 Interleukin 10-signalling pathway and the hsa04064 NF-kappa B signalling pathway.

Next, we aimed to decipher the differential signatures induced in myeloid cells by MEC1-sEVs or yRNA4 treatment. In a first step, upregulated proteins detected by the microarray analysis in MEC1-sEV treated myeloid cells, but considered to be of sEV-derived origin (*e.g.* the sEV-derived marker CD81 or B-cell marker CD19) where excluded by comparison of our data to previously published proteome data of MEC1 sEVs[278]. Then, the ratio of protein enrichment in both conditions, MEC1-sEV and yRNA4, was calculated for all proteins significantly upregulated in one or the other condition (Figure 18). For each ratio, the corresponding p-value is included in the Supplementary figure 3. Several candidates were selected for validation by RT-qPCR (Figure 19). In line with the microarray results, the transcripts of CR2, CCL22, IL5, NT5E and SLAMF8 were increased in MEC1-sEV-treated myeloid cells compared to yRNA4-treated myeloid cells, although not in a significant way. Furthermore, the IL12 transcript was more enriched in yRNA4-treated than MEC1-sEV-treated myeloid cells. The TRL7-downstream protein TNR5 was used as a control. As expected, TNR5 was upregulated in myeloid cells treated with MEC1-sEVs or yRNA4 alone. Surprisingly, CD86 was found downregulated in MEC1-sEV-treated myeloid cells compared to control cells at the transcriptome level. To investigate if the origin of CD86 detected on the microarray was from the signature of myeloid cells and not of sEV-derived origin, its expression was analysed at the surface of myeloid cells treated with MEC1-sEVs by flow cytometry (FC; Figure 19). FC data validated the upregulation at the protein level of CD86 at the surface of myeloid cells by both MEC1-sEVs and yRNA4, even though without reaching significance.

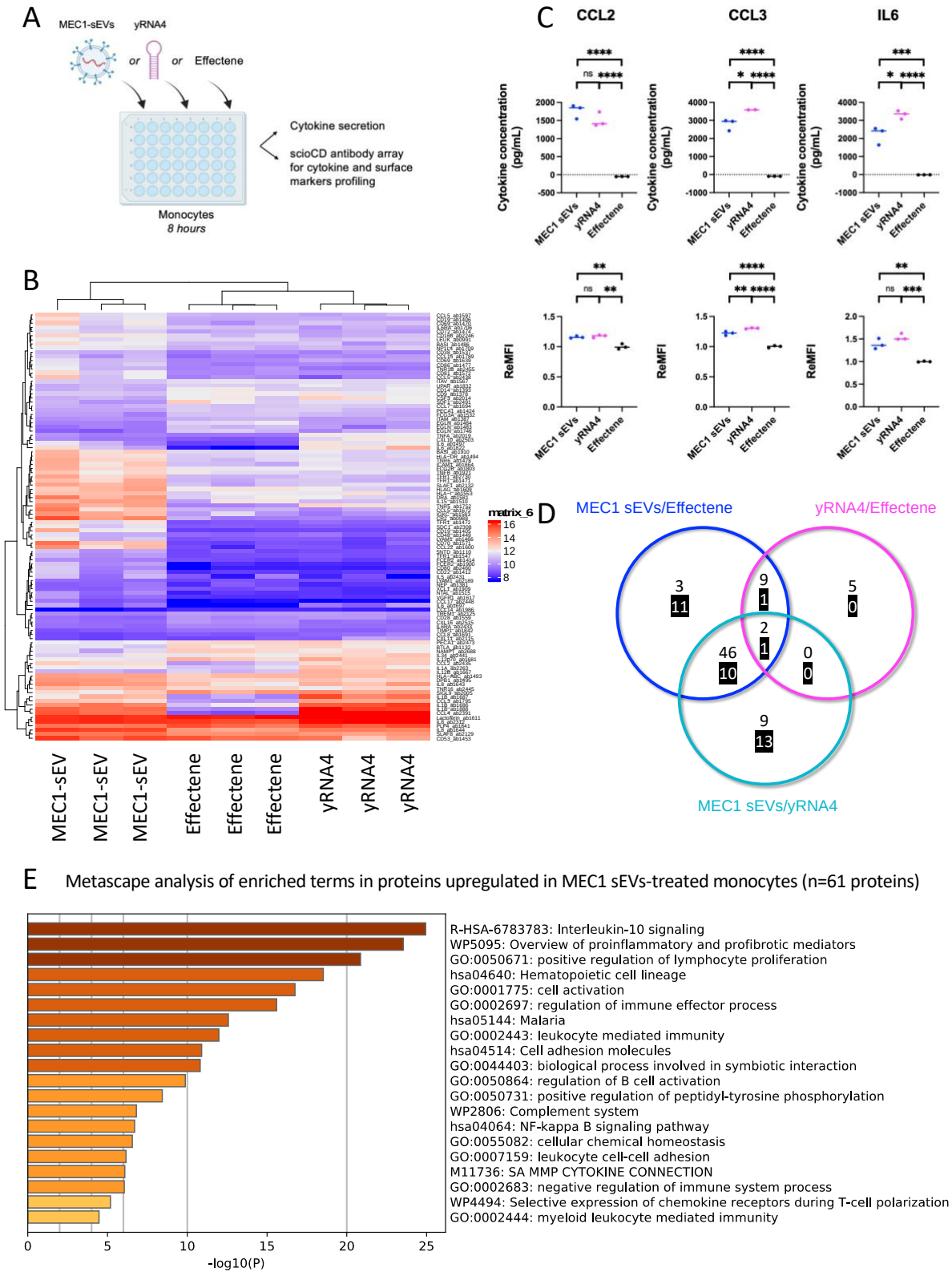

Figure 17: The response of myeloid cells upon MEC1-sEV treatment is broader compared to yRNA4 treatment. (**A**) Experimental overview. Myeloid cells were treated for 8 hours with MEC1-sEVs (40µg), effectene-encapsulated yRNA4 or effectene only. The supernatant was collected and used to assess the cytokine release into the medium, and the cells were collected for protein extraction, and analysis on a ScioCD microarray. (**B**) CCL2, CCL3 and IL-6

concentrations were assessed in the supernatant of the cells using a cytometric bead assay (top row). Similar results were obtained with the microarray (bottom row). P-values were determined by One-way ANOVA with Tukey's multiple comparisons test. *P < 0.05; **P < 0.0021; ***P < 0.0002; ****P < 0.0001 (**C**) Heat map of log protein expression data of significantly different proteins (p<0,05). (**D**) Venn diagram showing the significantly deregulated proteins between conditions compared two-per-two. The number of upregulated proteins is written in black, downregulated proteins in white over a black background. (**E**) Pathway enrichment analysis of proteins significantly upregulated in MEC1-sEV-treated myeloid cells compared to effectene-treated myeloid cells (Metascape analysis).

.

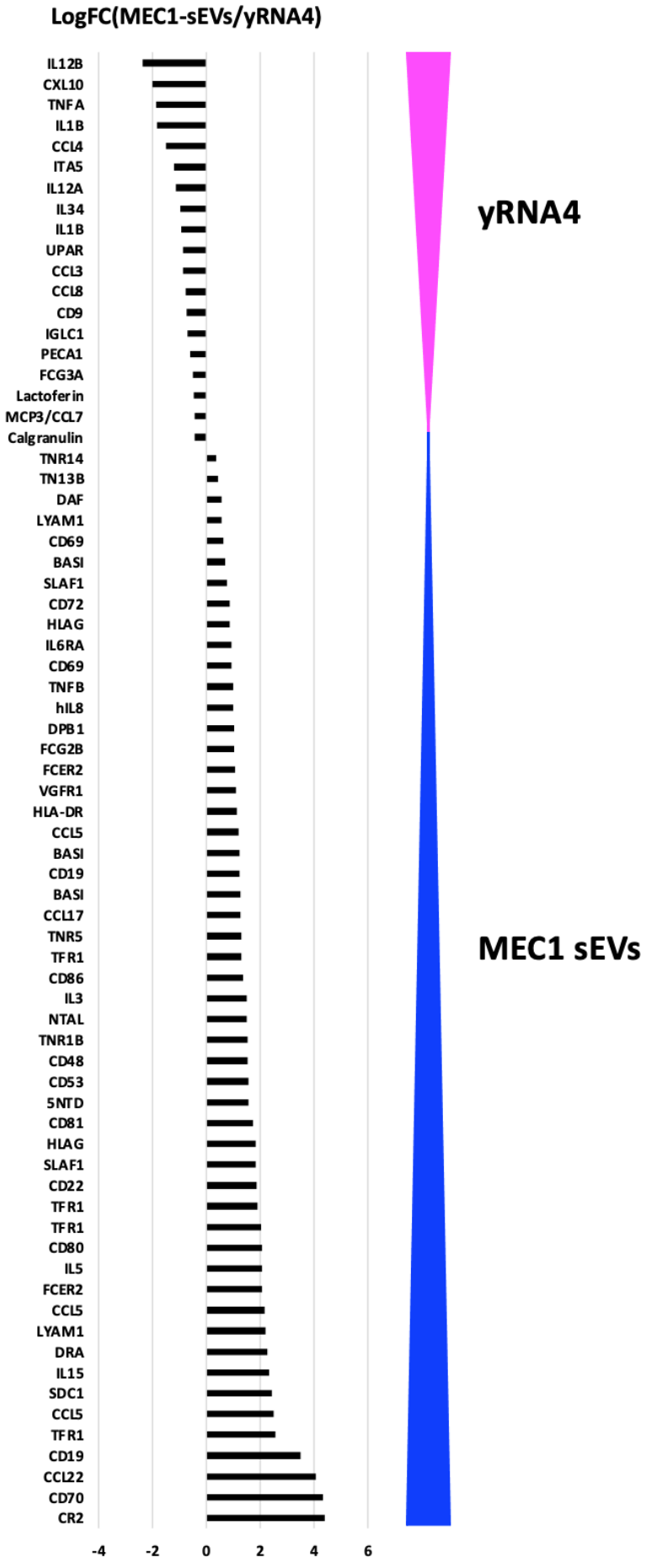
LogFC(MEC1-sEVs/yRNA4)
IL12B
CXL10
TNFA
IL1B
CCL4
ITA5
IL12A
IL34
IL1B
UPAR
CCL3
CCL8
CD9
IGLC1
PECA1
FCG3A
Lactoferin
MCP3/CCL7
Calgranulin
TNR14
TN13B
DAF
LYAM1
CD69
BASI
SLAF1
CD72
HLAG
IL6RA
CD69
TNFB
hIL8
DPB1
FCG2B
FCER2
VGFR1
HLA-DR
CCL5
BASI
CD19
BASI
CCL17
TNR5
TFR1
CD86
IL3
NTAL
TNR1B
CD48
CD53
5NTD
CD81
HLAG
SLAF1
CD22
TFR1
TFR1
CD80
IL5
FCER2
CCL5
LYAM1
DRA
IL15
SDC1
CCL5
TFR1
CD19
CCL22
CD70
CR2
-4
-2
0
2
4
6
yRNA4
MEC1 sEVs

Figure 18: Myeloid cells treated with MEC1-sEVs or yRNA4 alone show a differential protein signature. The ratio of protein enrichment was calculated and presented proteins are preferentially upregulated following treatment with MEC1-sEVs (down, blue) or yRNA4-alone (up, pink). Only proteins with a p-value < 10^{-5} are presented.

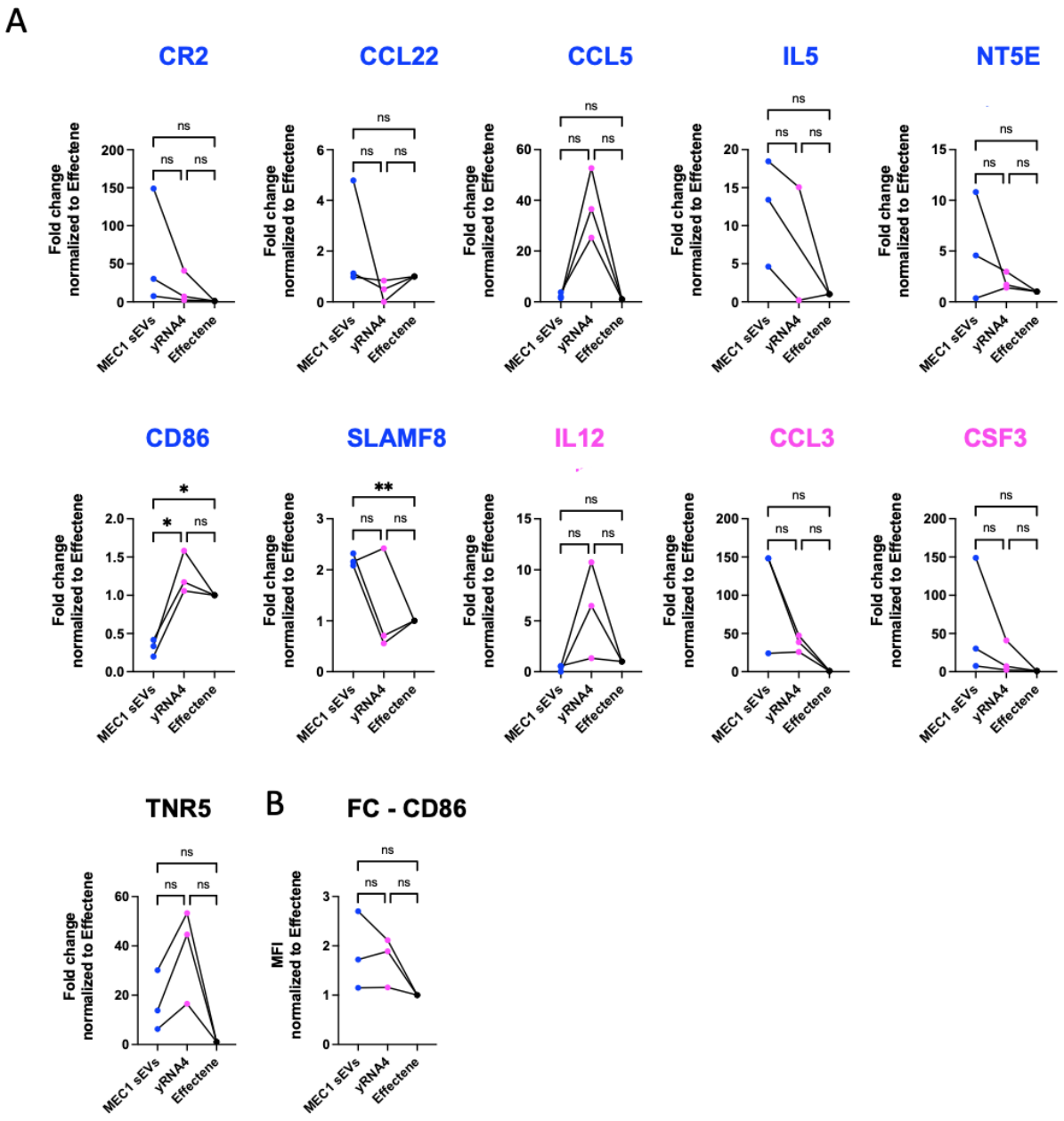

Figure 19: Myeloid cells treated with MEC1-sEVs or yRNA4 alone show a differential protein signature. (A) Validation of protein results by RT-qPCR using myeloid cells treated for 8 hours with 5µg of MEC1-sEVs or yRNA4-alone. The expression was normalized to the Effectene control (n=3). (B) The upregulation of CD86 expression was validated by flow cytometric analysis of myeloid cells following an 8-hour treatment with 5µg of MEC1-sEVs or yRNA4-alone. Median fluorescence intensity (MFI) normalized to Effectene control of CD86 staining is depicted. For all results, n=3 healthy donors. P-values were determined by One-way ANOVA with Tukey's multiple comparisons test. *P < 0.05; **P < 0.0021; ***P < 0.0002; ****P < 0.0001.

8.3.1. Conclusion

The above results show that both yRNA4 and MEC1-sEVs can induce an inflammatory response in myeloid cells, characterized by the secretion of cytokines like CCL2, CCL3 and IL6 among others. However, the signature induced by MEC1-sEVs includes many more proteins than the one induced by yRNA4. This signature seems to be linked to the induction of the immunosuppressive IL-10 pathway. Treatment of myeloid cells with MEC1-sEVs, and to lower extend with yRNA4-alone, also leads to the upregulation of the immune inhibitory enzyme CD73/NT5E [339]. However, the signature is also associated with the activation of immune system, highlighting the potential of tumor-derived sEVs to elicit both a pro- and anti-tumoral response in myeloid cells. The secretion of IL-10 is known to be driven by TLR2 and TLR4 in myeloid cells[340,341]. TLR signalling is linked to the the NF-κB pathway, also found enriched in myeloid cells treated with MEC1 sEVs. It was hypothesized that the response induced by yRNA4 is a global response of myeloid cells to small RNA, dependent on TLR7. Therefore, we hypothesize that the stronger signature seen in myeloid cells following treatment with MEC1-sEVs is dependent on other TLRs such as TLR2 and/or TLR4; and that bioactive molecules present in the sEVs other than small RNAs are playing a role in the sEV-induced polarization of myeloid cells. Due to their enrichment in sEVs, such bioactive molecules are most likely proteins.

Limitations of the study

In the initial set-up of the experiment, myeloid cells were treated with 40µg of sEVs, isolated on a density sucrose cushion. Therefore, separating proteins of sEV-derived origin or upregulated by the myeloid cells is particularly delicate. Ideally, an additional direct analysis of the proteins extracted from MEC1-sEVs on the same antibody microarray should have been performed. However, the isolation of sEV-derived proteins in sufficient quantities limited the inclusion of such a control. Additionally, some proteins such as CD86 were found upregulated by FC on the surface of myeloid cells although downregulated or not upregulated at the transcriptomic level following the treatment of myeloid cells with MEC1-sEVs. On the one side, it cannot be excluded that the difference results from post- translational regulation. On the other side, it is also known that the MEC1 cell line express high level of CD86, therefore the transfer of functional CD86 mRNAs from the MEC1-sEVs to the recipient myeloid cells cannot be excluded either[316] .

8.4. The response of myeloid cells to tumor-derived sEVs involves the activation of Toll-Like Receptors (TLRs)

8.4.1. Myd88

As it was previously shown by multiple teams, sEVs from multiple origins have the capacity to activate the TLRs (0). To test the hypothesis that TLRs are activated by CLL-derived sEVs, we used Myd88-KO mice. Myd88 is an adaptor protein essential to the transduction of signal following the activation of TLR, at the exception of TLR3. Myeloid cells were isolated from either C57BL/6J WT animals, or C57BL/6J Myd88$^{-/-}$ animals, as described in the Material and Methods section 7.2.12 and treated with 1, 5 or 10µg of TCL1-355 sEVs, or a positive control (yRNA4) and normalized to the control condition, the transfection reagent Effectene (Figure 20).

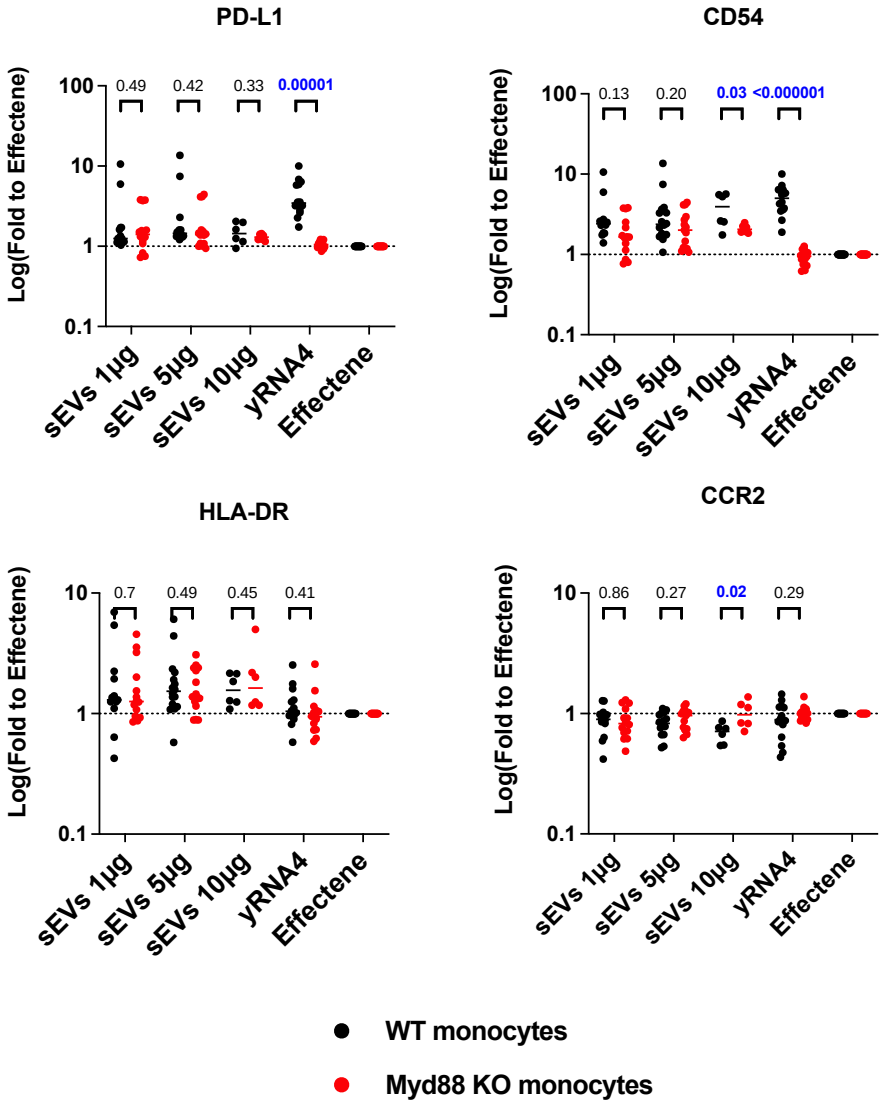

Figure 20: WT and Myd88-deficient myeloid cells respond similarly to treatment with CLL-derived sEVs. Myeloid cells from C57BL/6J WT animals or C57BL/6J Myd88$^{-/-}$ animals (n=3

per group) were treated with the indicated doses of TCL1-355 sEVs, effectene-encapsulated yRNA4 or Effectene, for 8 hours. The phenotype of myeloid cells was assessed by flow cytometry. The mean fluorescence intensities (MFIs) of PD-L1, CD54, HLA-DR and CCR2 were normalized to the MFIs of corresponding effectene-treated myeloid cells. The data are represented of 5 independent experiments. The normality of the data was validated by Shapiro test, and the p-values were calculated by unpaired t-test using GraphPad Prism 9.

TCL1-355 sEVs were able to induce an upregulation of PD-L1, CD54 and HLA-DR on both WT and Myd88$^{-/-}$ myeloid cells. Although the differences were statistically non-significant, the response of WT myeloid cells seemed to be slightly stronger for these three markers in response to sEV treatment in comparison to Myd88$^{-/-}$ myeloid cells. This difference was significant when looking at the expression of CD54 in WT or Myd88$^{-/-}$ myeloid cells treated with 10µg of sEVs. As expected, yRNA4 was able to induce PD-L1 and CD54 on WT myeloid cells but not Myd88$^{-/-}$ myeloid cells. Indeed, it has previously been shown that yRNA4 depends on the TLR7-Myd88 pathway to induce PD-L1 on myeloid cells [258]. Surprisingly, yRNA4 had in some experiments the potential to induce HLA-DR even in Myd88$^{-/-}$ myeloid cells. The use of increasing doses of sEVs seem to positively correlate with the upregulation of CD54 and HLA-DR, however a dose-response effect was not noticeable for PD-L1 upregulation. On the contrary, the downregulation of CCR2 seemed dose-dependent in WT but not Myd88$^{-/-}$myeloid cells. Altogether, the data seem to indicate a possible involvement of Myd88-dependant TLRs in response to sEV treatment. To further investigate if specific TLRs are of relevance for the effect of sEVs on myeloid cells, two additional murine models, TLR7$^{-/-}$and TLR4$^{-/-}$ mice, were used for a similar experimental set-up.

8.4.2. TLR7

In the next step, myeloid cells from WT and TLR7$^{-/-}$ animals were treated with different doses of TCL1-sEVs. The results are presented in Figure 21. As expected, the positive control yRNA4 was unable to induce PD-L1 and CD54 in TLR7$^{-/-}$ myeloid cells, whereas both markers were significantly induced in WT myeloid cells. No significant differences were observed for the yRNA4-mediated upregulation of HLA-DR, like the results obtained in Myd88$^{-/-}$ myeloid cells. However, the absence of TLR7 did not prevent the sEV-triggered upregulation of PD-L1, CD54 and HLA-DR. In this set of experiments, and contrary to the previous one, almost no downregulation of CCR2 was observed, most likely due to a technical difference as the source of sEVs was different between the two experiments. Although TLR7 is activated by sEV-derived small RNAs, in particular yRNA4, TLR7-ligands do not seem to be a major requirement for the activation of myeloid cells following treatment with sEVs. As ligands for TLR7 are single-stranded RNAs, the results above highlight an important involvement of other bioactive molecules such as double-stranded nucleic acids, proteins, and lipids for the activation of myeloid cells following sEV treatment.

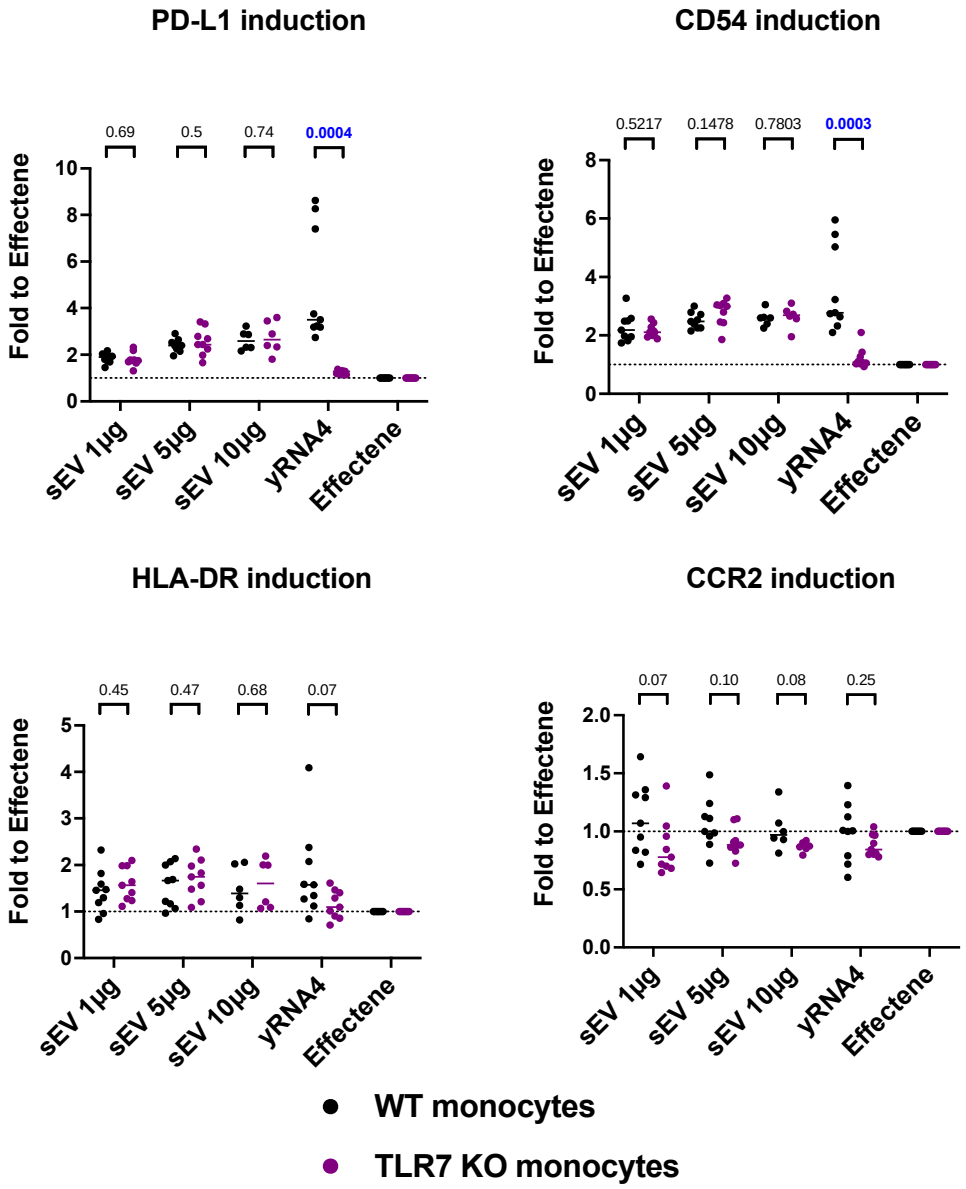

Figure 21: WT and TLR7-deficient myeloid cells respond similarly to treatment with CLL-derived sEVs. Myeloid cells from C57BL/6J WT animals or C57BL/6J TLR7$^{-/-}$ animals (n=3 per group) were treated with the indicated doses of Eμ-TCL1 sEVs, effectene-encapsulated yRNA4 or Effectene, for 8 hours. The phenotype of myeloid cells was assessed by flow cytometry. The mean fluorescence intensities (MFIs) of PD-L1, CD54, HLA-DR and CCR2 were normalized to the MFIs of corresponding effectene-treated myeloid cells. The data are represented of 5 independent experiments. The normality of the data was validated by Shapiro test, and the p-values were calculated by unpaired t-test using GraphPad Prism 9.

8.4.3. TLR4 and TLR2

8.4.3.1. TLR4

Several studies suggested that sEV-derived components have the capacity to activate TLR4 on the surface of recipient cells [271,342]. Candidate ligands for TLR4 include the Heat-Shock

Protein (HSP) family and HMGB1 [270,343–345]. Small RNAs seem to share the capacity to act as ligands for TLR4 [346]. However, if this is also the case for sEV-encapsulated small RNAs remains to be determined, although unlikely. To investigate a potential involvement of TLR4 in the response of myeloid cells to sEV treatment, both WT and TLR4$^{-/-}$ myeloid cells were treated with different doses of TCL1-355 sEVs, as described in the previous paragraphs.

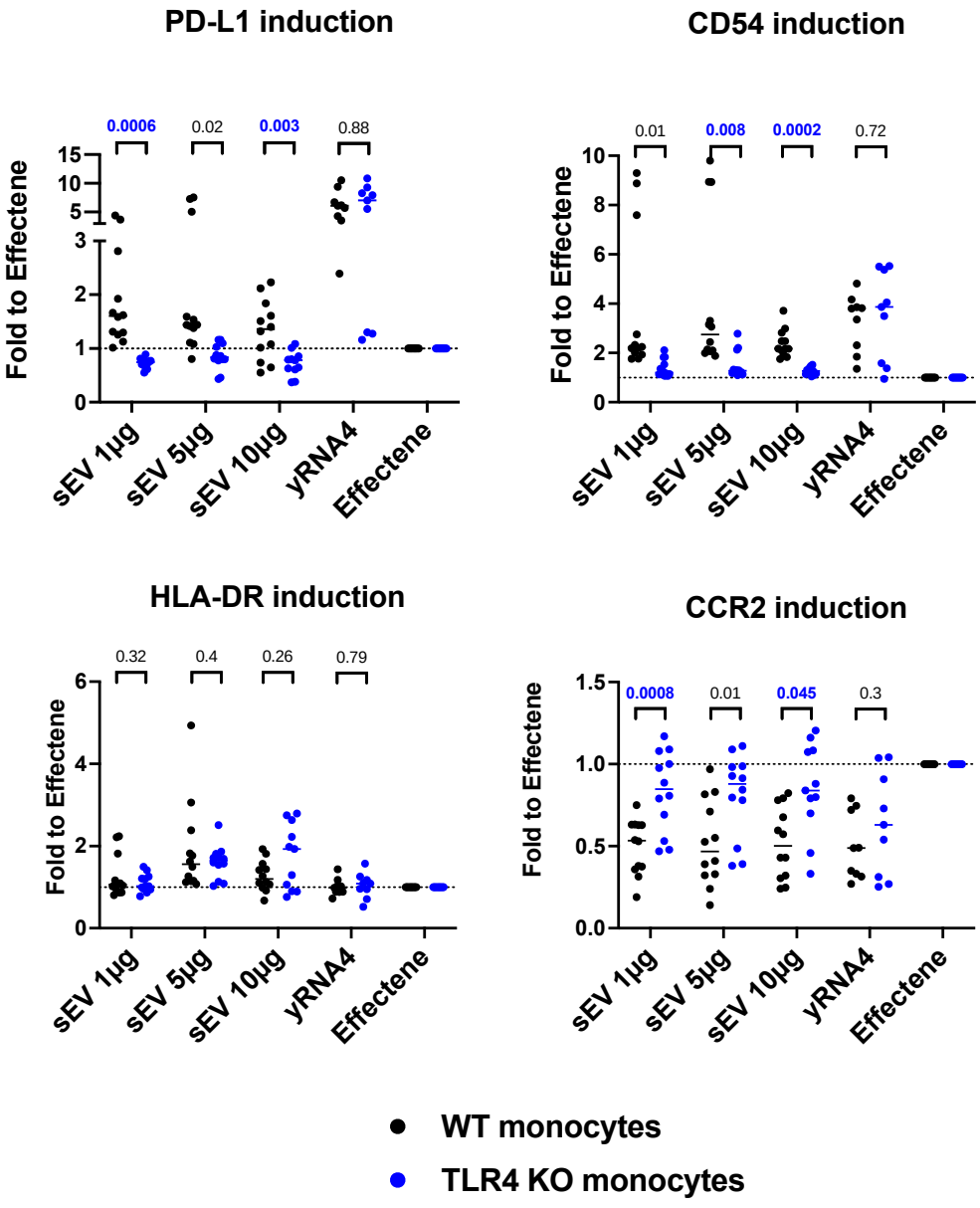

Figure 22: WT and TLR4-deficient myeloid cells respond differently to treatment with CLL-derived sEVs. Myeloid cells from C57BL/6J WT animals or C57BL/6J TLR4$^{-/-}$ animals (n=3 per group) were treated with the indicated doses of Eμ-TCL1 sEVs, effectene-encapsulated yRNA4 or Effectene, for 8 hours. The phenotype of myeloid cells was assessed by flow cytometry. The mean fluorescence intensities (MFIs) of PD-L1, CD54, HLA-DR and CCR2 were normalized to the MFIs of corresponding effectene-treated myeloid cells. The data are

represented of 5 independent experiments. The normality of the data was validated by Shapiro test, and the p-values were calculated by unpaired t-test using GraphPad Prism 9.

Interestingly, the obtained results showed statistically significant differences in the response of WT myeloid cells compared to TLR4$^{-/-}$ myeloid cells to sEV treatment, when considering PD-L1 and CD54 upregulation, as well as CCR2 downregulation, and this was true for all doses of sEVs used (1, 5 or 10 µg). On the contrary, the absence of TLR4 did not affect the capacity of sEVs to induce HLA-DR upregulation. Our results suggest that TLR4 may be an important receptor involved in the activation of myeloid cells following the contact with or uptake of tumor-derived sEVs. These results were furthermore investigated using a TLR4 reporter cell line.

8.4.3.2. Reporter cell lines

In addition to TLR4, TLR2 also appeared as a promising receptor activated by tumor-derived-sEVs [261,270,271,347]. To investigate the involvement of TLR4, and also TLR2, experiments involving the use of two reporter cell lines were set up in collaboration with Dr. Roman Hennel and Dr. Kirsten Lauber, at the Ludwig-Maximilians-Universität München. The sEVs were freshly isolated and sent on ice without prior freezing and thawing, and the experiments were performed by Dr. Hennel. The two cell lines (Invivogen, San Diego) are, genetically modified HEK293 cells stably expressing either the human TLR2 or human TLR4 proteins at the surface. In addition, the cells express the SEAP (secreted embryonic alkaline phosphatase) gene downstream of multiple NF-κB and AP1 binding sites (Figure 23, A). Activation of TLR2 or TLR4 leads to the activation NF-κB and AP1, which can be quantitatively assessed by chemiluminescence based on SEAP expression. For experiments involving TLR4 reporter cell lines, LPS (Lipopolysaccharide) was used as a positive control to activate TLR4 signalling. For experiments involving TLR2 reporter cell line, the synthetic diacylated lipoprotein FSL-1 was used a positive control. The activation of TLR4 and TLR2 was assessed following incubation for 8 hours with 1, 5 or 10µg of either MEC1 or HG3-sEVs. Although the experiments showed high heterogeneity from one sEV preparation to another, a dose-dependent activation of TLR4 and TLR2 was systematically observed upon sEV treatment (Figure 23, B). This observation was made for both source of CLL-derived sEVs.

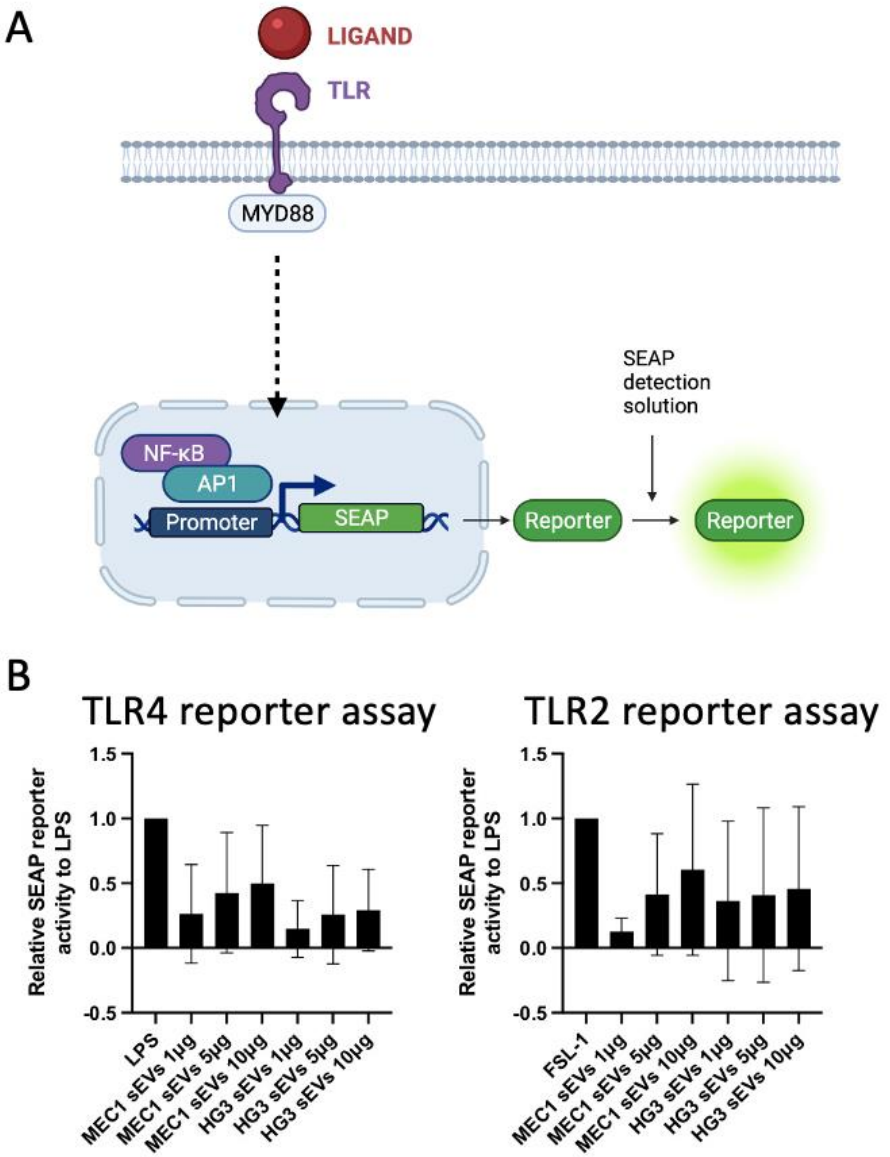

Figure 23: TLR4 and TLR2 are activated by CLL-derived sEVs in a dose-dependent way. (**A**) Schematic of the reporter cell lines. Following binding of the ligand to TLR, the signaling pathway leads to the binding of NF-κB and AP1 to the regulatory region of the SEAP protein. The amount of secreted SEAP can be assessed by fluorescence measurment and correlates to the promotor activity. (**B**) Relative SEAP promotor activity of TLR4 (left)) or TLR2 (right) normalized to the postive control: LPS for TLR4 reporter assay and FSL-1 for TLR2 reporter assay.The mean and standard deviation are plotted (n=4 independent sEV preparations).

8.4.3.3. Conclusion

The results described in this part are in line with the hypothesis that CLL-derived sEVs can induce TLRs on myeloid cells. Previously, our lab has shown that the yRNA4 and potentially all small RNAs activate TLR7 on recipient myeloid cells [258]. We bring here the evidence for an additional involvement of TLR4 and TLR2. Although TLR4$^{-/-}$ myeloid cells were clearly less responsive to sEV treatment than WT myeloid cells, only little differences were observed for

the TLR-adaptor protein Myd88$^{-/-}$ myeloid cells. A possible first explanation for such observations is that the signal transduction following TLR4 or TLR2 activation by sEV-derived bioactive molecules is not exclusively Myd88-independent, therefore could involve the TRIF-TRAM pathway. However, the classical upregulation of TNF-α or IFN-α expected following the activation of the TRIF-TRAM pathway was not detected in the microarray data (Supplementary figure 4). The involvement of Myd-88 independent Pattern Recognition Receptors (PRRs) such as TLR3, known to be activated by yRNA3 [348], or RIG-I-Like receptors [258] remains a possibility to be investigated. Our experiments suggest that the absence of TLR7 in myeloid cells, activated by small RNAs, does not prevent the sEV-induced polarization of myeloid cells when looking at the 4 markers PD-L1, CD54, HLA-DR or CCR2. Whether the signature induced in WT or TLR7$^{-/-}$ myeloid cells is truly similar or shows differences would require further investigations at a broader transcriptomic or proteomic level. However, the absence of TLR4 on myeloid cells clearly decreased the responsiveness of myeloid cells to sEV treatment. Interestingly, TLR4 is a surface receptor on myeloid cells, meaning that activation of TLR4 may depend on proteins presented on the surface of sEVs. Although the mechanisms of uptake of sEVs by recipient cells remains under investigation, it is unlikely that bioactive molecules present inside the sEVs interact with a surface receptor on recipient cells.

Limitations of the study

As previously mentioned, the culture conditions of the cells *in vitro* prior collection of the supernatant for sEV purification may impact the distribution of released sEV subpopulations. In addition, the storage conditions of sEV preparations were optimized and only fresh preparations were used towards the end of the project. Although it was attempted to reduce the bias and to ensure the same culture conditions of the cells at the time of sEV collection, it was still observed during the course of the above described experiments that the effect of one sEV preparation to another were slightly different, limiting to some extent the reproducibility of some of the results presented here. The use of reporter cell lines was firstly intended to overcome this limitation, however unsuccessfully. These observations underline the existence of numerous parameters influencing the cargo of secreted sEVs, a question being recurrently interrogated in the field, which would require intensive studies to address.

8.5. Mass-spectrometry analysis of LN-derived sEVs

To investigate the protein cargo of B-cell NHL sEVs, a proteomic analysis by mass spectrometry was performed on sEVs isolated from the LNs of 4 Diffuse Large B-Cell Lymphoma (DLBCL) patients, 4 Follicular Lymphoma (FL) patients and 4 patients presenting a reactive LN, an inflamed LN without any tumor detected during the histology analysis of the biopsy sample. The characteristics of the patients and received treatments are presented in the Material and Method section, Table 7.

The total number of detected proteins per sample showed large differences between the different samples (Figure 24, A). In particular, the proteome of sEVs isolated from rLNs were poor in protein diversity when compared to the sEVs from DLBCL or FL LNs. Additionally, one DLBCL and one FL sample (DLBCL3 and FL3) showed a low diversity of proteins as well. These results were compared to the protein concentration of the different sEV preparations (Figure 24, B). DLBCL3 and FL3 samples were lowly concentrated in protein, indicative of poorly enriched sEVs preparation. It was hypothesized that in those samples, non-sEV-derived proteins were highly enriched and contribute as an important part to the detected proteins. The differences were reflected by the results of the principal component analysis (Supplementary figure 5). Such differences are considered to be due to the original size of the biopsy sample, considered as small for the sample from DLBCL3 and FL3 patients, and highlight the importance of the starting material amount when collecting sEVs from tissues (Table 7). Additionally, the sEVs from the rLN2 showed a low number of detected proteins, probably linked to an overestimation of the protein concentration during the protein quantification (Figure 24, A and B). To overcome those limitations, only proteins present in 3 or more sample per group were considered for further analysis, and a rank-based analysis was performed to define the most enriched proteins per group.

In order to check the purity of our sEV preparations, the enrichment of sEV markers was checked in all samples. On this purpose, the list of the top 100 sEV-derived proteins from the Vesiclepedia database plus the sEV-derived biomarkers suggested in the studies from Hoshino, Kim, Bojmar (Lyden Lab) and colleagues and Kugeratski and colleagues (Kalluri lab) were analysed [239,349]. At the exception of the classical sEV-derived marker TSG101, most of these proteins were not only detected on the samples, but were highly enriched in all samples (Figure 24, C). Moreover, two markers suggested as sEV-derived biomarkers by the Kalluri lab, GNAI3 and GNAI2 were not detected in any of the samples. As expected, very little amounts of sEV-derived markers were detected in sEVs from the rLN2, therefore this sample was excluded from further analysis. In general, sEVs from rLNs were poorer in sEV-derived biomarkers, an observation that we link to the diminished enrichment in sEVs in those preparations. To investigate the B-cell origin of the sEVs, the presence of the B-cell markers CD20, CD19 and the lymphoma marker CD5 was verified. Surprisingly CD20, but not the other markers, represents one of the most enriched proteins in all samples (Supplementary figure 6). In addition, the presence of classical markers of contamination were checked and were not

detected or detected in very low amount (*Data not shown*). Altogether, these results suggest a strong purity of the sEV preparations and confirms the sEV-derived origin of the detected proteins.

Next, the three conditions were analysed individually. Across sEVs isolated from the LNs of DLBCL patients, a total of 5644 proteins were detected (Appendix). 3533 proteins (63% of all proteins) were common to 3 or more samples. These results highlight a high overlap of protein cargo between the different DLBCL samples. A total of 5446 proteins were detected across all sEVs from FL samples, out of which 3813 proteins (70% of all proteins) were common to 3 or more samples. Only 2507 proteins were detected across sEVs from rLNs, out of which 732 (29% of all proteins) were common to 3 or more samples.

The lists of proteins found in 3 or more samples for each condition were plotted as a Venn diagram (Figure 24, D). At the exception of one protein (IGHG2), all proteins detected in the sEVs from rLNs were commonly found in DLBCL or FL-derived sEVs.

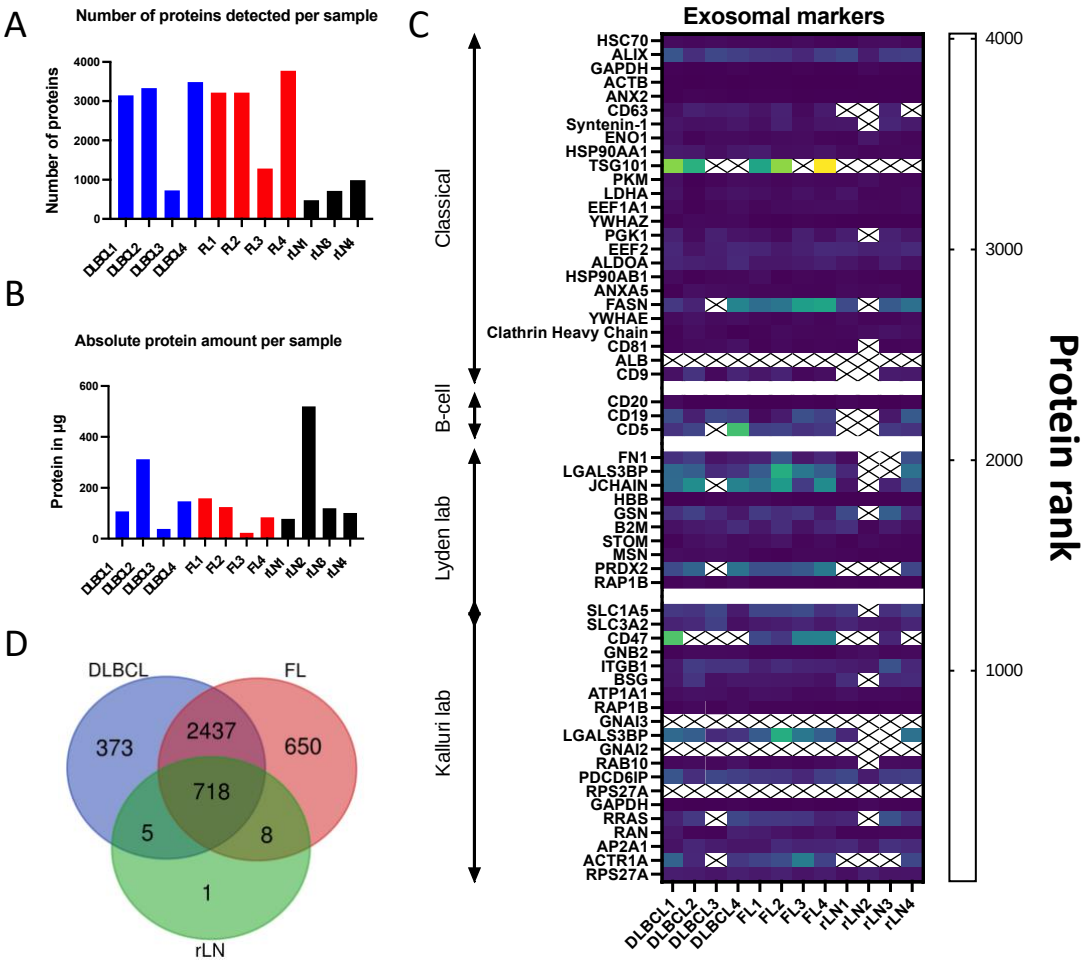

Figure 24: Characterization of LN-derived sEVs by Mass Spectrometry. (**A**) Total number of proteins detected in each sample (**B**) Absolute protein amount detected per sEV preparation, detected by BCA assay (**C**) Heatmap of the protein rank of indicated proteins for all samples.

“Classical” sEV markers correspond to the first 25 proteins on the Vesiclepedia List, “Lyden Lab” markers correspond to newly described sEV markers reported in Hoshino, Kim, Bojmar et al, and “Kalluri Lab” markers correspond to newly described sEV markers reported in Kugeratski et al[239,349]. Crossed fields indicate non-detected proteins.

As expected, the proteins common to all conditions were involved mainly in endosomal vesicle fusion (Figure 25, A); in addition to induction of immune tolerance, and cytokine production, among others. On the other side, an analysis of proteins common to DLBCL and FL sEV preparations revealed an enrichment of proteins involved in antigen presentation and subsequent T-cell activation (Figure 25, B). These results indicate that tumor-derived sEVs present both anti-tumor and pro-tumor functions, which may depend on the recipient cell type. A total of 38 proteins was found statistically differentially enriched between DLBCL and FL and is presented in Figure 26. Our data suggest that these proteins could be potentially considered as biomarkers to discriminate the two entities by analysing sEVs from the blood of patients, in particular when at risk of transformation from FL into DLBCL.

A

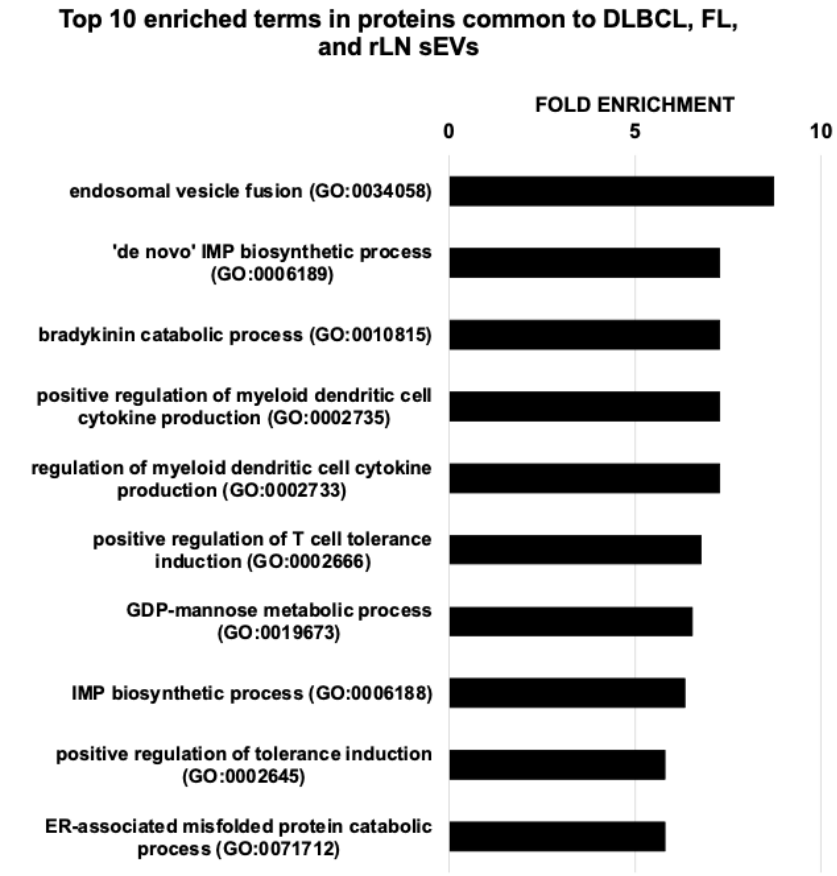
Top 10 enriched terms in proteins common to DLBCL, FL, and rLN sEVs
FOLD ENRICHMENT
0
5
10
endosomal vesicle fusion (GO:0034058)
'de novo' IMP biosynthetic process (GO:0006189)
bradykinin catabolic process (GO:0010815)
positive regulation of myeloid dendritic cell cytokine production (GO:0002735)
regulation of myeloid dendritic cell cytokine production (GO:0002733)
positive regulation of T cell tolerance induction (GO:0002666)
GDP-mannose metabolic process (GO:0019673)
IMP biosynthetic process (GO:0006188)
positive regulation of tolerance induction (GO:0002645)
ER-associated misfolded protein catabolic process (GO:0071712)

B

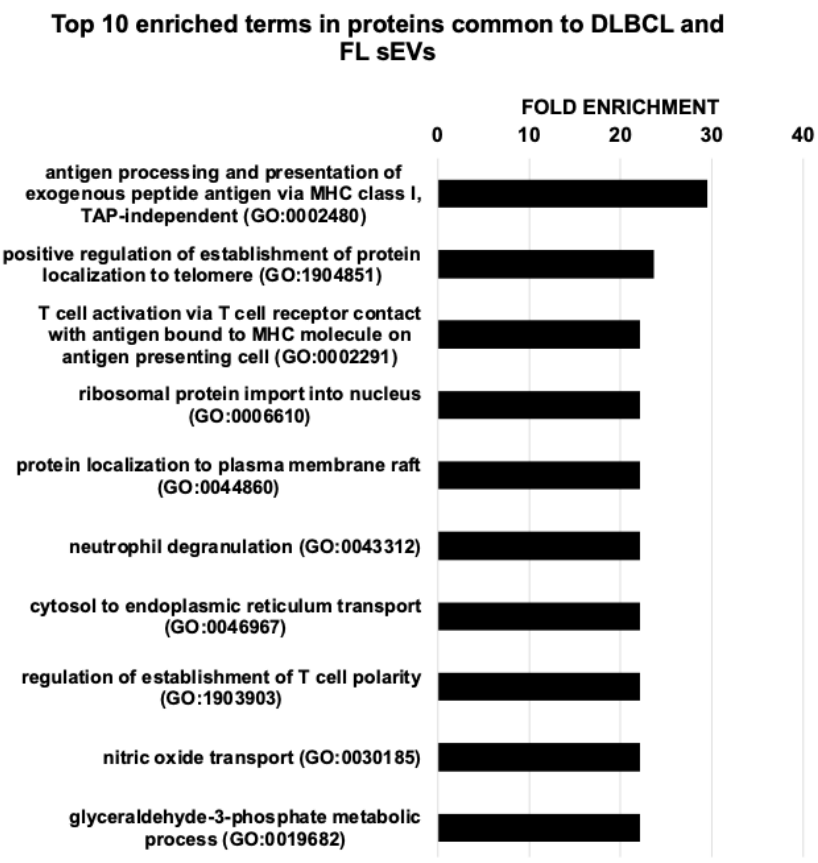
Top 10 enriched terms in proteins common to DLBCL and FL sEVs
FOLD ENRICHMENT
0
10
20
30
40
antigen processing and presentation of exogenous peptide antigen via MHC class I, TAP-independent (GO:0002480)
positive regulation of establishment of protein localization to telomere (GO:1904851)
T cell activation via T cell receptor contact with antigen bound to MHC molecule on antigen presenting cell (GO:0002291)
ribosomal protein import into nucleus (GO:0006610)
protein localization to plasma membrane raft (GO:0044860)
neutrophil degranulation (GO:0043312)
cytosol to endoplasmic reticulum transport (GO:0046967)
regulation of establishment of T cell polarity (GO:1903903)
nitric oxide transport (GO:0030185)
glyceraldehyde-3-phosphate metabolic process (GO:0019682)

Figure 25: Gene ontology analysis of enriched pathways among proteins common to DLBCL-, FL- and rLN-derived sEVs (A) or proteins unique to DLBCL- and FL-derived sEVs.

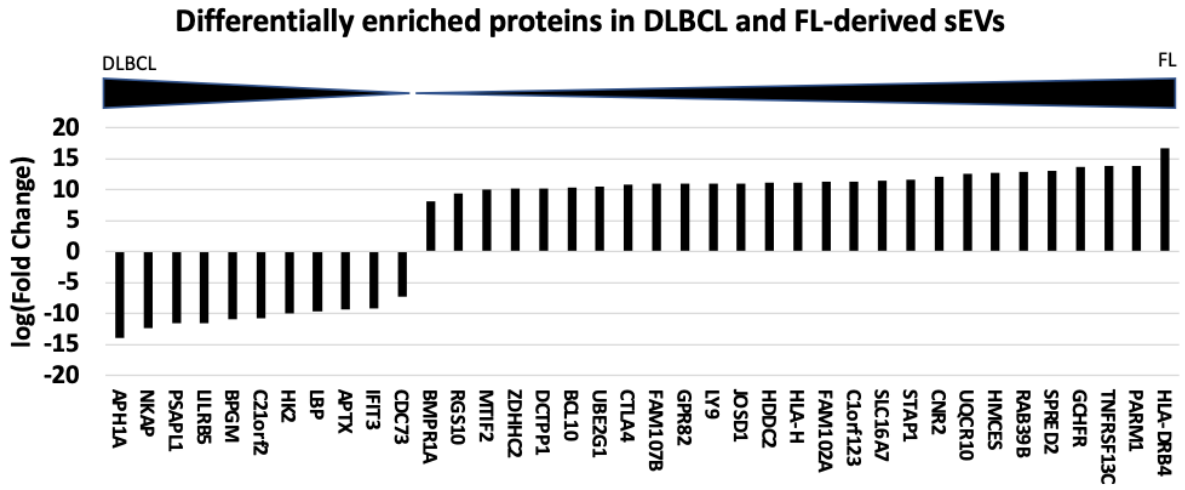

Figure 26: Differentially enriched proteins in the sEVs from DLBCL versus FL-derived sEVs.

Next, proteins specifically found enriched in DLBCL or FL-derived sEVs were analyzed further by performing Gene Ontology analysis (Figure 27) Interestingly, most of the top pathways related to DLBCL-sEV proteins were linked to RNA processing or maturation whereas the top pathways related to FL-sEVs proteins were linked to metabolism. These results tend to indicate important differences in the proteins cargo of DLBCL-derived or FL-derived sEVs.

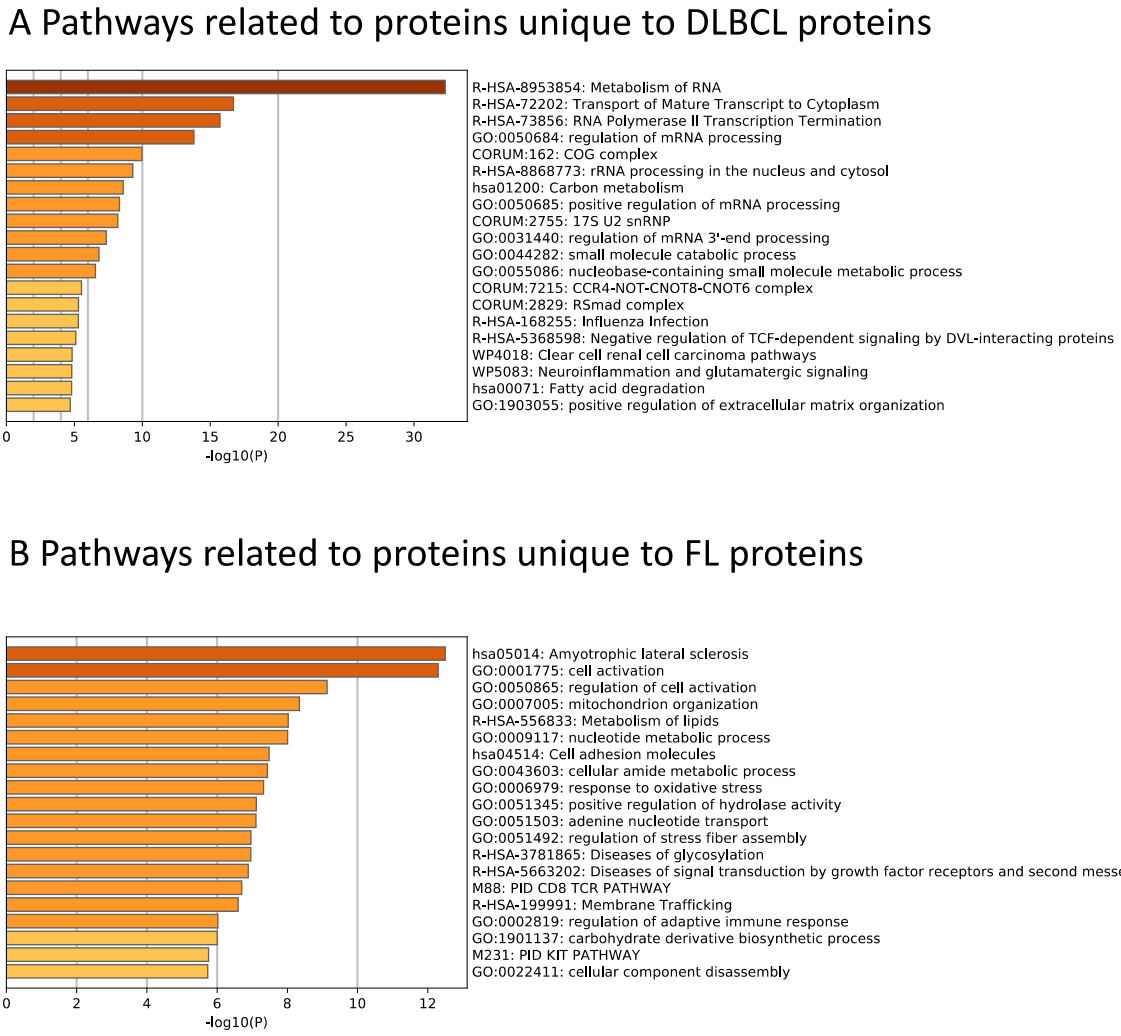

Figure 27: Pathway enrichment analysis of proteins specifically enriched in DLBCL-derived sEVs (**A**) or FL-sEVs (**B**); the analysis was performed using the Metascape software.

An additional gene set enrichment analysis (GSEA) analysis was performed to compare the proteome of DLBCL- and FL-derived sEVs. For this analysis the proteome data of the samples DLBCL3 and FL3 were removed due to the low number of detected proteins. The proteins exclusively detected in DLBCL sEVs or FL sEVs were analyzed using the Metascape platform. Interestingly, the proteins unique to DLBCL sEVs were mainly involved in pathways related to RNA processing, whereas the proteins unique to FL sEVs were mainly involved in pathways related to metabolism (Figure 27).

To search for candidate ligands for TLR2 and TLR4, the list of known endogenous ligands was crossed to the proteome dataset[344,350,351]. A multitude of TLR ligands were detected in DLBCL- and FL-derived sEVs but not detected in the sEVs originating from rLNs. This was the case for the S100A8, S100A9 and BGN and, in particular, for HMGB1 (Figure 28). In addition, some specific Heat Shock Proteins (HSPA1A, HSPB1, HSP90B1, and HSPA8), as well as fibrinogen and Myosin9 were found particularly enriched in the sEVs regardless of the origin of the LNs.

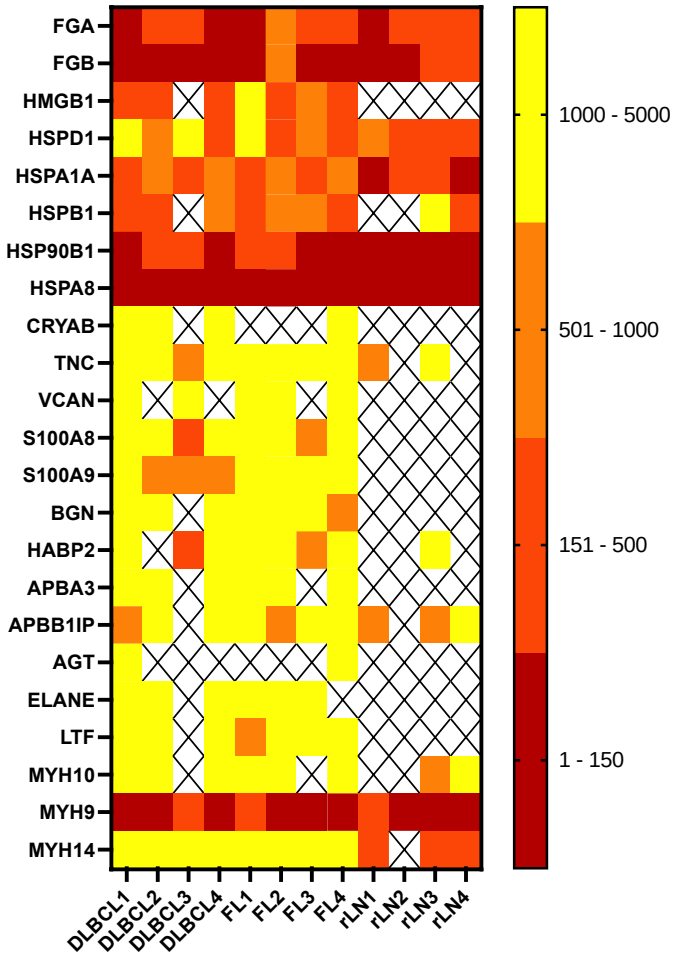

Figure 28: Tumor-derived sEVs are enriched in TLR ligands. Heat-map of the protein rank in each sample of known endogenous TLR ligand.

8.5.1.1. Conclusion

The results presented above suggest that reactive LNs were less enriched in sEVs than tumoral LNs. Indeed, the absolute number of proteins detected was lower in sEVs from rLNs compared to DLBCL or FL LNs. Additionally, it also remains possible that the cargo of tumor-derived sEVs was more enriched in proteins than the cargo of sEVs from rLNs. To answer this question, single-sEV approaches would represent an ideal tool; however, such techniques remained to be developed. Altogether, the data showed that numerous proteins can be detected in tumor-derived sEVs of DLBCL of FL origin, although absent from sEVs derived from rLNs. Among these proteins, a large proportion were present both in DLBCL and FL-derived sEVs. These observations suggest the existence of a protein signature present in tumor-derived sEVs, independently of the disease subtype. Nonetheless, proteins exclusively

detected in DLBCL or FL-derived sEVs allowed to propose several markers that can specifically differentiate DLBCL from FL-derived sEVs. A deeper analysis suggested that proteins specifically enriched in DLBCL-derived sEVs were involved in RNA processing, whereas proteins exclusively detected in FL-derived sEVs were linked to metabolism.

Finally, several endogenous ligands for TLRs were found enriched in both tumor-derived and rLN-derived sEVs, highlighting the capacity of sEVs to activate TLRs. Among those ligands were found the HSP family, including HSP90B and HSPA8 (HSP70).

Limitations to the study

Stronger conclusions would require the inclusion of more samples into the study. Additionally, the separation of B-cell-derived sEVs from sEVs of other cell origin would enhance the purity of the samples and strengthen our conclusions. In the future, the use of magnetic separation using, for example, antibodies against CD20, may represent a promising approach.

As I showed previously, TLR2 and TLR4 are activated following the treatment of cells with tumor-derived sEVs. However, TLR2 and TLR4 are two receptors expressed on the membrane of the cells. Therefore, it is likely that the TLR ligands present in tumor-derived sEVs are also presented on the surface of sEVs. Unfortunately, the analysis of sEVs' proteome does not allow to separate the proteins which are enriched at the surface of sEVs from the proteins enriched inside the sEVs. However, the development of techniques aiming at investigating the surface proteins on sEVs could help answer that question[184].

8.6. Investigating the function of yRNA4 in CLL-derived sEVs.

8.6.1. Creation of a new yRNA4-KO CLL cell line

The functions of the yRNA family remain poorly characterized. However, yRNAs can form complexes with proteins. This observation is of particular interest as yRNAs are among the most enriched small RNAs found in sEVs, independently of the sEV source. We therefore hypothesized that yRNAs may be required for the loading of specific proteins into the sEVs. As yRNAs were suggested to be involved in DNA replication, a deletion of multiple or all yRNAs is likely to lead to cell death and was therefore excluded. Instead, a deletion of the yRNA4 gene region was performed. Due to a higher transduction efficacy than MEC1 cells, the knock-out was performed in HG3 cells. A region of 908 base pairs was deleted from the cell lines' genome by CRISPR/Cas9-induced double strand breaks, targeting two PAM sequences located at the 5' and at the 3' ends of the yRNA4 gene. The deleted region did not contain any other coding region reported by the Human Genome Assembly GRCh38.p13. The deleted region was amplified by PCR and sequenced. An alignment to the sequence from the genome of reference containing yRNA4 clearly show that the deleted region was located, as expected, between the two guide RNAs (Figure 29, A). The genomic deletion was successfully visible by DNA amplification followed by gel electrophoresis (Figure 29, B). Total RNAs from the cells was extracted from three different replicates and the absence of yRNA4 transcript was validated by a Northern Blot approach (Figure 29, C). The Northern Blot was performed by Jeanette Seiler, in the lab of Prof. Dr. Sven Diederichs. From the cell pellet, only the full-length transcript but not the small fragment (31/32-nt) of yRNA4 was detected on the membrane. Two very weak, remaining bands were detected in the RNA samples from yRNA4-KO cells. We attribute this signal to the presence of two pseudogenes of yRNA4 RNY4P10 (95bp) and RNY4P7 (96bp), which also show a 100% homology with the yRNA4 primer. In particular, the RNYAP10 transcript is known to be found in the immune cells of the blood (www.genecards.org). Additionally, the RNYAP10 gene contains a binding site for FoxP2, a transcription factor expressed by the immune cells. RT-qPCR results also validated the efficient knock-down of yRNA4

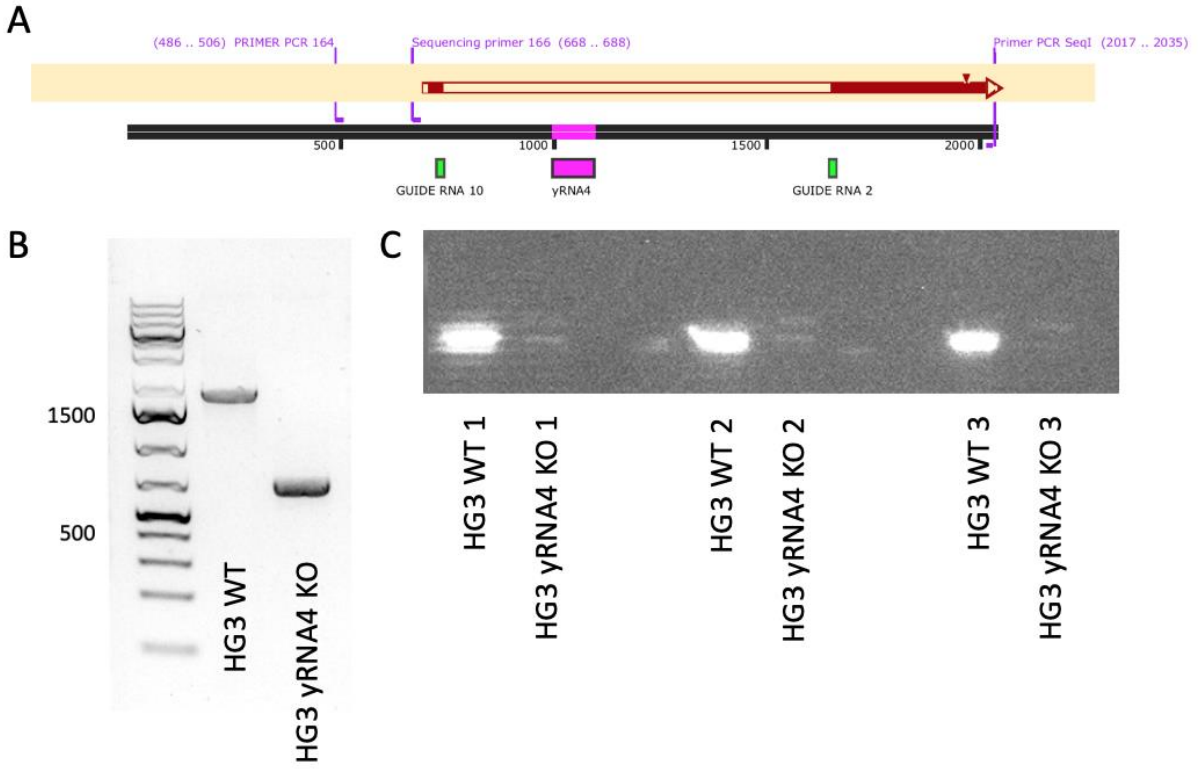

Figure 29: Validation of the yRNA4 deletion in the HG3 cell line (**A)** The genomic region containing the yRNA4 locus was amplified in HG3 WT and yRNA4-KO cell line and aligned. The region containing the yRNA4 gene and located between the two sequences targeted by the guide RNAs was absent from the yRNA4-KO cell line. (**B**) Analysis of the gel product size by electrophoresis. (**C**) Northern-Blot analysis of yRNA4 on total RNAs extracted from three technical replicates of HG3 WT and HG3 yRNA4-KO cells, isolated at different time points. A unique band with an estimated size of 96nt is visible in the WT samples.

HG3 yRNA4-KO cells did not differ from HG3 WT cell in terms of sEV secretion, or mean particle size as assessed by NTA (Figure 30, A and Supplementary figure 8). A difference in terms of protein per particle number was not detected (Figure 30, B). Furthermore, the protein profile of sEVs was compared by Ponceau staining and no differences were noticed (Data not shown). The deletion of yRNA4 did not impact the growth of the cells either (Figure 30, D).

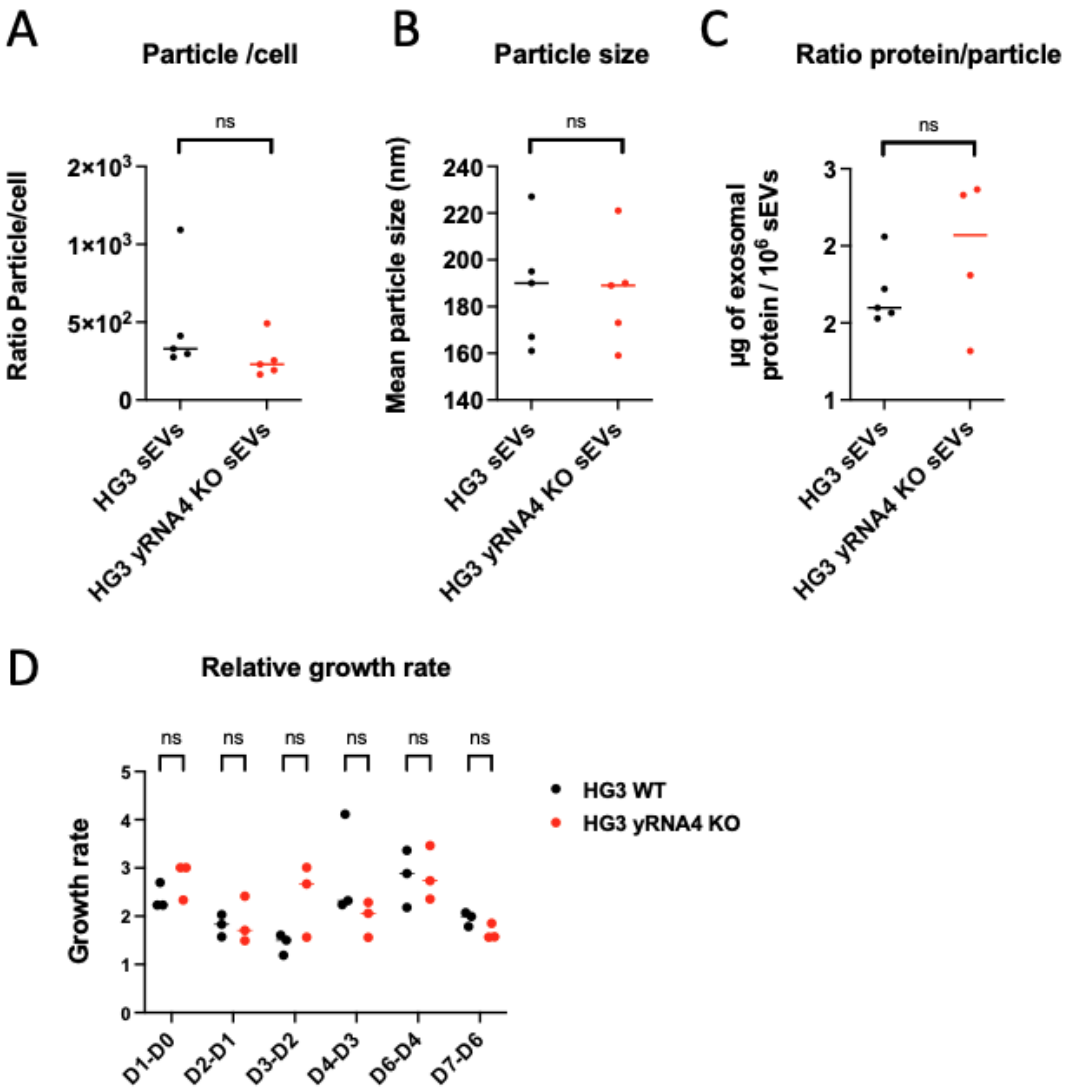

Figure 30: yRNA4 deletion in HG3 cell line does not affect the capacity of cells to produce sEVs. Comparison of the (**A**) Absolute number of particles isolated per cell, (**B**) Mean particle size and (**C**) absolute amount of protein isolated per million of sEV, in sEVs isolated from the HG3 WT or HG3 yRNA4-KO cell line. (**D**) Comparison of HG3 WT and HG3 yRNA4-KO cell growth rate between indicated time points.

It was recently suggested that EVs may be secreted from cell surface structures such as filopodia [190,352,353]. Scanning Electron Microscopy (SEM) analysis of HG3 and HG3 yRNA4-KO cell surface did not reveal differences in the shape of the cells, with filopodia and lamellipodia being similarly present at the surface of the cells (Figure 31). Analysis of the size and shape of sEVs from HG3 WT and HG3 yRNA4-KO cells by Transmission Electron Microscopy (TEM) did not reveal any noticeable difference in the size, shape or enrichment of sEVs (Figure 32).

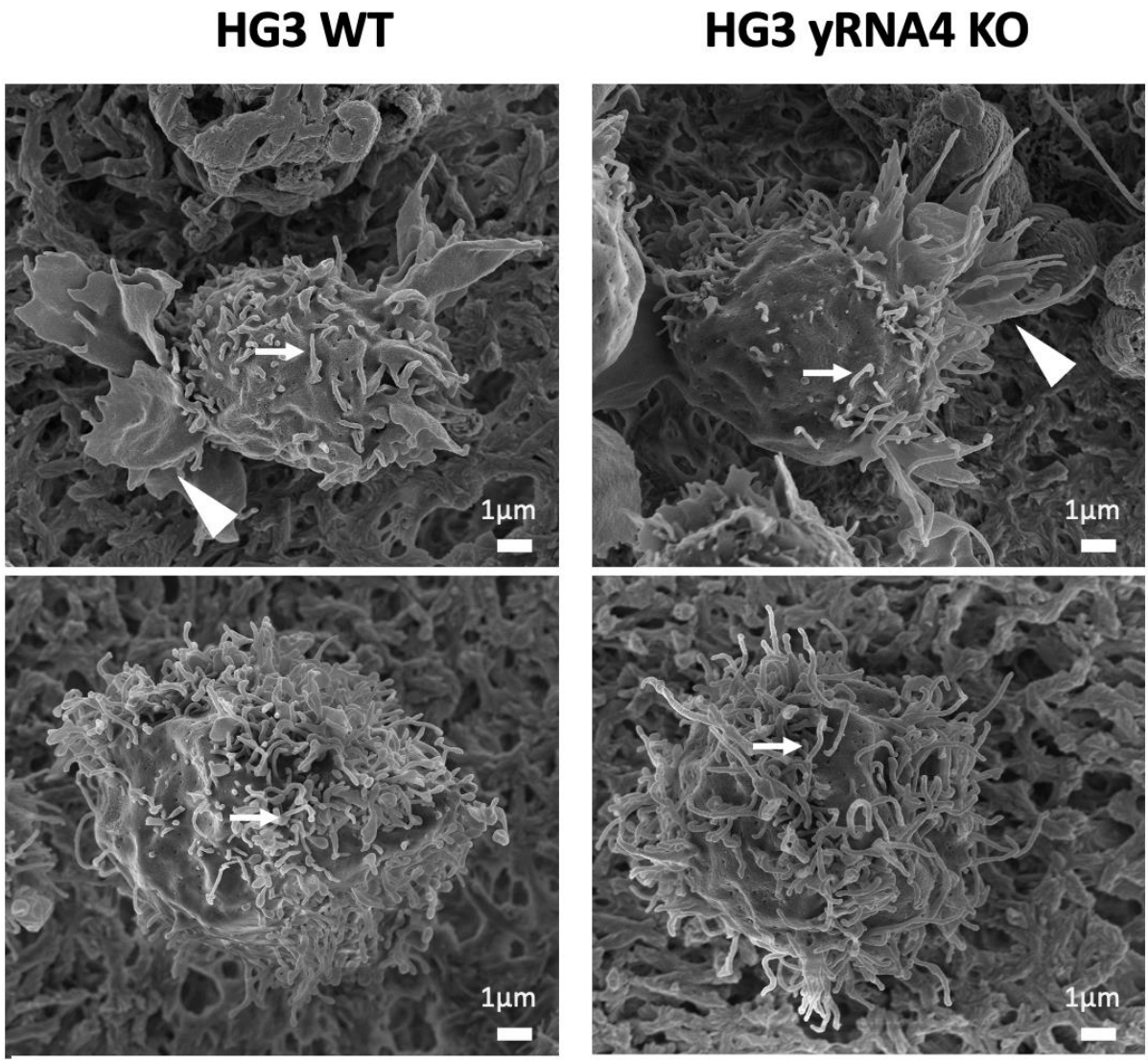

Figure 31: Scanning Electron Microscopy analysis of the surface of HG3 WT (left) and HG3 yRNA4-KO (right) cell lines. White arrows indicate lamellipodia structures, white arrowheads indicate examples of filopodia. Representative of n=3 samples.

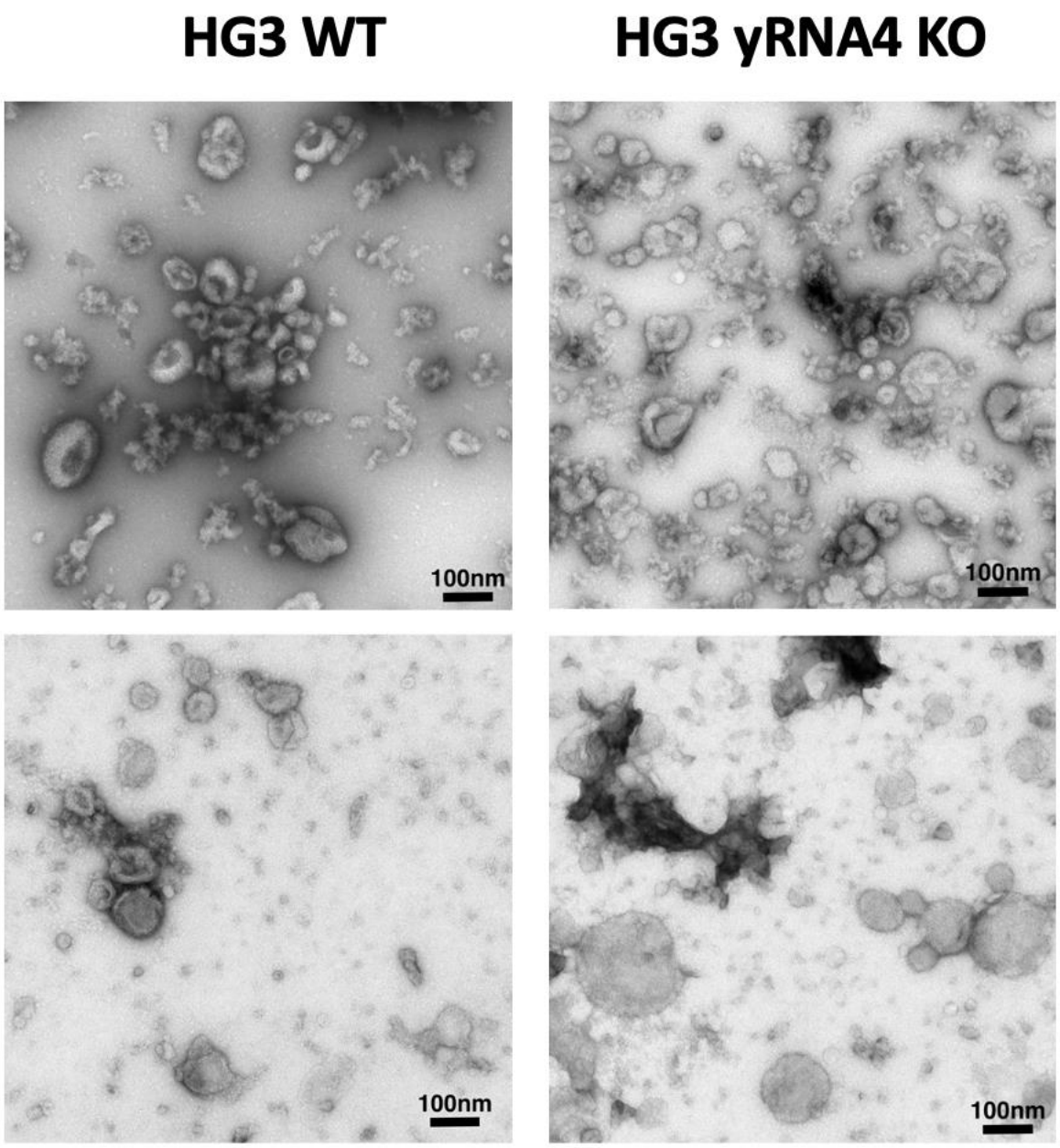

Figure 32: Transmission Electron Microscopy analysis of HG3 WT (left) and HG3 yRNA4-KO (right) cell-derived sEVs. Representative of n=3 samples.

8.6.2. yRNA4-deficient sEVs show a weaker potential to activate myeloid cells than control WT sEVs.

Next, small RNAs were extracted from WT or yRNA4-KO sEVs, and their profile analyzed on a Bioanalyzer No significant differences were detected in terms of RNA concentration per sEV nor in terms of its size profile (Figure 33, A and B). The capacity of both sources of sEVs in inducing an activation of myeloid cells was then compared. sEVs lacking yRNA4 clearly showed a decreased capacity to induce PD-L1 and CD54. Myeloid cells treated with 1 and 5µg

of HG3-WT sEVs showed a dose-dependent upregulation of PD-L1, while treatment with 10µg led to a weaker induction. This effect was repeatedly observed during the course of the project and attributed to a potential overstimulation, and potential cell death, of myeloid cells when using very high doses of sEVs. In comparison, treatment of myeloid cells with 10µg but not 1µg nor 5µg of HG3 yRNA4-KO sEVs lead to an upregulation of PD-L1. The upregulation of CD54 was similar when myeloid cells were treated with 1, 5 or 10µg of HG3 WT sEVs, although only the higher dose could induce an upregulation of CD54 when using HG3 yRNA4-KO sEVs (Figure 33, C).

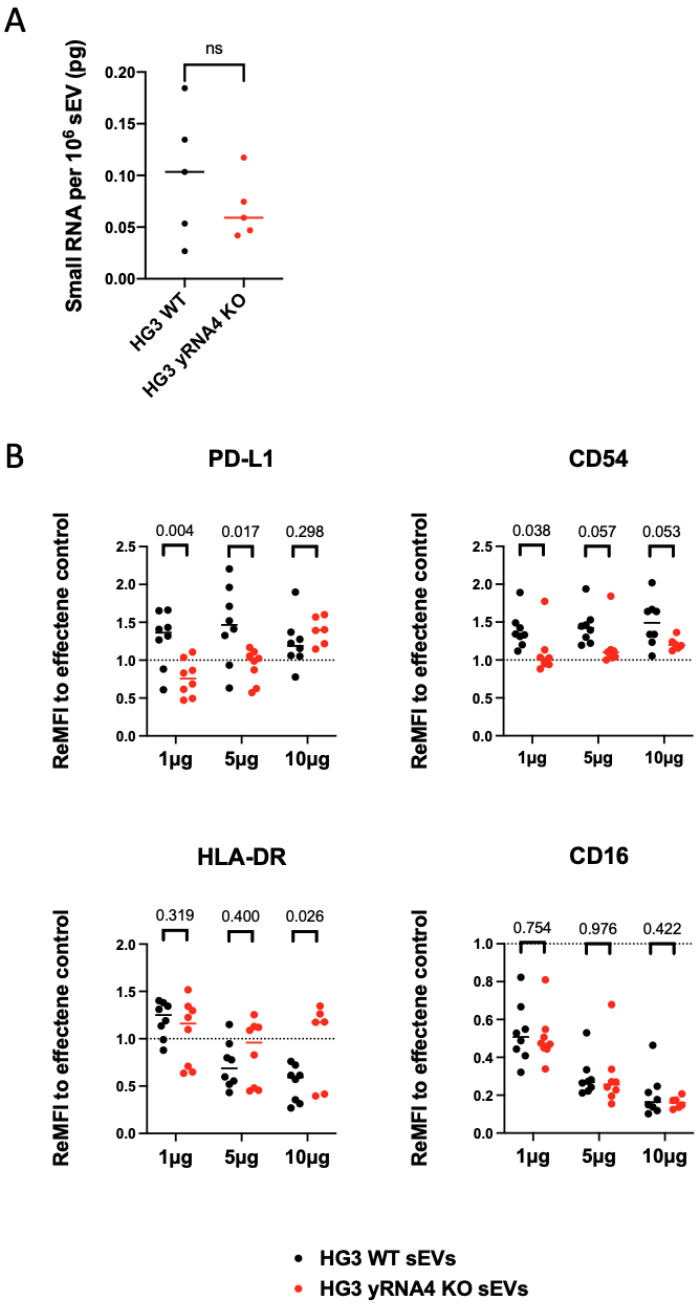

Figure 33: yRNA4-KO sEVs show a reduced capacity to activate myeloid cells. (**A**) Comparison of the absolute amount of small RNAs isolated per million sEVs between HG3-WT and HG3 yRNA4-KO. (**C**) Human myeloid cells from healthy donors were treated with the indicated

doses of HG3-WT or HG3 yRNA4-KO sEVs, or treated with Effectene for 8 hours. The phenotype of myeloid cells was assessed by flow cytometry. The mean fluorescence intensities (MFIs) of PD-L1, CD54, HLA-DR and CD16 were normalized to the MFIs of corresponding effectene-treated myeloid cells. The data are represented of 3 independent experiments. The normality of the data was validated by Shapiro test, and the p-values were calculated by unpaired t-test using GraphPad Prism 9.

8.6.3. Conclusion

It was previously observed that sEVs derived from CLL are particularly enriched in yRNA4, a small non-coding RNA. Similar to treatment with sEVs, myeloid cells treated with yRNA4 alone were polarized towards a pro-inflammatory phenotype characterized by the upregulation of PD-L1 and the secretion of pro-inflammatory cytokines such as CCL2, CCL3, or IL-6[258]. This dissertation presented for the first time a knock-out of the yRNA4 gene in the CLL cell line HG-3. This knock-out was validated by PCR, RT-qPCR as well as Northern Blot. The knock-out of the RNA4 gene did not affect the cells' capacity to secrete sEVs, nor the morphology of the sEVs. Additionally, SEM analysis also showed that the presence of lamellipodia nor filopodia, known to be the sites of sEVs secretion, was not affected at the surface of yRNA4-KO cells. However, sEVs derived from the yRNA4-KO HG-3 cells have a reduced capacity to induce a pro-inflammatory phenotype in myeloid cells than their WT counterpart. I hypothesize that the response of myeloid cells to yRNA4-KO sEVs was not only due to the absence of yRNA4 but also to the absence of specific proteins which require yRNA4 to be loaded into the sEVs. Indeed, the members of the yRNA family are known to form complexes with specific proteins (5.3.3.2). To assess this question, future experiments are ongoing to compare the proteome of WT and yRNA4-KO sEVs.

Limitations of the study

yRNA4 belongs to a family of 4 small non-coding RNAs, together with yRNA1, yRNA3, and yRNA5. Other yRNA family members have been found enriched in CLL-derived sEVs together with yRNA4. It is believed that yRNAs have overlapping functions. For these two reasons, ideally, a knock-out of all yRNA family members should have been performed. However, due to their role played in DNA replication, such a knock-out would likely lead to the cell line death and therefore was not attempted. Another possibility remains the additional knock-out of two, or three, yRNAs.

9. DISCUSSION AND FUTURE PERSPECTIVES

9.1. Optimization of cell culture, isolation and storage conditions for sEVs

9.1.1. Efficient isolation of sEVs from solid lymphoid tissues

sEVs are commonly isolated from biofluids, where they are enriched. This is the case for plasma, urine, milk, saliva, etc. Isolation of sEVs from biofluids is particularly interesting when searching for biomarkers of cancer diagnosis, progression, or to follow up the response to treatment in patients[354]. However, sEVs isolated from biofluids are of mixed parental origin. As an example, plasma is particularly enriched in platelet-derived sEVs[355]. This mixed origin remains a limitation when answering fundamental questions regarding the function of tumor-derived sEVs. So far, studies focusing on tumor-derived sEVs were limited to the use of primary cells or cell lines *in vitro*.

A way to partially overcome this limitation is to isolate sEVs from tumor biopsies highly enriched in tumor cells. This dissertation includes one of the first studies to isolate sEVs from lymphoid solid tissues. Two models were then used: the lymph nodes of B-cell NHL patients, known to be highly enriched in tumor cells, and the spleen of a CLL murine model, where the tumor cells accumulate until representing almost the sole cell population present in the organ.

Efficient enrichment of sEVs from these two tissues was obtained when using differential centrifugation combined with size-exclusion chromatography (SEC). On the contrary, using differential centrifugation combined with ultracentrifugation on a sucrose density cushion leads to a dramatic loss of material, with some final sEV products being poorly enriched in sEVs as analyzed by TEM. SEC also led to higher purity of the sEV preparations. Preliminary data have shown that two passages on the chromatography column do not show superiority over one passage regarding the efficient separation of protein complexes from sEVs. Nonetheless the approach presented here does not permit the selective sorting of tumor-derived sEVs. Such a selection may be however possible using magnetic separation[239] . However, magnetic separation is an approach requiring first finding an ideal cancer marker expressed in sufficient quantity at the surface of sEVs to use as target for magnetic bead-coupled antibodies. Moreover, it remains to be determined if labeling sEVs with magnetically-labeled antibodies does not affect their integrity or function, particularly due to their nanoscopic size.

For the tissue dissociation, prior to the isolation of the sEVs, it was decided not to use any enzymatic digestion to avoid possible degradation of surface proteins on sEVs. However, when working with murine spleens, a step to induce the lysis of red blood cells was included, whose effect on the integrity of sEVs was not tested.

Interestingly, the isolation of sEVs with the used protocols was easier when the tissue of origin was human lymph nodes compared to murine spleens. Indeed, the ultracentrifugation of

supernatant coming from spleens but not lymph nodes gives rise to a sticky pellet, which is hard to resuspend before the application onto the SEC column or onto the sucrose density cushion, and may contain an important part of the sEVs. This difference could be due to the co-isolation of extracellular matrix components present in the spleen. Therefore, optimization of organ processing to perform sEV isolation, especially from the spleen, remains open. Another approach would be to culture the biopsy samples *in vitro* and collect the sEVs from the supernatant of the cultures as recently suggested[356] . However, the cell viability would have to be carefully controlled to avoid the co-isolation of apoptotic bodies with sEVs.

As a limitation, the study presented in this dissertation did not aim to elucidate the superiority of one of the mentioned isolation protocols when it comes to efficient separation of sEVs from lipoproteins, viruses, or chylomicrons[357]. One suggested approach to increase the purity of sEV preparations would be the combination of both protocols [358,359]. This combination however leads to a drastic loss of material and requires very large volumes of starting supernatant.

To add a layer of complexity, it has been previously shown that cells can release different subpopulations of sEVs [360,361]. Our immunoblot data gave a first indication that the use of different isolation methods may also lead to the isolation of different subpopulations of sEVs. Single-exosome analysis would represent an ideal approach to investigate further to which extent the choice of the isolation method influences the isolated subpopulation but remains challenging. The use of asymmetrical flow field-flow fractionation or microfluidic devices, if these techniques become more accessible, represents promising techniques to efficiently separate sEV subpopulations [357,362]. Additionally, the use of the ImageStream® flow cytometry system could efficiently discriminate different subpopulations of sEVs based on their surface proteins.

Finally, sEVs is a generic term which includes both exosomes, present in the Multivesicular bodies (MVBs) and liberated into the extracellular space upon fusion of the MVB to the plasma membrane, and small size-ectosomes, directly released upon budding of the plasma membrane. Up to now, isolation techniques to separate those two populations are lacking, but new markers of each population are offering new opportunities to ensure a better separation[299].

9.1.2. Production of sEVs *in vitro*: factors influencing the function of isolated sEVs.

During the course of the project, most of the sEVs were isolated from immortalized cell lines cultured *in vitro* (MEC1, HG3, or TCL1-355). It was observed that the capacity of sEVs to induce polarization of myeloid cells could be relatively different from one preparation to another. In particular, preliminary results indicated that the sEVs collected from cells in a bioreactor show different effects than sEVs collected from cells in classical cell culture flasks. Although sEVs isolated from HG3 WT and HG3 yRNA4-KO cells show a differential impact on myeloid cells when originating from classical flasks, this effect was lost when they were of

bioreactor origin. One explanation is that the use of bioreactor does not only lead to the enrichment of sEVs in the cell compartment but also the strong enrichment of proteins. Comparison of negative sEV-derived markers by immunoblotting in both types of preparations could provide a first answer to that question.

Furthermore, some preliminary data indicate that the storage of sEVs at -80°C may change their integrity and therefore function. This effect may be due to the fusion of sEVs following freezing at –80°C, as recently reported[363]. TEM did not allow to notice a loss of integrity of the sEV membranes following a freezing step as the lipidic structures can reform following thawing[363]. In line with our hypothesis, several studies reported a change of mean particle size or zeta potential following the freezing of sEVs[294,364,365] . In the future, developing techniques to perform surface profiling of sEVs (*e.g.*, Nanoflow Cytometry) may allow for answering this interesting question. Although several studies recommended the use of cryopreservants for the storage of sEVs at -80°C, such as DMSO, such cryopreservants may have deleterious effects on the integrity of sEVs' membrane following thawing. To limit the effect of potential rupture of the sEVs membrane during a freeze-thaw cycle, it is recommended to use freshly isolated sEVs for all further applications, including functional assays or characterization.

9.2. Response of myeloid cells to B-cell NHL-derived sEVs

9.2.1. The polarization of myeloid cells through a hypothetical HSP/TLR/NF-kB pathway

Tumor-derived sEVs activate surface and intracellular TLRs

In this dissertation, it was shown that myeloid cells get polarized following treatment with tumor-derived sEVs. The next section will discuss whether this polarization is pro- or anti-tumoral. Contrary to other cell types, it is well described that sEVs do not only accumulate at the surface of myeloid cells but are also efficiently internalized by myeloid cells and macrophages [366–368]. Therefore, I imply that tumor-derived sEVs have a double way of polarizing myeloid cells: 1) through EV surface proteins interacting with cell surface receptors and 2) through the release of sEV-derived bioactive elements in the cytoplasm upon EV uptake by the recipient cells.

In line with the first part of the hypothesis, the results presented here highlight the activation of the cell surface receptors TLR2 and TLR4 following treatment with tumor-derived sEVs. In line with the second part of the hypothesis it was previously shown that the yRNA4, a small non-coding RNA enriched in tumor-derived sEVs, efficiently activate the intracellular TLR7. The analysis of the signature of myeloid cells following treatment with MEC1-sEVs also showed the activation of the NF-kB pathway, downstream of TLR2, TLR4, and TLR7. The activation of other TLRs (TLR1, TLR3, TLR5, TLR6, TLR9) following treatment of myeloid cells with tumor-derived sEVs remains to be investigated.

In this dissertation, I tried to investigate the potential ligands responsible for the activation of the TLR2, TLR4, and TLR7.

TLR7 is activated by single-stranded RNAs enriched in tumor-derived sEVs

TLR7 is known to be activated by single-stranded RNAs[369]. Therefore, it is likely that its activation in myeloid cells following treatment with tumor-derived sEVs results not only from the binding of yRNA4 to TLR7 but from potentially all single-stranded RNAs enriched in tumor-derived sEVs. One way of confirming this hypothesis would be to treat TLR7-reporter cells with tumor-derived sEVs, or tumor-derived sEVs depleted of RNAs. However, treatment of sEVs with RNase alone is not sufficient, the sEVs being protected from the RNase by their membrane. One solution to overcome this limitation is the combination of RNase to a detergent to ensure the entry of RNase into the sEVs. The concentration of detergent would have to be carefully chosen, in order to ensure the entry of RNase into the sEVs without disrupting the membrane.

TLR2 and TLR4 are potentially activated by HSPs present at the surface of sEVs

TLR2 and TLR4 being surface receptors on myeloid cells, their potential ligands must be localized at the surface of sEVs. An analysis of the proteome of B-cell NHL-derived sEVs was performed to answer this question, but did not allow to discriminate the proteins localized at the surface of sEVs from the proteins localized inside. Interestingly, the proteome analysis of B-cell NHL-derived sEVs revealed a strong enrichment of the HSP family members, particularly HSP90A, HSP90B, HSC70, and HSP70. HSPs are known endogenous ligands for TLR2 and TLR4, among others. HSPs are known to relocate to the cell membrane under stress conditions such as cancer; and this relocation may correlate with metastatic potential[370]. Therefore, it is likely that sEVs derived from tumor cells carry transmembrane forms of HSP family members. Due to its high enrichment in B-cell derived-sEVs, HSP70 represents a strong candidate as a ligand for TLR2 and TLR4.

Experiments investigating the transmembrane localization of HSP70 in sEVs were attempted. Tumor-derived sEVs were treated with proteinase K at different concentrations and the clearance of surface or intra-sEV proteins was tested as described before[371]. To analyze the clearance of surface HSP70, the signal of a classical anti-HSP70 antibody recognizing the intra-sEV form of the protein was compared to the signal of the cmHSP70.1 antibody recognizing the extracellular domain of the protein and kindly provided by Dr. Gabriele Multhoff at the Technische Universität München. However, the results of this experimental approach were non-conclusive.

Another approach would be to use a fluorochrome-conjugated form of the cmHSP70.1 antibody and perform nanoflow cytometry.

A third possibility would be to express a modified form of HSP family members carrying an HA-tag fused to the extracellular domain of the protein and analyze HA-signals on the surface of sEVs.
In addition, modulation of the expression of certain HSP family members expression in sEV-donor cells could be attempted, by using inhibitors or genetic engineering. The resulting sEVs, whether enriched or depleted for specific HSPs, would be functionaly tested for their capacity to induce the polarization of myeloid cells. However, it was described before that the downregulation of an HSP member may lead to a compensation mechanism leading to the upregulation of other members, particularly for HSP90 and HSP70[372].

TLR2 and TLR4 are potentially activated by other ligands than HSPs

The data presented here also indicate that other known endogenous TLR ligands are enriched in the proteome of sEVs from B-cell NHL patients, including the proteins of the S100 family, myosins, HMGB1, and fibrinogen. The S100 protein family was not investigated for the localization of family members on sEVs due to their poorer enrichment in the sEVs compared to other candidate ligands, and the fibrinogen proteins are likely contaminants of the ECM. As discussed in the introduction, the presence of HMGB1 in sEVs remains controversial; thus, considering HMGB1 as a candidate requires some additional validation steps. Myosin9 represents an interesting candidate due to its high enrichment in B-cell NHL-derived sEVs; nonetheless, its potential localization at the surface of sEV remains to be investigated.

Other Pattern-Recognition Receptors (PRRs) than TLRs are activated by tumor-derived sEVs

The data presented in this thesis have shown that myeloid cells deficient for Myd88, an adaptor protein required for the transduction of TLR2, TLR4 and TLR7 signals, still respond to the treatment by tumor-derived sEVs. These results are in line with the hypothesis that Myd88-independent PRRs are involved in the response of myeloid cells to tumor-derived sEVs. Such receptors include TLR3, a known receptor for yRNA3[373], RIG-I-like receptors (RLRs), or C-type lectin receptors (CLRs).

9.2.2. The polarization of myeloid cells by tumor-derived sEVs: pro- or anti-tumoral?

Analysis of the signature of myeloid cells following treatment with tumor-derived sEVs revealed an upregulation of PD-L1 combined with an enrichment of the IL10 pathway, a feature of M2 macrophages[374]. Additionally, it was shown that myeloid cells increased the secretion of IL6 and CCL2, considered M1-derived factors. Altogether, those data indicate that sEV-polarized myeloid cells have both pro- and anti-tumoral features.

To investigate the pro-tumoral function of sEV-treated myeloid cells, their capacity to inhibit the cytotoxic activity of CD8+ lymphocytes should be tested. The use of a co-culture of sEV-

polarized myeloid cells and CD8+ lymphocytes could provide further evidence. In particular, testing the cytotoxic potential of antigen specific CD8+ lymphocytes, by using *e.g.,* the OVA peptides, following coculture with sEV-treated or “naïve” myeloid cells would represent an efficient way to answer this question. Interestingly, myeloid cells treated with tumor-derived sEVs upregulated both PD-L1 and ICAM-1. The expression of both markers at the surface of myeloid cells-derived sEVs normally ensure an efficient PD-1-mediated inhibition of T cells at distant sites[375].

It was previously reported that myeloid cells and macrophages play a major role in the B-cell NHL microenvironment, and seem to be essential to tumor cell survival and proliferation. *In vivo*, depletion of myeloid cells delays tumor development[121,123,129,376]. It would be of interest to investigate by coculture assays if tumor cells gain a differential survival advantage when in contact with sEV-treated or “naïve” myeloid cells. The role of myeloid cells for the tumor microenvironment may also be investigated *in vivo*; by comparison of the effect of sEVs on the tumor growth in immunocompetent versus myeloid cell-depleted animals. Myeloid cell depletion can easily be achieved using clodronate liposomes.

To investigate the overall potential of sEVs to induce a pro- or anti-tumoral microenvironment, *in vivo* assays must be considered. The treatment of mice with tumor-derived sEVs followed by the injection of the tumor and follow-up of the tumor growth represent a straightforward direction to take in the future. Recently, García-Silva and colleagues have shown that sEVs injected in the footpad of mice leads to the internalization of the sEVs by cells from the LNs, in particular the myeloid and the endothelial cells. The education of mice by tumor-derived sEVs favors the development of metastasis[377].However, such experiments require to have access to murine-derived sEVs in large quantities, a condition which was not completed during the course of this project. Additionally, it is to be highlighted that the application of sEVs by intravenous injection often results in an accumulation of the sEVs in filtering organs such as kidney or liver and may not result in a physiological biodistribution of the injected sEVs. Another approach is the use of drugs to inhibit the secretion and/or internalization of sEVs [378,379]. Although attractive, the use of such drugs also leads to other effects on the organism which may impair the read-out of such studies. As an alternative, the deletion of a gene involved in sEV biogenesis in the tumor cells represents an attractive opportunity. This was particularly shown in melanoma using Rab27 deficient tumor cells, with a decrease of their capability to induce metastasis[380,381]. A combination of different approaches remains then the best option to interrogate the pro- or anti-tumoral function of sEVs.

In the context of NHL, it remains unknown if tumor-derived sEVs promote or prevent metastasis. One of the main metastatic sites for NHL remains the bone marrow. Preconditioning of the (BM) with tumor-derived sEVs could be achievable by intra-femoral injection of tumor-derived sEVs, in a murine model of NHL; and the colonization of the bone marrow by tumor cells, could be assessed by flow cytometry.

9.2.3. The role of yRNA4 in tumor-derived sEVs.

yRNA4 has been previously shown to be highly enriched in the sEVs from the B-cell NHL cell line MEC1[382]. yRNA4 was shown to act as a ligand for the endosomal TLR7 receptor and induce PD-L1 upregulation in myeloid cells, similarly to sEVs. The results of this dissertation showed that the deletion of yRNA4 from another B-cell NHL cell line, HG3, does not impact the capacity of the cells to secrete sEVs. However, sEVs depleted from yRNA4 showed a reduced capacity to induce a polarization of myeloid cells. Two hypotheses can explain the obtained results. First, the deletion of yRNA4 did not impact the rest of the cargo loaded into the sEVs and therefore the differential response of myeloid cells is the results of the sole absence of yRNA4 from the sEVs. Secondly, considering that yRNA4 is able to complex with multiple proteins, its deletion in the cell results in changes of the sEV proteome affecting their capacity to polarize myeloid cells. To investigate the second hypothesis, a proteome analysis by Mass Spectrometry of HG3 WT and HG3 yRNA4-KO sEVs should be performed. Preliminary results using immunoblot tend to indicate a depletion of the yRNA-binding partners APOBEC proteins in the sEVs from HG3 yRNA4-KO. Interestingly, the loading of APOBEC protein into the sEVs may lead to a deamination of RNAs present in the sEVs and modify their potential to activate PRRs[383].

Concerning the mechanism of action of the yRNA family, a recent study suggested that a part of yRNAs could be presented on the membrane of the cell in a glycosylated form[236]. Whether such forms of yRNAs are present as well on the surface of sEVs and to which extend they can functionally lead to myeloid cells' polarization remains to be investigated.

The different family members of yRNAs having overlapping function and binding partners, it would be of interest to perform single knock-outs of other yRNA family members as well as multiple yRNA knock-outs to deeper investigate the binding partners common to all yRNAs or specific for each. An RNA pulldown may represent an attractive way to validate the binding partners of yRNA family members, but remains challenging due to the accessibility of the probe to the yRNA. A recently described approach based on density gradient separation of RNA-proteins complexes combined to Mass-Spectrometry may represent an attractive method[384]

9.2.4. Conclusion

This dissertation questioned two isolation protocols for sEVs derived from lymphoid tissues and showed the superiority of differential centrifugation combined with size-exclusion chromatography over differential centrifugation combined with ultracentrifugation on a sucrose cushion. It was also shown that sEVs derived from B-cell NHL induced a polarization of myeloid cells characterized by the upregulation of PD-L1, CD54, HLA-DR and the downregulation of CCR2. This polarization could not be induced by yRNA4 only; and other bioactive elements contained in the sEVs were investigated for their capacity to polarize myeloid cells. Tumor-derived sEVs have the capacity to activate TLR2, TLR4 and TLR7, but also other Myd88-independent receptors on myeloid cells. Several candidate ligands were proposed: small non-coding RNAs contained in sEVs for TLR7, and the HSPs, potentially presented at the surface of sEVs, for TLR2 and TLR4. Additionally, it was observed that the proteome of tumor-derived sEVs differs between DLBCL and FL, with several proteins proposed as candidate biomarkers to differentiate the origin of sEVs. Finally, a new mechanism was proposed regarding the function of yRNA family members in sEVs: by binding to specific proteins, yRNAs may influence the protein cargo loaded into tumor-derived sEVs. A schematic of the findings and open questions derived from this dissertation is available on Figure 34.

Altogether these data highlight the role played by tumor-derived sEVs in promoting the polarization of myeloid cells into a pro-tumoral type, and indicate that tumor-derived sEVs are a possible target to delay tumor growth in B-cell NHL. Inhibition of sEVs' secretion by deletion of the Rab27 gene successfully diminished the tumor growth and the metastatic potential of mammary carcinoma and melanoma tumors[380,385,386]. Screening of new compounds to inhibit sEVs' secretion are ongoing and remain to be tested *in vivo,* in particular for B-cell NHL [387,388].

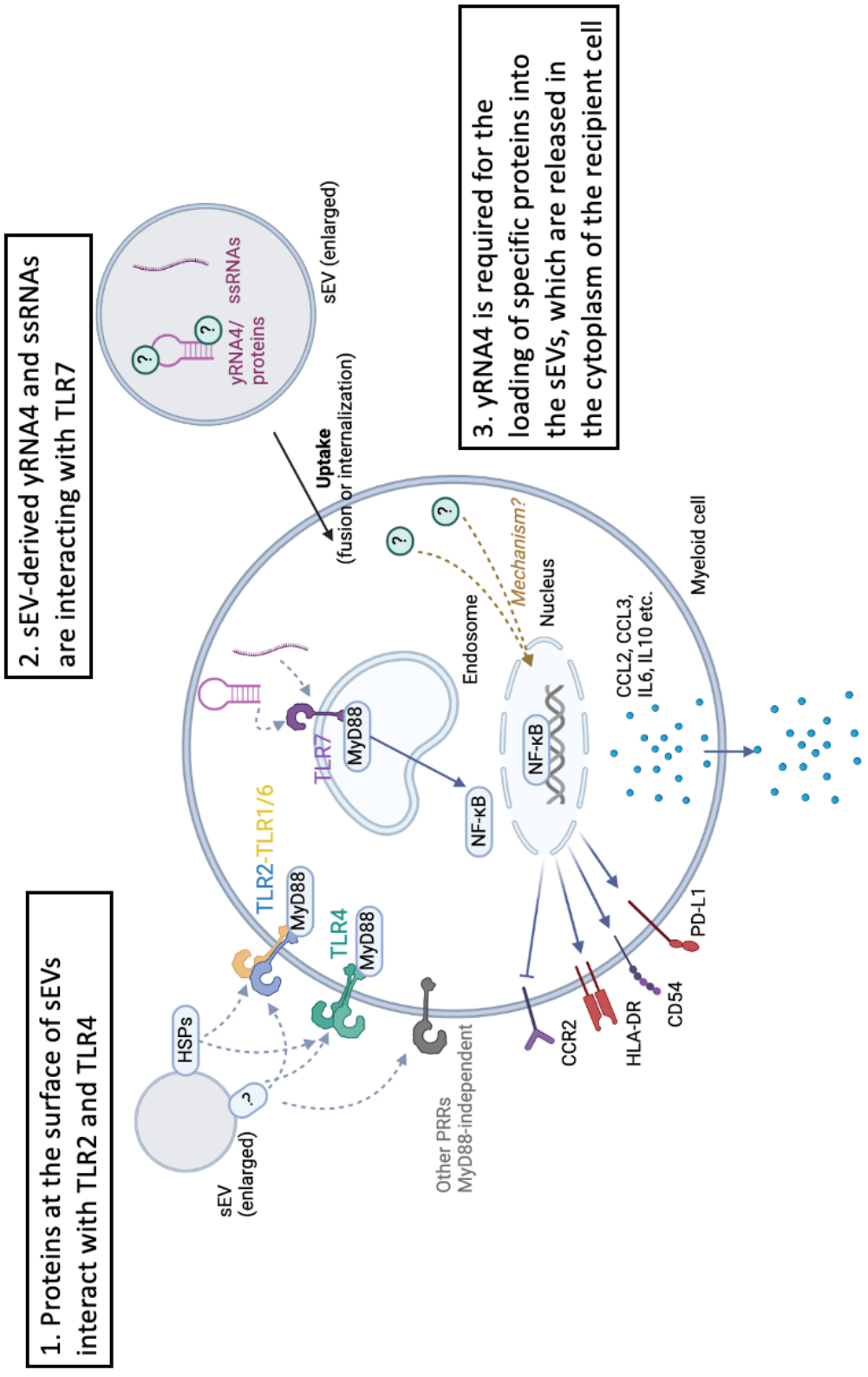

Figure 34: Summary schematic of the results presented in the dissertation; including three mechanisms by which tumor-derived sEVs may lead to the polarization of myeloid cells in the tumor microenvironment of B-cell NHL.

10. APPENDIX

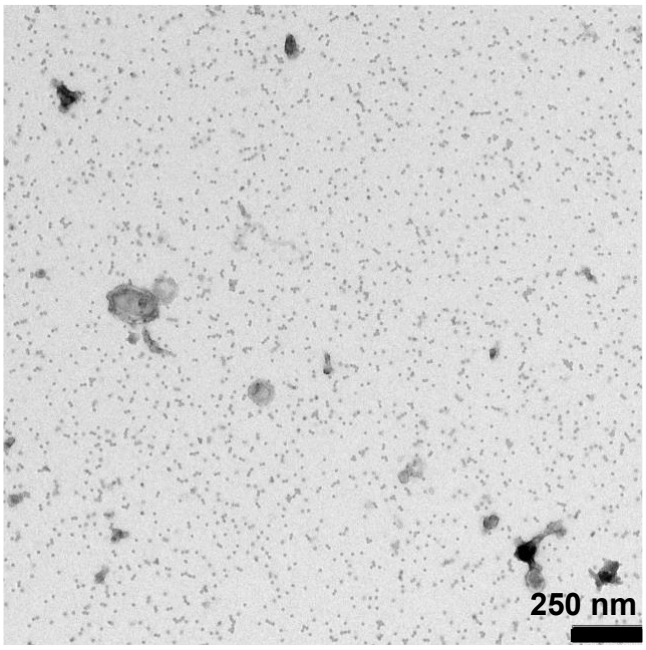

Supplementary figure 1: Representative Transmission Electron Microscopy image of sEVs isolated from the spleen of an adoptively transferred Eμ-TCL1 mouse, and isolated by differential centrifugation combined to ultracentrifugation on a sucrose density cushion.

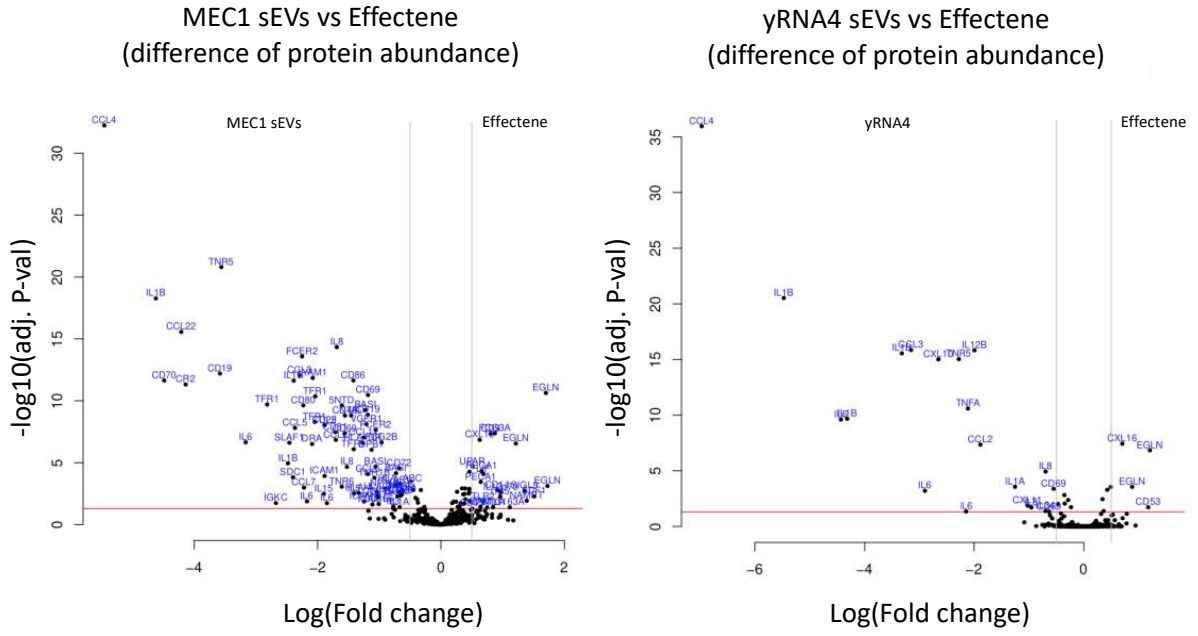

Supplementary figure 2: results of LIMMA analysis of differentially enriched proteins in myeloid cells treated with MEC1-sEVs (left) or yRNA4 (right) compared to the Effectene control condition.

Protein	AntibodyID	logFC yRNA/sEVs	adj.P.Val
IL12B	ab1667	2,39	1,6705E-18
CXL10	ab2503	2,02	2,6908E-12
TNFA	ab2019	1,88	3,4995E-10
IL1B	ab1687	1,84	0,00071412
CSF3	ab2014	1,52	0,0138898
CCL4	ab2391	1,52	7,7082E-15
SIGL9	ab2005	1,42	0,00095184
CD3deg	ab1524	1,27	0,00805217
IL6	ab1822	1,27	0,0288826
SDF1	ab2491	1,23	0,0259743
ITA5	ab1565	1,21	0,00044524
EGLN	ab1746	1,2	0,019338
IL12p70	ab1681	1,15	0,00032312
CXL11	ab2115	1,15	0,00119652
IL34	ab2441	0,97	0,00045883
IL1B	ab1686	0,93	0,00032747
CCL3	ab1795	0,86	0,00029809
UPAR	ab1832	0,86	7,2722E-10
IL1B	ab1888	0,85	0,00333857
CD15	ab1394	0,78	0,00153285
CD14	ab1393	0,76	0,00842069
CCL8	ab1691	0,76	5,2396E-06
CD9	ab1378	0,74	2,5166E-07
PERM	ab1514	0,73	0,0103948
CD28	ab1559	0,71	0,0361554
IGLC1	ab1584	0,71	0,00023147
PLF4	ab1841	0,71	0,0372218
TLR2	ab1868	0,65	0,0202989
PECA1	ab2473	0,62	0,0001084
CD44v2	ab2782	0,56	0,00748481
CCL7	ab1692	0,52	0,0455036
FCG3A	ab1532	0,51	0,00035752
DAF	ab1457	-0,55	0,00014428
HLA-ABC	ab1493	-0,55	0,00351967
LYAM1	ab2189	-0,56	4,7386E-05
CD69	ab1639	-0,63	1,7059E-05
CD80	ab1476	-0,65	0,0110195
BASI	ab1487	-0,68	0,00018706
NP1L4	ab1709	-0,7	0,012975
SLAF1	ab1033	-0,74	0,00044569
TNR5	ab1430	-0,78	0,0440222
CD38	ab1537	-0,81	0,0398286
CD72	ab1474	-0,84	6,396E-07

Protein	AntibodyID	logFC yRNA/sEVs	adj.P.Val
HLAG	ab1608	-0,85	3,1518E-05
NEP	ab1381	-0,9	0,0158693
XCL1	ab1909	-0,9	0,00372078
IL6RA	ab1706	-0,91	0,00014428
CD69	ab1470	-0,93	0,00033382
TNFB	ab1921	-0,98	2,0064E-05
IL8	ab1644	-0,99	2,9691E-09
FGF2	ab1714	-1	0,0356082
DPB1	ab1495	-1,02	5,8781E-06
FCG2B	ab1803	-1,03	6,006E-08
VGFR1	ab1617	-1,1	5,5757E-08
HLA-I	ab1553	-1,11	0,0133436
HLA-DR	ab1494	-1,12	2,807E-06
CCL5	ab1597	-1,2	6,8161E-05
BASI	ab1910	-1,21	8,6973E-10
ICAM1	ab1864	-1,23	0,0118107
BASI	ab1486	-1,24	1,2045E-06
CCL17	ab2448	-1,26	8,3333E-08
TNR5	ab1752	-1,28	3,0491E-09
TFR1	ab1547	-1,3	4,6732E-06
CD86	ab1477	-1,34	1,2722E-11
TNR6	ab1478	-1,34	0,0052748
CD166	ab2246	-1,44	0,00079172
IL3	ab2172	-1,48	4,9333E-05
NTAL	ab1515	-1,5	9,3507E-10
TNR1B	ab2455	-1,51	6,396E-07
5NTD	ab1110	-1,56	6,2092E-10
HLAG	ab1609	-1,82	5,774E-07
SLAF1	ab2132	-1,83	4,94E-05
CD22	ab1412	-1,85	1,4665E-08
TFR1	ab2730	-1,9	3,4995E-10
TFR1	ab1471	-2,02	6,5818E-09
CD80	ab2460	-2,04	2,1179E-09
IL5	ab2431	-2,05	2,9858E-05
CCL5	ab2438	-2,17	6,001E-10
LYAM1	ab1466	-2,2	5,1608E-13
DRA	ab1581	-2,24	8,3333E-08
IL15	ab1510	-2,32	0,00034812
SDC1	ab2308	-2,41	0,00014428
CCL5	ab1672	-2,49	5,2701E-09
TFR1	ab1472	-2,55	2,1179E-09
CCL22	ab1600	-4,06	1,5881E-15
CR2	ab0988	-4,38	1,6779E-12

Supplementary figure 3: Differentially enriched proteins in myeloid cells treated with MEC1-sEVs or yRNA4-alone, including the corresponding antibody, the fold enrichment and the adjusted p-value.

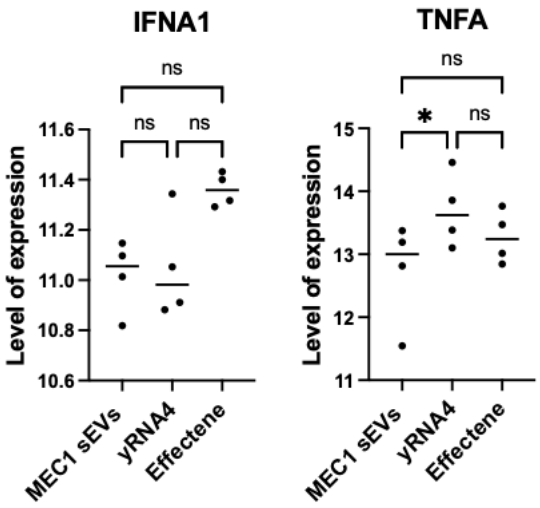

Supplementary figure 4: Enrichment of IFNA1 and TNFA in myeloid cells following treatment with MEC1-sEVs, effectene-encapsulated yRNA4 or effectene alone, detected by protein microarray.

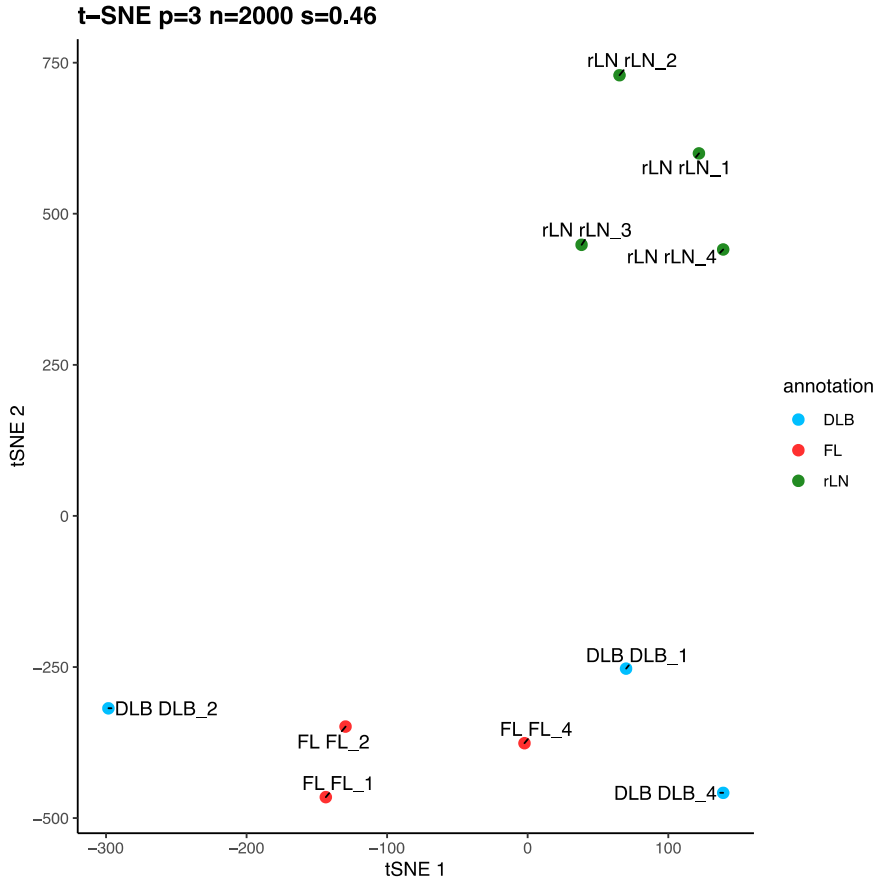

Supplementary figure 5: Principal component analysis (PCA) biplot of proteins identified in the sEVs isolated from the LNs of 4 DLBCL patients (DLB), 4 FL patients (FL) and 4 reactive LNs (rLN).

Rank	DLBCL1	DLBCL2	DLBCL3	DLBCL4	FL1	FL2	FL3	FL4	rLN1	rLN2	rLN3	rLN4
1	HIST1H4A	ACTB	HLA-DQB1	ACTB	HIST1H4A	HIST1H4A	ACTB	ACTB	ACTB	HIST1H4A	HIST1H4A	HIST1H4A
2	Histone group 1	TUBB4B	HIST1H4A	RPL18	Histone group 1	ACTB	HBB	BASP1	HBB	ACTB	ACTB	ACTB
3	ANXA2;ANXA2P2	HIST1H4A	ACTB	RPL7A	Histone group 2	Histone group 1	ANXA2;ANXA2P2	HLA-DRA	IGKC	Histone group 1	Histone group 1	Histone group 1
4	Histone group 2	TUBA1B	HLA-DRB1	RPLP0;RPLP0P6	ACTB	Histone group 2	RPL18	GAPDH	MVP	ANXA2;ANXA2P2	MARCKSL1	Histone group 2
5	HBB	HLA-DQB1	HLA-DRA	RPL7	CD20/MS4A1	GAPDH	RPS8	HLA-DRB1	RPS8	TMSB4X	HBB	ANXA2;ANXA2P2
6	ACTB	GAPDH	RPL18	HIST1H4A	TUBB4B	HLA-DRA	THY1	CD20/MS4A1	RPL18	YWHAZ	RPL18	HBB
7	RPL18	TUBB	HLA-DRB1	RPL23A	BASP1	CD20/MS4A1	HLA-DQB1	IGKC	RPL13A;RPL13AP3	CFL1	IGKC	G0I2
8	IGKC	HLA-DRA	HLA-DRB1	RPL22	Histone group 4	HLA-DRB1	RPL7A	HIST1H4A	IGHG1	HBB	CD20/MS4A1	IGKC
9	RPS8	RPL18	RPS8	RPS8	TUBA1B	BASP1	HIST1H4A	HLA-A	HIST1H4A	PLP2	CFL1	YWHAZ
10	Histone group 4	IGKC	Histone group 1	RPS14	RPL18	RPL18	RPL7	ANXA2;ANXA2P2	HLA-A	IGKC	ANXA2;ANXA2P2	RPL18
11	RPL7	HBB	HLA-DPB1	RPL6	G0I2	Histone group 4	MVP	THY1	ANXA2;ANXA2P2	PTCHD3	Histone group 2	CFL1
12	HLA-A	PKM	RPL13	RPL5	HLA-DRA	G0I2	RPL6	G0I2	RPL7	G0I2	YWHAZ	RPS8
13	G0I2	CD20/MS4A1	CD20/MS4A1	RPL14	MARCKSL1	YWHAZ	G0I2	RPL18	HLA-B	MARCKSL1	G0I2	RPL13A;RPL13AP3
14	THY1	RPL7A	RPL6	CLTC	GAPDH	RPS8	IGKC	TUBB4B	YWHAZ	RAP1B	BASP1	BASP1
15	RPL6	Coronin1a	GAPDH	RPL29	SYPL1	TUBB4B	RPS6	HBB	GAPDH	BASP1	HLA-A	ANXA6
16	Histone group 3	LDHB	RPL7A	ANXA2;ANXA2P2	HLA-DQB1	MARCKSL1	HLA-DRA	PTPRC	TUBB4B	RPL18	TUBB4B	MARCKSL1
17	RPL7A	HSP90AB1	CD44	RPL4	STX7	RPL7	PFN1	RPS8	RPL13	PFN1	RAP1B	HLA-B
18	TUBB4B	RPS8	RPL13A;RPL13AP3	CD20/MS4A1	RPS8	CFL1	CD20/MS4A1	TUBA1B	HLA-A	RPS8	HLA-DRB1	GAPDH
19	RPL14	RPL7	HLA-DQA1	CALR	RPL7	MSN	STX7	MARCKSL1	CFL1	Coronin1a	RPL13A;RPL13AP3	RAP1B
20	PPIB	EEF1A1;EEF1A1P5	RPL7	RPL13	HLA-A	TUBA1B	HLA-A	YWHAZ	G0I2	CD20/MS4A1	MARCKS	MARCKS

Histone group 1 HIST1H2BL;HIST1H2BH;HIST1H2BN;HIST1H2BC;HIST1H2BD;HIST1H2BK;HIST2H2BF;HIST1H2BM;H2BFS;HIST1H2BA

Histone group 2 HIST1H2AG;HIST1H2AJ;H2AFJ;HIST1H2AH;HIST1H2AD;HIST1H2AC;HIST3H2A;HIST1H2AB

Histone group 3 HIST1H2BB;HIST2H2BE;HIST1H2BO;HIST1H2BJ;HIST3H2BB

Histone group 4 H3F3A;HIST1H3A;HIST3H3;H3F3C

Supplementary figure 6: Top 20 proteins detected in each sample. Red: the B-cell protein CD20; green: the B-cell marker Ig kappa chain C region. In blue was detected the coronin-! protein, recently suggested as a marker of sEVs.

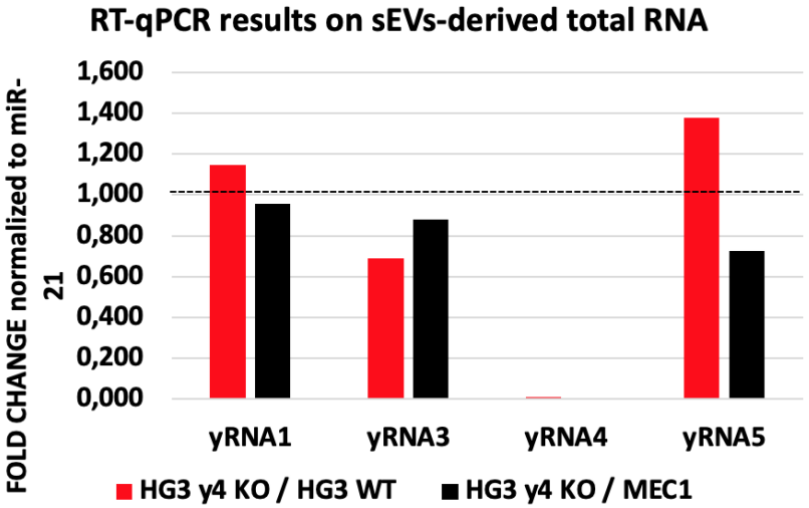

Supplementary figure 7: Validation of the RT-qPCR protocol to analyze the expression of yRNAs. The expression of the different yRNAs was normalized to the expression of miR-21 taken as a housekeeping control for sEV-derived small RNAs. n=1 sEV preparation

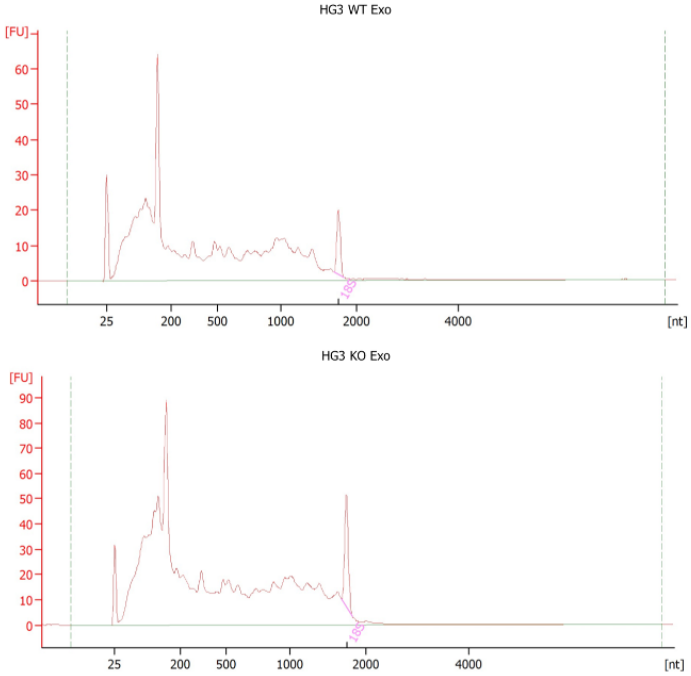

Supplementary figure 8: RNA size distribution profile of total RNAs isolated from HG3 WT (top) and HG3 yRNA4-KO sEVs.

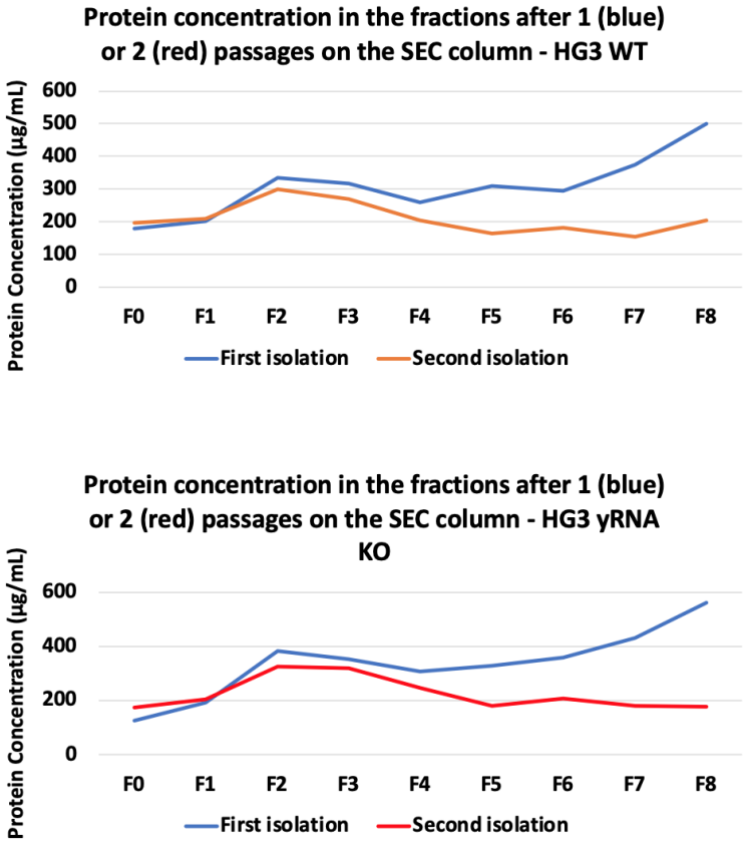

Supplementary figure 9: A second passage on a SEC column does not show superiority over one passage to efficiently separate protein complexes from sEVs. In blue, the protein concentration of each fraction following the first isolation (top: sEVs from HG3 WT cells; bottom: sEVs from HG3 yRNA4 KO cells). The peak fraction is F2 correspond to sEVs whether proteins complexes are generally eluted from fraction 5. The peak fraction product was re-isolated on a SEC column a second time (red). The protein concentration indicates that a second passage does not lead to additional separation of protein complexes.

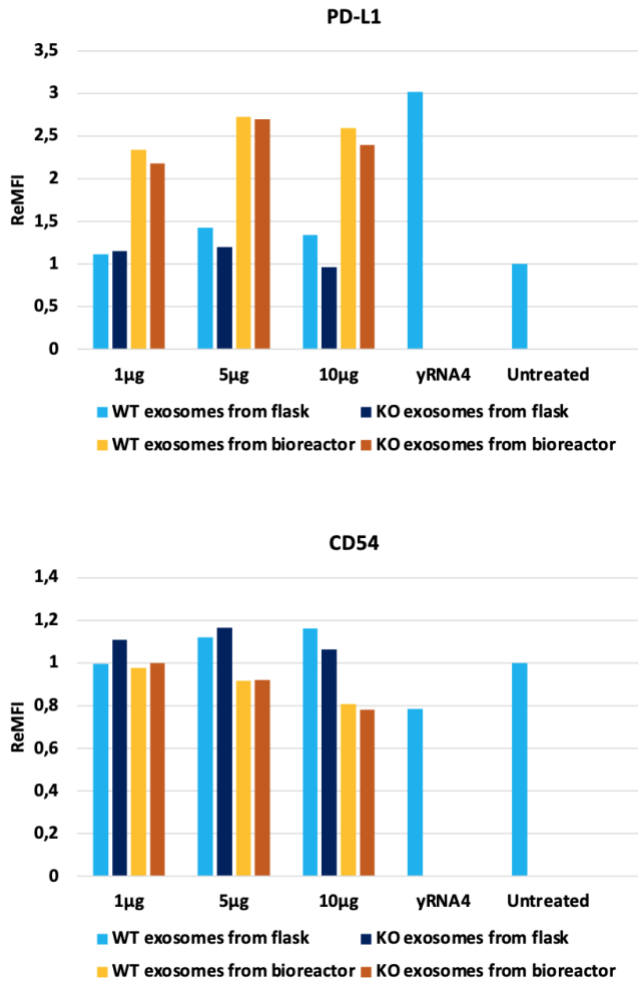

Supplementary figure 10: sEVs from cell cultured in classical flasks or bioreactors show different capacity to polarize myeloid cells *in vitro.* Myeloid cells were treated for 8 hours with 1,5, or 10 µg of sEVs and the phenotype of myeloid cells acquired by flow cytometry. On top, the expression of PD-L1 at the surface of myeloid cells, on the bottom, the surface expression of CD54 at on myeloid cells.

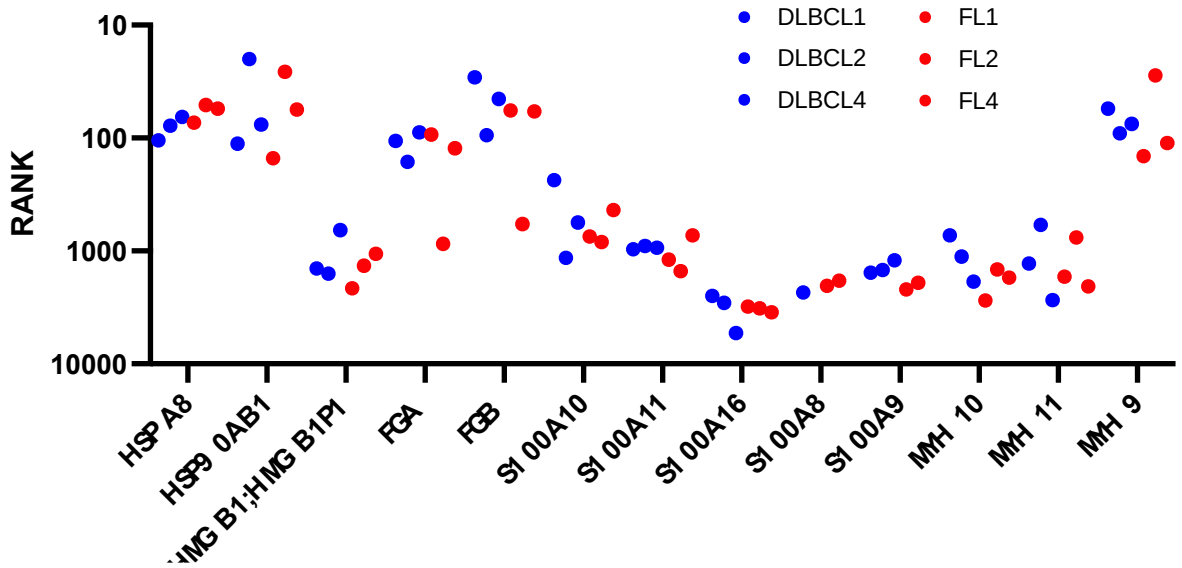

Supplementary figure 11: Analysis of the enrichment of known endogenous TLR ligands in the proteome data of sEV derived from the LNs of B-cell NHL patients. The proteins were plotted according to their rank.

11. SUPPLEMENTARY BOXES

Direct adhesion of tumor cells to stromal cells confers survival benefit

Stromal cells have been shown to promote B-cell NHL cell survival, both in a direct and indirect manner. Lwin et al. have shown that, in the bone marrow, the DLBCL cells adherent to stromal cells were more protected from mitoxantrone-induced apoptosis than suspension cells [389]. This drug resistance could be mediated by the interaction of VLA-4 on lymphoma cells to VCAM-1 on stromal cells [390]. The adhesion to stromal cells through the VCAM-1/VLA-4 axis leads to the upregulation of the NF-kB pathway in leukemic cells and confer them protection [391]. However, it is likely that the adhesion of lymphoma cells to mesenchymal stromal cells is reduced compared to normal B-cell [392], therefore highlighting the major role played by paracrine signals. VLA-1/VCAM-1 interaction can enhance the activation of BCR [393]

Stromal cells support tumor cells by paracrine signals

One of the most described paracrine signals sent by stromal cells is the secretion of CXCL12 [394,395]. CXCL12 binds to its receptor CXCR4, overexpressed at the surface of lymphoma cells [396,397]. In DLBCL patients, *CXCR4* expression is positively correlated to *C-MYC* and *BCL-2* expression; and high *CXCR4* expression is associated with a poor response to R-CHOP therapy[397,398]. In CLL, chemoattraction of the tumor cells via the CXCR4/CXCL12 axis induce the pseudoemperipolesis of CLL cells underneath BMSC where CLL cells are protected from chemotherapy [399]. Using xenograft murine models, Moreno et al. have shown that a high expression of *CXCR4* on lymphoma cells is not only associated with an increased dissemination of the tumor cells, but also with a poorer survival of the animals [400]. In line with those results, it has been shown that inhibition of CXCR4 induces lymphoma cells apoptosis [401,402], and combination of CXCR4 blockade with Rituximab has shown benefits over Rituximab treatment alone *in vitro* [402–405]. Clinical trials are ongoing to test further this therapeutic approach, with first results indicating that CXCR4 is increasing B-cell NHL cell mobilization into the circulation, therefore increasing their sensitivity to classical molecules [406]. Additionally, BMSC secrete Vascular Endothelial Growth Factor (VEGF) favorizing primary CLL survival *in vitro* [407,408]. Physical interaction of BMSC, and CLL cells induce the expression of the ZAP70 kinase, and CD38 on the tumor cells, and enhances their migratory, and proliferative potential [142,409–412].

B-cell NHL stromal cells crosstalk with immune cell subsets

Stromal cells from FL patients have also been shown to secrete more CCL2 than stromal cells from healthy donors [413]. The CCL2 cytokine promote myeloid cells recruitment and polarization into a pro-tumoral phenotype promoting the survival of FL cells.

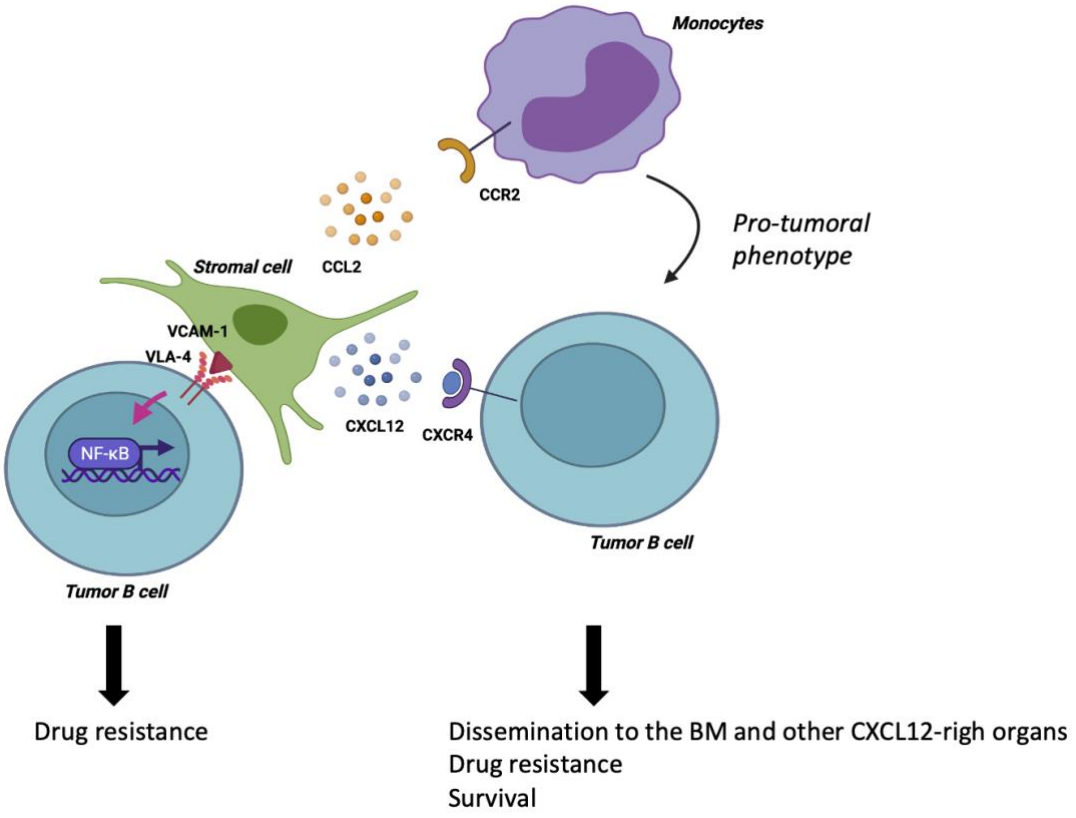

Stromal cells and B-cell NHL tumor cells interactions lead to tumor progression by both direct and indirect signals. The principal molecular interactions between stromal cells and B-cell NHL tumor cells are represented in the schematic above, as well as the downstream phenotype acquired in tumor cells associated with these interactions.

Supplementary box 1: Remodulation of the stromal cells in the context of B-cell NHL

One feature of many B-cell NHLs is the upregulation of *STAT3*, a downstream target of the BCR [414]. In ABC-DLBCL patients, the expression of *STAT3* is particularly high due to loss-of-function mutations of *BCL-6*, a STAT3 repressor, and *STAT3* upregulation was linked to tumor cell proliferation in ABC-DLBCL [415,416]. *STAT3* upregulation results in increased secretion of HIF-1 and VEGF [417–419]. VEGF induces angiogenesis in ABC-DLBCL patients [416,420].

Additionally, Menzel et al. used the Eμ-TCL1 murine model for CLL to show that, at an advanced disease stage, undifferentiated endothelial cells had a proliferative advantage over differentiated High Endothelial Venule (HEV) Cells compared to early-stage disease [421]. HEVs are secondary lymphoid organs (SLOs) structures made of endothelial cells expressing large amount of adhesion molecules on their surface, such as CD62L, and secreting chemoattractant cytokines as CCL21. Their regression in CLL was associated with an impaired transendothelial migration and priming of immune cells including naïve lymphocytes or dendritic cells. Surface expression of CD40L is increased on CLL B-cells [422,423]. Binding of CD40L to CD40 on endothelial cells results in secretion of BAFF, and APRIL factors, two factors known to promote B-cell survival, and proliferation signals through activation of both the canonical, and non-canonical NF-kB pathway, and downstream *BCL-2* [424–427]. Several studies studied the expression of BAFF and APRIL receptors on NHL B-cells although with contradictory conclusions [426,428]. However, *in vitro* treatment of murine TCL1 splenocytes with BAFF or APRIL resulted in survival advantage [426]. Overexpression of *APRIL* in the CLL murine model Eμ-TCL1 accelerates the progression of the disease although overexpression of *APRIL* alone did not affect WT animals [429]. Similarly, overexpression of *BAFF* in *c-MYC* transgenic mice drastically reduces the life expectancy of animals compared to *c-MYC* transgenic mice due to the proliferation of CD5+B220+ cells [430]. In the same animals were detected an increase of anti-apoptotic genes expression, including *BCL-2*, and decrease of the death receptor *FAS*. High expression of soluble APRIL in FL or BAFF in DLBCL was correlated to poor prognosis [431,432].

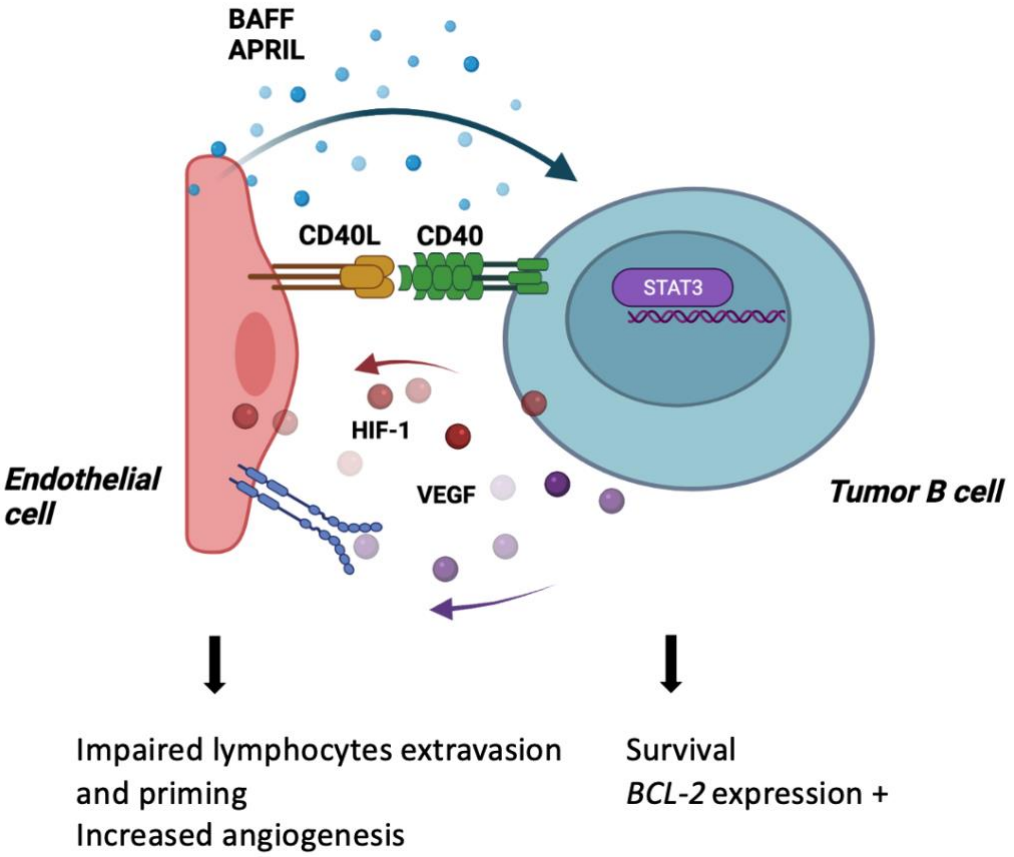

Schematic of the interactions between endothelial cells and B-cell NHL tumor cells. Following CD40L/CD40 interaction, endothelial cells induce the survival of B-cell NHL tumor cells through secretion of the BAFF and APRIL factors, leading to tumor cell survival. *STAT3* upregulation in the tumor cell leads to secretion of HIF-1 and VEGF, and acquisition of a pro-tumoral phenotype by endothelial cells.

Supplementary box 2: Remodulation of the endothelial cells in the context of B-cell NHL.

Regulatory T cells

B-cell NHL patients present high numbers of FoxP3$^+$CD4$^+$ Treg cells, both intratumorally and in peripheral blood[433,434]. However, studies investigating the prognostic value of intratumoral FoxP3$^+$ T cells lead to contradictory results [153,435–437]. It was recently suggested that the secretion of IL-10 would represent a major mechanism used by Treg cells to inhibit cytotoxic T cells [438,439].

Follicular helper T cells

Follicular Helper T cells (Tfh) are characterized by the surface expression of CXCR5, the receptor for the CXCL13 chemokine expressed by B-cells, and the absence of CD25 [440]. It is generally accepted that most of the helper T cells found in the lymphoma microenvironment are Tfh[104,441]. Tfh have both pro- and anti-tumoral properties. On the one side, Tfh induce the proliferation of malignant B cells, through expression of surface CD28 and ICOS and through the secretion of cytokines such as CD40L, IL-4 and IL-21[442–453]. On the other side, secretion of IL-2 and IL-21 leads to the expansion of cytotoxic CD8$^+$ T cells[454–456].

CD8+ T cells

CD8$^+$ T cells are cytotoxic T-cells which induce the cell death of infected or tumor cells through the release of cytotoxic granules containing factors as perforin, secretion of TNF-α and IFN-γ, and expression of the cell death ligand FASL. Such function requires the recognition by the T-cell Receptor (TCR) of antigenic peptides presented at the surface of MHC-I molecules. Using the Eμ-TCL1 murine model of CLL, our group has recently shown that CD8$^+$ T cell contribute to control disease progression[122]. In B-cell NHL, CD8$^+$ T cells present an exhausted phenotype, characterized by the co-expression of several inhibitory receptors also called immune checkpoints, the main ones being PD-1, LAG-3, TIM-3 [457–459]. The exhaustion of T-cells is driven by persistent antigen exposure and lead to a weakened effector function. The proportion of exhausted T cells in the tumor microenvironment is directly correlated to B-cell NHL overall survival[460]. On the other side, a lack of CD8$^+$ T cell stimulation can also be explained by decreased expression of MHC-I molecules in B-cell NHL[461]. Some of the new directions for the treatment of B-cell NHL are aiming at reactivating CD8$^+$ effector function, and are presented in the table below.

Therapeutical tool	Mechanism of action
Immune checkpoint	Not FDA-approved yet for the treatment of B-cell NHL, although approved for other cancer entities, currently tested in combination with classical therapies in clinical trials:

monoclonal antibodies	Anti-PD-1 (eg: Pembrolizumab, Nivolumab) Anti-PD-L1 antibodies (eg: Atezolizumab, Durvalumab, Avelumab) Anti-CTLA-4 (eg: Tremelimumab) Under clinical trial: anti-LAG-3 (eg: relatlimab), anti-CD80 (eg: galiximab) Under consideration: Anti-41BB (eg: urelumab), anti-CD27 [462,463]
Bispecific T-cell engagers (BiTes)	Bispecific antibodies can recognize two antigens simultaneously. The known bispecific antibodies are targeting both CD3 and CD120, and are aimed at specifically targeting T lymphocytes to malignant B cells and show promising results to treat relapsed or refractory patients in B-cell NHL (Kim et al, Oral Talk, ASH, 2020).
DC vaccines	Dendritic Cell therapy aims to produce autologous (sometimes allogeneic) DC *in vitro*, prime them with an antigenic peptide, expand them and reinject them into the patient. Multiple clinical trials performed in B-cell NHL have proven the efficacy of such therapy[464]. Antigenic peptides can be tumor cell lysates, apoptotic bodies, artificial neoantigen peptides, antigen mRNA, or inactivated tumor cells[464,465]. DC therapy could synergize with other treatments as anti-CD20 antibodies, to eradicate tumor cells[466].
CAR-T cells	The use of CAR-T cells to treat, and potentially cure B-cell NHL, is now approved both in Europe and in the USA[84]. CAR T cells are modified autologous T-cells with a chimeric TCR able to recognize a B-cell marker, generally CD19. Additionally, second- and third-generation CAR contain co-stimulatory domain as CD28 and OX40[467]z (Qu et al. Cell & Mol Immunol, 2020; Zhao and Cao, Front Immunol 2019). However, the response rate remains low, and limiting factors to the use of CAR-T-cells include T cell exhaustion phenotype, lack of *ex vivo* expansion, and adverse effects, in particular cytokine release syndrome and neurotoxicity (Fraietta et al., 2018; Lynn et al., 2019; Zhao and Cao, Frnt Immunol 2019). Recently, CAR-T-cells targeting CXCR5+ cells in B-cell NHL were shown to efficiently control B-cell NHL tumor growth *in vitro* and *in vivo* both through a direct killing effect on CXCR5+ lymphoma cells (Bunse et al Nat Comm, 2021).

Summarizing table of strategies developed in B-cell NHL aiming to reinvigorate $CD8^+$ antitumor immunity.

Supplementary box 3: Remodulation of the T cell compartment in the context of B-cell NHL

RNA family	Function in eukaryotic cells
piRNA	Non-coding transcripts. In complex with proteins to cleave RNAs, piRNAs modulate chromatin organization and silence transposable elements [468,469]. PiRNA use complementary to target RNA sequence to guide the Argonaute protein,and contributes to repress transposable elements Size: 21-31nt
mtRNA	Mix of non-coding, transfer or messenger RNAs coming from the mitochondrial genome [470]
SnRNA	Non-coding transcripts, with an important function for the splicing of introns (Valadkhan et al. Essays Biochem, 2013). Size: ~150nt
SnoRNA	Non-coding transcripts involved in maturation of ribosomal RNAs[471]. Size: 60-300nt
tRNA, tsRNA	Non-coding transcripts forming complex with ribosomal proteins to promote mRNA translation (Scitable database / Nature.com). Size: 70-100 nt for tRNA; 10-40 nt for tsRNA
lncRNA	Non-coding transcripts with unclear functions. They are found in complexes with different proteins depending on their localization: with RBP in the cytoplasm, in the mitochondria, or in organelles as sEVs. LncRNA-containing complexes are involved in cell migration, gene transcription, methylation. [472] Size: 1000-10.000nt
circRNA	Non-coding transcripts lacking a poly-A tail, poorly described. Circ RNa may serve as miRNA sponges[473,474]. Size: 100bp-1000bp

Supplementary box 4: summary of non-coding RNAs commonly found in sEVs. *The table does not include Y RNAs.*

12. REFERENCES

1. Nguyen, T. V., Pawlikowska, P., Firlej, V., Rosselli, F. & Aoufouchi, S. V(D)J recombination process and the Pre-B to immature B-cells transition are altered in Fanca -/- mice. *Sci. Rep.* **6**, 1–11 (2016).
2. Schatz, D. G., Oettinger, M. A. & Baltimore, D. The V(D)J recombination activating gene, RAG-1. *Cell* **59**, 1035–1048 (1989).
3. Schatz, D. G. & Swanson, P. C. V(D)J Recombination: Mechanisms of Initiation. *Annu. Rev. Genet.* **45**, 167–202 (2011).
4. Van Gent, D. C., Ramsden, D. A. & Gellert, M. The RAG1 and RAG2 proteins establish the 12/23 rule in V(D)J recombination. *Cell* **85**, 107–113 (1996).
5. Ghia, P. *et al.* Ordering of human bone marrow B lymphocyte precursors by single-cell polymerase chain reaction analyses of the rearrangement status of the immunoglobulin H and L chain gene loci. *J. Exp. Med.* **184**, 2217–2229 (1996).
6. Melchers, F. The pre-B-cell receptor: Selector of fitting immunoglobulin heavy chains for the B-cell repertoire. *Nat. Rev. Immunol.* **5**, 578–584 (2005).
7. Pieper, K., Grimbacher, B. & Eibel, H. B-cell biology and development. *J. Allergy Clin.*

Immunol. **131**, 959–971 (2013).
8. Pasqualucci, L. & Dalla-Favera, R. Genetics of diffuse large b-cell lymphoma. *Blood* **131**, 2307–2319 (2018).
9. Mesin, L., Ersching, J. & Victora, G. D. Germinal Center B Cell Dynamics. *Immunity* **45**, 471–482 (2016).
10. Wen, Y. *et al.* The regulators of BCR signaling during B cell activation. *Blood Sci.* **1**, 119–129 (2019).
11. Young, R. M., Phelan, J. D., Wilson, W. H., Staudt, L. M. & Branch, M. New Insights To Improve Treatment. *Immunol. Rev.* **291**, 190–213 (2020).
12. Avalos, A. M. & Ploegh, H. L. Early BCR events and antigen capture, processing, and loading on MHC class II on B cells. *Front. Immunol.* **5**, 1–5 (2014).
13. Wolf Bryant, P., Lennon-Duménil, A.-M., Fiebiger, E., Lagaudrière-Gesbert, C. & Ploegh, H. L. Proteolysis and Antigen Presentation by MHC Class II Molecules. *Adv. Immunol.* (2002).
14. Connors, J. M. *et al.* Hodgkin lymphoma. *Nat. Rev. Dis. Prim.* **6**, (2020).
15. Al-Hamadani, M. *et al.* Non-Hodgkin lymphoma subtype distribution, geodemographic patterns, and survival in the US: A longitudinal analysis of the National Cancer Data Base from 1998 to 2011. *Am. J. Hematol.* **90**, 790–795 (2015).
16. Pulte, D. *et al.* Survival of patients with non-Hodgkin lymphoma in Germany in the early 21st century. *Leuk. Lymphoma* **54**, 979–985 (2013).
17. Teras, L. R. *et al.* 2016 US lymphoid malignancy statistics by World Health Organization subtypes. *CA. Cancer J. Clin.* **66**, 443–459 (2016).
18. Miranda-Filho, A. *et al.* Global patterns and trends in the incidence of non-Hodgkin lymphoma. *Cancer Causes Control* **30**, 489–499 (2019).
19. Perry, A. M. *et al.* Non-hodgkin lymphoma in the developing world: Review of 4539 cases from the international Non-Hodgkin Lymphoma Classification Project. *Haematologica* **101**, 1244–1250 (2016).
20. Armitage, J. O., Gascoyne, R. D., Lunning, M. A. & Cavalli, F. Non-Hodgkin lymphoma. *Lancet* **390**, 298–310 (2017).
21. Shingleton, J. *et al.* Non-Hodgkin Lymphomas: Malignancies Arising from Mature B Cells. *Cold Spring Harb. Perspect. Med.* a034843 (2020) doi:10.1101/cshperspect.a034843.
22. Bakhshi, T. J. & Georgel, P. T. Genetic and epigenetic determinants of diffuse large B-cell lymphoma. *Blood Cancer J.* **10**, (2020).
23. Karube, K. *et al.* Integrating genomic alterations in diffuse large B-cell lymphoma identi fi es new relevant pathways and potential therapeutic targets. *Leukemia* 675–684 (2018) doi:10.1038/leu.2017.251.
24. Lenz, G. *et al.* Molecular subtypes of diffuse large B-cell lymphoma arise by distinct genetic pathways. *Proc. Natl. Acad. Sci. U. S. A.* **105**, (2008).
25. Pasqualucci, L. *et al.* Articles Analysis of the coding genome of diffuse large B-cell lymphoma. *Nat. Publ. Gr.* **43**, (2011).
26. Lohr, J. G. *et al.* Discovery and prioritization of somatic mutations in diffuse large B-cell lymphoma (DLBCL) by whole-exome sequencing. *Proc. Natl. Acad. Sci. U. S. A.* **109**, 3879–3884 (2012).
27. Schmitz, R. *et al.* Genetics and pathogenesis of diffuse large B-Cell lymphoma. *N. Engl. J. Med.* **378**, 1396–1407 (2018).
28. Reddy, A. *et al.* Genetic and Functional Drivers of DLBCL. *Cell* **344**, 1173–1178 (2015).
29. Bakhshi, A. *et al.* Cloning the chromosomal breakpoint of t(14;18) human lymphomas: clustering around Jh on chromosome 14 and near a transcriptional unit on 18. *Cell* **41**, 899–906 (1985).
30. Barrans, S. L. *et al.* The t(14;18) is associated with germinal center-derived diffuse large B-cell lymphoma and is a strong predictor of outcome. *Clin. Cancer Res.* **9**, 2133–2139 (2003).
31. Tsujimoto, Y., Finger, L., Yunis, J., Nowell, P. & Croce, C. Cloning of the Chromosome

Breakpoint of Neoplastic. *Science (80-.).* **7415**, 1097–1099 (1983).
32. Johnson, N. A. Functional and clinical impact of MYC mutations in diffuse large B cell lymphomas. *Transl. Cancer Res.* **5**, S257–S260 (2016).
33. Xia, Y. & Zhang, X. The Spectrum of MYC Alterations in Diffuse Large B-Cell Lymphoma. *Acta Haematol.* **730000**, 1–9 (2020).
34. Cerchietti, L. & Melnick, A. Targeting Bcl-6 in Diffuse Large B-Cell Lymphoma : *Expert Rev Hematol* **6**, 343–345 (2014).
35. Xiao, C. *et al.* Lymphoproliferative disease and autoimmunity in mice with increased miR-17-92 expression in lymphocytes. *Nat. Immunol.* **9**, 405–414 (2008).
36. Liou, H. *et al.* c-Rel is crucial for lymphocyte proliferation but dispensable for T cell effector function. *Int. Immunol.* **11**, 361–371 (1999).
37. Kober-Hasslacher, M. *et al.* c-Rel gain in B cells drives germinal center reactions and autoantibody production. *J. Clin. Invest.* (2020) doi:10.1172/jci124382.
38. Morin, R. D. *et al.* Somatic mutations altering EZH2 (Tyr641) in follicular and diffuse large B-cell lymphomas of germinal-center origin. *Nat. Genet.* **42**, 181–185 (2010).
39. Shen, C. *et al.* Gain-of-function mutations in chromatin regulators as an oncogenic mechanism and opportunity for drug intervention Chen. *Curr Opin Oncol.* **27**, 57–63 (2015).
40. Iqbal, J. *et al.* BCL2 expression is a prognostic marker for the activated B-cell-like type of diffuse large B-cell lymphoma. *J. Clin. Oncol.* **24**, 961–968 (2006).
41. Testoni, M., Zucca, E., Young, K. H. & Bertoni, F. Genetic lesions in diffuse large B-cell lymphomas. *Ann. Oncol.* **26**, 1069–1080 (2015).
42. Kraan, W. *et al.* High prevalence of oncogenic MYD88 and CD79B mutations in diffuse large B-cell lymphomas presenting at immune-privileged sites. *Blood Cancer J.* **3**, e136-4 (2013).
43. Davis, R. E. *et al.* B-Cell Receptor Signaling in Diffuse Large B-Cell lymphoma. *Semin. Hematol.* **52**, 77–85 (2015).
44. Ngo, V. N. *et al.* Oncogenically active MYD88 mutations in human lymphoma Vu. *Nature* **470**, 115–119 (2011).
45. Fogliatto, L. *et al.* Prognostic impact of MYD88 mutation, proliferative index and cell origin in diffuse large B cell lymphoma. *Hematol. Transfus. Cell Ther.* **41**, 50–56 (2019).
46. Honma, K. *et al.* SA - Designing and Reusing Architectural Evolution Knowledge.pdf. *Lymphoid Neoplasia* **114**, 2467–2476 (2018).
47. Wenzl, K. *et al.* Loss of TNFAIP3 enhances MYD88 L265P -driven signaling in non-Hodgkin lymphoma. *Blood Cancer J.* **8**, (2018).
48. Pasqualucci, L. *et al.* Inactivation of the PRDM1/BLIMP1 gene in diffuse large B cell lymphoma. *J. Exp. Med.* **203**, 311–317 (2006).
49. Mandelbaum, J. *et al.* BLIMP1 is a tumor suppressor gene frequently disrupted in activated B cell like diffuse large B cell lymphoma Jonathan. *Cancer Cell* **23**, 1–7 (2010).
50. Chapuy, B. *et al.* Molecular subtypes of diffuse large B cell lymphoma are associated with distinct pathogenic mechanisms and outcomes. *Nat. Med.* **24**, 679–690 (2018).
51. Sehn, L. H. & Salles, G. Diffuse large B-cell lymphoma. *N. Engl. J. Med.* (2021) doi:10.1157/13089865.
52. Wright, G. W. *et al.* A Probabilistic Classification Tool for Genetic Subtypes of Diffuse Large B Cell Lymphoma with Therapeutic Implications. *Cancer Cell* **37**, 551-568.e14 (2020).
53. Pasqualucci, L. *et al.* Genetics of Follicular Lymphoma Transformation. *Cell Rep.* **6**, 130–140 (2014).
54. Krysiak, K. *et al.* Recurrent somatic mutations affecting B-cell receptor signaling pathway genes in follicular lymphoma. *Blood* **129**, 473–483 (2017).
55. González-Rincón, J. *et al.* Unraveling transformation of follicular lymphoma to diffuse large B-cell lymphoma. *PLoS One* **14**, 1–16 (2019).
56. Caruso, S. & Poon, I. K. H. Apoptotic cell-derived extracellular vesicles: More than just

debris. *Front. Immunol.* **9**, (2018).
57. Damle, R. N. *et al.* Ig V gene mutation status and CD38 expression as novel prognostic indicators in chronic lymphocytic leukemia. *Blood* **94**, 1840–1847 (1999).
58. Hamblin, B. T. J., Davis, Z., Gardiner, A., Oscier, D. G. & Stevenson, F. K. Unmutated Ig V. *Blood* **94**, 1848–1854 (1999).
59. Gaidano, G. & Rossi, D. The mutational landscape of chronic lymphocytic leukemia and its impact on prognosis and treatment. *Hematology* **2017**, 329–337 (2017).
60. Klein, U. *et al.* The DLEU2/miR-15a/16-1 Cluster Controls B Cell Proliferation and Its Deletion Leads to Chronic Lymphocytic Leukemia. *Cancer Cell* **17**, 28–40 (2010).
61. Calin, G. A. *et al.* Frequent deletions and down-regulation of micro-RNA genes miR15 and miR16 at 13q14 in chronic lymphocytic leukemia. *Proc. Natl. Acad. Sci. U. S. A.* **99**, 15524–15529 (2002).
62. Cimmino, A. *et al.* miR-15 and miR-16 induce apoptosis by targeting BCL2. *Proc. Natl. Acad. Sci. U. S. A.* **102**, 13944–13949 (2005).
63. Hewitt, S. L. *et al.* RAG-1 and ATM coordinate monoallelic recombination and nuclear positioning of immunoglobulin loci. *Nat. Immunol.* **10**, 655–664 (2009).
64. Bredemeyer, A. L. *et al.* ATM stabilizes DNA double-strand-break complexes during V(D)J recombination. *Nature* **442**, 466–470 (2006).
65. Hathcock, K. S. *et al.* LYMPHOID NEOPLASIA ATM de fi ciency promotes development of murine B-cell lymphomas that resemble diffuse large B-cell lymphoma in humans. **126**, 2291–2302 (2015).
66. Yamamoto, K. *et al.* Early B-cell Specific Inactivation of ATM Synergizes with Ectopic CyclinD1 Expression to Promote Pre-germinal center B-cell Lymphomas in Mice. *Leukemia* **29**, 1414–1424 (2015).
67. Kalla, C. *et al.* Analysis of 11q22-q23 deletion target genes in B-cell chronic lymphocytic leukaemia: Evidence for a pathogenic role of NPAT, CUL5, and PPP2R1B. *Eur. J. Cancer* **43**, 1328–1335 (2007).
68. Zhao, G. *et al.* Cullin5 deficiency promotes small-cell lung cancer metastasis by stabilizing integrin β1. *J. Clin. Invest.* **129**, 972–987 (2019).
69. Fink, S. R. *et al.* Loss of TP53 is due to rearrangements involving chromosome region 17p10~p12 in chronic lymphocytic leukemia. *Cancer Genet. Cytogenet.* **167**, 177–181 (2006).
70. Dicker, F. *et al.* The detection of TP53 mutations in chronic lymphocytic leukemia independently predicts rapid disease progression and is highly correlated with a complex aberrant karyotype. *Leukemia* **23**, 117–124 (2009).
71. López, C. *et al.* A new genetic abnormality leading to TP53 gene deletion in chronic lymphocytic leukaemia. *Br. J. Haematol.* **156**, 612–618 (2012).
72. Abruzzo, L. V. *et al.* Trisomy 12 chronic lymphocytic leukemia expresses a unique set of activated and targetable pathways. *Haematologica* **103**, 2069–2078 (2018).
73. Balatti, V. *et al.* NIH Public Access. *Leukemia* **27**, 740–743 (2013).
74. Hallek, M. Chronic lymphocytic leukemia: 2017 update on diagnosis, risk stratification, and treatment. *Am. J. Hematol.* **92**, 946–965 (2017).
75. Landau, D. A. *et al.* Mutations driving CLL and their evolution in progression and relapse. *Nature* **526**, 525–530 (2015).
76. Puente, X. S. *et al.* Whole-genome sequencing identifies recurrent mutations in chronic lymphocytic leukaemia. *Nature* **475**, 101–105 (2011).
77. Quesada, V. *et al.* Exome sequencing identifies recurrent mutations of the splicing factor SF3B1 gene in chronic lymphocytic leukemia. *Nat. Genet.* **44**, 47–52 (2012).
78. Zhang, Z. *et al.* SF3B1 mutation is a prognostic factor in chronic lymphocytic leukemia: A meta-analysis. *Oncotarget* **8**, 69916–69923 (2017).
79. Coiffier, B. *et al.* Long-term outcome of patients in the LNH-98.5 trial, the first randomized study comparing rituximab-CHOP to standard CHOP chemotherapy in DLBCL patients: A study by the Groupe d'Etudes des Lymphomes de l'Adulte. *Blood* **116**, 2040–2045 (2010).
80. Coiffier, B. *et al.* CHOP CHEMOTHERAPY PLUS RITUXIMAB COMPARED WITH

CHOP ALONE IN ELDERLY PATIENTS WITH DIFFUSE LARGE-B-CELL LYMPHOMA B. *N Engl J Med* **346**, 235–242 (2002).
81. Coiffier, B. & Sarkozy, C. Diffuse large B-cell lymphoma : R-CHOP failure — what to do ? *Hematol. Am. Soc. Hematol. Educ. Progr.* 366–378 (2016).
82. Gisselbrecht, C. *et al.* Salvage Regimens With Autologous Transplantation for Relapsed Large B-Cell Lymphoma in the Rituximab Era. *J. Clin. Oncol.* **28**, (2010).
83. Westin, J. R. *et al.* Efficacy and safety of CD19-directed CAR-T cell therapies in patients with relapsed/refractory aggressive B-cell lymphomas: Observations from the JULIET, ZUMA-1, and TRANSCEND trials. *Am. J. Hematol.* **96**, 1295–1312 (2021).
84. Roschewski, M., Longo, D. L. & Wilson, W. H. CAR T-Cell Therapy for Large B-Cell Lymphoma — Who,When, and How? *N. Engl. J. Med.* 1547–1550 (2021).
85. Schuster, S. J. *et al.* Tisagenlecleucel in Adult Relapsed or Refractory Diffuse Large B-Cell Lymphoma. *N. Engl. J. Med.* **380**, 45–56 (2019).
86. Neelapu, S. S. *et al.* Axicabtagene Ciloleucel CAR T-Cell Therapy in Refractory Large B-Cell Lymphoma. *N. Engl. J. Med.* **377**, 2531–2544 (2017).
87. Chavez, J. C., Bachmeier, C. & Kharfan-Dabaja, M. A. CAR T-cell therapy for B-cell lymphomas: clinical trial results of available products. *Ther. Adv. Hematol.* **10**, 204062071984158 (2019).
88. Ardeshna, K. *et al.* Long-term effect of a watch and wait policy versus immediate systemic treatment for asymptomatic advanced-stage non-Hodgkin lymphoma : a randomised controlled trial. *Lancet* **362**, 516–522 (2003).
89. Ardeshna, K. M. *et al.* Rituximab versus a watch-and-wait approach in patients with advanced-stage , asymptomatic , non-bulky follicular lymphoma : an open-label randomised phase 3 trial. *Lancet Oncol.* **15**, 424–435 (2014).
90. Solal-Celigny, P. *et al.* Watchful Waiting in Low – Tumor Burden Follicular Lymphoma in the Rituximab Era : Results of an F2-Study Database. *J. Clin. Oncol.* **30**, 0–5 (2020).
91. Filippi, A. R., Ciammella, P. & Ricardi, U. Limited Stage Follicular Lymphoma : Current Role of Radiation Therapy. *Mediterr. J. Hematol. Infect. Dis.* 1–9 (2016).
92. Yahalom, J. Radiotherapy of Follicular Lymphoma : Updated Role and New Rules. *Curr. Treat. Options Oncol.* 262–268 (2014) doi:10.1007/s11864-014-0286-4.
93. Freeman, C. *et al.* Long-Term Results of PET-Guided Radiation in Advanced-Stage Diffuse Large B-Cell Lymphoma Patients Treated with R-CHOP. *Blood* (2021).
94. Norman, J. E., Schouten, H. C., Dreger, P. & Robinson, S. P. The role of stem cell transplantation in the management of relapsed follicular lymphoma in the era of targeted therapies. *Bone Marrow Transplant.* **54**, 787–797 (2019).
95. Eichhorst, B. *et al.* Chronic lymphocytic leukaemia: ESMO Clinical Practice Guidelines for diagnosis, treatment and follow-up. *Ann. Oncol.* **32**, 23–33 (2021).
96. De Rooij, M. F. M. *et al.* The clinically active BTK inhibitor PCI-32765 targets B-cell receptor- and chemokine-controlled adhesion and migration in chronic lymphocytic leukemia. *Blood* **119**, 2590–2594 (2012).
97. Herman, S. E. M. *et al.* Bruton tyrosine kinase represents a promising therapeutic target for treatment of chronic lymphocytic leukemia and is effectively targeted by PCI-32765. *Blood* **117**, 6287–6296 (2011).
98. Ponader, S. *et al.* The Bruton tyrosine kinase inhibitor PCI-32765 thwarts chronic lymphocytic leukemia cell survival and tissue homing in vitro and in vivo. *Blood* **119**, 1182–1189 (2012).
99. Barr, P. M. *et al.* Sustained efficacy and detailed clinical follow-up of first-line ibrutinib treatment in older patients with chronic lymphocytic leukemia: Extended phase 3 results from RESONATE-2. *Haematologica* **103**, 1502–1510 (2018).
100. Burger, J. A. *et al.* Long-term efficacy and safety of first-line ibrutinib treatment for patients with CLL/SLL: 5 years of follow-up from the phase 3 RESONATE-2 study. *Leukemia* **34**, 787–798 (2020).
101. Burger, J. A. *et al.* Randomized trial of ibrutinib vs ibrutinib plus rituximab in patients with chronic lymphocytic leukemia. *Blood* **133**, 1011–1019 (2019).

102. Fischer, K. *et al.* Venetoclax and Obinutuzumab in Patients with CLL and Coexisting Conditions. *N. Engl. J. Med.* **380**, 2225–2236 (2019).
103. Edelmann, J. & Gribben, J. G. Managing patients with TP53-deficient chronic lymphocytic leukemia. *J. Oncol. Pract.* **13**, 371–377 (2017).
104. Höpken, U. E. & Rehm, A. Targeting the Tumor Microenvironment of Leukemia and Lymphoma. *Trends in Cancer* **5**, 351–364 (2019).
105. Kapsenberg, M. L. Dendritic-cell control of pathogen-driven T-cell polarization. *Nat. Rev. Immunol.* **3**, 984–993 (2003).
106. Martín-Fontecha, A., Lanzavecchia, A. & Sallusto, F. Dendritic cell migration to peripheral lymph nodes. *Handb. Exp. Pharmacol.* **188**, 31–49 (2009).
107. Gutiérrez-Martínez, E. *et al.* Cross-presentation of cell-associated antigens by MHC class I in dendritic cell subsets. *Front. Immunol.* **6**, (2015).
108. McDonnell, A. M., Robinson, B. W. S. & Currie, A. J. Tumor antigen cross-presentation and the dendritic cell: Where it all begins? *Clin. Dev. Immunol.* **2010**, (2010).
109. Fu, C. & Jiang, A. Dendritic Cells and CD8 T Cell Immunity in Tumor Microenvironment. *Front. Immunol.* **9**, 1–11 (2018).
110. Van Gisbergen, K. P. J. M., Aarnoudse, C. A., Meijer, G. A., Geijtenbeek, T. B. H. & Van Kooyk, Y. Dendritic cells recognize tumor-specific glycosylation of carcinoembryonic antigen on colorectal cancer cells through dendritic cell-specific intercellular adhesion molecule-3-grabbing nonintegrin. *Cancer Res.* **65**, 5935–5944 (2005).
111. Fiore, F. *et al.* Dendritic cells are significantly reduced in non-Hodgkin's lymphoma and express less CCR7 and CD62L. *Leuk. Lymphoma* **47**, 613–622 (2006).
112. Chevalier, N. *et al.* Analysis of dendritic cell subpopulations in follicular lymphoma with respect to the tumor immune microenvironment. *Leuk. Lymphoma* **57**, 2150–2160 (2016).
113. Chang, K. C., Huang, G. C., Jones, D. & Lin, Y. H. Distribution patterns of dendritic cells and T cells in diffuse large B-cell lymphomas correlate with prognoses. *Clin. Cancer Res.* **13**, 6666–6672 (2007).
114. Chao, M. P. *et al.* Anti-CD47 Antibody Synergizes with Rituximab to Promote Phagocytosis and Eradicate Non-Hodgkin Lymphoma. *Cell* **142**, 699–713 (2010).
115. Zhang, W. *et al.* Therapy Strategy of CD47 in Diffuse Large B-Cell Lymphoma (DLBCL). *Dis. Markers* **2021**, (2021).
116. Gardner, A., de Mingo Pulido, Á. & Ruffell, B. Dendritic Cells and Their Role in Immunotherapy. *Front. Immunol.* **11**, 1–14 (2020).
117. Lwin, T. *et al.* Follicular dendritic cell-dependent drug resistance of non-Hodgkin lymphoma involves cell adhesion-mediated Bim down-regulation through induction of microRNA-181a. *Blood* **116**, 5228–5236 (2010).
118. Peng, Q. *et al.* PD-L1 on dendritic cells attenuates T cell activation and regulates response to immune checkpoint blockade. *Nat. Commun.* **11**, 1–8 (2020).
119. Oh, S. A. *et al.* PD-L1 expression by dendritic cells is a key regulator of T-cell immunity in cancer. *Nat. Cancer* **1**, 681–691 (2020).
120. Mueller, C. G. *et al.* Critical role of monocytes to support normal B cell and diffuse large B cell lymphoma survival and proliferation. *J. Leukoc. Biol.* **82**, 567–575 (2007).
121. Kocher, T. *et al.* CD4+ T cells, but not non-classical monocytes, are dispensable for the development of chronic lymphocytic leukemia in the TCL1-tg murine model. *Leukemia* **30**, 1409–1413 (2016).
122. Hanna, B. S. *et al.* Control of chronic lymphocytic leukemia development by clonally-expanded CD8 + T-cells that undergo functional exhaustion in secondary lymphoid tissues. *Leukemia* **33**, 625–637 (2019).
123. McKee, S. J. *et al.* B cell lymphoma progression promotes the accumulation of circulating Ly6Clo monocytes with immunosuppressive activity. *Oncoimmunology* **7**, (2018).
124. Le Gallou, S. *et al.* Nonclassical Monocytes Are Prone to Migrate Into Tumor in Diffuse

Large B-Cell Lymphoma. *Front. Immunol.* **12**, 1–12 (2021).
125. Maffei, R. *et al.* The monocytic population in chronic lymphocytic leukemia shows altered composition and deregulation of genes involved in phagocytosis and inflammation. *Haematologica* **98**, 1115–1123 (2013).
126. Friedman, D. R. *et al.* Relationship of blood monocytes with chronic lymphocytic leukemia aggressiveness and outcomes: a multi-institutional study. *Am. J. Hematol.* **91**, 687–691 (2016).
127. van Attekum, M. H. A. *et al.* CD40 signaling instructs chronic lymphocytic leukemia cells to attract monocytes via the CCR2 axis. *Haematologica* **102**, 2069–2076 (2017).
128. Kowalska, W. Expression of CD163 and HLA-DR molecules on the monocytes in chronic lymphocytic leukemia patients. *Folia Histochem. Cytobiol.* **58**, 17–24 (2020).
129. Hanna, B. S. *et al.* Depletion of CLL-associated patrolling monocytes and macrophages controls disease development and repairs immune dysfunction in vivo. *Leukemia* **30**, 570–579 (2016).
130. Liu, Y., Zhou, X. & Wang, X. Targeting the tumor microenvironment in B-cell lymphoma: challenges and opportunities. *J. Hematol. Oncol.* **14**, 1–17 (2021).
131. Ku, A. W. *et al.* Tumor-induced MDSC act via remote control to inhibit L-selectin-dependent adaptive immunity in lymph nodes. *Elife* **5**, 1–29 (2016).
132. Burger, J. A. *et al.* Blood-derived nurse-like cells protect chronic lymphocytic leukemia B cells from spontaneous apoptosis through stromal cell-derived factor-1. *Blood* **96**, 2655–2663 (2000).
133. Tsukada, N., Burger, J. A., Zvaifler, N. J. & Kipps, T. J. Distinctive features of " nurselike " cells that differentiate in the context of chronic lymphocytic leukemia. *Blood* **99**, 1030–1037 (2002).
134. Boissard, F., Fournié, J.-J., Quillet-Mary, A., Ysebaert, L. & Poupot, M. Nurse-like cells mediate ibrutinib resistance in chronic lymphocytic leukemia patients. *Blood Cancer J.* **5**, (2015).
135. Filip, A. A., Koczkodaj, D., Ewa, W., Piersiak, T. & Dmoszy, A. Blood Cells , Molecules and Diseases Circulating microenvironment of CLL : Are nurse-like cells related to tumor-associated macrophages ? *Blood cells, Mol. Dis.* **50**, 263–270 (2013).
136. Giannoni, P. *et al.* Chronic lymphocytic leukemia nurse-like cells express hepatocyte growth factor receptor (c-MET) and indoleamine 2,3-dioxygenase and display features of immunosuppressive type 2 skewed macrophages. *Haematologica* **99**, 1078–1087 (2014).
137. Croci, D. O. *et al.* Nurse-like cells control the activity of chronic lymphocytic leukemia B cells via galectin-1. *Leukemia* **27**, 1413–1416 (2013).
138. Ysebaert, L. & Fournié, J. Genomic and phenotypic characterization of nurse-like cells that promote drug resistance in chronic lymphocytic leukemia. *Leuk. Lymphoma* **8194**, (2011).
139. Nishio, M. *et al.* Nurselike cells express BAFF and APRIL, which can promote survival of chronic lymphocytic leukemia cells via a paracrine pathway distinct from that of SDF-1α. *Blood* **106**, 1012–1020 (2005).
140. McWilliams, E. M. *et al.* Anti–BAFF-R antibody VAY-736 demonstrates promising preclinical activity in CLL and enhances effectiveness of ibrutinib. *Blood Adv.* **3**, 447–460 (2019).
141. Gautam, S. *et al.* Reprogramming nurse-like cells with interferon γ to interrupt chronic lymphocytic leukemia cell survival. *J. Biol. Chem.* **291**, 14356–14362 (2016).
142. Deaglio, S. *et al.* CD38/CD31 interactions activate genetic pathways leading to proliferation and migration in chronic lymphocytic leukemia cells. *Mol. Med.* **16**, 87–91 (2010).
143. Poggi, A. *et al.* Engagement of CD31 delivers an activating signal that contributes to the survival of chronic lymphocytic leukaemia cells Alessandro. *Br. J. Haematol.* (2010).
144. Lee, K. Y. M1 and M2 polarization of macrophages: a mini-review. *Med. Biol. Sci. Eng.* **2**, 1–5 (2019).

145. Jayasingam, S. D. *et al.* Evaluating the Polarization of Tumor-Associated Macrophages Into M1 and M2 Phenotypes in Human Cancer Tissue: Technicalities and Challenges in Routine Clinical Practice. *Front. Oncol.* **9**, 1–9 (2020).
146. Ge, Z. & Ding, S. The Crosstalk Between Tumor-Associated Macrophages (TAMs) and Tumor Cells and the Corresponding Targeted Therapy. *Front. Oncol.* **10**, 1–23 (2020).
147. Palaga, T., Wongchana, W. & Kueanjinda, P. Notch signaling in macrophages in the context of cancer immunity. *Front. Immunol.* **9**, 1–9 (2018).
148. Wang, Y. C. *et al.* Notch signaling determines the M1 versus M2 polarization of macrophages in antitumor immune responses. *Cancer Res.* **70**, 4840–4849 (2010).
149. Shen, L. *et al.* M2 tumour-associated macrophages contribute to tumour progression via legumain remodelling the extracellular matrix in diffuse large B cell lymphoma. *Sci. Rep.* **6**, 1–10 (2016).
150. Canioni, D. *et al.* High numbers of tumor-associated macrophages have an adverse prognostic value that can be circumvented by rituximab in patients with follicular lymphoma enrolled onto the GELA-GOELAMS FL-2000 trial. *J. Clin. Oncol.* **26**, 440–446 (2008).
151. Taskinen, M., Karjalainen-Lindsberg, M. L., Nyman, H., Eerola, L. M. & Leppä, S. A high tumor-associated macrophage content predicts favorable outcome in follicular lymphoma patients treated with rituximab and cyclophosphamide- doxorubicin-vincristine-prednisone. *Clin. Cancer Res.* **13**, 5784–5789 (2007).
152. Marchesi, F. *et al.* High density of CD68+/CD163+ tumour-associated macrophages (M2-TAM) at diagnosis is significantly correlated to unfavorable prognostic factors and to poor clinical outcomes in patients with diffuse large B-cell lymphoma. *Hematol. Oncol.* **25**, 127–131 (2007).
153. Farinha, P. *et al.* Analysis of multiple biomarkers shows that lymphoma-associated macrophage (LAM) content is an independent predictor of survival in follicular lymphoma (FL). *Blood* **106**, 2169–2174 (2005).
154. Leidi, M. *et al.* M2 Macrophages Phagocytose Rituximab-Opsonized Leukemic Targets More Efficiently than M1 Cells In Vitro. *J. Immunol.* **182**, 4415–4422 (2009).
155. McCord, R. *et al.* PD-L1 and tumor-associated macrophages in de novo DLBCL. *Blood Adv.* **3**, 531–540 (2019).
156. Kiyasu, J. *et al.* Expression of programmed cell death ligand 1 is associated with poor overall survival in patients with diffuse large B-cell lymphoma. *Blood* **126**, 2193–2201 (2015).
157. Cencini, E., Fabbri, A., Sicuranza, A., Gozzetti, A. & Bocchia, M. The role of tumor-associated macrophages in hematologic malignancies. *Cancers (Basel).* **13**, (2021).
158. Riabov, V. *et al.* Role of tumor associated macrophages in tumor angiogenesis and lymphangiogenesis. *Front. Physiol.* **5 MAR**, 1–13 (2014).
159. Lenz, G. *et al.* Molecular subtypes of diffuse large B-cell lymphoma arise by distinct genetic pathways. *Proc. Natl. Acad. Sci. U. S. A.* **105**, 13520–13525 (2008).
160. Benner, B. *et al.* Generation of monocyte-derived tumor-associated macrophages using tumor-conditioned media provides a novel method to study tumor-associated macrophages in vitro. *J. Immunother. Cancer* **7**, 1–14 (2019).
161. Mesaros, O. *et al.* Macrophage polarization in chronic lymphocytic leukemia: Nurse-like cells are the caretakers of leukemic cells. *Biomedicines* **8**, 1–17 (2020).
162. Carbonnelle-Puscian, A. *et al.* The novel immunosuppressive enzyme IL4I1 is expressed by neoplastic cells of several B-cell lymphomas and by tumor-associated macrophages. *Leukemia* **23**, 952–960 (2009).
163. Willingham, S. B. *et al.* The CD47-signal regulatory protein alpha (SIRPa) interaction is a therapeutic target for human solid tumors. *Proc. Natl. Acad. Sci. U. S. A.* **109**, 6662–6667 (2012).
164. Mondal, A. *et al.* IDO1 is an Integral Mediator of Inflammatory Neovascularization. *EBioMedicine* **14**, 74–82 (2016).
165. Liu, M. *et al.* Targeting the IDO1 pathway in cancer: From bench to bedside. *J.*

Hematol. Oncol. **11**, 1–12 (2018).
166. Munn, D. H., Sharma, M. D., Johnson, T. S. & Rodriguez, P. IDO, PTEN-expressing Tregs and control of antigen-presentation in the murine tumor microenvironment. *Cancer Immunol. Immunother.* **176**, 139–148 (2017).
167. Sadik, A. *et al.* IL4I1 Is a Metabolic Immune Checkpoint that Activates the AHR and Promotes Tumor Progression. *Cell* **182**, 1252-1270.e34 (2020).
168. Yang, L. *et al.* IL-10 derived from M2 macrophage promotes cancer stemness via JAK1/STAT1/NF-κB/Notch1 pathway in non-small cell lung cancer. *Int. J. Cancer* **145**, 1099–1110 (2019).
169. Herishanu, Y. *et al.* The lymph node microenvironment promotes B-cell receptor signaling, NF-κB activation, and tumor proliferation in chronic lymphocytic leukemia. *Blood* **117**, 563–574 (2011).
170. Ye, H. *et al.* Tumor-associated macrophages promote progression and the Warburg effect via CCL18/NF-kB/VCAM-1 pathway in pancreatic ductal adenocarcinoma. *Cell Death Dis.* **9**, (2018).
171. Epron, G. *et al.* Monocytes and T cells cooperate to favor normal and follicular lymphoma B-cell growth: Role of IL-15 and CD40L signaling. *Leukemia* **26**, 139–148 (2012).
172. Grzywa, T. M. *et al.* Myeloid Cell-Derived Arginase in Cancer Immune Response. *Front. Immunol.* **11**, 1–24 (2020).
173. Blaker, Y. N. *et al.* The tumour microenvironment influences survival and time to transformation in follicular lymphoma in the rituximab era. *Br. J. Haematol.* **175**, 102–114 (2016).
174. Fleming, V. *et al.* Targeting myeloid-derived suppressor cells to bypass tumor-induced immunosuppression. *Front. Immunol.* **9**, (2018).
175. Li, T. *et al.* Targeting MDSC for Immune-Checkpoint Blockade in Cancer Immunotherapy: Current Progress and New Prospects. *Clin. Med. Insights Oncol.* **15**, (2021).
176. Arlauckas, S. P. *et al.* In vivo imaging reveals a tumor-associated macrophage-mediated resistance pathway in anti-PD-1 therapy. *Sci. Transl. Med.* **9**, 1–10 (2017).
177. Harding, C., Heuser, J. & Stahl, P. Receptor-mediated endocytosis of transferrin and recycling of the transferrin receptor in rat reticulocytes. *J. Cell Biol.* **97**, 329–339 (1983).
178. Pan, B. & Johnstone, R. M. Fate of the Transferrin Receptor during Maturation of Sheep Reticulocytes In Vitro : Selective Externalization of the Receptor. *Cell* **33**, 967–977 (1983).
179. Dautry Varsat, A., Ciechanover, A. & Lodish, H. F. pH and the recycling of transferrin during receptor-mediated endocytosis. *Proc. Natl. Acad. Sci. U. S. A.* **80**, 2258–2262 (1983).
180. Raposo, G. *et al.* B Lymphocytes Secrete Antigen-presentingVesicles. *J. Exp. Med.* **183**, (1996).
181. Raposo, G. *et al.* MHC_LAMP_mast cell_MBC.pdf. *Mol. Biol. cellcular Biol.* **8**, 2631–2645 (1997).
182. Harding, C. V., Heuser, J. E. & Stahl, P. D. Exosomes: Looking back three decades and into the future. *J. Cell Biol.* **200**, 367–371 (2013).
183. Samanta, S. *et al.* Exosomes : new molecular targets of diseases. *Nat. Publ. Gr.* **39**, 501–513 (2017).
184. Wu, D. *et al.* Profiling surface proteins on individual exosomes using a proximity barcoding assay. *Nat. Commun.* **10**, 1–10 (2019).
185. Campos-Silva, C. *et al.* High sensitivity detection of extracellular vesicles immune-captured from urine by conventional flow cytometry. *Sci. Rep.* **9**, 1–12 (2019).
186. Montecalvo, A. *et al.* Mechanism of transfer of functional microRNAs between mouse dendritic cells via exosomes. *Blood* **119**, 3–5 (2012).
187. Ratajczak, J. *et al.* Embryonic stem cell-derived microvesicles reprogram hematopoietic progenitors : evidence for horizontal transfer of mRNA and protein

delivery. *Leukemia* 847–856 (2006) doi:10.1038/sj.leu.2404132.
188. Lenzini, S., Bargi, R., Chung, G. & Shin, J. Matrix mechanics and water permeation regulate extracellular vesicle transport. *Nat. Nanotechnol.* **15**, (2020).
189. Bebelman, M. P., Smit, M. J., Pegtel, D. M. & Baglio, S. R. Biogenesis and function of extracellular vesicles in cancer. *Pharmacol. Ther.* **188**, 1–11 (2018).
190. Mathieu, M., Martin-Jaular, L., Lavieu, G. & Théry, C. Specificities of secretion and uptake of exosomes and other extracellular vesicles for cell-to-cell communication. *Nat. Cell Biol.* **21**, 9–17 (2019).
191. Xu, X., Lai, Y. & Hua, Z. C. Apoptosis and apoptotic body: Disease message and therapeutic target potentials. *Biosci. Rep.* **39**, 1–17 (2019).
192. Hessvik, N. P. & Llorente, A. Current knowledge on exosome biogenesis and release. *Cell. Mol. Life Sci.* **75**, 193–208 (2018).
193. Maas, S. L. N., Breakefield, X. O. & Weaver, A. M. Extracellular Vesicles: Unique Intercellular Delivery Vehicles. *Trends Cell Biol.* **27**, 172–188 (2017).
194. Boyiadzis, M. & Whiteside, T. L. Exosomes in acute myeloid leukemia inhibit hematopoiesis. *Curr. Opin. Hematol.* **25**, 279–284 (2018).
195. Sork, H. *et al.* Heterogeneity and interplay of the extracellular vesicle small RNA transcriptome and proteome. *Sci. Rep.* **8**, 1–12 (2018).
196. Théry, C. *et al.* Minimal information for studies of extracellular vesicles 2018 (MISEV2018): a position statement of the International Society for Extracellular Vesicles and update of the MISEV2014 guidelines. *J. Extracell. Vesicles* **7**, (2018).
197. Zhang, H. *et al.* Identification of distinct nanoparticles and subsets of extracellular vesicles by asymmetric flow field-flow fractionation. *Nat. Cell Biol.* **20**, 332–343 (2018).
198. Zhang, Q. *et al.* Transfer of Functional Cargo in Exomeres. *Cell Rep.* **27**, 940-954.e6 (2019).
199. Kalluri, R. & LeBleu, V. S. The biology, function, and biomedical applications of exosomes. *Science (80-.).* **367**, (2020).
200. Colombo, M., Raposo, G. & Théry, C. Biogenesis, Secretion, and Intercellular Interactions of Exosomes and Other Extracellular Vesicles. *Annu. Rev. Cell Dev. Biol.* **30**, 255–289 (2014).
201. Alenquer, M. & Amorim, M. J. Exosome biogenesis, regulation, and function in viral infection. *Viruses* **7**, 5066–5083 (2015).
202. Colombo, M. *et al.* Analysis of ESCRT functions in exosome biogenesis, composition and secretion highlights the heterogeneity of extracellular vesicles. *J. Cell Sci.* **126**, 5553–5565 (2013).
203. Kowal, J. *et al.* Biogenesis and secretion of exosomes. *Curr. Protoc. Cell Biol.* 116–125 (2014).
204. Wollert, T. *et al.* The ESCRT machinery at a glance. *J. Cell Sci.* **122**, 2163–2166 (2009).
205. Van Niel, G., D'Angelo, G. & Raposo, G. Shedding light on the cell biology of extracellular vesicles. *Nat. Rev. Mol. Cell Biol.* **19**, 213–228 (2018).
206. Baietti, M. F. *et al.* Syndecan – syntenin – ALIX regulates the biogenesis of exosomes. *Nat. Cell Biol.* **14**, (2012).
207. Perez-Hernandez, D. *et al.* The intracellular interactome of tetraspanin-enriched microdomains reveals their function as sorting machineries toward exosomes. *J. Biol. Chem.* **288**, 11649–11661 (2013).
208. Wei, D. *et al.* RAB31 marks and controls an ESCRT-independent exosome pathway. *Cell Res.* **31**, 157–177 (2021).
209. Krishnan, P. D. G., Golden, E., Woodward, E. A., Pavlos, N. J. & Blancafort, P. Rab gtpases: Emerging oncogenes and tumor suppressive regulators for the editing of survival pathways in cancer. *Cancers (Basel).* **12**, (2020).
210. Thakur, B. K. *et al.* Double-stranded DNA in exosomes: A novel biomarker in cancer detection. *Cell Res.* **24**, 766–769 (2014).
211. Kahlert, C. *et al.* Identification of doublestranded genomic dna spanning all chromosomes with mutated KRAS and P53 DNA in the serum exosomes of patients

with pancreatic cancer. *J. Biol. Chem.* **289**, 3869–3875 (2014).
212. Yokoi, A. *et al.* Mechanisms of nuclear content loading to exosomes. *Sci. Adv.* **5**, 1–17 (2019).
213. Jeppesen, D. K. *et al.* Reassessment of Exosome Composition Article Reassessment of Exosome Composition. *Cell* **177**, 428-445.e18 (2019).
214. Lucchetti, D. *et al.* Mutational status of plasma exosomal KRAS predicts outcome in patients with metastatic colorectal cancer. *Sci. Rep.* **11**, 1–14 (2021).
215. Valadi, H. *et al.* Exosome-mediated transfer of mRNAs and microRNAs is a novel mechanism of genetic exchange between cells. *Nat. Cell Biol.* **9**, 654–659 (2007).
216. Tsai, S. J. *et al.* Exosome-mediated mRNA delivery in vivo is safe and can be used to induce SARS-CoV-2 immunity. *J. Biol. Chem.* **297**, 101266 (2021).
217. Bhome, R. *et al.* Exosomal microRNAs (exomiRs): Small molecules with a big role in cancer. *Cancer Lett.* **420**, 228–235 (2018).
218. Liu, X. M., Ma, L. & Schekman, R. Selective sorting of micrornas into exosomes by phase-separated ybx1 condensates. *Elife* **10**, 1–31 (2021).
219. Mittelbrunn, M. *et al.* Unidirectional transfer of microRNA-loaded exosomes from T cells to antigen-presenting cells. *Nat. Commun.* **2**, (2011).
220. Shin, S. *et al.* Urinary exosome microRNA signatures as a noninvasive prognostic biomarker for prostate cancer. *npj Genomic Med.* **6**, 1–6 (2021).
221. Liu, F., Mao, H., Chai, S. & Mao, H. Meta-analysis of the diagnostic value of exosomal miR-21 as a biomarker for the prediction of cancer. *J. Clin. Lab. Anal.* **35**, 1–10 (2021).
222. Feng, Y. *et al.* Exosome-derived miRNAs as predictive biomarkers for diffuse large B-cell lymphoma chemotherapy resistance. *Epigenomics* **11**, 35–51 (2019).
223. Decruyenaere, P., Offner, F. & Vandesompele, J. Circulating RNA biomarkers in diffuse large B-cell lymphoma: a systematic review. *Exp. Hematol. Oncol.* **10**, 1–22 (2021).
224. Mahati, S., Fu, X., Ma, X., Zhang, H. & Xiao, L. Delivery of miR-26a Using an Exosomes-Based Nanosystem Inhibited Proliferation of Hepatocellular Carcinoma. *Front. Mol. Biosci.* **8**, 1–9 (2021).
225. O'Brien, K., Breyne, K., Ughetto, S., Laurent, L. C. & Breakefield, X. O. RNA delivery by extracellular vesicles in mammalian cells and its applications. *Nat. Rev. Mol. Cell Biol.* **21**, 585–606 (2020).
226. McKenzie, A. J. *et al.* KRAS-MEK Signaling Controls Ago2 Sorting into Exosomes. *Cell Rep.* **15**, 978–987 (2016).
227. Driedonks, T. A. P. & Hoen, E. N. M. N.-. Circulating Y-RNAs in Extracellular Vesicles and Ribonucleoprotein Complexes ; Implications for the Immune System. *Front. Immunol.* **9**, 1–15 (2019).
228. Groot, M. & Lee, H. Sorting Mechanisms for MicroRNAs into Extracellular Vesicles and Their Associated Diseases. *Cells* **9**, 1–16 (2020).
229. Boccitto, M. & Wolin, S. L. Ro60 and Y RNAs: structure, functions, and roles in autoimmunity. *Crit. Rev. Biochem. Mol. Biol.* **54**, 133–152 (2019).
230. Gulìa, C. *et al.* Y RNA: An overview of their role as potential biomarkers and molecular targets in human cancers. *Cancers (Basel).* **12**, 1–21 (2020).
231. Lerner, M. R., Boyle, J. A., Hardin, J. A. & Steitz, J. A. Two novel classes of small ribonucleoproteins detected by antibodies associated with lupus erythematosus. *Science (80-.).* **211**, 400–402 (1981).
232. Sim, S., Hughes, K., Chen, X. & Wolin, S. L. The Bacterial Ro60 Protein and Its Noncoding y RNA Regulators. *Annu. Rev. Microbiol.* **74**, 387–407 (2020).
233. Christov, C. P., Gardiner, T. J., Szuts, D. & Krude, T. Functional Requirement of Noncoding Y RNAs for Human Chromosomal DNA Replication. *Mol. Cell. Biol.* **26**, 6993–7004 (2006).
234. Krude, T., Christov, C. P., Hyrien, O. & Marheineke, K. Y RNA functions at the initiation step of mammalian chromosomal DNA replication. *J. Cell Sci.* **122**, 2836–2845 (2009).
235. Collart, C., Christov, C. P., Smith, J. C. & Krude, T. The Midblastula Transition Defines

the Onset of Y RNA-Dependent DNA Replication in Xenopus laevis. *Mol. Cell. Biol.* **31**, 3857–3870 (2011).
236. Flynn, R. A. *et al.* Small RNAs are modified with N-glycans and displayed on the surface of living cells ll Article Small RNAs are modified with N-glycans and displayed on the surface of living cells. 3109–3124 (2021).
237. Lovisa, F. *et al.* RNY4 in Circulating Exosomes of Patients With Pediatric Anaplastic Large Cell Lymphoma: An Active Player? *Front. Oncol.* **10**, 1–8 (2020).
238. Wei, Z., Batagov, A. O., Carter, D. R. F. & Krichevsky, A. M. Fetal Bovine Serum RNA Interferes with the Cell Culture derived Extracellular RNA. *Sci. Rep.* **6**, 1–6 (2016).
239. Kugeratski, F. G. *et al. Quantitative proteomics identifies the core proteome of exosomes with syntenin-1 as the highest abundant protein and a putative universal biomarker*. *Nature Cell Biology* vol. 23 (Springer US, 2021).
240. Shurtleff, M. J., Temoche-Diaz, M. M., Karfilis, K. V., Ri, S. & Schekman, R. Y-box protein 1 is required to sort microRNAs into exosomes in cells and in a cell-free reaction. *Elife* **5**, 1–23 (2016).
241. Fabbiano, F. *et al.* RNA packaging into extracellular vesicles: An orchestra of RNA-binding proteins? *J. Extracell. Vesicles* **10**, (2020).
242. Tran, N. Cancer Exosomes as miRNA Factories. *Trends in Cancer* **2**, 329–331 (2016).
243. Leidal, A. M. *et al.* The LC3-conjugation machinery specifies the loading of RNA-binding proteins into extracellular vesicles. *Nat. Cell Biol.* **22**, 187–199 (2020).
244. Stavrou, S. & Ross, S. R. APOBEC3 Proteins in Viral Immunity. *J. Immunol.* **195**, 4565–4570 (2015).
245. Vasudevan, A. A. J. *et al.* Structural features of antiviral DNA cytidine deaminases. *Biol. Chem.* **394**, 1357–1370 (2013).
246. Liu, C. *et al.* APOBEC3G inhibits microRNA-mediated repression of translation by interfering with the interaction between Argonaute-2 and MOV10. *J. Biol. Chem.* **287**, 29373–29383 (2012).
247. Ali, S. *et al.* APOBEC3 inhibits DEAD-END function to regulate microRNA activity. *BMC Mol. Biol.* **14**, 1–9 (2013).
248. Sharma, S. *et al.* APOBEC3A cytidine deaminase induces RNA editing in monocytes and macrophages. *Nat. Commun.* **6**, (2015).
249. Granadillo Rodríguez, M., Flath, B. & Chelico, L. The interesting relationship between APOBEC3 deoxycytidine deaminases and cancer: A long road ahead: APOBEC3 cytidine deaminases and cancer. *Open Biol.* **10**, (2020).
250. Venkatesan, S. *et al.* Induction of apobec3 exacerbates dna replication stress and chromosomal instability in early breast and lung cancer evolution. *Cancer Discov.* **11**, 2456–2473 (2021).
251. Cervantes-Gracia, K., Gramalla-Schmitz, A., Weischedel, J. & Chahwan, R. APOBECs orchestrate genomic and epigenomic editing across health and disease. *Trends Genet.* **37**, 1028–1043 (2021).
252. Skotland, T., Sandvig, K. & Llorente, A. Lipids in exosomes: Current knowledge and the way forward. *Prog. Lipid Res.* **66**, 30–41 (2017).
253. Czernek, L., Chworos, A. & Duechler, M. The Uptake of Extracellular Vesicles is Affected by the Differentiation Status of Myeloid Cells. *Scand. J. Immunol.* **82**, 506–514 (2015).
254. Gabrusiewicz, K. *et al.* Glioblastoma stem cell-derived exosomes induce M2 macrophages and PD-L1 expression on human monocytes. *Oncoimmunology* **7**, (2018).
255. Li, B. *et al.* Tumor-derived exosomal HMGB1 promotes esophageal squamous cell carcinoma progression through inducing PD1 + TAM expansion. *Oncogenesis* **8**, (2019).
256. Whiteside, T. L. Tumor-derived exosomes and their role in tumor-induced immune suppression. *Vaccines* **4**, (2016).
257. Gärtner, K. *et al.* Tumor-derived extracellular vesicles activate primary monocytes. *Cancer Med.* **7**, 2013–2020 (2018).

258. Haderk, F. *et al.* Tumor-derived exosomes modulate PD-L1 expression in monocytes. *Sci. Immunol.* **2**, 1–12 (2017).
259. Han, C., Zhang, C., Wang, H. & Zhao, L. Exosome-mediated communication between tumor cells and tumor-associated macrophages: implications for tumor microenvironment. *Oncoimmunology* **10**, 1–16 (2021).
260. Olejarz, W., Dominiak, A., Zołnierzak, A., Kubiak-Tomaszewska, G. & Lorenc, T. Tumor-Derived Exosomes in Immunosuppression and Immunotherapy. *J. Immunol. Res.* **2020**, (2020).
261. Arkhypov, I. *et al.* Myeloid cell modulation by tumor-derived extracellular vesicles. *Int. J. Mol. Sci.* **21**, 1–22 (2020).
262. Kawasaki, T. & Kawai, T. Toll-like receptor signaling pathways. *Front. Immunol.* **5**, 1–8 (2014).
263. Akira, S. & Takeda, K. Toll-like receptor signalling. *Nat. Rev. Immunol.* **4**, 499–511 (2004).
264. Cervantes, J. L., Weinerman, B., Basole, C. & Salazar, J. C. TLR8: The forgotten relative revindicated. *Cell. Mol. Immunol.* **9**, 434–438 (2012).
265. El-Zayat, S. R., Sibaii, H. & Mannaa, F. A. Toll-like receptors activation, signaling, and targeting: an overview. *Bull. Natl. Res. Cent.* **43**, (2019).
266. Premkumar, V., Dey, M., Dorn, R. & Raskin, I. MyD88-dependent and independent pathways of toll-like receptors are engaged in biological activity of triptolide in ligand-stimulated macrophages. *BMC Chem. Biol.* **10**, (2010).
267. Kawai, T. *et al.* Lipopolysaccharide Stimulates the MyD88-Independent Pathway and Results in Activation of IFN-Regulatory Factor 3 and the Expression of a Subset of Lipopolysaccharide-Inducible Genes. *J. Immunol.* **167**, 5887–5894 (2001).
268. Zhou, M. *et al.* Pancreatic cancer derived exosomes regulate the expression of TLR4 in dendritic cells via miR-203. *Cell. Immunol.* **292**, 65–69 (2014).
269. Morrissey, S. M. *et al.* Tumor-derived exosomes drive immunosuppressive macrophages in a pre-metastatic niche through glycolytic dominant metabolic reprogramming. *Cell Metab.* **33**, 2040-2058.e10 (2021).
270. Shen, Y. *et al.* Tumor-derived exosomes educate dendritic cells to promote tumor metastasis via HSP72/HSP105-TLR2/TLR4 pathway. *Oncoimmunology* **6**, 1–16 (2017).
271. Bretz, N. P. *et al.* Body fluid exosomes promote secretion of inflammatory cytokines in monocytic cells via Toll-Like receptor signaling. *J. Biol. Chem.* **288**, 36691–36702 (2013).
272. Chow, A. *et al.* Macrophage immunomodulation by breast cancer-derived exosomes requires Toll-like receptor 2-mediated activation of NF-κ B. *Sci. Rep.* **4**, (2014).
273. Gao, S. *et al.* Histidine-Rich Glycoprotein Inhibits High-Mobility Group Box-1-Mediated Pathways in Vascular Endothelial Cells through CLEC-1A. *iScience* **23**, 101180 (2020).
274. Fleming, V. *et al.* Melanoma extracellular vesicles generate immunosuppressive myeloid cells by upregulating PD-L1 via TLR4 signaling. *Cancer Res.* **79**, 4715–4728 (2019).
275. Wang, J. Der *et al.* Exosomal hmgb1 promoted cancer malignancy. *Cancers (Basel).* **13**, 1–16 (2021).
276. Yeh, Y. Y. *et al.* Characterization of CLL exosomes reveals a distinct microRNA signature and enhanced secretion by activation of BCR signaling. *Blood* **125**, 3297–3305 (2015).
277. Navarro-Tableros, V., Gomez, Y., Camussi, G. & Brizzi, M. F. Extracellular vesicles: New players in lymphomas. *Int. J. Mol. Sci.* **20**, 1–19 (2019).
278. Paggetti, J. *et al.* Exosomes released by chronic lymphocytic leukemia cells induce the transition of stromal cells into cancer-associated fibroblasts. *Blood* **126**, 1106–1117 (2015).
279. Carvalho, A. S. *et al.* Proteomic landscape of extracellular vesicles for diffuse large b-cell lymphoma subtyping. *Int. J. Mol. Sci.* **22**, (2021).

280. Farahani, M., Rubbi, C., Liu, L., Slupsky, J. R. & Kalakonda, N. CLL exosomes modulate the transcriptome and behaviour of recipient stromal cells and are selectively enriched in MIR-202-3p. *PLoS One* **10**, 1–18 (2015).
281. Lou, X. *et al.* MiR-7e-5p downregulation promotes transformation of low-grade follicular lymphoma to aggressive lymphoma by modulating an immunosuppressive stroma through the upregulation of FasL in M1 macrophages. *J. Exp. Clin. Cancer Res.* **39**, 1–15 (2020).
282. Feng, Y. *et al.* The Role and Underlying Mechanism of Exosomal CA1 in Chemotherapy Resistance in Diffuse Large B Cell Lymphoma. *Mol. Ther. - Nucleic Acids* **21**, 452–463 (2020).
283. Palviainen, M. *et al.* Metabolic signature of extracellular vesicles depends on the cell culture conditions. *J. Extracell. Vesicles* **8**, (2019).
284. Bost, J. P. *et al.* Growth Media Conditions Influence the Secretion Route and Release Levels of Engineered Extracellular Vesicles. *Adv. Healthc. Mater.* **2101658**, 1–15 (2021).
285. Burger, D. *et al.* High glucose increases the formation and pro-oxidative activity of endothelial microparticles. *Diabetologia* **60**, 1791–1800 (2017).
286. Lehrich, B. M., Liang, Y. & Fiandaca, M. S. Foetal bovine serum influence on in vitro extracellular vesicle analyses. *J. Extracell. Vesicles* **10**, (2021).
287. Ludwig, N., Whiteside, T. L. & Reichert, T. E. Challenges in exosome isolation and analysis in health and disease. *Int. J. Mol. Sci.* **20**, (2019).
288. Patel, G. K. *et al.* Comparative analysis of exosome isolation methods using culture supernatant for optimum yield, purity and downstream applications. *Sci. Rep.* **9**, 1–10 (2019).
289. Lane, R. E., Korbie, D., Anderson, W., Vaidyanathan, R. & Trau, M. Analysis of exosome purification methods using a model liposome system and tunable-resistive pulse sensing. *Sci. Rep.* **5**, 1–7 (2015).
290. Brennan, K. *et al.* A comparison of methods for the isolation and separation of extracellular vesicles from protein and lipid particles in human serum. *Sci. Rep.* **10**, 1039 (2020).
291. Tang, Y. T. *et al.* Comparison of isolation methods of exosomes and exosomal RNA from cell culture medium and serum. *Int. J. Mol. Med.* **40**, 834–844 (2017).
292. Benedikter, B. J. *et al.* Ultrafiltration combined with size exclusion chromatography efficiently isolates extracellular vesicles from cell culture media for compositional and functional studies. *Sci. Rep.* **7**, 1–13 (2017).
293. Witwer, K. W. *et al.* Updating the MISEV minimal requirements for extracellular vesicle studies: building bridges to reproducibility. *J. Extracell. Vesicles* **6**, (2017).
294. Jeyaram, A. & Jay, S. M. Preservation and Storage Stability of Extracellular Vesicles for Therapeutic Applications. *AAPS J.* **20**, 1–7 (2018).
295. Lee, M., Ban, J. J., Im, W. & Kim, M. Influence of storage condition on exosome recovery. *Biotechnol. Bioprocess Eng.* **21**, 299–304 (2016).
296. Lorincz, Á. M. *et al.* Effect of storage on physical and functional properties of extracellular vesicles derived from neutrophilic granulocytes. *J. Extracell. Vesicles* **3**, (2014).
297. Zhang, Y. *et al.* Exosome: A review of its classification, isolation techniques, storage, diagnostic and targeted therapy applications. *Int. J. Nanomedicine* **15**, 6917–6934 (2020).
298. Sung, B. H. *et al.* A live cell reporter of exosome secretion and uptake reveals pathfinding behavior of migrating cells. *Nat. Commun.* **11**, 1–15 (2020).
299. Mathieu, M. *et al.* Specificities of exosome versus small ectosome secretion revealed by live intracellular tracking of CD63 and CD9. *Nat. Commun.* **12**, (2021).
300. Verweij, F. J. *et al.* Quantifying exosome secretion from single cells reveals a modulatory role for GPCR signaling. *J. Cell Biol.* **217**, 1129–1142 (2018).
301. Hikita, T., Miyata, M., Watanabe, R. & Oneyama, C. In vivo imaging of long-term accumulation of cancer-derived exosomes using a BRET-based reporter. *Sci. Rep.* **10**,

1–10 (2020).
302. Paolillo, M. & Schinelli, S. Integrins and exosomes, a dangerous liaison in cancer progression. *Cancers (Basel).* **9**, (2017).
303. Hoshino, A. *et al.* Tumour exosome integrins determine organotropic metastasis. *Nature* **527**, 329–335 (2015).
304. Wiklander, O. P. B. *et al.* Extracellular vesicle in vivo biodistribution is determined by cell source, route of administration and targeting. *J. Extracell. Vesicles* **4**, 1–13 (2015).
305. Riau, A. K., Ong, H. S., Yam, G. H. F. & Mehta, J. S. Sustained delivery system for stem cell-derived exosomes. *Front. Pharmacol.* **10**, 1–7 (2019).
306. Kamerkar, S. *et al.* Exosomes facilitate therapeutic targeting of oncogenic KRAS in pancreatic cancer. *Nature* **546**, 498–503 (2017).
307. Cully, M. Exosome-based candidates move into the clinic. *Nat. Rev. Drug Discov.* **20**, 6–7 (2021).
308. Khongkow, M. *et al.* Surface modification of gold nanoparticles with neuron-targeted exosome for enhanced blood–brain barrier penetration. *Sci. Rep.* **9**, 1–9 (2019).
309. Cocozza, F. *et al.* Extracellular vesicles containing ACE2 efficiently prevent infection by SARS-CoV-2 Spike protein-containing virus. *J. Extracell. Vesicles* **10**, (2020).
310. Yang, Z. *et al.* Large-scale generation of functional mRNA-encapsulating exosomes via cellular nanoporation. *Nat. Biomed. Eng.* **4**, 69–83 (2020).
311. Luan, X. *et al.* Engineering exosomes as refined biological nanoplatforms for drug delivery. *Acta Pharmacol. Sin.* **38**, 754–763 (2017).
312. Cha, J. M. *et al.* Efficient scalable production of therapeutic microvesicles derived from human mesenchymal stem cells. *Sci. Rep.* **8**, 1–16 (2018).
313. Haraszti, R. A. *et al.* Exosomes Produced from 3D Cultures of MSCs by Tangential Flow Filtration Show Higher Yield and Improved Activity. *Mol. Ther.* **26**, 2838–2847 (2018).
314. Thangaraju, K., Neerukonda, S. N., Katneni, U. & Buehler, P. W. Extracellular vesicles from red blood cells and their evolving roles in health, coagulopathy and therapy. *Int. J. Mol. Sci.* **22**, 1–25 (2021).
315. Usman, W. M. *et al.* Efficient RNA drug delivery using red blood cell extracellular vesicles. *Nat. Commun.* **9**, (2018).
316. Stacchini, A. *et al.* MEC1 and MEC2: Two new cell lines derived from B-chronic lymphocytic leukaemia in prolymphocytoid transformation. *Leuk. Res.* **23**, 127–136 (1999).
317. Rosén, A. *et al.* Lymphoblastoid cell line with B1 cell characteristics established from a chronic lymphocytic leukemia clone by in vitro EBV infection. *Oncoimmunology* **1**, 18–27 (2012).
318. Chakrabortty, S. K., Prakash, A., Nechooshtan, G., Hearn, S. & Gingeras, T. R. Extracellular vesicle-mediated transfer of processed and functional RNY5 RNA. *Rna* **21**, 1966–1979 (2015).
319. Dhahbi, J. M., Spindler, S. R., Atamna, H., Boffelli, D. & Martin, D. I. K. Deep Sequencing of Serum Small RNAs Identifies Patterns of 5′ tRNA Half and YRNA Fragment Expression Associated with Breast Cancer. *Biomark. Cancer* **6**, BIC.S20764 (2014).
320. Driedonks, T. A. P. *et al.* Y-RNA subtype ratios in plasma extracellular vesicles are cell type- specific and are candidate biomarkers for inflammatory diseases. *J. Extracell. Vesicles* **9**, (2020).
321. Bordas, M. *et al.* Optimized protocol for isolation of small extracellular vesicles from human and murine lymphoid tissues. *Int. J. Mol. Sci.* **21**, 1–16 (2020).
322. Most, J., Schwaeble, W., Drach, J., Sommerauer, A. & Dierich, M. P. Regulation of the expression of ICAM-1 on human monocytes and monocytic tumor cell lines. *J. Immunol.* **148**, 1635–1642 (1992).
323. Mcdermott, D. F. & Atkins, M. B. PD-1 as a potential target in cancer therapy. *Cancer Med.* **2**, 662–673 (2013).
324. Sheikh, N. A. & Jones, L. A. CD54 is a surrogate marker of antigen presenting cell

activation. *Cancer Immunol. Immunother.* **57**, 1381–1390 (2008).
325. Doyle, I. S., Hollmann, C. A., Crispe, I. N. & Owens, T. Specific blockade by CD54 and MHC II of CD40-mediated signaling for B cell proliferation and survival. *Exp. Cell Res.* **265**, 312–318 (2001).
326. Slavin-Chiorini, D. C. *et al.* Amplification of the lytic potential of effector/memory CD8+ cells by vector-based enhancement of ICAM-1 (CD54) in target cells: Implications for intratumoral vaccine therapy. *Cancer Gene Ther.* **11**, 665–680 (2004).
327. Wang, Y. *et al.* CCR2 and CXCR4 regulate peripheral blood monocyte pharmacodynamics and link to efficacy in experimental autoimmune encephalomyelitis. *J. Inflamm.* **6**, 1–15 (2009).
328. Kuroda, N. *et al.* Infiltrating CCR2+ monocytes and their progenies, fibrocytes, contribute to colon fibrosis by inhibiting collagen degradation through the production of TIMP-1. *Sci. Rep.* **9**, 1–17 (2019).
329. Fantuzzi, L. *et al.* Loss of CCR2 expression and functional response to monocyte chemotactic protein (MCP-1) during the differentiation of human monocytes: Role of secreted MCP-1 in the regulation of the chemotactic response. *Blood* **94**, 875–883 (1999).
330. Lim, J. K. *et al.* Chemokine Receptor Ccr2 Is Critical for Monocyte Accumulation and Survival in West Nile Virus Encephalitis. *J. Immunol.* **186**, 471–478 (2011).
331. Kwiecień, I. *et al.* Blood monocyte subsets with activation markers in relation with macrophages in non-small cell lung cancer. *Cancers (Basel).* **12**, 1–13 (2020).
332. Xu, H., Manivannan, A., Crane, I., Dawson, R. & Liversidge, J. Critical but divergent roles for CD62L and CD44 in directing blood monocyte trafficking in vivo during inflammation. *Blood* **112**, 1166–1174 (2008).
333. Yeap, W. H. *et al.* CD16 is indispensable for antibodydependent cellular cytotoxicity by human monocytes. *Sci. Rep.* **6**, (2016).
334. Haderk, F. *et al.* Extracellular vesicles in chronic lymphocytic leukemia. *Leuk. Lymphoma* **54**, 1826–1830 (2013).
335. Willms, E. *et al.* Cells release subpopulations of exosomes with distinct molecular and biological properties. *Sci. Rep.* **6**, 1–12 (2016).
336. Luo, P., Jiang, C., Ji, P., Wang, M. & Xu, J. Exosomes of stem cells from human exfoliated deciduous teeth as an anti-inflammatory agent in temporomandibular joint chondrocytes via miR-100-5p/mTOR. *Stem Cell Res. Ther.* **10**, 1–12 (2019).
337. McAndrews, K. M. & Kalluri, R. Mechanisms associated with biogenesis of exosomes in cancer. *Mol. Cancer* **18**, 1–11 (2019).
338. Willms, E., Cabañas, C., Mäger, I., Wood, M. J. A. & Vader, P. Extracellular vesicle heterogeneity: Subpopulations, isolation techniques, and diverse functions in cancer progression. *Front. Immunol.* **9**, (2018).
339. Sciaraffia, E. *et al.* Human monocytes respond to extracellular cAMP through A2A and A2B adenosine receptors. *J. Leukoc. Biol.* **96**, 113–122 (2014).
340. Saraiva, M. & O'Garra, A. The regulation of IL-10 production by immune cells. *Nat. Rev. Immunol.* **10**, 170–181 (2010).
341. Sanin, D. E., Prendergast, C. T. & Mountford, A. P. IL-10 Production in Macrophages Is Regulated by a TLR-Driven CREB-Mediated Mechanism That Is Linked to Genes Involved in Cell Metabolism. *J. Immunol.* **195**, 1218–1232 (2015).
342. Bhatnagar, S., Shinagawa, K., Castellino, F. J. & Schorey, J. S. Exosomes released from macrophages infected with intracellular pathogens stimulate a proinflammatory response in vitro and in vivo. *Blood* **110**, 3234–3244 (2007).
343. Zhang, X. *et al.* Tumor-derived exosomes induce N2 polarization of neutrophils to promote gastric cancer cell migration. *Mol. Cancer* **17**, 1–16 (2018).
344. Yu, L., Wang, L. & Chen, S. Endogenous toll-like receptor ligands and their biological significance. *J. Cell. Mol. Med.* **14**, 2592–2603 (2010).
345. Erridge, C. Endogenous ligands of TLR2 and TLR4: agonists or assistants? *J. Leukoc. Biol.* **87**, 989–999 (2010).
346. Bayraktar, R., Bertilaccio, M. T. S. & Calin, G. A. The interaction between two worlds:

MicroRNAs and Toll-like receptors. *Front. Immunol.* **10**, 1–11 (2019).
347. Li, X. *et al.* Lung tumor exosomes induce a pro-inflammatory phenotype in mesenchymal stem cells via NFκB-TLR signaling pathway. *J. Hematol. Oncol.* **9**, 1–12 (2016).
348. Driedonks, T. A. P. & Nolte-T'Hoen, E. N. M. Circulating Y-RNAs in extracellular vesicles and ribonucleoprotein complexes; Implications for the immune system. *Front. Immunol.* **10**, 1–15 (2019).
349. Hoshino, A. *et al.* Extracellular Vesicle and Particle Biomarkers Define Multiple Human Cancers ll Resource Extracellular Vesicle and Particle Biomarkers Define Multiple Human Cancers. *Cell* 1044–1061 (2020) doi:10.1016/j.cell.2020.07.009.
350. Erridge, C. Endogenous ligands of TLR2 and TLR4: agonists or assistants? *J. Leukoc. Biol.* **87**, 989–999 (2010).
351. Midwood, K. S. & Piccinini, A. M. DAMPening inflammation by modulating TLR signalling. *Mediators Inflamm.* **2010**, (2010).
352. Rilla, K. Diverse plasma membrane protrusions act as platforms for extracellular vesicle shedding. *J. Extracell. Vesicles* **10**, (2021).
353. Virgintino, D. *et al.* Plasma membrane-derived microvesicles released from tip endothelial cells during vascular sprouting. *Angiogenesis* **15**, 761–769 (2012).
354. Makler, A. & Asghar, W. Exosomal biomarkers for cancer diagnosis and patient monitoring. *Expert Rev. Mol. Diagn.* **20**, 387–400 (2020).
355. Buzas, E. I., György, B., Nagy, G., Falus, A. & Gay, S. Emerging role of extracellular vesicles in inflammatory diseases. *Nat. Rev. Rheumatol.* **10**, 356–364 (2014).
356. Crescitelli, R., Lässer, C. & Lötvall, J. Isolation and characterization of extracellular vesicle subpopulations from tissues. *Nat. Protoc.* **16**, 1548–1580 (2021).
357. Liangsupree, T., Multia, E. & Riekkola, M. L. Modern isolation and separation techniques for extracellular vesicles. *J. Chromatogr. A* **1636**, 461773 (2021).
358. Wei, R. *et al.* Combination of Size-Exclusion Chromatography and Ultracentrifugation Improves the Proteomic Profiling of Plasma-Derived Small Extracellular Vesicles. *Biol. Proced. Online* **22**, 1–11 (2020).
359. Onódi, Z. *et al.* Isolation of high-purity extracellular vesicles by the combination of iodixanol density gradient ultracentrifugation and bind-elute chromatography from blood plasma. *Front. Physiol.* **9**, 1–11 (2018).
360. Willms, E. *et al.* Cells release subpopulations of exosomes with distinct molecular and biological properties. *Sci. Rep.* **6**, 1–12 (2016).
361. Smith, Z. J. *et al.* Single exosome study reveals subpopulations distributed among cell lines with variability related to membrane content. *J. Extracell. Vesicles* **4**, 1–15 (2015).
362. Jia, Y., Ni, Z., Sun, H. & Wang, C. Microfluidic Approaches Toward the Isolation and Detection of Exosome Nanovesicles. *IEEE Access* **7**, 45080–45098 (2019).
363. Gelibter, S. *et al.* The impact of storage on extracellular vesicles: A systematic study. *J. Extracell. Vesicles* **11**, (2022).
364. Bosch, S. *et al.* Trehalose prevents aggregation of exosomes and cryodamage. *Sci. Rep.* **6**, 1–11 (2016).
365. Cheng, Y., Zeng, Q., Han, Q. & Xia, W. Effect of pH, temperature and freezing-thawing on quantity changes and cellular uptake of exosomes. *Protein Cell* **10**, 295–299 (2019).
366. Arteaga-Blanco, L. A. *et al.* Characterization and internalization of small extracellular vesicles released by human primary macrophages derived from circulating monocytes. *PLoS One* **15**, 1–23 (2020).
367. Vallhov, H. *et al.* Exosomes Containing Glycoprotein 350 Released by EBV-Transformed B Cells Selectively Target B Cells through CD21 and Block EBV Infection In Vitro. *J. Immunol.* **186**, 73–82 (2011).
368. Verweij, F. J. *et al.* Live Tracking of Inter-organ Communication by Endogenous Exosomes In Vivo. *Dev. Cell* **48**, 573-589.e4 (2019).
369. Lund, J. M. *et al.* Recognition of single-stranded RNA viruses by Toll-like receptor 7.

Proc. Natl. Acad. Sci. U. S. A. **101**, 5598–5603 (2004).
370. Shevtsov, M. *et al.* Membrane-Associated Heat Shock Proteins in Oncology: From Basic Research to New Theranostic Targets. *Cells* **9**, 1–24 (2020).
371. Lima, L. G. *et al.* Tumor microenvironmental cytokines bound to cancer exosomes determine uptake by cytokine receptor-expressing cells and biodistribution. *Nat. Commun.* **12**, (2021).
372. Maloney, A. *et al.* Gene and protein expression profiling of human ovarian cancer cells treated with the heat shock protein 90 inhibitor 17-allylamino-17-demethoxygeldanamycin. *Cancer Res.* **67**, 3239–3253 (2007).
373. Driedonks, T. A. P. & Nolte-T'Hoen, E. N. M. Circulating Y-RNAs in extracellular vesicles and ribonucleoprotein complexes; Implications for the immune system. *Front. Immunol.* **10**, 1–15 (2019).
374. Lopes, R. L., Borges, T. J., Zanin, R. F. & Bonorino, C. IL-10 is required for polarization of macrophages to M2-like phenotype by mycobacterial DnaK (heat shock protein 70). *Cytokine* **85**, 123–129 (2016).
375. Zhang, W. *et al.* ICAM-1-mediated adhesion is a prerequisite for exosome-induced T cell suppression. *Dev. Cell* **57**, 329-343.e7 (2022).
376. Galletti, G. *et al.* Targeting Macrophages Sensitizes Chronic Lymphocytic Leukemia to Apoptosis and Inhibits Disease Progression. *Cell Rep.* **14**, 1748–1760 (2016).
377. García-Silva, S. *et al.* Melanoma-derived small extracellular vesicles induce lymphangiogenesis and metastasis through an NGFR-dependent mechanism. *Nat. Cancer* **2**, 1387–1405 (2021).
378. Datta, A. *et al.* High-Throughput screening identified selective inhibitors of exosome biogenesis and secretion: A drug repurposing strategy for advanced cancer. *Sci. Rep.* **8**, 1–13 (2018).
379. Zheng, Y., Tu, C., Zhang, J. & Wang, J. Inhibition of multiple myeloma-derived exosomes uptake suppresses the functional response in bone marrow stromal cell. *Int. J. Oncol.* **54**, 1061–1070 (2019).
380. Guo, D. *et al.* RAB27A promotes melanoma cell invasion and metastasis via regulation of pro-invasive exosomes. *Int. J. Cancer* **144**, 3070–3085 (2019).
381. Poggio, M. *et al.* Suppression of Exosomal PD-L1 Induces Systemic Anti-tumor Immunity and Memory. *Cell* **177**, 414-427.e13 (2019).
382. Franziska Haderk1, Ralph Schulz1, Murat Iskar1, Laura Llaó Cid1, Thomas Worst2, Karolin V. Willmund1, Angela Schulz1, 3, Uwe Warnken3, Jana Seiler4, Axel Benner5, Michelle Nessling6, Thorsten Zenz7, Maria Göbel8, Jan Dürig8, Sven Diederichs4, 9, 10, Jérôm, and M. S. Tumor-derived exosomes modulate PD-L1 expression in monocytes. *Sci. Immunol.* (2017).
383. Treger, R. S. *et al.* Human APOBEC3G Prevents Emergence of Infectious Endogenous Retrovirus in Mice. *J. Virol.* **93**, (2019).
384. Caudron-Herger, M. *et al.* Identification, quantification and bioinformatic analysis of RNA-dependent proteins by RNase treatment and density gradient ultracentrifugation using R-DeeP. *Nat. Protoc.* (2020) doi:10.1038/s41596-019-0261-4.
385. Peinado, H. *et al.* Melanoma exosomes educate bone marrow progenitor cells toward a pro-metastatic phenotype through MET. *Nat. Med.* **18**, 883–891 (2012).
386. Bobrie, A. *et al.* Rab27a supports exosome-dependent and -independent mechanisms that modify the tumor microenvironment and can promote tumor progression. *Cancer Res.* **72**, 4920–4930 (2012).
387. Im, E. *et al.* Sulfisoxazole inhibits the secretion of small extracellular vesicles by targeting the endothelin receptor A. *Nat. Commun.* 1–17 (2019) doi:10.1038/s41467-019-09387-4.
388. Zhang, H., Lu, J., Liu, J., Zhang, G. & Lu, A. Advances in the discovery of exosome inhibitors in cancer. *J. Enzyme Inhib. Med. Chem.* **35**, 1322–1330 (2020).
389. Lwin, T. *et al.* Bone marrow stromal cells prevent apoptosis of lymphoma cells by upregulation of anti-apoptotic proteins associated with activation of NF-κB (RelB/p52) in non-Hodgkin's lymphoma cells. *Leukemia* **21**, 1521–1531 (2007).

390. Mraz, M. *et al.* Bone marrow stromal cells protect lymphoma B-cells from rituximab-induced apoptosis and targeting integrin α-4-β-1 (VLA-4) with natalizumab can overcome this resistance. *Br. J. Haematol.* **155**, 53–64 (2011).
391. Jacamo, R. *et al.* Reciprocal leukemia-stroma VCAM-1/VLA-4-dependent activation of NF-κB mediates chemoresistance. *Blood* **123**, 2691–2702 (2014).
392. Duś-Szachniewicz, K. *et al.* Differentiation of single lymphoma primary cells and normal B-cells based on their adhesion to mesenchymal stromal cells in optical tweezers. *Sci. Rep.* **9**, 1–13 (2019).
393. Carrasco, Y. R. & Batista, F. D. B-cell activation by membrane-bound antigens is facilitated by the interaction of VLA-4 with VCAM-1. *EMBO J.* **25**, 889–899 (2006).
394. Pandey, S. *et al.* IL-4 / CXCL12 loop is a key regulator of lymphoid stroma function in follicular lymphoma. **129**, 2507–2518 (2017).
395. Arai, J., Yasukawa, M., Yakushijin, Y., Miyazaki, T. & Fujita, S. Stromal cells in lymph nodes attract B-lymphoma cells via production of stromal cell-derived factor-1. *Eur. J. Haematol.* **64**, 323–332 (2000).
396. Cojoc, M. & Peitzsch, C. Emerging targets in cancer management : role of the CXCL12 / CXCR4 axis. 1347–1361 (2013).
397. Chen, J. *et al.* Dysregulated CXCR4 expression promotes lymphoma cell survival and independently predicts disease progression in germinal center B-cell-like diffuse large B-cell lymphoma. *Oncotarget* **6**, 5597–5614 (2015).
398. Laursen, M. B. *et al.* High CXCR4 expression impairs rituximab response and the prognosis of R-CHOP-treated diffuse large B-cell lymphoma patients. **10**, 717–731 (2019).
399. Burger, J. A., Burger, M. & Kipps, T. J. Chronic lymphocytic leukemia B cells express functional CXCR4 chemokine receptors that mediate spontaneous migration beneath bone marrow stromal cells. *Blood* **94**, 3658–3667 (1999).
400. Moreno, M. J. *et al.* CXCR4 expression enhances diffuse large B cell lymphoma dissemination and decreases patient survival. *J. Pathol.* 445–455 (2015) doi:10.1002/path.4446.
401. Lymphoma, N. *et al.* CXCR4 Neutralization , a Novel Therapeutic Approach for. 3106–3112 (2002).
402. Beider, K. *et al.* Targeting the CD20 and CXCR4 Pathways in Non-Hodgkin Lymphoma with Rituximab and High-Af fi nity CXCR4 Antagonist BKT140. 3495–3508 (2013) doi:10.1158/1078-0432.CCR-12-3015.
403. Reinholdt, L. *et al.* The CXCR4 antagonist plerixafor enhances the effect of rituximab in diffuse large B-cell lymphoma cell lines. *Biomark. Res.* 1–12 (2016) doi:10.1186/s40364-016-0067-2.
404. Kashyap, M. K. *et al.* Targeting the CXCR4 pathway using a novel anti-CXCR4 IgG1 antibody (PF-06747143) in chronic lymphocytic leukemia. *J. Hematol. Oncol.* **10**, 1–16 (2017).
405. Zeng, Z. *et al.* Inhibition of CXCR4 with the novel RCP168 peptide overcomes stroma-mediated chemoresistance in chronic and acute leukemias. *Mol. Cancer Ther.* **5**, 3113–3121 (2006).
406. Andritsos, L. A. *et al.* A multicenter phase 1 study of plerixafor and rituximab in patients with chronic lymphocytic leukemia. *Leuk. Lymphoma* **60**, 3461–3469 (2019).
407. Gehrke, I., Gandhirajan, R. K., Poll-Wolbeck, S. J., Hallek, M. & Kreuzer, K. A. Bone marrow stromal cell-derived vascular endothelial growth factor (VEGF) rather than chronic lymphocytic leukemia (CLL) cell-derived VEGF is essential for the apoptotic resistance of cultured CLL cells. *Mol. Med.* **17**, 619–627 (2011).
408. Wang, L., Coad, J. E., Fortney, J. M. & Gibson, L. F. VEGF-induced survival of chronic lymphocytic leukemia is independent of Bcl-2 phosphorylation [2]. *Leukemia* **19**, 1486–1487 (2005).
409. Calpe, E. *et al.* ZAP-70 Promotes the infiltration of malignant B-lymphocytes into the bone marrow by enhancing signaling and migration after CXCR4 stimulation. *PLoS One* **8**, 4–13 (2013).

410. Purroy, N. *et al.* Co-culture of primary CLL cells with bone marrow mesenchymal cells, CD40 ligand and CpG ODN promotes proliferation of chemoresistant CLL cells phenotypically comparable to those proliferating in vivo. *Oncotarget* **6**, 7632–7643 (2015).
411. Vaisitti, T. *et al.* CD38 increases CXCL12-mediated signals and homing of chronic lymphocytic leukemia cells. *Leukemia* **24**, 958–969 (2010).
412. Deaglio, S. *et al.* CD38 and CD100 lead a network of surface receptors relaying positive signals for B-CLL growth and survival. *Blood* **105**, 3042–3050 (2005).
413. Guilloton, F. *et al.* Mesenchymal stromal cells orchestrate follicular lymphoma cell niche through the CCL2-dependent recruitment and polarization of monocytes. **119**, 2556–2567 (2012).
414. Su, L., Rickert, R. C. & David, M. Rapid STAT Phosphorylation via the B Cell Receptor. *J. Biol. Chem.* **274**, 31770–31774 (1999).
415. Ding, B. B. *et al.* Constitutively activated STAT3 promotes cell proliferation and survival in the activated B-cell subtype of diffuse large B-cell lymphomas. **111**, 1515–1523 (2008).
416. Tamma, R. *et al.* Tr a n s l a t i o n a l O n c o l o g y STAT-3 RNAscope Determination in Human Diffuse Large B-Cell Lymphoma 1. *Transl. Oncol.* **12**, 545–549 (2019).
417. Akiyama, Y. *et al.* Effect of STAT3 Inhibition on the Metabolic Switch in a Highly STAT3-activated Lymphoma Cell Line. *Cancer Genomics and Proteomics* **142**, 133–142 (2015).
418. Marzec, M. *et al.* Oncogenic kinase NPM / ALK induces expression of HIF1 a mRNA. *Oncogene* 1372–1378 (2011) doi:10.1038/onc.2010.505.
419. Niu, G. *et al.* Signal Transducer and Activator of Transcription 3 Is Required for Hypoxia-Inducible Factor-1 A RNA Expression in Both Tumor Cells and Tumor-Associated Myeloid Cells. **6**, 1099–1106 (2008).
420. Solimando, A. G., Summa, S. De, Vacca, A. & Ribatti, D. Cancer-Associated Angiogenesis : The Endothelial Cell as a Checkpoint for Immunological Patrolling. 1–24 (2020).
421. Menzel, L. *et al.* Lymphocyte access to lymphoma is impaired by high endothelial venule regression ll ll Lymphocyte access to lymphoma is impaired by high endothelial venule regression. *Cell Rep.* (2021) doi:10.1016/j.celrep.2021.109878.
422. Brugnoni, D., Rossi, G., Tucci, A., Cattaneo, R. & Airo, P. Study of CD40 ligand expression in B-cell chronic lymphocytic leukemia. *Haematologica* **80**, 440–442 (1995).
423. Schattner, E. J. *et al.* Chronic lymphocytic leukemia B cells can express CD40 ligand and demonstrate T-cell type costimulatory capacity. *Blood* **91**, 2689–2697 (1998).
424. Mackay, F., Schneider, P., Rennert, P. & Browning, J. BAFF AND APRIL: A Tutorial on B Cell Survival . *Annu. Rev. Immunol.* **21**, 231–264 (2003).
425. Cols, M. *et al.* Stromal Endothelial Cells Establish a Bidirectional Crosstalk with Chronic Lymphocytic Leukemia Cells through the TNF-Related Factors BAFF, APRIL, and CD40L. *J. Immunol.* **188**, 6071–6083 (2012).
426. Endo, T. *et al.* BAFF and APRIL support chronic lymphocytic leukemia B-cell survival through activation of the canonical NF-κB pathway. *Blood* **109**, 703–710 (2007).
427. Kanakaraj, P. *et al.* BLyS binds to B cells with high affinity and induces activation of the transcription factors NF-κB and ELF-1. *Cytokine* **13**, 25–31 (2001).
428. Rodig, S. J., Shahsafaei, A., Li, B., Mackay, C. R. & Dorfman, D. M. BAFF-R, the major B cell-activating factor receptor, is expressed on most mature B cells and B-cell lymphoproliferative disorders. *Hum. Pathol.* **36**, 1113–1119 (2005).
429. Lascano, V. *et al.* Chronic lymphocytic leukemia disease progression is accelerated by APRIL-TACI interaction in the TCL1 transgenic mouse model. **122**, 3960–3963 (2013).
430. Zhang, W. *et al.* B-cell activating factor and v-Myc myelocytomatosis viral oncogene homolog (c-Myc) influence progression of chronic lymphocytic leukemia. *Proc. Natl. Acad. Sci. U. S. A.* **107**, 18956–18960 (2010).
431. Li, Y., Li, Z., Xia, Z. & Li, S. High APRIL but not BAFF serum levels are associated

with poor outcome in patients with follicular lymphoma. **2**, 79–88 (2015).
432. Kim, S. J. *et al.* Serum BAFF predicts prognosis better than APRIL in diffuse large B-cell lymphoma patients treated with rituximab plus CHOP chemotherapy. 177–184 (2008) doi:10.1111/j.1600-0609.2008.01099.x.
433. Serag El-DIen, M. M., Abdou, A. G., Asaad, N. Y., Abd El-Wahed, M. M. & Kora, M. A. E. H. M. Intratumoral FOXP3+ Regulatory T Cells in Diffuse Large B-Cell Lymphoma. *Appl. Immunohistochem. Mol. Morphol.* **25**, 534–542 (2017).
434. Han, Y. *et al.* Malignant B cells induce the conversion of CD4 +CD25 - T cells to regulatory T cells in B-cell non-Hodgkin lymphoma. *PLoS One* **6**, 4–13 (2011).
435. Tzankov, A. *et al.* Correlation of high numbers of intratumoral FOXP3+ regulatory T cells with improved survival in germinal center-like diffuse large B-cell lymphoma, follicular lymphoma and classical Hodgkin's lymphoma. *Haematologica* **93**, 193–200 (2008).
436. Zhao, Y. *et al.* Expression of Foxp3 and interleukin-7 receptor and clinicopathological characteristics of patients with diffuse large B-cell lymphoma. *Oncol. Lett.* **19**, 2755–2764 (2020).
437. Carreras, J. *et al.* High numbers of tumor-infiltrating FOXP3-positive regulatory T cells are associated with improved overall survival in follicular lymphoma. *Blood* **108**, 2957–2964 (2006).
438. Chinen, T. *et al.* An essential role for the IL-2 receptor in T reg cell function. *Nat. Immunol.* **17**, 1322–1333 (2016).
439. de la Rosa, M., Rutz, S., Dorninger, H. & Scheffold, A. Interleukin-2 is essential for CD4+CD25+ regulatory T cell function. *Eur. J. Immunol.* **34**, 2480–2488 (2004).
440. Moser, B. Editorial: History of Chemoattractant Research. *Front. Immunol.* **6**, 26–28 (2015).
441. Kumar, D. & Xu, M. L. Microenvironment Cell Contribution to Lymphoma Immunity. *Front. Oncol.* **8**, 1–11 (2018).
442. Elgueta, R. *et al.* Molecular mechanism and function of CD40/CD40L engagement in the immune system. *Immunol. Rev.* **229**, 152–172 (2009).
443. Luo, W., Weisel, F. & Shlomchik, M. J. B cell receptor and CD40 Signaling are Rewired for Synergistic induction of the c-Myc transcription factor in Germinal Center B cells. *Immunity* **176**, 139–148 (2018).
444. Schleiss, C. *et al.* BCR-associated factors driving chronic lymphocytic leukemia cells proliferation ex vivo. *Sci. Rep.* **9**, 1–12 (2019).
445. Roider, T. *et al.* Dissecting intratumour heterogeneity of nodal B-cell lymphomas at the transcriptional, genetic and drug-response levels. *Nat. Cell Biol.* **22**, 896–906 (2020).
446. Haxhinasto, S. A. & Bishop, G. A. Synergistic B cell activation by CD40 and the B cell antigen receptor: Role of B lymphocyte antigen receptor-mediated kinase activation and tumor necrosis factor receptor-associated factor regulation. *J. Biol. Chem.* **279**, 2575–2582 (2004).
447. Rauert-Wunderlich, H., Rudelius, M., Berberich, I. & Rosenwald, A. CD40L mediated alternative NFκB-signaling induces resistance to BCR-inhibitors in patients with mantle cell lymphoma article. *Cell Death Dis.* **9**, (2018).
448. Mizuno, T. & Rothstein, T. L. B Cell Receptor (BCR) Cross-Talk: CD40 Engagement Creates an Alternate Pathway for BCR Signaling That Activates IκB Kinase/IκBα/NF-κB without the Need for PI3K and Phospholipase Cγ. *J. Immunol.* **174**, 6062–6070 (2005).
449. Tromp, J. M. *et al.* Dichotomy in NF-B signaling and chemoresistance in immunoglobulin variable heavy-chain-mutated versus unmutated CLL cells upon CD40/TLR9 triggering. *Oncogene* **29**, 5071–5082 (2010).
450. Ochando, J. & Braza, M. S. T follicular helper cells: A potential therapeutic target in follicular lymphoma. *Oncotarget* **8**, 112116–112131 (2017).
451. Bhatt, S. *et al.* Anti-CD20-interleukin-21 fusokine targets malignant B cells via direct apoptosis and NK-cell–dependent cytotoxicity. *Blood* **129**, 2246–2256 (2017).
452. Saito, T. *et al.* Effective collaboration between IL-4 and IL-21 on B cell activation.

Immunobiology **213**, 545–555 (2008).
453. Chevrier, S., Kratina, T., Emslie, D., Tarlinton, D. M. & Corcoran, L. M. IL4 and IL21 cooperate to induce the high Bcl6 protein level required for germinal center formation. *Immunol. Cell Biol.* **95**, 925–932 (2017).
454. Yu, L. *et al. Blastocyst-like structures generated from human pluripotent stem cells*. *Nature* vol. 591 (2021).
455. Ross, S. H. & Cantrell, D. A. Signaling and Function of Interleukin-2 in T Lymphocytes. *Annu. Rev. Immunol.* **36**, 411–433 (2018).
456. Du, L. *et al.* IL-21 Optimizes the CAR-T Cell Preparation Through Improving Lentivirus Mediated Transfection Efficiency of T Cells and Enhancing CAR-T Cell Cytotoxic Activities. *Front. Mol. Biosci.* **8**, 1–11 (2021).
457. Wherry, E. J. & Kurachi, M. Molecular and cellular insights into T cell exhaustion. *Nat. Rev. Immunol.* **15**, 486–499 (2015).
458. Keane, C. *et al.* LAG3: A novel immune checkpoint expressed by multiple lymphocyte subsets in diffuse large B-cell lymphoma. *Blood Adv.* **4**, 1367–1377 (2020).
459. Roussel, M. *et al.* Functional characterization of PD11TIM31 tumor-infiltrating T cells in DLBCL and effects of PD1 or TIM3 blockade. *Blood Adv.* **5**, 1816–1829 (2021).
460. Autio, M. *et al.* Immune cell constitution in the tumor microenvironment predicts the outcome in diffuse large B-cell lymphoma. *Haematologica* **106**, 718–729 (2021).
461. Xu-Monette, Z. Y., Zhou, J. & Young, K. H. PD-1 expression and clinical PD-1 blockade in B-cell lymphomas. *Blood* **131**, 68–83 (2018).
462. Armengol, M., Santos, J. C., Fern, M., Ribeiro, M. L. & Rou, G. *Immune-Checkpoint Inhibitors in B-Cell Lymphoma*. (2021).
463. Ghahremanloo, A., Soltani, A., Modaresi, S. M. S. & Hashemy, S. I. Recent advances in the clinical development of immune checkpoint blockade therapy. *Cell. Oncol.* **42**, 609–626 (2019).
464. Weinstock, M., Rosenblatt, J. & Avigan, D. Dendritic Cell Therapies for Hematologic Malignancies. *Mol. Ther. - Methods Clin. Dev.* **5**, 66–75 (2017).
465. Filin, I. Y., Kitaeva, K. V., Rutland, C. S., Rizvanov, A. A. & Solovyeva, V. V. Recent Advances in Experimental Dendritic Cell Vaccines for Cancer. *Front. Oncol.* **11**, 1–7 (2021).
466. Cox, M. C. *et al.* Clinical and antitumor immune responses in relapsed/refractory follicular lymphoma patients after intranodal injections of IFNα-Dendritic cells and rituximab: A phase i clinical trial. *Clin. Cancer Res.* **25**, 5231–5241 (2019).
467. Zhao, L. & Cao, Y. J. Engineered T Cell Therapy for Cancer in the Clinic. *Front. Immunol.* **10**, (2019).
468. Ozata, D. M., Gainetdinov, I., Zoch, A., O'Carroll, D. & Zamore, P. D. PIWI-interacting RNAs: small RNAs with big functions. *Nat. Rev. Genet.* **20**, 89–108 (2019).
469. Anzelon, T. A. *et al.* Structural basis for piRNA targeting. *Nature* **597**, 285–289 (2021).
470. Jedynak-Slyvka, M., Jabczynska, A. & Szczesny, R. J. Human mitochondrial rna processing and modifications: Overview. *Int. J. Mol. Sci.* **22**, (2021).
471. Liang, H., Kidder, K. & Liu, Y. Extracellular microRNAs initiate immunostimulation via activating toll-like receptor signaling pathways. *ExRNA* **1**, 4–8 (2019).
472. Statello, L., Guo, C. J., Chen, L. L. & Huarte, M. Gene regulation by long non-coding RNAs and its biological functions. *Nat. Rev. Mol. Cell Biol.* **22**, 96–118 (2021).
473. Thomson, D. W. & Dinger, M. E. Endogenous microRNA sponges: Evidence and controversy. *Nat. Rev. Genet.* **17**, 272–283 (2016).
474. Li, Z., Chen, Z., Hu, G. H. & Jiang, Y. Roles of circular RNA in breast cancer: Present and future. *Am. J. Transl. Res.* **11**, 3945–3954 (2019).

13. Acknowledgments

The very first person I would like to thank is my supervisor, **Dr. Martina Seiffert**. Thank you, Tina, for being an enthusiastic science lover, for sharing many great ideas, helping me troubleshoot my experiments, for always being supportive about starting new collaborations, and for your patience.

I would like to thank **Prof. Dr. Peter Lichter** for allowing me to join his extraordinary division, creating and maintaining such an excellent environment where we can simply feel free to knock at any door when in need of scientific support.

I would like to thank **Sibylle Ohl** for being a fantastic colleague and for contributing in such a significant way to this thesis. Thank you for your investment, for teaching me many techniques and tricks, and for promoting a Rock'n'roll spirit in the lab.

I would like to thank the two brilliant postdocs who scientifically (and emotionally) supported me during numerous meetings and discussions, helped me unlock my project many times, and inspired me every single day during those last years. I was so lucky to have you by my side during this journey! **Dr.Geraldine Genard** and **Dr.Kendra Maass**.

I would like to thank all the collaborators and colleagues who helped me at one point or another in this project and not only shared with me their incredible knowledge but also performed experiments for this project; your enthusiasm was a driving force to me: **Dr.Karsten Richter**, **Dr.Michelle Nessling**, **Dr.Steffen Schmidt**, **Dr.Tobias Roider**, **Prof.Dr.Sascha Dietrich**, **Dr.Gabrielle Muhltoff**, **Dr.Roman Henkel**, **Dr.Kirsten Lauber**, **Dr.Torsten Müller**, **Prof.Dr.Jeroen Krijgsveld**, **Jeanette Seiler**, **Dr.Sven Diederichs**.

I would like to thank **Prof. Dr. Viktor Umansky**, **Dr. Jérôme Paggetti** and **Dr. Etienne Moussay** for their input as part of my Thesis Advisory Committee. I also would like to thank **Prof. Dr. Suat Özbek** and **Dr. Sevin Turcan** for their willingness to evaluate and discuss my PhD thesis as part of my examination committee.

I would like to thank **Verena Kalter** for being such a supportive colleague and always being available to help us.

I would like to thank my amazing student **Maisra Kasim**, for trusting me and choosing me as a supervisor. I was fortunate to work with such a motivated and talented student.

I would like to thank all the members of the Seiffert group for their scientific support and for sharing their experience and knowledge with me: **Alessa, Ebru, Franziska, Hanniyeh, Ibrahim, Laura, Lavinia, Lena, Mariana, Philipp, Ralph, Selcen**, as well as all the students who transiently joined our lab during my stay.

I would like to thank the Dietrich lab for their scientific support during the lab meetings. Particularly, I would like to address a huge thank you to **Angela**, **Caro**, **Felix,** and **Mareike,** who adapted their protocol so I could collect patients' sEVs.

I would like to thank **Michael Hain** for always being helpful with IT-related tasks. Thank you for ensuring that we could all work efficiently, especially during the pandemic.

I would like to thank **Jasmin Müller** for always being so helpful when we were having administrative problems and for organizing the life of the division so well.

I would like to thank my badminton gang: **Umar**, **Himanshu**, **Venu**, **Yashna**, **Michael**, **Mona**, **Silja, Tolga, and Thorsten** for memorable games, as well as other B06x friends for their support: **Lilo, Jasmin, Theresa, Emma, Yuan, Matt, Karol, and Milena.**

Je voudrais remercier, une fois encore, **Geraldine**, pour ses petits plats, nos journées home-office, nos aventures en tout genre. Merci d'avoir été d'un tel soutien. Je n'y serais jamais parvenue sans toi.

Thank you, **Christoph**, **Mariana,** and **Felipe** for being there for me, sharing numerous precious moments, and accepting me as the fifth roommate.

Je voudrais remercier **Charlène** pour son amitié si précieuse, pour sa générosité débordante, pour avoir été à l'écoute si souvent, et pour sa folie qui résonne si bien avec la mienne quand on est ensemble.

Je voudrais remercier **Nassim**, pour être le plus beau public de mes raps improvisés, et un excellent confident.

Je voudrais remercier **Marie** et **Lauriane** pour leur amitié durant ces dix dernières années malgré la distance. Rien ne peut effacer les souvenirs de nos sessions karaoké d'exception, nos tatouages éphémères et nos aventures en tout genre.

Je voudrais remercier **Samantha** et **Rosie** pour leur amitié et pour tous nos moments précieux passés ensemble que ce soit à Metz, à Strasbourg, à Reims, à Munich ou à Berlin.

Je voudrais remercier mes rayons de soleil **Aurore**, **Elodie**, et **Laura**. Pour nos fous rires exceptionnels, quelques péripéties inoubliables. Merci d'être présentes à mes côtés, tout simplement.

I would like to thank **Ayman** for his friendship and support, especially during the pandemic. Thank you for encouraging me and never complaining when I was singing in the car.

Je voudrais remercier ma petite sœur, **Mélanie**, de m'avoir soutenue tout au long de cette aventure et d'avoir toujours été une source d'inspiration.

Je voudrais remercier mes parents, **Luc et Solange**, pour avoir toujours cru en moi et d'avoir été présents pour célébrer chaque succès et transformer chaque défaite en tremplin. Il n'existe pas de mot assez fort pour vous exprimer toute la gratitude que j'ai envers vous.